JUSTUS-LIEBIG-
UNIVERSITÄT
GIESSEN

Kumulative Inauguraldissertation zur Erlangung

des Doktorgrades der Naturwissenschaften

- Dr. rer. nat. -

Riboregulation in der bakteriellen Anpassung zur Umwelt: Neue Funktionen der RNase E, RNase III und des kleinen RNA-Bindeproteins CcaF1

Riboregulation in bacterial adaptation to the environment: Novel functions of RNase E, RNase III and the small RNA binding protein CcaF1

vorgelegt von

Janek Maximilian Börner

Justus-Liebig-Universität Gießen

Institut für Mikro- und Molekularbiologie

November 2023

Die vorliegende Arbeit wurde am Institut für Mikro- und Molekularbiologie im Fachbereich 08 der Justus-Liebig-Universität Gießen im Zeitraum von Oktober 2019 bis November 2023 angefertigt und von Prof. Dr. Gabriele Klug betreut.

Dekan:	Prof. Dr. Thomas Wilke Institut für Tierökologie und Spezielle Zoologie Justus-Liebig-Universität Gießen
1. Gutachterin:	Prof. Dr. Gabriele Klug Institut für Mikrobiologie und Molekularbiologie Justus-Liebig-Universität Gießen
2. Gutachter:	Prof. Dr. Marek Bartkuhn Biomedical Informatics and Systems Medicine Science Justus-Liebig-Universität Gießen

Inhaltsverzeichnis

Summary

Ribonuclease E (RNase E) is likely the most important endoribonuclease in Gram-negative bacteria. As a frequently essential enzyme, RNase E is involved in the processing of numerous RNA species. In order to investigate the transcriptome-wide activity of RNase E, mutants with thermosensitive RNase E enzymes have been analysed through TIER-seq in recent years. Thereby, >20,000 RNase E-dependent RNA 5'-ends were detected in the transcriptomes of *Salmonella enterica*, *Vibrio cholerae* and *Rhodobacter sphaeroides*. Interestingly, in *R. sphaeroides* the reduction of RNase E activity led to a severe growth deficit under phototrophic conditions in addition to an altered stress resistance. A recent follow-up study of this phenotype revealed that important transcriptional activators of photosynthesis-related genes of *R. sphaeroides* are regulated in an RNase E-dependent manner. Furthermore, the data show that RNase E has a function in the growth condition-dependent control of RNA degradation rates. While the mRNA stabilities of three important transcriptional regulators were not significantly affected under microaerobic conditions, the reduced enzyme activity led to a significant change in RNA half-lives under phototrophic conditions.

As one of the few known double-strand-specific endoribonucleases, RNase III, like RNase E, plays an important role in bacterial gene regulation. However, compared to RNase E, RNase III is much higher conserved and can be found in all known bacteria and eukaryotes. RNase III has long been known to be involved in the maturation of bacterial rRNAs. Especially since the discovery of numerous new sRNAs in the last 15 years, which can form RNA-RNA hybrids with cellular target mRNAs, RNase III has again become a focus of research as a global regulator of gene expression. Recent RNA-seq studies have identified numerous substrates of RNase III, particularly among the sRNA-mRNA hybrids, and thus revealed important functions of the enzyme, for example in the production of antibiotics, regulation of virulence, maturation of CRISPR-RNAs or regulation of toxin/anti-toxin systems. A recent study on RNase III in *R. sphaeroides* demonstrated for the first time an involvement of the enzyme in the bacterial quorum sensing system in addition to functions in stress resistance and the formation of the photosynthetic apparatus.

RNA-binding proteins regulate gene expression by interacting with cellular transcripts and thus influence intramolecular RNA folding, intermolecular base pairing or the accessibility of RNase cleavage sites. The small DUF1127-protein CcaF1 was recently identified as a novel RNA-binding protein in *R. sphaeroides*. A comparison of the CcaF1 binding partners identified by RIP-seq revealed an partially overlapping binding spectrum between microaerobic and phototrophic growth conditions. An interaction with the pigment binding protein-encoding *pufBA* mRNA was detected under both microaerobic and phototrophic conditions by RIP-seq analysis. Interestingly, overexpression of CcaF1 had an opposite effect on the stability of *pufBA* under the two conditions: While destabilization of *pufBA* was observed under microaerobic conditions, the overexpression of CcaF1 had a stabilizing effect on *pufBA* under phototrophic conditions.

This work examines the present state of research on posttranscriptional gene regulation in bacteria by discussing step-by-step current research results on the function of RNase E, RNase III as well as the novel RNA binding protein CcaF1 from *R. sphaeroides* in the context of the latest state of knowledge. In addition, this work provides an important scientific contribution by investigating the effects of different environmental conditions on posttranscriptional gene regulation and revealing new functions of RNase E, RNase III and CcaF1.

Zusammenfassung

Ribonuklease E (RNase E) ist die wohl einflussreichste Endoribonuklease in Gram-negativen Bakterien. Als häufig essentielles Enzym, ist RNase E an der Prozessierung zahlreicher RNA-Spezies beteiligt. Um das transkriptomweite Wirkspektrum der RNase E zu untersuchen, wurden in den letzten Jahren Mutanten mit thermosensitiven RNase E Enzymen mittels TIER-seq analysiert. Dabei wurden >20.000 RNase E-abhängige RNA 5'-Enden in den Transkriptomen von *Salmonella enterica*, *Vibrio cholerae* und *Rhodobacter sphaeroides* detektiert. In *R. sphaeroides* führte die Reduktion der RNase E Aktivität interessanterweise neben einer veränderten Stressresistenz zu einem schwerwiegenden Wachstumsdefizit unter phototrophen Bedingungen. Eine aktuelle Folgeuntersuchung dieses Phänotyps ergab, dass wichtige Transkriptionsaktivatoren der Photosynthese-Gene in *R. sphaeroides* RNase E-abhängig reguliert werden. Weiterhin zeigen die Daten, dass RNase E eine Funktion in der Umweltbedingungs-abhängigen Kontrolle der RNA-Abbauraten besitzt. Während die mRNA-Stabilitäten dreier wichtiger Transkriptionsregulatoren unter mikroaeroben Bedingungen nicht signifikant beeinflusst wurden, führte die verminderte Enzymaktivität unter phototrophen Bedingungen zu einer signifikanten Veränderung der RNA-Halbwertszeiten.

Als eine der wenigen bekannten Doppelstrang-spezifischen Endoribonukleasen besitzt RNase III ebenso wie RNase E eine wichtige Bedeutung in der bakteriellen Genregulation. Im Vergleich zur RNase E ist RNase III jedoch deutlich stärker konserviert und kommt in allen bekannten Bakterien und Eukaryonten vor. Dabei ist RNase III schon seit längerer Zeit für ihre Beteiligung an der Reifung bakterieller rRNAs bekannt. Spätestens mit der Entdeckung zahlreicher neuer sRNAs in den letzten 15 Jahren, welche RNA-RNA Hybride mit zellulären Ziel-mRNAs bilden können, ist RNase III als globaler Regulator der Genexpression wieder in den Fokus der Forschung gerückt. Neuere RNA-seq Studien konnten insbesondere unter den sRNA-mRNA-Hybriden zahlreiche Substrate der RNase III identifizieren und somit wichtige Funktionen des Enzyms zum Beispiel in der Antibiotikaproduktion, Virulenz, Reifung von CRISPR-RNAs oder Regulation von Toxin/Anti-Toxin-Systemen aufzeigen. Eine kürzlich durchgeführte Studie zur RNase III in *R. sphaeroides* demonstrierte hierbei neben interessanten Funktionen in der Stressresistenz und der Ausbildung des Photosynthese-Apparates erstmals eine Beteiligung des Enzyms im bakteriellen *Quorum sensing* System.

RNA-Bindeproteine regulieren die Genexpression indem sie mit zellulären Transkripten interagieren und so die intramolekulare RNA-Faltung, intermolekulare Basenpaarungen oder die Zugänglichkeit von RNase-Schnittstellen beeinflussen. Das kleine DUF1127-Protein CcaF1 wurde kürzlich als neuartiges RNA-Bindeprotein in *R. sphaeroides* identifiziert. Ein Vergleich der mittels RIP-seq identifizierten CcaF1 Bindepartner ergab ein nur teilweise überlappendes Bindespektrum unter mikroaeroben und phototrophen Wachstumsbedingungen. Eine Interaktion mit der Pigmentbindeprotein-kodierenden *pufBA* mRNA wurde sowohl unter mikroaeroben als auch unter phototrophen Bedingungen mittels RIP-seq Analyse nachgewiesen. Interessanterweise hatte die Überexpression von CcaF1 einen gegensätzlichen Effekt auf die Stabilität von *pufBA* unter den beiden Bedingungen: Während unter mikroaeroben Bedingungen eine Destabilisierung von *pufBA* beobachtet wurde, wirkte die Überexpression von CcaF1 unter phototrophen Bedingungen stabilisierend auf *pufBA*.

Die vorliegende Arbeit befasst sich mit dem gegenwärtigen Stand der Forschung zur posttranskriptionellen Genregulation in Bakterien, indem schrittweise aktuelle Forschungsergebnisse zur Funktion der RNase E und RNase III sowie des neuartigen RNA-Bindeproteins CcaF1 aus *R. sphaeroides* im Kontext des aktuellen Wissensstandes diskutiert werden. Darüber hinaus leistet diese Arbeit einen wichtigen wissenschaftlichen Beitrag, da sie die Auswirkungen unterschiedlicher Umweltbedingungen auf die posttranskriptionelle Genregulation untersucht und anhand dessen neue Funktionen von RNase E, RNase III und CcaF1 aufdeckt.

Meister der Anpassung

Bakterien gehören zu den ältesten Bewohnern unseres Planeten. Durch ihre besonders lange evolutionäre Entwicklungshistorie konnte eine große Artenvielfalt entstehen. Von der Spitze des Mount Everests bis in die Tiefen des Marianengrabens, unsere Welt ist voller Bakterien. Dabei besiedeln sie nicht nur nahezu alle erdenklichen Habitate um uns herum, sondern begleiten uns auch auf und sogar in uns. Während die meisten der uns bekannten Bakterienarten in einer überschaubaren Auswahl an standardisierten Wachstumsbedingungen kultiviert werden können, benötigen einige stärker spezialisierte und viele bisher unerforschte Arten teilweise komplexe Wachstumsvoraussetzungen, welche oft nur an besonderen Standorten existieren.

Obwohl sich die heutige bakterielle Artenvielfalt im Laufe der Evolution an verschiedenste Standorte anpassen konnte, sind die umweltbedingten Standortgegebenheiten in der Natur nicht immer gleichbleibend, sondern verändern sich dynamisch. Schwankende abiotische Parameter, wie Feuchtigkeit, Temperatur, Osmolarität, pH-Wert, Strahlung, Sauerstoffverfügbarkeit und Nährstoffangebot beeinflussen die Wachstumsbedingungen eines jeden Individuums. Gleichzeitig wirken biotische Faktoren, wie die Zusammensetzung mikrobieller Lebensgemeinschaften sowie Interaktionen mit Artgenossen und fremden Spezies, auf das Leben bakterieller Zellen ein. Um sich stetig wechselnden Umweltbedingungen anpassen zu können und somit die evolutionäre Fitness zu steigern, haben Bakterien diverse Mechanismen zur Regulation ihrer Genexpression entwickelt.

Das von Francis Crick am 19. September 1957 auf einem Symposium der *Society of Experimental Biology* präsentierte und 1958 schriftlich veröffentlichte „Zentrale Dogma der Molekularbiologie“[1] stellt bis heute einen Meilenstein im Verständnis des Mechanismus der Genexpression dar. Als erste Publikation beschrieb dieser Aufsatz die Linearität der Genexpression und den Fluss der genetischen Information von der DNA über die Transkription in die RNA, welche schließlich durch die Translation in ein funktionelles Protein übersetzt werden kann. Darauffolgend konnte durch zahlreiche Experimente ein großer Wissensschatz angesammelt werden, welcher für unser heutiges Verständnis der Genexpression in Lebewesen essentiell ist.

Erstmals 15 Jahre nach Francis Cricks Hypothesenformulierung diskutierte David Apirion, dass sich der damals aktuelle Wissenstand besonders ausführlich mit der *de novo* Synthese von RNA (Transkription) befasste, wobei ein vergleichsweises spärliches Verständnis zum Abbau von RNA herrschte. Während seine relativ simple Arbeitshypothese darin bestand, dass der RNA-Abbau in *Escherichia coli* eine Art einfacher Recycling-Prozess zur Freigabe von Nukleotiden sein muss, diente diese Annahme als Grundlage für eine Bandbreite nachfolgender Untersuchungen[2]. Heute, 50 Jahre später, ist klar, dass die bakterielle Genexpression ein hochkomplexer Prozess ist, welcher zahlreiche Mechanismen beinhaltet und gleichermaßen durch RNA-Syntheserate und -Abbaurate definiert wird.

Die RNA-Polymerase

Damit die Genexpression effizient gesteuert werden kann, besitzen Bakterien die Möglichkeit, auf mehreren Ebenen der Genexpression regulierend eingreifen zu können. Auf Ebene der Transkription spielt die Zusammensetzung der DNA-abhängigen RNA-Polymerase (im Folgenden verkürzt als RNA-Polymerase bezeichnet) eine wichtige Rolle.

Da höhere Lebewesen, wie die meisten Eukaryonten, ein sehr dicht durch Histone kondensiertes Genom besitzen, können eukaryontische RNA-Polymerasen im Gegensatz zu bakteriellen RNA-Polymerasen zumeist nicht unmittelbar an die

chromosomale DNA binden. Häufig müssen sie zuerst in einem Prä-Initiationskomplex assembliert werden[3]. Dabei steuern Eukaryonten ihre Genexpression bereits durch eine sehr komplexe Regulation auf Chromatin-Ebene, indem sie die Zugänglichkeit der DNA stark variieren können, zum Beispiel mittels einer veränderten Zusammensetzung der Histon-DNA-Komplexe (Nukleosomen). Interessanterweise besitzen Archaeen, welche spätestens seit 1990 als eigenständige prokaryontische Domäne des Lebens gelten[4], ebenfalls Histone. Diese ähneln zwar in ihrer Tertiärstruktur den eukaryontischen Histonen, bilden allerdings Quartärstrukturen aus, welche sich deutlich von den eukaryontischen Nukleosomen unterscheiden[5,6].

Weiterhin besitzen Eukaryonten drei verschiedene RNA-Polymerase Enzyme, welche über unterschiedliche DNA-Bindespezifitäten verfügen. Im Gegensatz dazu besitzen Prokaryonten nur eine einzige RNA-Polymerase[7], wobei die archaelle RNA-Polymerase der eukaryontischen RNA-Polymerase II ähnelt und mit 12-14 Untereinheiten relativ komplex aufgebaut ist[8]. Die bakterielle RNA-Polymerase ist deutlich einfacher aufgebaut und besteht im Kern aus den beiden großen Untereinheiten β und β´, zwei α-Untereinheiten und einer ω-Untereinheit[9]. Als zusätzliche Untereinheit, kann ein σ-Faktor an den bakteriellen RNA-Polymerase-Kernkomplex binden, wodurch das so genannte RNA-Polymerase-Holoenzym entsteht. Aufgrund der Affinität des σ-Faktors zu spezifischen -10 und -35 lokalisierten Erkennungsmotiven an den DNA-Promotoregionen, kann das RNA-Polymerase-Holoenzym gezielt an bestimmte Promotorregionen geführt werden, um die Transkription zu initiieren[10,11]. Durch den Einsatz verschiedener σ-Faktoren können Bakterien die DNA-Bindespezifität der RNA-Polymerase modulieren.

Viele Bakterienarten besitzen einen *house keeping* σ-Faktor, welcher zur RNA-Synthese während des exponentiellen Wachstums verwendet wird. Um auf Umweltveränderungen reagieren und zum Beispiel eine Stoffwechselanpassung einleiten zu können, werden oft alternative σ-Faktoren aktiv, welche den *house keeping* σ-Faktor ersetzen und somit die DNA-Bindespezifität der RNA-Polymerase verändern[12]. Dies führt dazu, dass die genetische Information des Stoffwechselprogramms auf RNA-Ebene umgestellt werden kann. Häufig leiten prägnante Veränderungen abiotischer Umweltfaktoren, wie zum Beispiel eine starke Abweichung von der optimalen Wachstumstemperatur[13–15], die Anwesenheit reaktiver Sauerstoffspezies[16,17] oder Nährstoffmangelsituationen[18] die Synthese oder Aktivierung alternativer σ-Faktoren ein. Dabei kann ein σ-Faktor direkt die Transkription von mehr als 100 Genen kontrollieren[19,20]. Um die Transkription einzelner Gene feiner regulieren zu können, verwenden Bakterien zusätzlich eine Vielzahl weiterer Transkriptionsfaktoren, welche entweder als Transkriptionsaktivator oder -repressor wirken können.

Transkriptionsregulation am Beispiel der *Rhodobacter sphaeroides* Photosynthese-Gene

Das fakultativ-phototrophe α-Proteobakterium *Rhodobacter sphaeroides*[21,22] (mittlerweile phylogenetisch dem neu entstandenen Genus *Cereibacter* zugeordnet[23]) ist für seinen vielfältigen Metabolismus bekannt und dient in zahlreichen Studien als Modellorganismus zur Erforschung der transkriptionellen Regulation der Photosynthese-Genexpression[24–26]. Auch durch die frühe Sequenzierung des *R. sphaeroides* Genoms[27] und dessen Zugänglichkeit für genetische Modifikationen, erhielt das Bakterium als metabolisches Multitalent große Aufmerksamkeit bei der Entwicklung interessanter Anwendungen in der Biotechnologie. Dabei wird *R. sphaeroides* zum Beispiel in der grünen Wasserstoffproduktion[28,29], der Produktion von Polyhydroxyalkanoaten (Ressource zur Herstellung biologisch

abbaubaren Plastiks)[30–32], der Bioremediation von kontaminierten Böden und Gewässern[33–35] oder der *in vitro* CO_2-Fixierung verwendet[36–38].

Die Expression Photosynthese-relevanter Gene ist in *R. sphaeroides* eng an den Sauerstoffgehalt und die Lichtverfügbarkeit am Wachstumsstandort gekoppelt. Während bei Vorherrschen eines hohen Sauerstoffpartialdrucks Energie durch aerobe Respiration konserviert wird, bildet das Bakterium bei einem sinkenden Sauerstoffgehalt photosynthetisch-aktive Pigment-Proteinkomplexe in Membraneinstülpungen der inneren Zellmembran aus (siehe Abbildung 1).

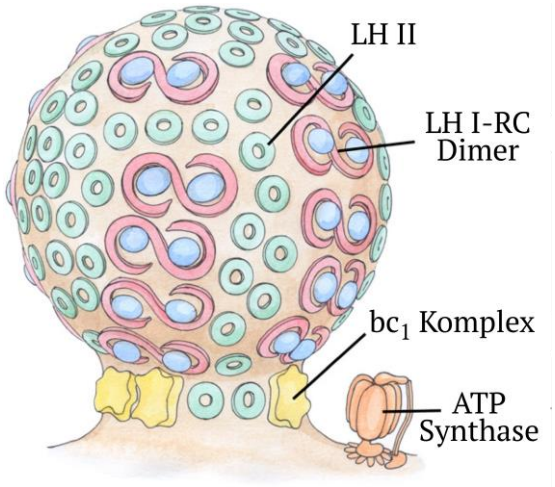

Abbildung 1: Schematische Darstellung der photosynthetischen Membran von *R. sphaeroides*. Der Photosynthese-Apparat von *R. sphaeroides* befindet sich in intrazytoplasmatischen Membraninvaginationen und besteht unter anderem aus dem Lichtsammelkomplex I *(LH I: light harvesting complex I)*, welcher ein Dimer mit dem photochemischen Reaktionszentrum *(RC: reaction center)* bildet und von mehreren Lichtsammelkomplexen II *(LH II: light harvesting complex II)* umgeben ist. In räumlicher Nähe befindet sich ein Cytochromkomplex (bc_1 Komplex). Dieser kann einen Protonengradienten durch zyklischen Elektronentransport entlang der Membran generieren, welcher durch eine ATP-Synthase zum Aufbau von ATP und somit zur Energiekonservierung genutzt wird. (Grafik modifiziert nach: [41]).

Bei der simultanen Abwesenheit von Sauerstoff und dem Vorhandensein einer geeigneten Lichtquelle stellt *R. sphaeroides* den Stoffwechsel auf eine anoxygene Photosynthese um[24]. Die strikte Koordinierung der Photosynthese-Genexpression ist für *R. sphaeroides* notwendig, da das Bakteriochlorophyll der photosynthetischen Lichtsammelkomplexe bei Anwesenheit von Sauerstoff als *photosensitizer* wirkt[39]. Dabei kann zytotoxischer Singulett-Sauerstoff, durch Energieübertragung auf molekularen Sauerstoff im Triplett-Grundzustand[40], produziert werden. Für die präzise Regulation der Photosynthese-Gen Transkription in Anpassung an Sauerstoff- und Lichtverfügbarkeit in der Umgebung besitzt *R. sphaeroides* multiple Transkriptionsfaktorsysteme, welche teilweise synergetisch und überlappend agieren.

Das PrrA/PrrB Zwei-Komponenten-System

Das aktivierende Zwei-Komponenten-System bestehend aus PrrA und PrrB (Prr: *photosynthetic response regulator*) reguliert die Transkription zahlreicher Photosynthese-Gene in Abhängigkeit vom Redox-Zustand[42,43]. Durch ihre Transmembran-Domäne kann die Zytoplasmamembran-gebundene Phosphokinase PrrB die Sauerstoffverfügbarkeit wahrnehmen. Hierbei führt der Elektronfluss in Gegenwart von Sauerstoff durch die cbb_3 Oxidase zu einer Stimulierung der Phosphatase-Aktivität von PrrB[44], wodurch dessen Autokinase-Aktivität reduziert wird und PrrB vorwiegend in einem unphosphorylierten Zustand vorliegt.

Eine Abnahme des Elektronenflusses durch cbb_3 bei Abwesenheit von Sauerstoff dient als Signal zur Stimulierung der PrrB Autokinase Funktion, wodurch Histidin-Seitenketten der zytoplasmatisch lokalisierten Proteinregion phosphoryliert werden[45]. Durch die Autophosphorylierung aktiviert, kann PrrB die angefügte Phosphat-Gruppe auf eine Aspartat-Seitenkette der N-terminalen Domäne des *response regulator* PrrA übertragen. Infolgedessen geht PrrA in den aktiven Zustand (PrrA-P) über und dimerisiert[46]. Die C-terminalen Helix-Turn-Helix Strukturen des aktiven Homodimers können

schließlich ein spezifisches Konsensusmotiv, bestehend aus zwei invertierten GCGNC-Sequenzen, an der DNA binden und dort die Transkription aktivieren[47]. Dieses Konsensusmotiv findet sich beispielweise in den Promotorregionen der *puf* und *puc* Gene[48], welche Pigmentbindeproteine des Lichtsammelkomplex I und Lichtsammelkomplex II kodieren (siehe Abbildung 1 und 2).

Das AppA/PpsR Anti-Repressor/Repressor-System

Ein weiteres Regulationssystem der Photosynthese-Gen Transkription in *R. sphaeroides* besteht aus dem Transkriptionsrepressor PpsR (*photopigment suppression*) und seinem Anti-Repressor AppA (*activation of photopigment and puc expression*). Als Gegenspieler zum aktivierenden PrrA/PrrB-System inhibiert PpsR die Transkription zahlreicher Photosynthese-Gene, unter anderem *puf*, *puc,* sowie einige Gene zur Häm-Synthese (*hem* Gene), Bakteriochlorophyll-Synthese (*bch* Gene) und Karotinoid-Synthese (*crt* Gene)[49–51] (siehe Abbildung 2). Die höchste DNA-Bindeaffinität zum TCT-N_{12}-AGA Konsensusmotiv[49] besitzt PpsR unter aeroben Bedingungen. Unter anaeroben Bedingungen (gelöste Sauerstoffkonzentration $[O_2] \leq 3$ µM) können für die Proteinfaltung wichtige Cystein-Disulfid-Brücken durch Reduktion gebrochen und folglich die Bindeaffinität zum Konsensusmotiv reduziert werden[52,53].

Der Anti-Repressor des Systems, AppA, kann die Lichtintensität in der Umwelt durch eine N-terminale BLUF-Domäne (*blue light sensing using FAD*)[54] wahrnehmen. Diese absorbiert Blaulicht mit Hilfe eines nicht-kovalent gebundenen FAD-Chromophors[55,56], wodurch eine Konformationsänderung von AppA induziert werden kann[57–59]. Bemerkenswerterweise kann die BLUF-Domäne unabhängig vom C-terminalen Rest des AppA Proteins funktionieren[60] und stellt aufgrund struktureller Unterschiede zur FAD-bindenden PAS-Domäne von Photolyasen und pflanzlichen Cryptochromen einen neuartigeren Typ biologischer Blaulichtrezeptoren dar[54]. Neben seiner lichtwahrnehmenden Eigenschaft kann AppA ebenfalls den Redox-Zustand in der Umgebung messen und wurde somit Anfang der 2000er Jahre als erstes Protein beschrieben, welches die Perzeption von Licht- und Redox-Zustand zugleich integriert[56]. Während man anfänglich eine Redox-Wahrnehmung mittels FAD-Cofaktor der BLUF-Domäne vermutete[61], konnte in späteren Arbeiten gezeigt werden, dass AppA den Redox-Zustand durch einen nicht-kovalent gebundenen Häm-Cofaktor erkennen kann[62–64]. Die Sauerstoff- und Licht-abhängige Konformationsänderung des Anti-Repressors AppA erhöht die Bindeaffinität gegenüber PpsR und es kann sich ein AppA-$PpsR_2$ Komplex bilden. Durch Bindung des Anti-Repressors AppA wird die DNA-Bindeaktivität von PpsR vollständig inhibiert. Folglich ist die PpsR-abhängige Repression der Photosynthese-Gen Transkription außer Kraft gesetzt[52].

Der Transkriptionsaktivator FnrL

Neben dem aktivierenden PrrA/PrrB Zwei-Komponenten-System, verfügt *R. sphaeroides* über einen weiteren zentralen Transkriptionsaktivator der Photosynthese-Gene, das FnrL Protein. FnrL besitzt ebenfalls eine Helix-Turn-Helix-Domäne und ist ein Homolog des Fnr (*fumarate nitrate regulator*) Transkriptionsfaktor aus *E. coli*, welcher spezifisch an DNA mit der Konsensussequenz TTGAT-N_4-ATCAA bindet[65]. Zur signalbedingten Regulation der Genexpression kann FnrL den vorherrschenden Redox-Zustand mit Hilfe eines Eisen-Schwefel-Cluster wahrnehmen. Dieses wird über vier Cystein-Seitenketten in der N-terminalen Region des Proteins gebunden[66]. Eisen-Schwefel-Cluster sind ubiquitär in nahezu allen Lebewesen vorkommend[67] und können als Cofaktor von Eisen-Schwefel-Cluster-Proteinen genutzt werden, welche unterschiedlichste

biologischen Funktionen ausüben[67–69]. Die Bindung des Eisen-Schwefel-Clusters aktiviert Fnr-Proteine, wie FnrL, indem es eine Homodimerisierung des Proteins induziert[70,71]. Neben dem *puc* Operon werden Gene zur Häm-Synthese und Bakteriochlorophyll-Synthese transkriptionell positiv durch das aktive FnrL kontrolliert[72–76] (siehe Abbildung 2). Interessanterweise reguliert FnrL auch das PrrA-abhängige Regulon indirekt, indem es die Expression von CcoN (Komponente der *cbb*$_3$ Cytochrom-Oxidase) kontrolliert[77]. Durch Anwesenheit von Säure, Sauerstoff oder anderen Oxidationsmitteln können Eisen-Schwefel-Cluster rapide beschädigt werden[78,79], wodurch FNR-Proteine zumeist monomerisieren und ihre DNA-Bindeaffinität drastisch reduziert wird[71,80].

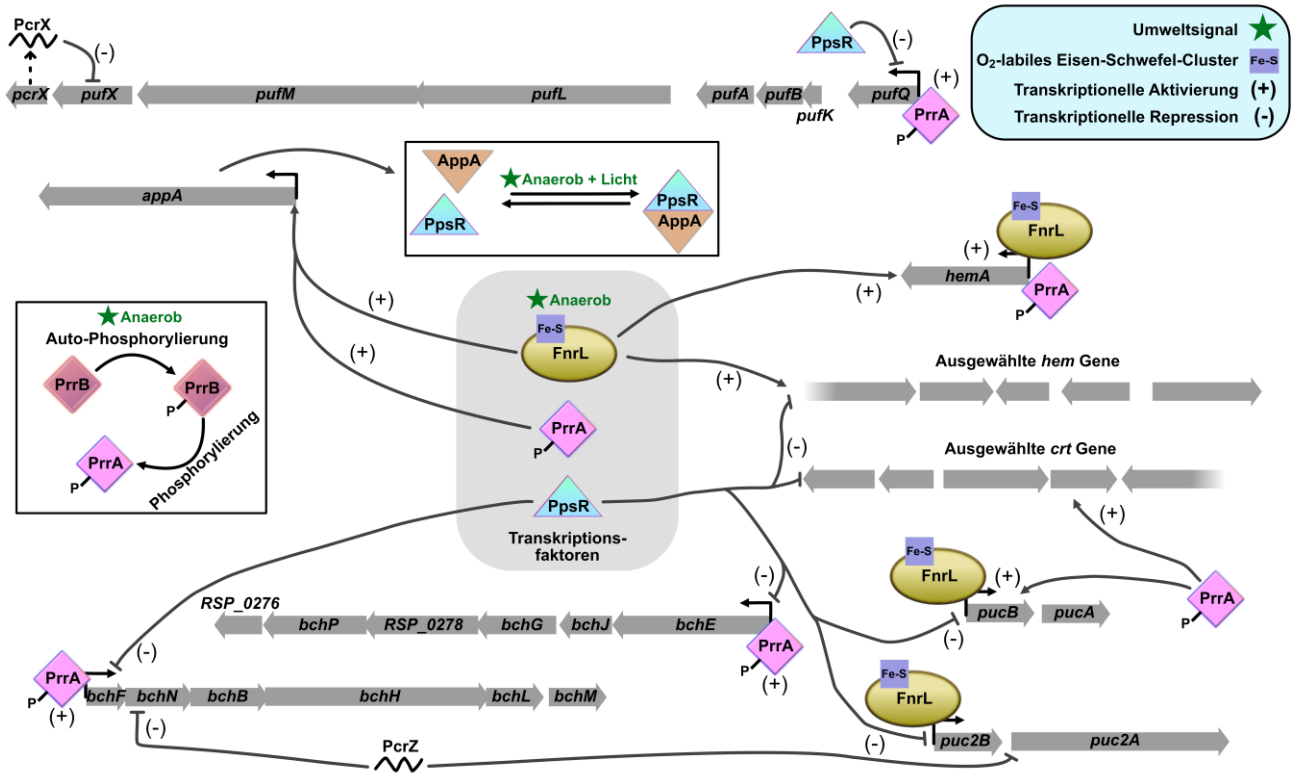

Abbildung 2. Die zentralen Transkriptionsfaktoren der Photosynthese-Genexpression und deren Regulons in *R. sphaeroides*. Das Schema zeigt den Einfluss der drei wichtigen Transkriptionsregulationssysteme FnrL, PrrB/PrrA und AppA/PpsR auf die Expression der Photosynthese-Gene in *R. sphaeroides*. Das Zwei-Komponenten-System bestehend aus der Sensorkinase PrrB und dem *response regulator* PrrA aktiviert die Transkription von *bch*, *crt*, *puc* und *puf* Genen in Abwesenheit von Sauerstoff. PpsR reprimiert die Transkription zahlreicher *bch*, *crt* und *hem* Gene, sowie die Operons der *puf* und *puc* Gene. In Abwesenheit von Sauerstoff wird der Anti-Repressor AppA exprimiert, welcher bei ausreichender Lichtintensität PpsR komplexiert und dessen reprimierende Wirkung inhibiert. FnrL nimmt den Redoxzustand durch einen Eisen-Schwefel-Cluster Cofaktor wahr. In Abwesenheit von Sauerstoff liegt das Eisen-Schwefel-Cluster intakt vor und ermöglicht die Homodimerisierung von FnrL, wodurch die Transkription der beiden *puc* Operons und einiger *hem* Gene aktiviert wird. PcrX und PcrZ sind zwei kleine nicht-kodierende RNAs, welche ihre Ziel-mRNAs in *trans* binden und dadurch reprimierend wirken. *bch Gene: kodieren Komponenten der Bakteriochlorophyll a-Synthese; crt Gene: kodieren Komponenten der Karotinoid-Synthese; hem Gene: kodieren Komponenten der Tetrapyrrol-Synthese; puf Gene: kodieren Pigmentbindeproteine des Lichtsammelkomplex I; puc Gene: kodieren Pigmentbindeproteine des Lichtsammelkomplex II.* (Grafik modifiziert nach: [81])

Kleine RNAs als Regulatoren der Photosynthese-Gene

Kleine, nicht-kodierende RNAs (in Bakterien sRNAs genannt) können durch Basenkomplementarität mit bestimmten Ziel-mRNAs in der Zelle direkt interagieren und so die Stabilität oder Translationseffizienz der Ziel-mRNA regulieren[82–85]. Durch moderne Hochdurchsatztranskriptomik, untestützt von Northern blot Analysen, konnten seit 2009 [86] zahlreiche sRNAs in *R. sphaeroides* identifiziert werden. Während für einige dieser sRNAs ein modulierender Einfluss auf die Stressresistenz[87–92] oder die Wachstumsrate[93,94] beschrieben werden konnte, wurden drei sRNAs im posttranskriptionellen Photosynthese-Genregulationsnetzwerk von *R. sphaeroides* identifiziert.

Die zuerst entdeckte sRNA im Photosynthese-Regulationsnetzwerk von *R. sphaeroides*, PcrZ (*photosynthesis control RNA Z*), hemmt die Expression von *bchE* und *puc2A* durch direkte sRNA-mRNA Interaktion. Des Weiteren konnte gezeigt werden, dass die Abundanzen vieler zusätzlicher Photosynthese-mRNAs in Abhängigkeit von PcrZ beeinflusst werden[95,96].

Als zusätzliche sRNA, entsteht PcrX *(photosynthesis control RNA X)* durch Co-Transkription der *puf* Gene und anschließender Prozessierung aus der 3´-UTR (*untranslated region*) des polycistronischen *puf* Transkripts. PcrX bindet an das *pufX* Segment der *puf* mRNA, wodurch deren Halbwertszeit herabgesetzt und die zelluläre Stöchiometrie der Puf-Proteine (beschrieben in: [97–99]) beeinflusst wird[100].

asPcrL *(anti-sense photosynthesis control RNA L)* ist eine weitere sRNA, welche direkt die Expression des *puf* Operons moduliert. Anders als PcrZ und PcrX entsteht asPcrL durch Transkription vom *anti-sense* DNA-Strang seiner Ziel-mRNA, dem *pufL* Segment. Durch perfekte Basenkomplementarität bindet asPcrL an das *pufL* Segment der polycistronischen *pufBALMX* mRNA. Das asPcrL-*pufBALMX* sRNA-mRNA Hybrid wird im Folgenden von der Doppelstrang-spezifischen Endoribonuklease III (RNase III) erkannt und prozessiert, was zur posttranskriptionellen Feinregulation der *puf* Genexpression und als weiterer Kontrollmechanismus zur Etablierung der Puf-Protein Stöchiometrie beiträgt[101].

Riboregulation in Bakterien

Durch die Formulierung des zentralen Dogmas der Molekularbiologie angestoßen, wurden in den folgenden Jahren nach Francis Cricks Hypothesenformulierung zahlreiche Komponenten der transkriptionellen Regulation der Genexpression entdeckt. Auf Grund dessen ging man ursprünglich davon aus, dass die zentrale Regulation der Genexpression vor allem auf transkriptioneller Ebene stattfindet.

Interessanterweise stellt die differentielle Expression der *Rhodobacter puf* Gene ein anschauliches Gegenbeispiel zu dieser Vermutung dar. Da die Transkription der *puf* Gene in einer gemeinsamen Transkriptionseinheit exakt identisch reguliert wird, ließe sich vermuten, dass auch die kodierten Proteine in einem quantitativ ähnlichen Verhältnis zueinander vorliegen. Entgegen dieser Vermutung, führt eine überraschend komplexe posttranskriptionelle Regulation der *puf* RNA dazu, dass eine mehr als 10-fach unterschiedliche Proteinmenge der einzelnen Komponenten generiert werden kann[97,102–104] (siehe Abbildung 3).

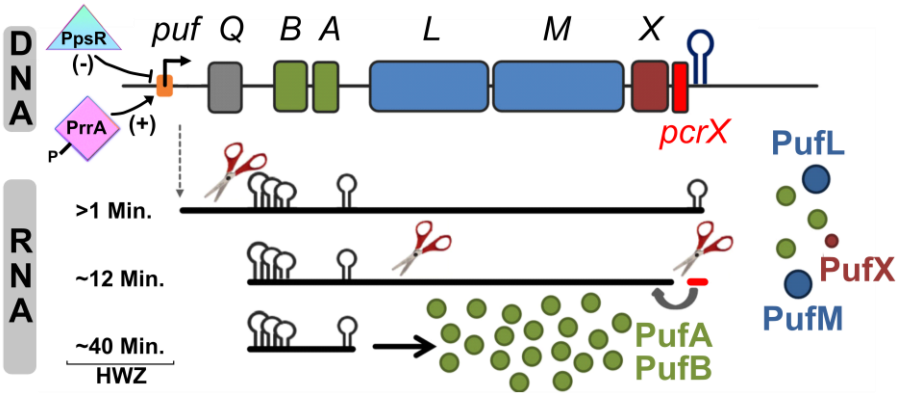

Abbildung 3: Posttranskriptionelle Regulation der *puf* Genexpression in *Rhodobacter*. Die *puf* Gene *(Q, B, A, L, M und X)* sind auf dem Negativ-DNA-Strang des ersten Chromosoms in einem gemeinsamen Operon organisiert. Die Transkription wird positiv durch PrrA und negativ durch PpsR kontrolliert. Im Gegensatz zur nah verwandten Spezies *Rhodobacter capsulatus*, befindet sich keine FnrL Bindestelle in der *puf* Genregion von *R. sphaeroides*.[73,74] Die polycistronische *pufQBALMX* mRNA besitzt eine Halbwertszeit (HWZ) von unter einer Minute. Durch einen endonukleolytischen Schnitt wird das 5´-lokalisierte *pufQ* Segment abgetrennt, wodurch ein neues 5´-Ende generiert wird, welches mehrere stabilisierende RNA-Sekundärstrukturen trägt[105]. Das Prozessierungsprodukt *pufBALMX* besitzt eine Halbwertszeit von ~12 Minuten und wird durch einen RNase E-abhängigen endonukleolytischen Schnitt in der 5´-Region des *pufL* Segments weiter prozessiert[106]. Das resultierende *pufBA* Prozessierungsprodukt ist durch 5´- und 3´- Sekundärstrukturen stabilisiert und besitzt eine Halbwertszeit von ~40 Minuten. Durch die räumlich und zeitlich versetzte Prozessierung der *puf* RNA, stehen die einzelnen ORFs (*open reading frame:* offener Leserahmen) unterschiedlich lange zur Translation zur Verfügung, wodurch PufA und PufB Proteine zahlreich am meisten, gefolgt von PufL und PufM, und am wenigsten PufX, synthetisiert werden. (Grafik modifiziert nach: [100]).

Während bei Eukaryonten die Transkription (im Zellkern) und Translation (im Zytoplasma) räumlich voneinander getrennt sind, finden sie bei Bakterien simultan statt. Hierbei wird die synthetisierte RNA meist unmittelbar von den Ribosomen gebunden und die Translation initiiert. Weiterhin können Ribonukleasen, RNA-Bindeproteine und sRNAs in Bakterien direkt am Ort der Transkription wirken, wodurch die Stabilität und Translationseffizienz von RNAs moduliert werden kann. Diese posttranskriptionelle Expressionsregulierung durch Ribonukleasen, RNA-Bindeproteine oder sRNAs wird auch Riboregulation genannt.

Dass eine rasche und durchaus komplexe Riboregulation vor allem von bakteriellen Spezies genutzt wird, deutet sich bereits beim Vergleich der generellen RNA-Halbwertszeiten in den beiden Domänen des Lebens an: Bei Bakterien beträgt diese zwischen wenigen Minuten bis einigen Stunden, wobei eukaryontische RNAs oftmals mehrere Stunden bis teilweise sogar tagelang stabil sind[107–110], zum Beispiel mRNAs für Crystalline[111], Kollagene[112] oder Globine[113,114]. In einer Untersuchung zur RNA-Stabilität im Dinoflagellaten *Karenia brevis*, welcher vermehrt im Golf von Mexiko vorkommt und dort regelmäßig für die Entstehung der roten Algenblüte verantwortlich ist, konnte erstaunlicherweise eine durchschnittliche RNA-Halbwertszeit von 33,3 Stunden ermittelt werden, wobei einige RNAs sogar Halbwertszeiten von mehr als 144 Stunden besaßen[115].

Ribonukleasen: Die Katalysatoren

Zu den Schlüsselkomponenten der bakteriellen Riboregulation zählen allen voran Ribonukleasen (RNasen). RNasen sind ubiquitär in allen Lebewesen vorkommende Enzyme, welche die Spaltung von RNA katalysieren. Zumeist geschieht dies durch eine irreversible Hydrolyse des RNA-Phosphatrückgrats.

Funktionell werden RNasen in Exo- oder Endoribonukleasen unterteilt, wobei Exoribonukleasen RNA vom 5´- oder 3´-Ende beginnend abbauen und dabei schrittweise einzelne Nukleotide vom Substrat entfernen. Endoribonukleasen hydrolysieren RNA-Substrate intern. Hierbei wird die RNA gespalten wodurch zwei kürzere RNA-Fragmente entstehen, welche jeweils ein neues 5´- oder 3´-Ende an Position der Hydrolyse besitzen (siehe Abbildung 4).

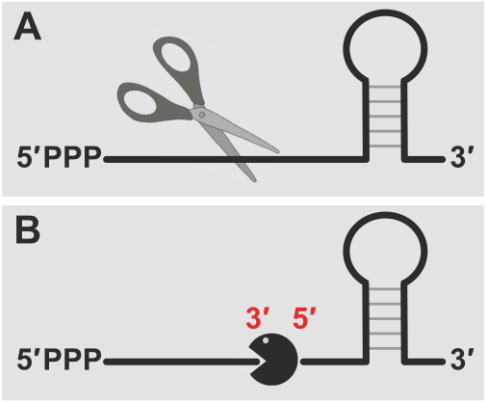

Abbildung 4: Unterscheidung zwischen Exo- und Endoribonukleasen. Skizziert ist ein bakterielles Primärtranskripte, welches typischerweise ein 5´-Triphosphat und eine 3´-Sekundärstruktur besitzt. **A** Endoribonukleasen (Schere) spalten RNA intern. **B** Durch endonukleolytische Wirkung werden neue 5´- und 3´-Enden (rot) erzeugt. Diese können von Exoribonukleasen (Pacman) abgebaut werden.

Die Polynukleotidphosphorylase

Die meisten RNasen bestehen mindestens aus einer katalytischen Domäne, welche zur Hydrolyse des Substrats benötigt wird, und einer RNA-Bindedomäne, welche den RNasen eine Substratspezifität verleiht. Die Polynukleotidphosphorylase (PNPase) ist eine wichtige Exoribonuklease, vorkommend in Bakterien, Tieren und Pflanzen[116], und eine der wenigen RNasen, welche ihre Substrate nicht durch hydrolytische Spaltung, sondern durch Phosphorolyse prozessiert (nukleophiler Angriff durch Verwendung einer Phosphatgruppe anstelle eines H_2O-Moleküls). Durch Addition der Phosphatgruppe, entstehen dabei Nukleosiddiphosphate. Bemerkenswerterweise ist die durch PNPase katalysierte Phosphorolyse reversibel, wobei das Enzym in der Umkehrreaktion auch eine Matrizen-unabhängige 5´ zu 3´ Polymerisierung von Nukleosiddiphosphaten katalysieren kann[117–119].

In Gram-negativen Bakterien übernimmt die PNPase die Prozessierung von rRNAs, tRNAs, sRNAs und verschiedensten mRNAs, wobei sie eine zentrale Rolle in der posttranskriptionellen Genregulation einnimmt[120]. Dabei konnte gezeigt werden, dass eine vollständige Abwesenheit der PNPase-Aktivität (zum Beispiel durch genomische Deletion) oder eine reduzierte Aktivität (zum Beispiel durch Entfernen der C-terminalen RNA-Bindedomäne) zahlreiche Phänotypen hervorruft, wie erhöhte Stresssensitivität[121–123], eine verminderte Virulenz[124–126] oder eine veränderte Motilität und Biofilmbildung[127–129].

Weitere Exoribonukleasen

Nicht nur in Bakterien besitzen die meisten Exoribonukleasen eine 3´ zu 5´ RNA-Abbauspezifität. Vertreter dieser Enzyme finden sich in allen Domänen des Leben[130]. Bakterielle 3´ zu 5´ Exoribonukleasen werden auf Grundlage ihrer Struktur zu den Superfamilien RNR (RNase R und RNase II), PDX (PNPase) oder DEED (Oligoribonuklease) zugeordnet[131]. Im Gram-negativen Modellorganismus *E. coli* geht der größte Teil der katalytischen 3´ zu 5´ Exoribonuklease-Aktivität in der Zelle von drei Exoribonukleasen aus: RNase R, RNase II und PNPase[132,133]. Während das Substratspektrum dieser RNasen teilweise überlappend ist, üben sie auch spezifische Funktionen aus.

RNase R ist in der Lage, strukturierte RNAs durch hydrolytische Spaltung zu prozessieren, wobei zur Substratbindung einzelsträngige RNA-Bereiche benötigt werden. In *E. coli* besitzt RNase R eine wichtige Funktion in der Qualitätskontrolle von RNAs

und Proteinen, da sie spezifisch beschädigte tRNAs und rRNAs abbaut[134,135] und bei der Befreiung festgesetzter Ribosomen beteiligt ist, indem sie die Ribosom-blockierende RNA degradiert[136–138]. Des Weiteren ist RNase R maßgeblich am Abbau von RNAs mit Polyadenyl-Anhängen beteiligt[139–141], welche häufig in Bakterien (im Gegensatz zu Eukaryonten) als Abbau-Signal und nicht zur Stabilisierung verwendet werden[142].

RNase II ist eine weitere hydrolysierende 3´ zu 5´ Exoribonuklease der RNR Superfamilie. Im Gegensatz zur strukturell ähnlich aufgebauten RNase R, baut RNase II spezifisch einzelsträngige RNA-Enden ab und gerät beim Erreichen einer RNA-Sekundärstruktur ins Stocken, wobei der RNase II-Substrat-Komplex dissoziieren kann[143,144]. In *E. coli* prozessiert RNase II hauptsächlich verschiedene mRNAs und tRNAs, wobei Adenin-reiche Regionen besonders schnell degradiert werden können. Interessanterweise begünstigt die Anheftung eines Polyadenyl-Anhangs am RNA 3´-Ende, welcher zum Beispiel durch die Polyadenylatpolymerase (nicht in α-Proteobakterien vorkommend[145]) generiert wird, den Abbau vorausliegender RNA-Sekundärstrukturen durch RNase II[146–148].

Schließlich spielt auch die Oligoribonuklease eine wichtige Rolle in der RNA-Degradation in vielen Gram-negativen Bakterien. Im Gegensatz zu den drei anderen wichtigen 3´ zu 5´ Exoribonukleasen aus *E. coli*, RNase R, RNase II und PNPase, ist die Oligoribonuklease essentiell[149], besitzt keine spezifische RNA-Bindedomäne und ist nahezu ausschließlich für den Abbau von Oligoribonukleinsäuren (bevorzugt RNA-Moleküle mit bis zu fünf Nukleotiden) zu Mononukleotiden verantwortlich[150].

Endoribonukleasen: Die Initiatoren

Apirion hielt bereits 1973 fest, dass die RNA-Degradation aus einer Reihe von exo- und endonukleolytischen Katalyseevents bestehen muss[2]. Hierbei erklärte er, dass die bakteriellen Ribosomen die neu synthetisierte mRNA unmittelbar durch Bindung stabilisieren können. Weiterhin stellte er fest, dass eine Verzögerung der Ribosomen-mRNA Bindung das Transkript zugänglich für eine endonukleolytische Prozessierung macht, woraufhin das neu entstehende RNA 3´-Ende von Exoribonukleasen attackiert werden kann. Auch 50 Jahre später ist diese Zusammenfassung noch richtig, wenn auch stark vereinfacht.

Erwähnenswert ist, dass die meisten Gram-positiven Bakterien eine spezielle Ribonuklease besitzen, RNase J, welche sowohl 5´ zu 3´ Exoribonuklease-Aktivität als auch Endoribonuklease-Aktivität besitzt[151]. Durch die 5´ zu 3´ Exoribonuklease-Aktivität ist es RNase J möglich, Endoribonuklease-unabhängig mRNA-Degradation zu initiieren. Da die 5´ zu 3´ Exoribonuklease-Prozessierung jedoch stark von den RNA 5´-Triphosphaten bakterieller Primärtranskripte inhibiert wird[152,153], benötigt die Endoribonuklease-unabhängige Degradation häufig eine zusätzliche Konvertierung des 5´ RNA-Triphosphats zu einem Monophosphat durch enzymatische Wirkung der Pyrophosphatase RppH[154]. Interessanterweise besitzt auch *R. sphaeroides*, im Gegensatz zu vielen Gram-Negativen, ein Homolog der RNase J, welches jedoch hauptsächlich als Endoribonuklease vor allem in der Prozessierung der rRNA[155] wirkt und nur sehr limitierte 5´ zu 3´ Exoribonuklease-Aktivität zeigt[156].

Endoribonuklease E (RNase E)

Zuerst Ende der 1970er Jahre identifiziert[157,158], ist RNase E mittlerweile die meist untersuchte Endoribonuklease in Gram-negativen Bakterien. Struk-

turell besteht das Enzym etwa zur Hälfte aus einer N-terminalen katalytischen Domäne, welche in den meisten Gram-Negativen stark konserviert ist, gefolgt von einer C-terminalen nicht-katalytischen Domäne, welche weniger stark konserviert und eher unstrukturiert ist[159,160]. In der N-terminalen katalytischen Domäne befinden sich strukturgebende RNase H1 Domänen, die katalysierende DNase I Domäne, eine S1 RNA-Bindedomäne und ein sensorischer Bereich zur Interaktion mit 5´ monophosphorylierten RNA-Substraten[161].

Die C-terminale Domäne der RNase E hat selbst keine katalytische Wirkung und ist Spezies-spezifisch unterschiedlich aufgebaut, wobei sich der Aufbau innerhalb einiger Proteobakterien stark ähnelt. Auf der C-terminalen Domäne des bestuntersuchten RNase E-Modells aus *E. coli* befinden sich zwei weitere RNA-Bindedomänen (AR2 und RBD)[162,163] und Proteinstrukturen zur Interaktion mit der RNA-Helikase RhlB, der glykolytischen Enolase und der exonukleolytischen PNPase, sowie eine Membran-Bindedomäne zur Lokalisierung des Enzyms entlang der inneren Zellmembran. Durch Protein-Protein-Interaktion mit RhlB, Enolase und PNPase bildet sich ein Multienzymkomplex, auch Degradosom genannt (siehe Abbildung 5), welcher durch die räumliche Zusammenführung der Helikase-, Exo- und Endoribonuklease-Aktivität besonders effizient eine Vielzahl zellulärer Transkripte abbauen kann. Dabei variiert die Zusammensetzung des Degradosoms nicht nur Art-spezifisch, sondern auch dynamisch in Abhängigkeit von Umweltbedingungen oder Wachstumsphasen[164–166]. Für *R. capsulatus*, eine nah verwandte Art von *R. sphaeroides*, konnte mittels Proteinaufreinigung gezeigt werden, dass das Degradosom des Organismus neben RNase E aus dem Transkriptionsterminations-Faktor Rho und zwei DEAD-box Helikasen besteht[167]. Interessanterweise demonstrierte eine Folgestudie, dass die Zusammensetzung und Aktivität des *R. capsulatus* Degradosoms in Abhängigkeit zur Sauerstoffverfügbarkeit variiert. Dabei co-eluierten erhöhten Mengen des Rho-Faktors unter aeroben Bedingungen, während unter mikroaeroben Bedingungen deutlich geringere Mengen des Rho-Faktors, aber eine erhöhte Menge der 65 kDa DEAD-box Helikase mit RNase E co-eluiert wurden[165].

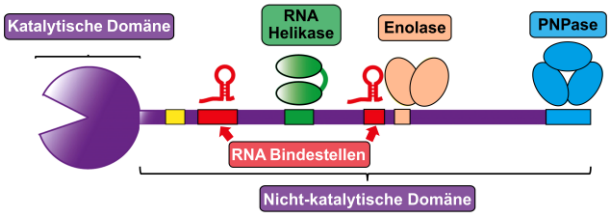

Abbildung 5: Schematische Darstellung des *E. coli* Degradosoms. Die RNase E (lila) dient als Gerüst zur Assemblierung des RNA-degradierenden Multienzymkomplexes. Der N-terminale Bereich der RNase E (Pacman) ist in der Lage RNA-Substrate endonukleolytisch zu hydrolysieren. Die C-terminale Domäne ist nicht katalytisch aktiv und besitzt eine Membranbinderegion (gelb), zwei RNA-Bindestellen (rot) und exponierte Strukturregionen zur Interaktion mit der RNA-Helikase RhlB (grün), der glykolytischen Enolase (hellbraun) und der exoribonukleolytischen PNPase (blau). (Grafik modifiziert nach: [168]).

RNase E ist in Bakterien weit konserviert vorkommend[161] und dabei häufig essentiell. Als wichtige Endoribonuklease prozessiert RNase E nicht nur zahlreiche mRNAs[169–173] und sRNAs[90,93,174,175], sondern ist auch häufig an der Reifung von tRNAs[176–178] und rRNAs[170,179,180] beteiligt. Im Gram-positiven Modellorganismus *Bacillus subtilis* ist RNase E nicht vorzufinden. Hier übernimmt ein Homolog, RNase Y, eine zentrale RNA-prozessierende Funktion anstelle von RNase E. Dass beide RNasen funktionell überlappend wirken, konnte zuletzt anschaulich demonstriert werden, wobei das *E. coli* RNase E Enzym eine Vielzahl zellulärer RNAs an gleichen Schnittstellen wie RNase Y prozessierte und dabei die Wiederherstellung eines Wildtyp-ähnlichen Wachstumsverhaltens der *B. subtilis* Δ*rny* Mutante (Deletion des RNase Y kodierenden Gens)

ermöglichte. Weiterhin postulierten die Autoren, dass die Membranlokalisierung der RNase E aus *E. coli* (ebenso wie RNase Y aus *B. subtilis*) einen wichtigen Teil zur Kompensationseffizienz beiträgt, da eine mutierte RNase E mit fehlender Membranbindesequenz das RNase Y-bedingte RNA-Prozessierungsmuster und Wachstumsdefizit geringfügiger kompensieren konnte als intakte RNase E[181].

Hierbei ist zu bemerken, dass eine Dysfunktion der Membranbindeeigenschaft keinen generellen Einfluss auf die enzymatische RNase E-Aktivität *in vitro*[182] und *in vivo*[183] hat, aber dennoch zu einer leichten Erhöhung der Gesamt-RNA-Stabilität in *E. coli* (von ~2,4 Minuten auf ~3,1 Minuten) führte[183]. Während die Stabilität von 1.792 ORFs nicht signifikant durch die fehlende Membranlokalisierung beeinflusst wurde, konnten 246 ORFs mit signifikant erhöhter Stabilität in *E. coli* gefunden werden.

Abschließend sollte darauf hingewiesen werden, dass nicht alle RNase E Enzyme eine Membran-Bindedomäne besitzen. Während RNase E aus *E. coli* und vielen β- und γ-Proteobakterien der Typ I RNase E zugeordnet werden, welche eine Membran-Bindedomäne besitzen, zählt RNase E aus *R. sphaeroides* und vielen anderen α-Proteobakterien zur Typ II RNase E, welche über keine erkennbare Membran-Bindedomäne verfügt[184,185]. Dabei demonstrierte eine aktuelle Studie mit *Caulobacter crescentus*, einem α-Proteobakterien mit Typ II Enzym, dass RNase E in Phasen-separierten *BR bodies* (ähnlich den eukaryontischen Ribonukleoprotein-Granula) im Zytoplasma lokalisiert, welche dynamisch gebildet werden und zur membranlosen Kompartimentierung innerhalb der Zelle dienen. In den *BR bodies* befinden sich hier vor allem Ribosom-ungebundene mRNAs, welche mit dem RNA-Degradaosom assoziiert sind, während tRNAs und rRNAs durch eine selektive Permeabilität aus den *BR bodies* ausgeschlossen werden[186–191].

RNase E als zentraler Regulator der globalen Genexpression

Als Endoribonuklease kann RNase E auch unabhängig vom Degradosom wirken. In ihrer aktiven Form bildet sie dabei ein aus zwei Homodimeren bestehendes Tetramer[161] und hydrolysiert spezifisch in einzelsträngigen Adenin/Uracil-reichen RNA-Regionen[192,193]. Weiterhin besitzt RNase E eine stark erhöhte Affinität gegenüber monophosphorylierten RNA-Substraten (etwa 20- bis 30-fach höher verglichen zu triphosphorylierten Substraten)[194].

Monophosphorylierte RNA 5´-Enden entstehen in Gram-Negativen häufig durch endonukleolytische Prozessierung, zum Beispiel durch RNase III, RNase G (ein Mitglied der RNase E-Familie) oder durch RNase E selbst. In weiteren Fällen können monophosphorylierte Substrate durch Wirkung der RNA 5´ Pyrophosphohydrolase RppH generiert werden, welche in *E. coli* durch direkte Proteininteraktion mit DapF (einer Diaminopimelat-Epimerase) reguliert werden kann[195,196].

Das neu generierte monophosphorylierte RNA 5´-Ende kann wiederum durch die C-terminale Bindetasche der RNase E erkannt werden. Infolgedessen kann RNase E in eine geschlossene Konformation übergehen und allosterisch aktiviert werden[197–200]. Als Resultat besitzt RNase E zumeist eine stark erhöhte Hydrolyseaktivität gegenüber prozessierten RNAs. Da dieser Mechanismus (auch 5´-abhängiger RNA-Abbaumechanismus genannt) eine Art positive Rückkopplungs-Schleife darstellt, kann folglich das Substrat vollständig fragmentiert werden. Bei Vorhandensein einer RNA-Sekundärstruktur oder Abwesenheit einer geeigneten RNase E-Erkennungssequenz wird der 5´-abhängige Abbau durch RNase E unterbrochen. Somit kann RNase E

einerseits stabile RNA 5´-Enden generieren, welche zur Reifung von RNAs beitragen können, oder andererseits den Abbau einer RNA in zahlreiche Einzelfragmente bewerkstelligen.

Mit modernen Hochdurchsatzverfahren wie RNA-seq ist es möglich, die Gesamtheit der RNAs innerhalb einer Zelle (das Transkriptom) zu analysieren, zum Beispiel hinsichtlich Qualität und Quantität verschiedener Transkripte. Hierbei werden RNA-Isolate durch reverse Transkription in cDNA umgeschrieben, welche anschließend mit terminalen Adaptern versehen und durch ein schrittweises Fluoreszenz-basiertes Amplifikationsverfahren sequenziert wird (mehr zur RNA-seq Technologie in: [201,202]). Aufgrund der immensen Zeit- und Kostenersparnis hat RNA-seq die zuvor etablierten Transkriptomanalyseverfahren wie Microarray-Studien[203] in vielen Laboren weltweit abgelöst und ein neues Zeitalter der Transkriptomik eingeleitet.

Um das Prozessierungsmuster von essentiellen Endoribonukleasen, wie RNase E, auf transkriptomweiter Ebene untersuchen zu können, wurde das TIER-seq Protokoll (*transiently inactivating an endoribonuclease followed by RNA-seq*)[204] auf Grundlage der einige Jahre vorher publizierten Studie von Clarke und Kollegen[205] entwickelt. Hierbei wird ein Bakterienstamm verwendet, welcher eine temperatursensitive RNase E kodiert (zum Beispiel durch das Gen *rne-3071* in *E. coli* [157]). Durch eine Erhöhung der Wachstumstemperatur (oftmals auf 39-44 °C) kann die temperatursensitive RNase E irreversibel inaktiviert werden. Resultierend daraus verändert sich das 5´-Prozessierungsmuster des Transkriptoms, welches durch RNA-seq erfasst und mit dem nativen Prozessierungsmuster verglichen werden kann.

Durch Anwendung von TIER-seq konnte zuerst in *Salmonella enterica*[204] und darauffolgend in *R. sphaeroides*[206], *Vibrio cholerae*[207] und *Synechocysists* sp. PC 6803[208] eine transkriptomweite Kartierung von RNase E-Prozessierungsstellen erfolgen. Während in *S. enterica* (~22.000), *R. sphaeroides* (~23.000) und *V. cholerae* (~25.000) eine ähnliche Anzahl RNase E-abhängiger Schnittstellen gefunden wurde, konnten in *Synechocystis* deutlich weniger RNase E-Schnittstellen (1472) identifiziert werden. Obwohl die bloße Anzahl der 5´-Enden vermuten lässt, dass RNase E in *Synechocystis* ein verringertes Substratspektrum besitzt, ist die erhebliche Reduktion der festgestellten RNase E-Schnittstellen sicherlich auch auf die etwas verfeinerte Methodik (tagRNA-seq) zur spezifischen Detektion Prozessierungs-bedingter RNA-Enden zurückzuführen, welche in dieser Studie angewandt wurde. Da die Genomgrößen der vier mittels TIER-seq untersuchten Organismen in einer ähnlichen Größenordnung von ~5.000.0000 Basenpaaren liegen, ist eine Diskrepanz in der Anzahl der detektierten Schnittstellen aufgrund unterschiedlicher Genomgrößen eher unwahrscheinlich.

Interessanterweise konnte in den vier bisherigen TIER-seq Studien eine ähnliche Verteilung der RNase E-Schnittstellen beobachtet werden, wobei die meisten Schnittstellen in kodierenden RNAs entdeckt wurden. Ebenso konnte das zuvor beschriebene Adenin-Uracil-reiche Erkennungsmotiv[192,193] der RNase E bestätigt werden, wobei die identifizierten Schnittstellen eine erhöhte Wahrscheinlichkeit für Uracil an Position +2 (relativ zur Hydrolyseposition) zeigten. Die TIER-seq Studie in *R. sphaeroides* ergab im Vergleich zu den Studien in *Salmonella*, *Vibrio* und *Synechocystis* ein nur sehr schwach Adenin-Uracil-angereichertes Erkennungsmotiv, was vermutlich durch den generell höheren Guanin-Cytosin-Gehalt des *Rhodobacter* Genoms (~69%) zustande kommt[206].

Während die übrigen TIER-seq Studien unter Normalbedingungen keine besonderen phänotypischen Auswirkungen durch die temperatursensitive RNase E (*rne*^{ts}) berichteten, zeigte die *Rhodobacter*

Mutante eine verringerte Zellüberlebensrate nach Singulett-Sauerstoff und Superoxid Exposition, eine verminderte Ausbildung von Photosynthese-komplexen und ein drastisches Wachstumsdefizit unter phototrophen Bedingungen (anaerob im Licht)[206].

Obgleich der wichtige regulatorische Einfluss von RNase E auf die Prozessierung des *puf* Operons und damit die Ausbildung des Photosynthese-Apparats in *Rhodobacter* bereits seit einiger Zeit beschrieben ist[104], war es vorerst unklar, ob ausschließlich die verminderte *puf* Prozessierung der *Rhodobacter* *rne*^{ts} Mutante für das limitierte Wachstum unter phototrophen Bedingungen verantwortlich ist. Auch zur Beantwortung dieser Fragestellung wurde in einer Folgestudie das Transkriptom der *R. sphaeroides* *rne*^{ts} Mutante unter drei verschiedenen Wachstumsbedingungen analysiert: aerob (hoher Sauerstoffpartialdruck in Dunkelheit), mikroaerob (geringer Sauerstoffpartialdruck in Dunkelheit) und phototroph (anaerob im Licht). Hierbei konnte gezeigt werden, dass nicht nur die *puf* mRNA Abundanz, sondern auch die Level vieler weiterer Photosynthese-relevanter Transkripte, wie *puc*, *hem* und *bch* mRNAs, in der *rne*^{ts} Mutante exklusiv unter phototrophen Bedingungen stark reduziert sind. Auffallend dabei war, dass die mRNA-Abundanz und -Stabilität der wichtigen Regulatoren AppA und PrrB ebenfalls ausschließlich unter phototrophen Bedingungen in der Mutante reduziert wird, was im Umkehrschluss eine Erklärung für die gesamtheitliche Verringerung der Photosynthese-Transkriptlevel und das Wachstumsdefizit ergab (siehe auch Kapitel 2: [81]).

Regulation der RNase E-Aktivität

Da RNasen besonders einflussreiche Enzyme sind, welche das Schicksal einer mRNA und damit die genetische Informationsumwandlung vorgeben können, ist es für den Organismus notwendig, dass die destruktive Wirkung der RNasen gerichtet ablaufen kann. Während die Biosynthese von RNasen unter anderem auf transkriptioneller Ebene reguliert wird[209], besitzen einige RNasen posttranskriptionelle Rückkopplungs-Schleifen, wobei die jeweilige RNase die Stabilität der eigenen mRNA kontrollieren kann. Eine Mitwirkung am Abbau der eigenen mRNA konnte unter anderem für die wichtigen Enzyme PNPase, RNase E und RNase III in *E. coli* und anderen Organismus mehrfach gezeigt werden[210].

Weiterhin wird das Substratspektrum von RNasen maßgeblich durch die Bindeaffinität zum Substrat definiert. Dafür existieren natürlicherweise unterschiedliche RNA-Bindemotive, welche von RNasen genutzt werden. Die PNPase besitzt eine KH und eine S1 RNA-Bindedomäne, wodurch spezifisch einzelsträngige RNAs erkannt und in die innere Pore des PNPase Homotrimers geführt werden können[211,212]. RNase E trägt zur Erkennung einzelsträngiger RNAs ein AR2 und ein RBD RNA-Bindeelement. Interessanterweise kann die RNA-Erkennung von RNase E nicht nur durch Entstehung und Zusammensetzung des Degradosoms kontrolliert werden.

RraA und RraB (*regulator of ribonuclease acitivity A/B*) sind Proteininhibitoren, welche die RNase E-Aktivität durch direkte Proteinbindung herabsetzen können[213]. Während RraA an die AR2 und RBD Region der RNase E bindet und mit der RNA-Helikase RhlB des Degradosoms interagiert[214], bindet RraB im Aminosäuresequenzbereich 694-727 [215], welcher zwischen der AR2 und RhlB Binderegion liegt. Globale Transkriptomstudien haben ergeben, dass zahlreiche RNA-Stabilitäten durch die RraA- und RraB-abhängige RNase E-Inhibition reguliert werden können, wobei die Effekte der beiden Inhibitoren nicht exakt überlappend sind, sondern einige Transkripte auch RraA- oder RraB-spezifisch stabilisiert werden[215,216].

RapZ aus *E. coli* (ehemals: YhbJ) ist ein RNA-Bindeprotein, welches direkt mit der katalytischen Domäne der RNase E interagieren und dabei als eine Art Adapter für RNase E fungieren kann, wodurch es die RNase E-Substratspezifität moduliert[217,218]. Die Bindung von RapZ ist dabei notwendig, um eine RNase E-abhängige Prozessierung der GlmZ sRNA herbeizuführen, welche die Glucosamin-6-Phosphat Synthase in *E. coli* reguliert[219]. Interessanterweise zeigte eine Folgestudie, dass GlmZ eine distinkte Aptamer Struktur enthält, welche spezifisch von RapZ erkannt wird. Weiterhin konnte demonstriert werden, dass die Fusion des Aptamers mit dem 5'-Ende einer beliebigen RNA ausreichend ist, um Prozessierung durch RNase E in diesen RNA-Fusionssubstraten einzuleiten[220]. Somit bietet sich RapZ als potentielles Werkzeug zur feineren Modulierung der Genexpression an, zum Beispiel für gentechnische Anwendungen.

RNase III: Ein alter Bekannter mit neuen Funktionen

Dass Bakterien eine Doppelstrang-spezifische Endoribonuklease besitzen, wurde bereits 10 Jahre vor der Entdeckung von RNase E, zuerst von Robertson und Kollegen für *E. coli* berichtet[221,222]. In den folgenden Jahre wurde RNase III hinsichtlich ihrer Beteiligung an der rRNA-Reifung und als Wirtsfaktor in der Prozessierung viraler RNAs intensiv untersucht[223–225]. Während RNase III in *E. coli* unter anderem für die vollständige Reifung der 23S rRNA notwendig ist[226], besitzen einige α-Proteobakterien eine spezielle RNase III-abhängige rRNA Fragmentierung. Beispielsweise wird in *Rhodobacter* das größere 23S rRNA-Molekül RNase III-abhängig in eine stabile 14S, 5.8S und eine zusätzliche 16S rRNA-Spezies prozessiert[227,228].

Interessanterweise kommt RNase III in allen bekannten Bakterien und Eukaryonten vor[229–232] und ist damit deutlich stärker konserviert als RNase E. Dabei besitzt die katalytische Domäne der RNase III ein besonders hoch konserviertes Signaturmotiv (neun Aminosäuren), welches ein strikt konserviertes Leucin an Position 3, Glycin an Position 7 und Aspartat an Position 8 beherbergt[233]. Eine Mutation dieser Positionen kann genutzt werden, um die Enzymkatalyse zu inaktivieren, während die dsRNA-Bindeaktivität erhalten bleibt[234–238].

Auf struktureller Basis wird die RNase III-Enzymfamilie in mindestens drei Klasen unterteilt (siehe Abbildung 6). Bakterielle RNase III Enzyme bestehen oftmals nur aus einer katalytisch aktiven N-terminalen RNase III-Domäne und einer C-terminalen Doppelstrang-RNA (dsRNA) Bindedomäne (Klasse 1). Eukaryontische RNase III Enzyme sind zumeist komplexer aufgebaut, wobei Drosha (Klasse 2) und Dicer (Klasse 3) als bekannte Vertreter zu nennen sind[239].

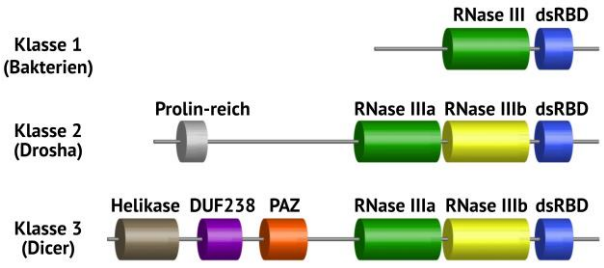

Abbildung 6: Strukturelle Unterschiede zwischen RNase III-Familienmitgliedern. Das bakterielle Klasse 1 RNase III Enzym besteht zumeist aus einer N-terminalen katalytischen RNase III-Domäne (grün) und einer C-terminalen dsRNA-Bindedomäne (blau). Eukaryontische RNase III Enzyme besitzen häufig eine weitere katalytische RNase III-Domäne (gelb). Während Klasse 2 Vertreter wie Drosha eine Prolin-reiche unstrukturierte Domäne (grau) am N-Terminus tragen, besitzen Klasse 3 Vertreter wie Dicer eine Helikase Domäne (braun), eine konservierte Domäne unbekannter Funktion (DUF238, lila) und eine PIWI-Argonaut-Zwille Domäne (PAZ, rot). (Grafik modifiziert nach: [240]).

Neben der zuerst dokumentierten, wichtigen Beteiligung in der rRNA-Reifung prozessiert RNase III auch zahlreiche mRNAs und sRNAs in Gram-positiven und Gram-negativen Bakterien, wodurch es direkt in die Regulation der Genexpression eingreifen kann. Auch durch Entwicklung der Hochdurch-

satztranskriptomik konnten in den letzten Jahren zahlreiche neue RNase III-Substrate identifiziert werden, wodurch eine Beteiligung der RNase III in vielen physiologischen Prozessen entdeckt wurde.

Eine erste Microarray-Studie zur RNase III in *E. coli* zeigte, dass eine Deletion des Enzyms zu einer Abundanzveränderung bei ~12% der kodierenden RNAs führte, was die Autoren als eine unerwartet hohe Beteiligung an der zellulären mRNA-Prozessierung beschrieben[241]. In einer kurz darauf veröffentlichten Microarray-Studie in *B. subtilis* wurde ein quantitativ ähnlicher globaler Effekt einer RNase III-Depletion (in Abwesenheit des IPTG-Induktors) beschrieben, wobei ~11% der annotierten Transkripte eine mindestens zweifache Abundanzveränderung aufwiesen. Da eine exemplarische Anzahl von analysierten RNA-Halbwertszeiten jedoch keine signifikante RNase III-abhängige Stabilisierung anzeigte, schlossen die Autoren auf eine hauptsächlich indirekte Regulation durch RNase III, zum Beispiel durch eine Modulierung der Transkriptionsraten[242].

Interessanterweise ist RNase III in *B. subtilis*, im Gegensatz zu den meisten anderen Organismen, essentiell[243]. Dies liegt daran, dass RNase III zwei Prophagen-kodierte Toxin-mRNAs destabilisiert, welche mit den beiden endogen-produzierten Anti-Toxin sRNAs RatA und SR6 (ehemals: as-yonT) hybridisieren[244,245]. Dabei ist schon länger bekannt, dass RNase III durch ihre dsRNA-spezifische Endoribonuklease-Aktivität eine wichtige Rolle in posttranskriptionell regulierten Toxin/Anti-Toxin-Systemen spielt, indem sie beispielsweise das Hybrid der Toxin-mRNA/Anti-Toxin-sRNA abbauen kann[246,247].

Auch aufgrund der RNA-seq basierten Entdeckung zahlreicher neuer sRNAs, welche durch RNA-RNA-Hybridbildung expressionsregulierend wirken und somit ein potentielles RNase III-Substrat darstellen, entstand in den letzten Jahren ein gesteigertes Interesse für weitere globale Analysen mit RNase III. Erstaunlicherweise zeigt eine frühe RNA-seq basierte Studie, welche sich mit der genomweiten *sense/anti-sense* Transkription in etlichen Gram-Positiven beschäftigte, dass die kodierenden RNA-Sequenzen von >75% aller annotierten Gene in *Staphylococcus aureus* einer RNase III-abhängigen Regulation unterliegen, wobei durch überlappende Transkription entstehende *anti-sense* Transkripte (siehe auch *„pervasive transcripts“*: [248–250]) mit den *sense* RNAs hybridisieren[251]. In der Tat konnte eine kurz darauf veröffentlichte Untersuchung via Co-Immunopräzipitation mit einer katalytisch inaktivierten RNase III bestätigen, dass eine Vielzahl dieser allgegenwärtigen *sense/anti-sense* Hybride in *S. aureus* von RNase III gebunden wird. Weiterhin zeigten die Daten, dass RNase III etliche mRNAs bindet und dabei teilweise translational reguliert, indem sie zum Beispiel die translationsinhibierende 5´-UTR-Struktur von *cspA* (kodiert ein wichtiges Kälteschockprotein) entfernt oder *leaderless* mRNAs durch 5´-UTR-Prozessierung erzeugt. Zu den häufigsten Bindepartnern der untersuchten RNase III zählten auch einige abundante regulatorische RNAs, wie tmRNA, 6S RNA, RNase P und 4.5S RNA[252], aber auch weniger abundante sRNAs wie RsaA und RsaE[253], welche durch RNase III destabilisiert wurden[254]. Durch einen ähnlichen integrierten Versuchsansatz von RNA-seq basierter Expressionsanalyse und Co-Immunopräzipitation wurde in *Streptomyces coelicolor* eine RNase III-abhängige Regulation der Antibiotikaproduktion festgestellt[255].

Mit Hilfe eines CLASH-Protokolls (*cross-linking ligation and sequencing of hybrids*)[256], also einer weiterentwickelten Form der Co-Immunopräzipitation, wurden kürzlich mehrere Hundert sRNA-mRNA Regulationspaare in Methicillin-resistenten *S. aureus* Isolaten entdecket, welche mit RNase III interagieren und unter anderem an der

Toxinproduktion des Erregers beteiligt sind[257]. In einer parallel veröffentlichten Studie wurden multiresistente *S. aureus* Isolate ebenfalls durch CLASH untersucht[258]. Hier konnten die Autoren eine unerwartet hohe Menge an mRNA-mRNA Hybriden entdecken. Deren besondere Funktion konnte unter anderem anhand der *vigR* mRNA beschrieben werden, welche eine untypisch lange 3´-UTR besitzt (657 nt) und eine Vancomycin-Resistenz vermittelt. Dabei konnte gezeigt werden, dass die *vigR* mRNA durch ihre 3´-UTR mit den kodierenden Sequenzen der *folD* und *isaA* mRNAs interagiert und diese stabilisiert, vermutlich durch Maskierung potentieller RNase III-Schnittstellen[258]. Zusammenfassend konnten beiden Gruppen zeigen, dass sich RNase III aufgrund ihrer strikten dsRNA-Spezifität und der relativ einfachen katalytischen Inaktivierung sehr gut als „Köder" im CLASH-Protokoll zur Identifizierung regulatorischer RNA-RNA Hybride eignet.

Eine umfassende Studie in *Streptococcus pyogenes* konnte durch globale Kartierung der 5´- und 3´-RNA-Enden insgesamt 92 RNase III-spezifische Schnittstellen detektieren[259]. Während 48 dieser Schnittstellen bereits bekannt waren und den bioinformatischen Detektionsalgorithmus bestätigten, konnten 42 neue Schnittstellen identifiziert werden. Die meisten wurden dabei in untranslatierten Regionen gefunden. Interessanterweise zeigte nur ~1/4 aller RNAs mit Schnittstelle eine differentielle Abundanz in Abwesenheit von RNase III. Schlussfolgernd fassten die Autoren den direkten Einfluss der RNase III auf die RNA-Abundanz als eher geringfügig zusammen, schlossen allerdings einen translationsregulierenden Effekt durch RNase III nicht aus[259], zum Beispiel durch Modulierung der Substrat-mRNA-Struktur[233].

Eine andere Gruppe konnte durch RNA-seq basiertes Transkriptomprofiling eines RNase III-Deletionsstamms von *S. pyogenes* 12 RNAs aus intergenen Regionen mit RNase III-abhängiger Abundanz erfassen, wovon sechs als neue putative sRNAs identifiziert wurden[260]. Interessant ist auch, dass ebenfalls in *S. pyogenes* erstmals die RNase III-abhängige Reifung der prä-crRNA (CRISPR RNA) beschrieben wurde. Hierbei bildet die neu entdeckte tracrRNA (*trans activating* crRNA) ein RNase III-sensitives RNA-RNA Hybrid mit der prä-crRNA[261].

Eine katalytisch inaktivierte RNase III Variante, ähnlich der untersuchten *S. pyogenes* Mutante, wurde auch in einer aktuellen Studie in *R. sphaeroides* untersucht (siehe auch Kapitel 3: [262]). Durch komparative Analyse der RNase III-abhängigen RNA 5´-Enden, basierend auf dem Protokoll von Chao *et al.*[204], konnte eine, vergleichend zur RNase E[81], deutlich geringere Anzahl potentieller RNase III-Schnittstellen im Transkriptom identifiziert werden. Diese Dokumentation deutet auf einen eher geringfügigeren globalen Effekt der RNase III in *R. sphaeroides* hin, übereinstimmend mit den vorherigen Berichten zu *E. coli*[241,263,264], *B. subtilis*[242] und *S. pyogenes*[259]. Ein Vergleich der Schnittstellen-Verteilung in *R. sphaeroides*, ermittelt unter aeroben, mikroaeroben und phototrophen Bedingungen, ergab eine bemerkenswerte Variation zwischen den Wachstumsbedingungen. Dabei konnten die meisten RNAs mit Schnittstellen unter aeroben Bedingungen (~15% des Transkriptoms) und am wenigsten RNAs mit Schnittstellen unter phototrophen Bedingungen (~5% des Transkriptoms) identifiziert wurden. Parallel dazu deutete eine Reporter-RNA-basierte *in vivo* Messung der RNase III-Aktivität auf eine leicht erhöhte Hydrolyseaktivität unter aeroben Bedingungen hin. Neben den beobachteten globalen Effekten konnte weiterhin eine wichtige Funktion in der posttranskriptionellen Expressionskontrolle des *R. sphaeroides Quorum sensing*-Systems festgestellt werden. Hier destabilisierte RNase III die mRNA der AHL-Synthase, was wiederum zu einer drastisch reduzierten mRNA- und

Autoinduktor-Abundanz führte (siehe auch Kapitel 3: [262]). *Quorum sensing* ist eine Zelldichte-abhängige interzelluläre Kommunikation mittels sekretierter Autoinduktor-Signalmoleküle (bei Gram-Negativen zumeist in Form von AHLs). Bakterien dient diese Kommunikation zur Wahrnehmung der mikrobiotischen Umgebung und wird beispielsweise zur koordinierten Expression von Genen für die Antibiotikaproduktion, Biofilmbildung oder Virulenz verwendet[265].

Interessanterweise ergab eine Transkriptomanalyse im Keuchhusten-Erreger *Bordetella pertussis*, dass in Mutanten mit inaktivierter RNase III oder reduzierter RNase E-Aktivität ein quantitativ ähnlicher Anteil des Transkriptoms (jeweils ~25%) signifikant differentiell exprimiert wird. Da die Mehrheit der regulierten Transkripte allerdings eine verringerte Abundanz in Abwesenheit der RNase III-Aktivität zeigten, deutete dies auf eine stabilisierende und ebenfalls insgesamt eher indirekte Regulation durch RNase III in *B. pertussis* hin[266].

Das wachsende Feld der RNA-Bindeproteine: Nichtkatalytische Mediatoren der Riboregulation

Durch Entwicklung der RNA-seq basierten Transkriptomik konnten in den letzten Jahren zahlreiche, vorher unbekannte, sRNAs in Bakterien identifiziert werden, welche posttranskriptionell die unterschiedlichsten physiologischen Prozesse kontrollieren. Viele sRNAs regulieren die Genexpression dabei in *trans*. Diese werden oft von eigenständigen Genen kodiert (zum Beispiel PcrZ in *R. sphaeroides*) oder durch RNase-abhängige Prozessierung aus UTRs anderer RNAs generiert (zum Beispiel PcrX in *R. sphaeroides*), wodurch sie charakteristischerweise keine perfekt-komplementäre Basensequenz zur regulierten Ziel-mRNA besitzen[267]. Damit *trans*-wirkende sRNAs eine Bindung mit ihren Ziel-mRNAs herstellen können, wird häufig das RNA-Chaperon Hfq benötigt, welches die beiden RNAs in räumlicher Nähe zusammenführt[268,269].

Hfq ist das wohl bekannteste bakterielle RNA-Bindeprotein. Es ist sowohl in Gram-Negativen als auch Gram-Positiven konserviert und wurde erstmals 1968 als wichtiger Wirtsfaktor während der Phageninfektion in *E. coli* entdeckt[270]. Als Homohexamer bildet Hfq einen ringförmigen Proteinkomplex. Dieser beherbergt 12 konservierte Sm-ähnliche RNA-Bindemotive (zwei je Protomer). Dabei bildet das Hexamer mindestens drei RNA-Kontaktflächen aus: Eine distale Plattform (an der vermehrt mRNAs[271] und eher selten sRNAs binden[272]), sowie den äußeren Rand des Rings und eine proximale Plattform (an denen zumeist der Kontakt mit sRNAs stattfindet[273,274]). Generell binden Sm RNA-Bindemotive präferiert an Adenin-Uracil-reiche RNA-Sequenzen, zum Beispiel dem 3´-gelegenen Polyuracil-Ende bakterieller Rho-unabängiger Transkriptionsterminatoren. Bekannte eukaryontische Sm-Proteine findet man unter anderem in den Proteinkomponenten des RNA-Spleißosoms, wobei dort besonders die Erkennung des eukaryontischen Polyadenyl-mRNA-Endes durch Sm-Proteine eine wichtige Rolle spielt[275]. Während Hfq vor allem für seine Wirkung als Mediator in der sRNA-vermittelten Riboregulation bekannt ist[276], interagiert das RNA Chaperon auch mit anderen RNA-Spezies in der Zelle. In *E. coli* wurde beobachtet, dass die Deletion von Hfq eine gestörte Ribosom-Biogenese verursacht, welche auf eine fehlerhafte Prozessierung und Mißfaltung von rRNAs zurückgeführt werden kann[277]. In Eukaryonten hingegen ist eine Beteiligung von Sm-Proteinen an der rRNA-[278] und tRNA-Reifung[279] schon länger bekannt. Interessanterweise wurde in einer frühen Studie während der Proteinaufreinigung von Hfq aus *E. coli* beobachtet, dass Hfq zusammen mit nicht-reifen prä-tRNAs eluiert, was erstmals auf eine mögliche Interaktion hindeutete[280]. Eine direkte Beteiligung von Hfq in

der tRNA-Biogenese konnte einige Jahre später von Lee & Feig genauer erläutert werden[281].

In *R. sphaeroides* resultierte die genomische Deletion von *hfq* unter mikroaeroben Bedingungen in einer erhöhten Sensitivität gegenüber Singulett-Sauerstoff, einer drastisch verminderten Photopigment-Produktion und einer *minicell* Morphologie. Mittels Co-Immunopräzipitation und RNA-seq konnten 25 sRNAs als Hfq Bindepartner in *R. sphaeroides* ermittelt werden[282]. Während in einem ähnlichen Versuchsansatz in *S. enterica* >700 verschiedene mRNAs nach Co-Elution mit Hfq angereichert waren (verglichen mit der Gesamt-RNA Kontrolle)[283], war der mRNA-Gehalt in den *R. sphaeroides* Proben mit 47 angereicherten mRNAs relativ niedrig[282].

Parallel zu Hfq ist in den letzten Jahren auch das RNA-Bindeprotein ProQ als ein Schlüsselspieler der bakteriellen Riboregulation ins Rampenlicht der Forschung gerückt. Obwohl ProQ bereits recht früh während eines Transposon-Screenings als Regulator der Prolin-Aufnahme in *E. coli* entdeckt wurde[284], konnte erst 22 Jahre später, durch eine Kristallisationsstudie aus 2004 angestoßen[285], eine RNA-Bindeaktivität des Proteins dokumentiert werden[286]. Durch darauffolgende Co-Immunopräzipitationsstudien in *E. coli* und *S. enterica* konnten mehr als 100 potentielle RNA-Interaktionspartner identifiziert werden, weshalb man mittlerweile von einer globalen regulatorischen Funktion von ProQ in diesen Organismen ausgeht[287,288].

Eine komparative Studie des ProQ- und Hfq-abhängigen RNA-RNA Interaktoms in *E. coli* ergab, dass das ProQ-abhängige Interaktom um ein Vielfaches kleiner ist (n_{total} ≈ 300 RNA-RNA Paare) und ein Drittel der ProQ interagierenden RNA-Hybride ebenfalls an Hfq bindet (n_{total} ≈ 1900 RNA-Paare). Eine teilweise konkurrierende Rolle der beiden Proteine konnte weiterhin anhand der Interaktion von Hfq und ProQ mit der sRNA RbsZ, welche durch Transkription von einem internen Promotor des Chemotaxis-relevanten *rbsB* Gens entsteht[289], veranschaulicht werden. RbsZ wird in Abwesenheit von ProQ in einem Hfq-abhängigen Mechanismus durch die sRNA RybB gebunden, was zur endonukleolytischen Prozessierung des Hybrids durch RNase III und einer Destabilisierung von RbsZ führt. Im Gegensatz zur kurzweiligen Interaktion der RNAs auf Hfq, war ein auf ProQ assembliertes RbsZ-RybB Hybrid stabil, was auf eine schützende Rolle von ProQ gegenüber RNase III-initiiertem Abbau hindeutete[290]. Dass ProQ Homologe (FinO-Domäne-Proteine) nur in Bakterien zu finden sind, welche ebenfalls Hfq besitzen, suggeriert neben der konkurrierenden auch eine komplementäre Funktion der beiden Proteine. Dabei kommen ProQ Homologe in vielen β- und γ-Proteobakterien vor, sind aber, bis auf Ausnahme einiger Rhizobien, nicht in α-Proteobakterien und Firmicutes zu finden (von denen zahlreiche Spezies Hfq besitzen)[291]. Interessanterweise konnte in einer umfassenden Strukturanalyse zu ProQ aus *E. coli* festgestellt werden, dass das Protein eine Tudor-ähnliche Domäne besitzt, welche häufig in Eukaryonten vorkommt und vermutlich durch horizontalen Gentransfer akquiriert wurde[292].

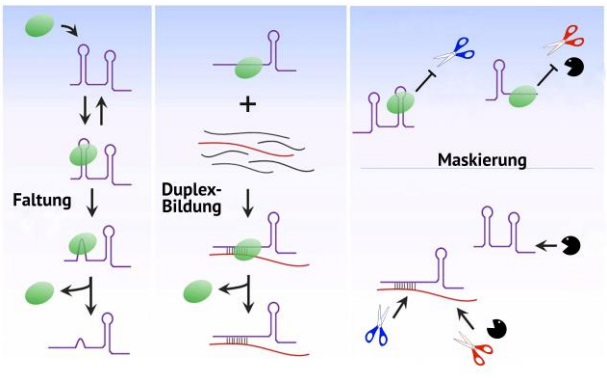

Abbildung 7: Regulatorische Funktionsmechanismen von RNA-Bindeproteinen. RNA-Bindeproteine (grün), wie Hfq oder ProQ, können die Sekundärstrukturen von sRNAs (violett) durch Protein-RNA Bindung modifizieren. Zusätzlich können zelluläre Ziel-mRNAs (rot) an Hfq oder ProQ binden, wodurch ein RNA-RNA Duplex gebildet werden kann. Außerdem können RNA-

Bindeproteine RNA-stabilisierend wirken, indem sie mit doppelsträngigen Bereichen interagieren und potentielle RNase III (blaue Schere) Schnittstellen maskieren, oder mit einzelsträngigen Bereichen interagieren und potentielle RNase E (rote Schere) Schnittstellen maskieren. Durch Interaktion mit dem RNA 3´-Ende kann der Abbau durch Exoribonukleasen (Pacman) inhibiert werden. (Grafik modifiziert nach: [293]).

DUF1127-Proteine als neue Klasse von RNA-Bindeproteinen?

Insbesondere durch die Entdeckung von ProQ und anderen FinO-Domäne-Proteinen, wie RocC (*repressor of competence*) aus *Legionella pneumophila*[294] oder NMB1681 aus *Neisseria meningitidis*[295], besteht derzeit ein starkes Forschungsinteresse, den globalen Einfluss RNA-bindender Proteine auf die bakterielle Genexpression besser zu verstehen.

Eine aktuelle Studie in *R. sphaeroides* entdeckte hierbei ein neuartiges kleines RNA-Bindeprotein, CcaF1 (ehemals RSP_6037), welches durch seine Arginin-reiche DUF1127-Domäne (DUF: *domain of unknown function*) charakterisiert wird[88]. Das *ccaF1* Gen wird interessanterweise von einem gemeinsamen genomischen Lokus mit vier homologen sRNAs co-transkribiert, welche RNase E-abhängig aus dem 3´-UTR Bereich des Transkripts prozessiert werden[87]. In früheren Studien konnte gezeigt werden, dass die genomische Organisation des kleinen Proteins und der sRNAs (in *R. sphaeroides*: CcsR1-4) in *Rhodobacteraceae, Brucellaceae, Rhizobiaceae* und *Phylobacteraceae* konserviert ist[296].

Während die Funktion von CcaF1 zunächst ungeklärt war, konnte für die CcsR sRNAs eine wichtige Funktion in der oxidativen Stressabwehr von *R. sphaeroides* demonstriert werden, indem sie die Expression von *flhR* durch direkte sRNA-mRNA Interaktion negativ regulieren. *flhR* kodiert einen Aktivator des Glutathion-abhängigen Methanol/Formaldehyd Stoffwechselwegs. Die Repression von *flhR* führt dabei zur einer Akkumulation von antioxidativem Glutathion[87].

In einer Folgestudie konnte eine RNA-Bindeaktivität von CcaF1 *in vitro* mittels EMSA (*electro mobility shift assay*) und *in vivo* mittels RIP-seq Analyse (*RNA immunoprecipitation followed by RNA-seq*) festgestellt werden. Ein zusätzliches komparatives Transkriptomprofiling via RNA-seq ergab, dass während einer Überexpression des kleinen Proteins 61 RNAs signifikant differentiell exprimiert wurden, darunter 23S und 16S rRNA, etliche tRNAs, drei sRNAs und mRNAs für einen ABC-Mangantransporter, drei Kälteschockproteine und ein σ-Faktor/Anti-σ-Faktor-System[88].

Phänotypisch resultierte die Überexpression von CcaF1 in einer erhöhten Sensitivität gegenüber oxidativem Stress, vermutlich verursacht durch eine verringerte Abundanz der CcsR sRNAs, sowie in einem drastisch reduzierten Wachstumsverhalten unter mikroaeroben Wachstumsbedingungen. Andererseits konnte unter phototrophen Bedingungen, konträr zu den Resultaten unter mikroaeroben Bedingungen, ein leicht wachstumsfördernder Effekt der CcaF1 Überexpression beobachtet werden. Damit einhergehend zeigte die Überexpression einen positiven Effekt auf die Ausbildung der Photosynthesekomplexe unter phototrophen Bedingungen[297]. Diese werden in *R. sphaeroides* zwar bereits unter mikroaeroben Bedingungen assembliert, dabei jedoch nicht durch die CcaF1 Überexpression beeinflusst[88]. Ein Vergleich der mit Hilfe von RIP-seq identifizierten CcaF1 RNA-Bindepartnern unter mikroaeroben und phototrophen Bedingungen ergab ein nur teilweise überlappendes Spektrum, wobei einige Photosynthese-relevante mRNAs exklusiv unter phototrophen Bedingungen mit CcaF1 co-eluierten (siehe auch Kapitel 4: [297]). Beispielweise konnte eine Interaktion mit der *pufBA* mRNA sowohl unter phototrophen als auch mikroaeroben Bedingungen gezeigt werden. In diesem

Zusammenhang war interessant, dass eine RNA-Halbwertszeitenanalyse in einem gegensätzlichen Effekt der CcaF1 Überexpression auf die Stabilität der *pufBA* mRNA zwischen den beiden Wachstumsbedingungen resultierte. Unter phototrophen Bedingungen stabilisierte die CcaF1 Überexpression *pufBA,* während unter mikroaeroben Bedingungen eine Destabilisierung gemessen wurde[297]. Da es eher unwahrscheinlich scheint, dass die Sekundärstruktur der RNA Umweltbedingungs-abhängig variiert, liegt es nahe, dass weitere Faktoren, wie die Abundanz von RNasen oder anderer RNA-Bindeproteine, eine wichtige Rolle in der CcaF1-vermittelten Riboregulation spielen. Interessant ist auch, dass die Studie von Grützner *et al.*[94] ebenfalls die RNA-Bindeaktivität eines weiteren DUF1127-Proteins aus *R. sphaeroides*, RSP_0557, mittels RIP-seq Analyse belegt.

Die InterPro Datenbank (aktuelle Version 96.0)[298] listet >18.000 DUF1127-Proteine in fast 4.300 Spezies, wobei ungefähr 1.000 neue Einträge von DUF1127-Proteinen in den letzten drei Jahren (seit Version 77.0) neu hinzukamen (vergleiche Referenz: [299]. Dabei befinden sich fast alle DUF1127-Proteine in α- und γ-Proteobakterien (>99% der Einträge) und sind bislang uncharakterisiert. Lediglich zwei weitere Studien beschäftigten sich derweil mit der Charakterisierung von DUF1127-Proteinen. In einer Studie mit *Brucella abortus*, häufiger Verursacher der Brucellose bei Rindern und seltener beim Menschen, resultierte die Deletion eines DUF1127-Proteins in einer Sensitivität gegenüber L-Fucose[300]. L-Fucose ist ein Zucker, der unter anderem häufig im menschlichen Darm vorkommt[301]. Für die Pathogenen *Klebsiella pneumonia* und *Campylobacter jejuni* konnte gezeigt werden, dass ein Defekt des Fucose-Metabolismus die Virulenz herabsetzen kann[302,303]. Auch andere Bakterien wie enterohämorrhagischer *E. coli* (EHEC) und *Roseburia inulinivorans* nehmen Fucose als Wirtssignal wahr und induzieren daraufhin die Expression von Fucosestoffwechsel-relevanten Genen, um Fucose als Energiequelle nutzen zu können[304,305]. Da der beobachtete Effekt des DUF1127-Proteins auf das Wachstum von *Brucella* in Anwesenheit von L-Fucose jedoch nur sehr schwach war, wurde der genauere Wirkmechanismus des DUF1127-Proteins nicht tiefergehend untersucht[300].

In einer anderen Studie an *Agrobacterium tumefaciens* berichteten die Autoren von einer starken Transkriptomveränderung vor allem in späteren Wachstumsphasen, welche durch simultane Deletion dreier DUF1127-Proteine verursacht wurde. Während zum Ende der exponentiellen Wachstumsphase bereits 78 RNAs in der Dreifachmutante signifikant differentiell exprimiert waren, stieg diese Anzahl auf ~2.600 RNAs in der späteren Transitionsphase. Auch wenn die zugrundeliegende Wirkungsweise der DUF1127-Proteine ungeklärt blieb, konnte ein drastisches Wachstumsdefizit der *A. tumefaciens* DUF1127-Mutante in Übereinstimmung mit den starken Transkriptomveränderungen in späteren Wachstumsphasen beobachtet werden[299].

Da die Entdeckung der RNA-Bindeeigenschaft des *R. sphaeroides* DUF1127-Proteins, CcaF1, erst sehr kürzlich berichtet wurde, ist momentan noch unsicher, inwiefern die RNA-Bindeaktivität eine generelle Funktion der DUF1127-Domäne darstellt. Das weitverbreitete Vorkommen dieser Domäne in α- und γ-Proteobakterien deutet allerdings auf eine konservierte Funktion hin.

Ausblick

Zuerst in Worte gefasst von Sokrates „Ich weiß, dass ich nicht weiß“ (sinnbildlich verkürztes Zitat), war diese Erkenntnis nicht nur seit Beginn ein grundlegender Baustein, sondern ist gleichzeitig

auch bis heute die treibende Kraft allen wissenschaftlichen Handelns.

Auch wenn die letzten Jahre der Forschung maßgeblich dazu beigesteuert haben, komplexe Regulationsnetzwerke in bakteriellen Systemen zu identifizieren, und uns dadurch gezeigt wurde, dass die Riboregulation eine weit wichtigere Rolle in der Genexpression einnimmt als ursprünglich vermutet, so bleiben viele Fragen dennoch ungeklärt. So war es beispielsweise überraschend, dass obwohl RNase E, RNase III und PNPase als die wichtigsten Ribonukleasen in Gram-Negativen gelten, dennoch eine erstaunliche Vielzahl zellulärer RNAs existiert, bei denen keine Hinweise für eine Prozessierung durch diese Enzyme gefunden wurden. Während dies einerseits an einer nicht vollständigen Optimierung des Detektionsverfahrens liegen mag, ist andererseits davon auszugehen, dass weitere RNasen und andere Riboregulatoren, wie nicht-identifizierte RNA-Bindeproteine und sRNAs existieren, welche wichtige Funktionen in der Kontrolle der Genexpression ausüben. Abseits der DUF1127-Proteine, listet die Pfam (*protein family*) Datenbank 4.424 DUFs, was ~25% aller bekannten Domänen-Familien ausmacht[306]. Ungefähr 60% davon können in Bakterien gefunden werden, wobei mehrere Hundert sogar essentiell zu sein scheinen[307]. Alleine durch die bloße Betrachtung dieser Zahlen ist davon auszugehen, dass viele DUF-Proteine neuartige Funktion besitzen, welche unser Verständnis wichtiger physiologischer Prozesse zumindest erweitern, wahrscheinlich sogar reformieren, werden.

In zukünftigen Untersuchungen sind wir hierbei mit modernen Technologien wie CRISPR-Cas-basierten Werkzeugen zur Genommodifikation, feinauflösenden Kristallisations-basierten Strukturgebungsverfahren, Hochdurchsatzsequenzierungsmethoden, neuartigen bioinformatischen Algorithmen und moderner künstlicher Intelligenz gewappnet. Weiterhin werden der analytischen Molekularbiologie, zum Beispiel durch die stetige Weiterentwicklung und Anpassung der CLIP-basierten Methoden (*cross-linking and immunoprecipitation*)[308], potente Protokolle zur Verfügung gestellt, welche es erlauben werden, die Interaktome von RNasen, RNA-Bindeproteinen und regulatorischen RNAs weitreichend erfassen und besser verstehen zu können.

Auch wenn bisher viele bekannte Mechanismen unter kontrollierten *in vitro* Bedingungen aufgeklärt werden konnten, ist eine Übertragung von variierenden Umweltbedingungen auf *in vitro* Studien nur sehr limitiert möglich. Insbesondere aufgrund der teilweise enormen Umweltschwankungen in der Natur ist es daher für ein umfassenderes Verständnis der Biologie zunehmend wichtig, biologische Systeme durch weitere *in vivo* Experimente zu untersuchen.

Abkürzungsverzeichnis

AHL	N-Acyl-Homoserin-Lacton
BLUF	*blue light sensing using FAD*
CLASH	*cross-linking ligation and sequencing of hybrids*
CLIP	*cross-linking and immunoprecipitation*
CRISPR	*clustered regularly interspaced short palindromic repeats*
crRNA	CRISPR RNA
DNA	Desoxyribonukleinsäure (*deoxyribonulceic acid*)
dsRNA	Doppelstrang-RNA
DUF	Domäne mit unbekannter Funktion (*domain of unknown function*)
EMSA	*electro mobility shift assay*
FAD	Flavin-Adenin-Dinukleotid
IPTG	Isopropyl-β-thiogalactosid
kDa	Kilodalton
mRNA	Boten-RNA (*messenger* RNA)
nt	Nukleotide
ORF	Offener Leserahmen (*open reading frame*)
RIP-seq	*RNA immunoprecipitation followed by RNA-seq*
RNA	Ribonukleinsäure (*ribonucleic acid*)
RNase	Ribonuklease
RNA-seq	RNA *sequencing*
rRNA	Ribosomale RNA
sRNA	Kleine regulatorische RNA (*small* RNA)
TIER-seq	*transiently inactivating an endoribonuclease followed by RNA-seq*
tracrRNA	*trans activating* crRNA
tRNA	Transfer RNA
UTR	Nicht-translatierte Region (*untraslated region*)

References

1. Crick, F. H. On protein synthesis. *Symposia of the Society for Experimental Biology* **12,** 8 (1958).
2. Apirion, D. Degradation of RNA in *Escherichia coli*. A hypothesis. *Molecular & general genetics : MGG* **122,** 313–322 (1973).
3. Hahn, S. Structure and mechanism of the RNA polymerase II transcription machinery. *Nature structural & molecular biology* **11,** 394–403 (2004).
4. Woese, C. R., Kandler, O. & Wheelis, M. L. Towards a natural system of organisms: proposal for the domains Archaea, Bacteria, and Eucarya. *Proceedings of the National Academy of Sciences of the United States of America* **87,** 4576–4579 (1990).
5. Stevens, K. M. & Warnecke, T. Histone variants in archaea - An undiscovered country. *Seminars in cell & developmental biology* **135,** 50–58 (2023).
6. Henneman, B., van Emmerik, C., van Ingen, H. & Dame, R. T. Structure and function of archaeal histones. *PLOS Genetics* **14,** e1007582 (2018).
7. Kwapisz, M., Beckouët, F. & Thuriaux, P. Early evolution of eukaryotic DNA-dependent RNA polymerases. *Trends in genetics : TIG* **24,** 211–215 (2008).
8. Karr, E. A. Chapter Three - Transcription Regulation in the Third Domain. In *Advances in Applied Microbiology,* edited by S. Sariaslani & G. M. Gadd (Academic Press), Vol. 89, pp. 101–133 (2014).
9. Decker, K. B. & Hinton, D. M. Transcription regulation at the core: similarities among bacterial, archaeal, and eukaryotic RNA polymerases. *Annual review of microbiology* **67,** 113–139 (2013).
10. Paget, M. S. Bacterial sigma factors and anti-sigma factors: Structure, function and distribution. *Biomolecules* **5,** 1245–1265 (2015).
11. Paget, M. S. B. & Helmann, J. D. The σ^{70} family of sigma factors. *Genome biology* **4,** 203; 10.1186/gb-2003-4-1-203 (2003).
12. Gruber, T. M. & Gross, C. A. Multiple sigma subunits and the partitioning of bacterial transcription space. *Annual review of microbiology* **57,** 441–466 (2003).
13. Ades, S. E., Grigorova, I. L. & Gross, C. A. Regulation of the alternative sigma factor σ^{E} during initiation, adaptation, and shutoff of the extracytoplasmic heat shock response in *Escherichia coli*. *Journal of bacteriology* **185,** 2512–2519 (2003).
14. Chan, Y. C. *et al.* Contributions of two-component regulatory systems, alternative sigma factors, and negative regulators to *Listeria monocytogenes* cold adaptation and cold growth. *Journal of Food Protection* **71,** 420–425 (2008).
15. Kullik, I. & Giachino, P. The alternative sigma factor sigmaB in *Staphylococcus aureus*: regulation of the *sigB* operon in response to growth phase and heat shock. *Archives of Microbiology* **167,** 151–159 (1997).
16. Nuss, A. M., Glaeser, J., Berghoff, B. A. & Klug, G. Overlapping alternative sigma factor regulons in the response to singlet oxygen in *Rhodobacter sphaeroides*. *Journal of bacteriology* **192,** 2613–2623 (2010).
17. Raman, S. *et al.* The alternative sigma factor SigH regulates major components of oxidative and heat stress responses in *Mycobacterium tuberculosis*. *Journal of bacteriology* **183,** 6119–6125 (2001).
18. DeMaio, J., Zhang, Y., Ko, C., Young, D. B. & Bishai, W. R. A stationary-phase stress-response sigma factor from *Mycobacterium tuberculosis*. *Proceedings of the National Academy of Sciences of the United States of America* **93,** 2790–2794 (1996).

19. Blanka, A. *et al.* Identification of the alternative sigma factor SigX regulon and its implications for *Pseudomonas aeruginosa* pathogenicity. *Journal of bacteriology* **196,** 345–356 (2014).
20. Feklístov, A., Sharon, B. D., Darst, S. A. & Gross, C. A. Bacterial sigma factors: a historical, structural, and genomic perspective. *Annual review of microbiology* **68,** 357–376 (2014).
21. Imhoff, J. F., Trüper, H. G. & Pfennig, N. Rearrangement of the species and genera of the phototrophic "Purple Nonsulfur Bacteria". *International Journal of Systematic Bacteriology* **34,** 340–343 (1984).
22. van Niel, C. B. The culture, general physiology, morphology, and classification of the non-sulfur purple and brown bacteria. *Bacteriological Reviews* **8,** 1–118 (1944).
23. Hördt, A. *et al.* Analysis of 1,000+ type-strain genomes substantially improves taxonomic classification of *Alphaproteobacteria*. *Frontiers in microbiology* **11,** 468 (2020).
24. Kiley, P. J. & Kaplan, S. Molecular genetics of photosynthetic membrane biosynthesis in *Rhodobacter sphaeroides*. *Microbiological Reviews* **52,** 50–69 (1988).
25. Klug, G. Regulation of expression of photosynthesis genes in anoxygenic photosynthetic bacteria. *Archives of microbiology* **159,** 397–404 (1993).
26. Zeilstra-Ryalls, J. H., Gomelsky, M., Yeliseev, A. A., Eraso, J. M. & Kaplan, S. Transcriptional regulation of photosynthesis operons in *Rhodobacter sphaeroides* 2.4.1. *Methods in enzymology* **297,** 151–166 (1998).
27. Mackenzie, C. *et al.* The home stretch, a first analysis of the nearly completed genome of *Rhodobacter sphaeroides* 2.4.1. *Photosynthesis research* **70,** 19–41 (2001).
28. Kim, E.-J., Lee, M.-K., Kim, M.-S. & Lee, J. K. Molecular hydrogen production by nitrogenase of *Rhodobacter sphaeroides* and by Fe-only hydrogenase of *Rhodospirillum rubrum*. *International Journal of Hydrogen Energy* **33,** 1516–1521 (2008).
29. Franchi, E. *et al.* Metabolically engineered *Rhodobacter sphaeroides* RV strains for improved biohydrogen photoproduction combined with disposal of food wastes. *Marine biotechnology* **6,** 552–565 (2004).
30. Arumugam, A., Sandhya, M. & Ponnusami, V. Biohydrogen and polyhydroxyalkanoate co-production by *Enterobacter aerogenes* and *Rhodobacter sphaeroides* from *Calophyllum inophyllum* oil cake. *Bioresource Technology* **164,** 170–176 (2014).
31. Li, S. *et al.* Electron uptake from solid electrodes promotes the more efficient conversion of CO_2 to polyhydroxybutyrate by using *Rhodobacter sphaeroides*. *Chemical Engineering Journal* **469,** 143785 (2023).
32. Sangkharak, K. & Prasertsan, P. Optimization of polyhydroxybutyrate production from a wild type and two mutant strains of *Rhodobacter sphaeroides* using statistical method. *Journal of Biotechnology* **132,** 331–340 (2007).
33. Sasaki, K. *et al.* Practical removal of radioactivity from sediment mud in a swimming pool in Fukushima, Japan by immobilized photosynthetic bacteria. *Bioscience, biotechnology, and biochemistry* **76,** 859–862 (2012).
34. Li, X., Peng, W., Jia, Y., Lu, L. & Fan, W. Bioremediation of lead contaminated soil with *Rhodobacter sphaeroides*. *Chemosphere* **156,** 228–235 (2016).
35. Bai, H.-J., Zhang, Z.-M., Yang, G.-E. & Li, B.-Z. Bioremediation of cadmium by growing *Rhodobacter sphaeroides*: kinetic characteristic and mechanism studies. *Bioresource Technology* **99,** 7716–7722 (2008).
36. Alber, B. E. Biotechnological potential of the ethylmalonyl-CoA pathway. *Applied microbiology and biotechnology* **89,** 17–25 (2011).
37. Erb, T. J. *et al.* Synthesis of C_5-dicarboxylic acids from C_2-units involving crotonyl-CoA carboxylase/reductase: the ethylmalonyl-CoA pathway. *Proceedings of the National Academy of Sciences of the United States of America* **104,** 10631–10636 (2007).
38. McLean, R. *et al.* Exploring alternative pathways for the *in vitro* establishment of the HOPAC cycle for synthetic CO_2 fixation. *Science advances* **9,** eadh4299 (2023).
39. Beems, E. M. *et al.* Photosensitizing properties of bacteriochlorophyllin a and bacteriochlorin a, two derivatives of bacteriochlorophyll a. *Photochemistry and photobiology* **46,** 639–643 (1987).
40. Borland, C. F., McGarvey, D. J., Truscott, T. G., Codgell, R. J. & Land, E. J. Photophysical studies of bacteriochlorophyll a and bacteriopheophytin a — singlet oxygen generation. *Journal of Photochemistry and Photobiology B: Biology* **1,** 93–101 (1987).
41. Chandler, D. E., Hsin, J., Harrison, C. B., Gumbart, J. & Schulten, K. Intrinsic curvature properties of photosynthetic proteins in chromatophores. *Biophysical journal* **95,** 2822–2836 (2008).
42. Eraso, J. M. & Kaplan, S. *prrA*, a putative response regulator involved in oxygen regulation of photosynthesis gene expression in *Rhodobacter sphaeroides*. *Journal of bacteriology* **176,** 32–43 (1994).
43. Oh, J. I. & Kaplan, S. Generalized approach to the regulation and integration of gene expression. *Molecular microbiology* **39,** 1116–1123 (2001).
44. Oh, J.-I., Ko, I.-J. & Kaplan, S. Reconstitution of the *Rhodobacter sphaeroides* cbb_3-PrrBA signal transduction pathway *in vitro*. *Biochemistry* **43,** 7915–7923 (2004).
45. Oh, J. I., Ko, I. J. & Kaplan, S. The default state of the membrane-localized histidine kinase PrrB of *Rhodobacter sphaeroides* 2.4.1 is in the kinase-positive mode. *Journal of bacteriology* **183,** 6807–6814 (2001).
46. Laguri, C., Stenzel, R. A., Donohue, T. J., Phillips-Jones, M. K. & Williamson, M. P. Activation of the global gene regulator PrrA (RegA) from *Rhodobacter sphaeroides*. *Biochemistry* **45,** 7872–7881 (2006).
47. Laguri, C., Phillips-Jones, M. K. & Williamson, M. P. Solution structure and DNA binding of the effector domain from the global regulator PrrA (RegA) from *Rhodobacter sphaeroides*: insights into DNA binding specificity. *Nucleic Acids Research* **31,** 6778–6787 (2003).
48. Eraso, J. M. & Kaplan, S. Complex regulatory activities associated with the histidine kinase PrrB in expression of photosynthesis genes in *Rhodobacter*

sphaeroides 2.4.1. *Journal of bacteriology* **178,** 7037–7046 (1996).
49. Gomelsky, M. & Kaplan, S. Genetic evidence that PpsR from *Rhodobacter sphaeroides* 2.4.1 functions as a repressor of *puc* and *bchF* expression. *Journal of bacteriology* **177,** 1634–1637 (1995).
50. Penfold, R. J. & Pemberton, J. M. Sequencing, chromosomal inactivation, and functional expression in *Escherichia coli* of *ppsR*, a gene which represses carotenoid and bacteriochlorophyll synthesis in *Rhodobacter sphaeroides*. *Journal of bacteriology* **176,** 2869–2876 (1994).
51. Zeng, X., Choudhary, M. & Kaplan, S. A second and unusual *pucBA* operon of *Rhodobacter sphaeroides* 2.4.1: genetics and function of the encoded polypeptides. *Journal of bacteriology* **185,** 6171–6184 (2003).
52. Masuda, S. & Bauer, C. E. AppA is a blue light photoreceptor that antirepresses photosynthesis gene expression in *Rhodobacter sphaeroides*. *Cell* **110,** 613–623 (2002).
53. Gomelsky, M. *et al.* Domain structure, oligomeric state, and mutational analysis of PpsR, the *Rhodobacter sphaeroides* repressor of photosystem gene expression. *Journal of bacteriology* **182,** 2253–2261 (2000).
54. Gomelsky, M. & Klug, G. BLUF: a novel FAD-binding domain involved in sensory transduction in microorganisms. *Trends in biochemical sciences* **27,** 497–500 (2002).
55. Gomelsky, M. & Kaplan, S. AppA, a redox regulator of photosystem formation in *Rhodobacter sphaeroides* 2.4.1, is a flavoprotein. Identification of a novel FAD binding domain. *The Journal of biological chemistry* **273,** 35319–35325 (1998).
56. Braatsch, S., Gomelsky, M., Kuphal, S. & Klug, G. A single flavoprotein, AppA, integrates both redox and light signals in *Rhodobacter sphaeroides*. *Molecular microbiology* **45,** 827–836 (2002).
57. Jung, A., Reinstein, J., Domratcheva, T., Shoeman, R. L. & Schlichting, I. Crystal structures of the AppA BLUF domain photoreceptor provide insights into blue light-mediated signal transduction. *Journal of molecular biology* **362,** 717–732 (2006).
58. Anderson, S. *et al.* Structure of a novel photoreceptor, the BLUF domain of AppA from *Rhodobacter sphaeroides*. *Biochemistry* **44,** 7998–8005 (2005).
59. Dragnea, V., Waegele, M., Balascuta, S., Bauer, C. & Dragnea, B. Time-resolved spectroscopic studies of the AppA blue-light receptor BLUF domain from *Rhodobacter sphaeroides*. *Biochemistry* **44,** 15978–15985 (2005).
60. Han, Y., Braatsch, S., Osterloh, L. & Klug, G. A eukaryotic BLUF domain mediates light-dependent gene expression in the purple bacterium *Rhodobacter sphaeroides* 2.4.1. *Proceedings of the National Academy of Sciences of the United States of America* **101,** 12306–12311 (2004).
61. Gomelsky, M. & Kaplan, S. Molecular genetic analysis suggesting interactions between AppA and PpsR in regulation of photosynthesis gene expression in *Rhodobacter sphaeroides* 2.4.1. *Journal of bacteriology* **179,** 128–134 (1997).
62. Moskvin, O. V., Kaplan, S., Gilles-Gonzalez, M.-A. & Gomelsky, M. Novel heme-based oxygen sensor with a revealing evolutionary history. *The Journal of biological chemistry* **282,** 28740–28748 (2007).
63. Han, Y., Meyer, M. H. F., Keusgen, M. & Klug, G. A haem cofactor is required for redox and light signalling by the AppA protein of *Rhodobacter sphaeroides*. *Molecular microbiology* **64,** 1090–1104 (2007).
64. Jäger, A. *et al.* The AppA and PpsR proteins from *Rhodobacter sphaeroides* can establish a redox-dependent signal chain but fail to transmit blue-light signals in other bacteria. *Journal of bacteriology* **189,** 2274–2282 (2007).
65. Eiglmeier, K., Honoré, N., Iuchi, S., Lin, E. C. & Cole, S. T. Molecular genetic analysis of FNR-dependent promoters. *Molecular microbiology* **3,** 869–878 (1989).
66. Fleischhacker, A. S. & Kiley, P. J. Iron-containing transcription factors and their roles as sensors. *Current opinion in chemical biology* **15,** 335–341 (2011).
67. Beinert, H., Holm, R. H. & Münck, E. Iron-sulfur clusters: nature's modular, multipurpose structures. *Science* **277,** 653–659 (1997).
68. Johnson, D. C., Dean, D. R., Smith, A. D. & Johnson, M. K. Structure, function, and formation of biological iron-sulfur clusters. *Annual review of biochemistry* **74,** 247–281 (2005).
69. Lill, R. Function and biogenesis of iron-sulphur proteins. *Nature* **460,** 831–838 (2009).
70. Khoroshilova, N., Popescu, C., Münck, E., Beinert, H. & Kiley, P. J. Iron-sulfur cluster disassembly in the FNR protein of *Escherichia coli* by O_2: [4Fe-4S] to [2Fe-2S] conversion with loss of biological activity. *Proceedings of the National Academy of Sciences of the United States of America* **94,** 6087–6092 (1997).
71. Lazazzera, B. A., Beinert, H., Khoroshilova, N., Kennedy, M. C. & Kiley, P. J. DNA binding and dimerization of the Fe-S-containing FNR protein from *Escherichia coli* are regulated by oxygen. *Journal of Biological Chemistry* **271,** 2762–2768 (1996).
72. Zeilstra-Ryalls, J. H. & Kaplan, S. Aerobic and anaerobic regulation in *Rhodobacter sphaeroides* 2.4.1: the role of the *fnrL* gene. *Journal of bacteriology* **177,** 6422–6431 (1995).
73. Imam, S., Noguera, D. R. & Donohue, T. J. Global analysis of photosynthesis transcriptional regulatory networks. *PLoS genetics* **10,** e1004837 (2014).
74. Kumka, J. E. & Bauer, C. E. Analysis of the FnrL regulon in *Rhodobacter capsulatus* reveals limited regulon overlap with orthologues from *Rhodobacter sphaeroides* and *Escherichia coli*. *BMC genomics* **16,** 895 (2015).
75. Oh, J. I., Eraso, J. M. & Kaplan, S. Interacting regulatory circuits involved in orderly control of photosynthesis gene expression in *Rhodobacter sphaeroides* 2.4.1. *Journal of bacteriology* **182,** 3081–3087 (2000).
76. Zeilstra-Ryalls, J. H., Gabbert, K., Mouncey, N. J., Kaplan, S. & Kranz, R. G. Analysis of the *fnrL* gene and its function in *Rhodobacter capsulatus*. *Journal of bacteriology* **179,** 7264–7273 (1997).
77. Mouncey, N. J. & Kaplan, S. Oxygen regulation of the *ccoN* gene encoding a component of the cbb_3 oxidase in *Rhodobacter sphaeroides* $2.4.1^T$: involvement of the

FnrL protein. *Journal of bacteriology* **180,** 2228–2231 (1998).
78. Jang, S. & Imlay, J. A. Micromolar intracellular hydrogen peroxide disrupts metabolism by damaging iron-sulfur enzymes. *Journal of Biological Chemistry* **282,** 929–937 (2007).
79. Imlay, J. A. Iron-sulphur clusters and the problem with oxygen. *Molecular microbiology* **59,** 1073–1082 (2006).
80. Khoroshilova, N., Beinert, H. & Kiley, P. J. Association of a polynuclear iron-sulfur center with a mutant FNR protein enhances DNA binding. *Proceedings of the National Academy of Sciences of the United States of America* **92,** 2499–2503 (1995).
81. Börner, J., Friedrich, T., Bartkuhn, M. & Klug, G. Ribonuclease E strongly impacts bacterial adaptation to different growth conditions. *RNA biology* **20,** 120–135 (2023).
82. Papenfort, K. & Melamed, S. Small RNAs, Large Networks: Posttranscriptional regulons in gram-negative bacteria. *Annual review of microbiology* **77,** 23–43 (2023).
83. Storz, G., Vogel, J. & Wassarman, K. M. Regulation by small RNAs in bacteria: expanding frontiers. *Molecular Cell* **43,** 880–891 (2011).
84. Wagner, E. G. H. & Romby, P. Chapter Three - Small RNAs in bacteria and archaea: Who they are, what they do, and how they do it. In *Advances in Genetics,* edited by T. Friedmann, J. C. Dunlap & S. F. Goodwin (Academic Press), Vol. 90, pp. 133–208 (2015).
85. Jørgensen, M. G., Pettersen, J. S. & Kallipolitis, B. H. sRNA-mediated control in bacteria: An increasing diversity of regulatory mechanisms. *Biochimica et biophysica acta. Gene regulatory mechanisms* **1863,** 194504 (2020).
86. Berghoff, B. A., Glaeser, J., Sharma, C. M., Vogel, J. & Klug, G. Photooxidative stress-induced and abundant small RNAs in *Rhodobacter sphaeroides*. *Molecular microbiology* **74,** 1497–1512 (2009).
87. Billenkamp, F., Peng, T., Berghoff, B. A. & Klug, G. A cluster of four homologous small RNAs modulates C_1 metabolism and the pyruvate dehydrogenase complex in *Rhodobacter sphaeroides* under various stress conditions. *Journal of bacteriology* **197,** 1839–1852 (2015).
88. Grützner, J. *et al.* The small DUF1127 protein CcaF1 from *Rhodobacter sphaeroides* is an RNA-binding protein involved in sRNA maturation and RNA turnover. *Nucleic Acids Research* **49,** 3003–3019 (2021).
89. Müller, K. M. H., Berghoff, B. A., Eisenhardt, B. D., Remes, B. & Klug, G. Characteristics of Pos19 - A small coding RNA in the oxidative stress response of *Rhodobacter sphaeroides*. *PloS one* **11,** e0163425 (2016).
90. Peng, T. *et al.* Regulation of a polyamine transporter by the conserved 3' UTR-derived sRNA SorX confers resistance to singlet oxygen and organic hydroperoxides in *Rhodobacter sphaeroides*. *RNA biology* **13,** 988–999 (2016).
91. Adnan, F., Weber, L. & Klug, G. The sRNA SorY confers resistance during photooxidative stress by affecting a metabolite transporter in *Rhodobacter sphaeroides*. *RNA biology* **12,** 569–577 (2015).
92. Eisenhardt, K. M. H. *et al.* A complex network of sigma factors and sRNA StsR regulates stress responses in *R. sphaeroides*. *International journal of molecular sciences* **22,** 7557 (2021).
93. Weber, L. *et al.* The conserved *dcw* gene cluster of *R. sphaeroides* is preceded by an uncommonly extended 5' leader featuring the sRNA UpsM. *PloS one* **11,** e0165694 (2016).
94. Grützner, J. *et al.* sRNA-mediated RNA processing regulates bacterial cell division. *Nucleic Acids Research* **49,** 7035–7052 (2021).
95. Mank, N. N., Berghoff, B. A., Hermanns, Y. N. & Klug, G. Regulation of bacterial photosynthesis genes by the small noncoding RNA PcrZ. *Proceedings of the National Academy of Sciences of the United States of America* **109,** 16306–16311 (2012).
96. Mank, N. N., Berghoff, B. A. & Klug, G. A mixed incoherent feed-forward loop contributes to the regulation of bacterial photosynthesis genes. *RNA biology* **10,** 347–352 (2013).
97. Klug, G., Adams, C. W., Belasco, J., Doerge, B. & Cohen, S. N. Biological consequences of segmental alterations in mRNA stability: effects of deletion of the intercistronic hairpin loop region of the *Rhodobacter capsulatus puf* operon. *The EMBO journal* **6,** 3515–3520 (1987).
98. Olsen, J. D. *et al.* Aberrant assembly complexes of the reaction center light-harvesting 1 PufX (RC-LH1-PufX) core complex of *Rhodobacter sphaeroides* imaged by atomic force microscopy. *Journal of Biological Chemistry* **289,** 29927–29936 (2014).
99. Donohue, T. J., Kiley, P. J. & Kaplan, S. The *puf* operon region of *Rhodobacter sphaeroides*. *Photosynthesis research* **19,** 39–61 (1988).
100. Eisenhardt, K. M. H., Reuscher, C. M. & Klug, G. PcrX, an sRNA derived from the 3'- UTR of the *Rhodobacter sphaeroides puf* operon modulates expression of *puf* genes encoding proteins of the bacterial photosynthetic apparatus. *Molecular microbiology* **110,** 325–334 (2018).
101. Reuscher, C. M. & Klug, G. Antisense RNA asPcrL regulates expression of photosynthesis genes in *Rhodobacter sphaeroides* by promoting RNase III-dependent turn-over of *puf* mRNA. *RNA biology* **18,** 1445–1457 (2021).
102. Klug, G. & Cohen, S. N. Combined actions of multiple hairpin loop structures and sites of rate-limiting endonucleolytic cleavage determine differential degradation rates of individual segments within polycistronic *puf* operon mRNA. *Journal of bacteriology* **172,** 5140–5146 (1990).
103. Belasco, J. G., Beatty, J. T., Adams, C. W., Gabain, A. von & Cohen, S. N. Differential expression of photosynthesis genes in *R. capsulata* results from segmental differences in stability within the polycistronic *rxcA* transcript. *Cell* **40,** 171–181 (1985).
104. Klug, G. The role of mRNA degradation in the regulated expression of bacterial photosynthesis genes. *Molecular microbiology* **9,** 1–7(1993).
105. Heck, C., Balzer, A., Fuhrmann, O. & Klug, G. Initial events in the degradation of the polycistronic *puf* mRNA in *Rhodobacter capsulatus* and consequences

for further processing steps. *Molecular microbiology* **35,** 90–100 (2000).
106. Fritsch, J., Rothfuchs, R., Rauhut, R. & Klug, G. Identification of an mRNA element promoting rate-limiting cleavage of the polycistronic *puf* mRNA in *Rhodobacter capsulatus* by an enzyme similar to RNase E. *Molecular microbiology* **15,** 1017–1029 (1995).
107. Belasco, J. G. *Control of RNA stability* (Academic Press) pp. 3-11 (1993).
108. Rauhut, R. & Klug, G. mRNA degradation in bacteria. *FEMS Microbiology Reviews* **23,** 353–370 (1999).
109. Kushner, S. R. mRNA decay in prokaryotes and eukaryotes: different approaches to a similar problem. *IUBMB life* **56,** 585–594 (2004).
110. Hui, M. P., Foley P. L. & Belasco J. G. Messenger RNA degradation in bacterial cells. *Annual Reviews of Genetics* **48,** 537-559 (2014).
111. Li, X. A. & Beebe, D. C. Messenger RNA stabilization in chicken lens development: a reexamination. *Developmental biology* **146,** 239–241 (1991).
112. Dozin, B., Quarto, R., Rossi, F. & Cancedda, R. Stabilization of the mRNA follows transcriptional activation of type II collagen gene in differentiating chicken chondrocyte. *Journal of Biological Chemistry* **265,** 7216–7220 (1990).
113. Ross, J. & Sullivan, T. D. Half-lives of beta and gamma globin messenger RNAs and of protein synthetic capacity in cultured human reticulocytes. *Blood* **66,** 1149–1154 (1985).
114. Aviv, H., Voloch, Z., Bastos, R. & Levy, S. Biosynthesis and stability of globin mRNA in cultured erythroleukemic Friend cells. *Cell* **8,** 495–503 (1976).
115. Morey, J. S. & van Dolah, F. M. Global analysis of mRNA half-lives and *de novo* transcription in a dinoflagellate, *Karenia brevis*. *PloS one* **8,** e66347 (2013).
116. Lin-Chao, S., Chiou, N.-T. & Schuster, G. The PNPase, exosome and RNA helicases as the building components of evolutionarily-conserved RNA degradation machines. *Journal of biomedical science* **14,** 523–532 (2007).
117. Grunberg-Manago, M., Oritz, P. J. & Ochoa, S. Enzymatic synthesis of nucleic acidlike polynucleotides. *Science* **122,** 907–910 (1955).
118. Grunberg-Manago, M., Oritz, P. J. & Ochoa, S. Enzymic synthesis of polynucleotides. I. Polynucleotide phosphorylase of *Azotobacter vinelandii*. *Biochimica et Biophysica Acta* **20,** 269–285 (1956).
119. Littauer, U. Z. & Soreq, H. 17 Polynucleotide Phosphorylase. In *Nucleic Acids Part B* (Elsevier), pp. 517–553 (1982).
120. Briani, F., Carzaniga, T. & Dehò, G. Regulation and functions of bacterial PNPase. *Wiley Interdisciplinary Reviews: RNA* **7,** 241–258 (2016).
121. Goverde, R. L., Huis in't Veld, J. H., Kusters, J. G. & Mooi, F. R. The psychrotrophic bacterium *Yersinia enterocolitica* requires expression of *pnp*, the gene for polynucleotide phosphorylase, for growth at low temperature (5°C). *Molecular microbiology* **28,** 555–569 (1998).
122. Henry, A., Shanks, J., van Hoof, A. & Rosenzweig, J. A. The *Yersinia pseudotuberculosis* degradosome is required for oxidative stress, while its PNPase subunit plays a degradosome-independent role in cold growth. *FEMS Microbiology Letters* **336,** 139–147 (2012).
123. Spanka, D.-T., Reuscher, C. M. & Klug, G. Impact of PNPase on the transcriptome of *Rhodobacter sphaeroides* and its cooperation with RNase III and RNase E. *BMC Genomics* **22,** 106 (2021).
124. Clements, M. O. *et al.* Polynucleotide phosphorylase is a global regulator of virulence and persistency in *Salmonella enterica*. *Proceedings of the National Academy of Sciences of the United States of America* **99,** 8784–8789 (2002).
125. Rosenzweig, J. A. & Chopra, A. K. The exoribonuclease polynucleotide phosphorylase influences the virulence and stress responses of yersiniae and many other pathogens. *Frontiers in cellular and infection microbiology* **3,** 81 (2013).
126. Chen, R. *et al.* Polynucleotide phosphorylase regulates multiple virulence factors and the stabilities of small RNAs RsmY/Z in *Pseudomonas aeruginosa*. *Frontiers in microbiology* **7,** 247 (2016).
127. Quendera, A. P. *et al.* The ribonuclease PNPase is a key regulator of biofilm formation in *Listeria monocytogenes* and affects invasion of host cells. *npj Biofilms Microbiomes* **9,** 34 (2023).
128. Pobre, V. & Arraiano, C. M. Next generation sequencing analysis reveals that the ribonucleases RNase II, RNase R and PNPase affect bacterial motility and biofilm formation in *E. coli*. *BMC Genomics* **16,** 72 (2015).
129. Palanisamy, S. K. A., Fletcher, C., Tanjung, L., Katz, M. E. & Cheetham, B. F. Deletion of the C-terminus of polynucleotide phosphorylase increases twitching motility, a virulence characteristic of the anaerobic bacterial pathogen *Dichelobacter nodosus*. *FEMS Microbiology Letters* **302,** 39–45 (2010).
130. Mian, I. S. Comparative sequence analysis of ribonucleases HII, III, II PH and D. *Nucleic Acids Research* **25,** 3187–3195 (1997).
131. Zuo, Y. & Deutscher, M. P. Exoribonuclease superfamilies: structural analysis and phylogenetic distribution. *Nucleic Acids Research* **29,** 1017–1026 (2001).
132. Arraiano, C. M. *et al.* The critical role of RNA processing and degradation in the control of gene expression. *FEMS Microbiolgy Reviews* **34,** 883–923 (2010).
133. Andrade, J. M., Pobre, V., Silva, I. J., Domingues, S. & Arraiano, C. M. The role of 3'-5' exoribonucleases in RNA degradation. *Progress in molecular biology and translational science* **85,** 187–229 (2009).
134. Vincent, H. A. & Deutscher, M. P. Substrate recognition and catalysis by the exoribonuclease RNase R. *The Journal of biological chemistry* **281,** 29769–29775 (2006).
135. Cheng, Z.-F. & Deutscher, M. P. Quality control of ribosomal RNA mediated by polynucleotide phosphorylase and RNase R. *Proceedings of the National Academy of Sciences of the United States of America* **100,** 6388–6393 (2003).
136. Richards, J., Mehta, P. & Karzai, A. W. RNase R degrades non-stop mRNAs selectively in an SmpB-tmRNA-dependent manner. *Molecular microbiology* **62,** 1700–1712 (2006).

137. Venkataraman, K., Zafar, H. & Karzai, A. W. Distinct tmRNA sequence elements facilitate RNase R engagement on rescued ribosomes for selective non-stop mRNA decay. *Nucleic Acids Research* **42,** 11192–11202 (2014).
138. Domingues, S. *et al.* The role of RNase R in trans-translation and ribosomal quality control. *Biochimie* **114,** 113–118 (2015).
139. Cheng, Z.-F. & Deutscher, M. P. An important role for RNase R in mRNA decay. *Molecular Cell* **17,** 313–318 (2005).
140. Cheng, Z.-F. & Deutscher, M. P. Purification and characterization of the *Escherichia coli* exoribonuclease RNase R. Comparison with RNase II. *Journal of Biological Chemistry* **277,** 21624–21629 (2002).
141. Andrade, J. M., Hajnsdorf, E., Régnier, P. & Arraiano, C. M. The poly(A)-dependent degradation pathway of *rpsO* mRNA is primarily mediated by RNase R. *RNA* **15,** 316–326 (2009).
142. Dreyfus, M. & Régnier, P. The poly(A) tail of mRNAs: bodyguard in eukaryotes, scavenger in bacteria. *Cell* **111,** 611–613 (2002).
143. Cannistraro, V. J. & Kennell, D. The reaction mechanism of ribonuclease II and its interaction with nucleic acid secondary structures. *Biochimica et Biophysica Acta* **1433,** 170–187 (1999).
144. Spickler, C. & Mackie, G. A. Action of RNase II and polynucleotide phosphorylase against RNAs containing stem-loops of defined structure. *Journal of bacteriology* **182,** 2422–2427 (2000).
145. Martin, G. & Keller, W. Sequence motifs that distinguish ATP(CTP):tRNA nucleotidyl transferases from eubacterial poly(A) polymerases. *RNA* **10,** 899–906 (2004).
146. Mohanty, B. K. & Kushner, S. R. Polynucleotide phosphorylase, RNase II and RNase E play different roles in the *in vivo* modulation of polyadenylation in *Escherichia coli*. *Molecular microbiology* **36,** 982–994 (2000).
147. Marujo, P. E. *et al.* RNase II removes the oligo(A) tails that destabilize the *rpsO* mRNA of *Escherichia coli*. *RNA* **6,** 1185–1193 (2000).
148. Folichon, M. *et al.* Fate of mRNA extremities generated by intrinsic termination: detailed analysis of reactions catalyzed by ribonuclease II and poly(A) polymerase. *Biochimie* **87,** 819–826 (2005).
149. Ghosh, S. & Deutscher, M. P. Oligoribonuclease is an essential component of the mRNA decay pathway. *Proceedings of the National Academy of Sciences of the United States of America* **96,** 4372–4377 (1999).
150. Lee, V. T., Sondermann, H. & Winkler, W. C. Nano-RNases: oligo- or dinucleases? *FEMS Microbiology Reviews* **46** (2022).
151. La Li de Sierra-Gallay, I., Zig, L., Jamalli, A. & Putzer, H. Structural insights into the dual activity of RNase J. *Nature structural & molecular biology* **15,** 206–212 (2008).
152. Mathy, N. *et al.* 5'-to-3' exoribonuclease activity in bacteria: role of RNase J1 in rRNA maturation and 5' stability of mRNA. *Cell* **129,** 681–692 (2007).
153. Hasenöhrl, D., Konrat, R. & Bläsi, U. Identification of an RNase J ortholog in *Sulfolobus solfataricus*: implications for 5'-to-3' directional decay and 5'-end protection of mRNA in Crenarchaeota. *RNA* **17,** 99–107 (2011).
154. Richards, J. *et al.* An RNA pyrophosphohydrolase triggers 5'-exonucleolytic degradation of mRNA in *Bacillus subtilis*. *Molecular cell* **43,** 940–949 (2011).
155. Rische, T. & Klug, G. The ordered processing of intervening sequences in 23S rRNA of *Rhodobacter sphaeroides* requires RNase J. *RNA biology* **9,** 343–350 (2012).
156. Rische-Grahl, T., Weber, L., Remes, B., Förstner, K. U. & Klug, G. RNase J is required for processing of a small number of RNAs in *Rhodobacter sphaeroides*. *RNA biology* **11,** 855–864 (2014).
157. Apirion, D. & Lassar, A. B. A conditional lethal mutant of *Escherichia coli* which affects the processing of ribosomal RNA. *Journal of Biological Chemistry* **253,** 1738–1742 (1978).
158. Ono, M. & Kuwano, M. A conditional lethal mutation in an *Escherichia coli* strain with a longer chemical lifetime of messenger RNA. *Journal of molecular biology* **129,** 343–357 (1979).
159. Callaghan, A. J. *et al.* Studies of the RNA degradosome-organizing domain of the *Escherichia coli* ribonuclease RNase E. *Journal of molecular biology* **340,** 965–979; 10.1016/j.jmb.2004.05.046 (2004).
160. Kaberdin, V. R. *et al.* The endoribonucleolytic N-terminal half of *Escherichia coli* RNase E is evolutionarily conserved in *Synechocystis* sp. and other bacteria but not the C-terminal half, which is sufficient for degradosome assembly. *Proceedings of the National Academy of Sciences of the United States of America* **95,** 11637–11642 (1998).
161. Mackie, G. A. RNase E: at the interface of bacterial RNA processing and decay. *Nature reviews. Microbiology* **11,** 45–57 (2013).
162. Leroy, A., Vanzo, N. F., Sousa, S., Dreyfus, M. & Carpousis, A. J. Function in *Escherichia coli* of the non-catalytic part of RNase E: role in the degradation of ribosome-free mRNA. *Molecular microbiology* **45,** 1231–1243 (2002).
163. Taraseviciene, L., Björk, G. R. & Uhlin, B. E. Evidence for an RNA binding region in the *Escherichia coli* processing endoribonuclease RNase E. *Journal of Biological Chemistry* **270,** 26391–26398 (1995).
164. Prud'homme-Généreux, A. *et al.* Physical and functional interactions among RNase E, polynucleotide phosphorylase and the cold-shock protein, CsdA: evidence for a 'cold shock degradosome'. *Molecular microbiology* **54,** 1409–1421 (2004).
165. Jäger, S., Hebermehl, M., Schiltz, E. & Klug, G. Composition and activity of the *Rhodobacter capsulatus* degradosome vary under different oxygen concentrations. *Journal of molecular microbiology and biotechnology* **7,** 148–154 (2004).
166. Hardwick, S. W., Chan, V. S. Y., Broadhurst, R. W. & Luisi, B. F. An RNA degradosome assembly in *Caulobacter crescentus*. *Nucleic Acids Research* **39,** 1449–1459 (2011).
167. Jäger, S. *et al.* An mRNA degrading complex in *Rhodobacter capsulatus*. *Nucleic Acids Research* **29,** 4581–4588 (2001).

168. Bandyra, K. J., Bouvier, M., Carpousis, A. J. & Luisi, B. F. The social fabric of the RNA degradosome. *Biochimica et Biophysica Acta* **1829,** 514–522 (2013).
169. Mudd, E. A., Krisch, H. M. & Higgins, C. F. RNase E, an endoribonuclease, has a general role in the chemical decay of *Escherichia coli* mRNA: evidence that *rne* and *ams* are the same genetic locus. *Molecular microbiology* **4,** 2127–2135 (1990).
170. Ow, M. C., Liu, Q. & Kushner, S. R. Analysis of mRNA decay and rRNA processing in *Escherichia coli* in the absence of RNase E-based degradosome assembly. *Molecular microbiology* **38,** 854–866 (2000).
171. Cam, K., Rome, G., Krisch, H. M. & Bouché, J. P. RNase E processing of essential cell division genes mRNA in *Escherichia coli*. *Nucleic Acids Res* **24,** 3065–3070 (1996).
172. Naureckiene, S. & Uhlin, B. E. *In vitro* analysis of mRNA processing by RNase E in the *pap* operon of *Escherichia coli*. *Molecular microbiology* **21,** 55–68 (1996).
173. Klug, G., Jock, S. & Rothfuchs, R. The rate of decay of *Rhodobacter capsulatus*-specific *puf* mRNA segments is differentially affected by RNase E activity in *Escherichia coli*. *Gene* **121,** 95–102 (1992).
174. Davis, B. M. & Waldor, M. K. RNase E-dependent processing stabilizes MicX, a *Vibrio cholerae* sRNA. *Molecular microbiology* **65,** 373–385 (2007).
175. Sinha, D. & Lay, N. R. de. Target recognition by RNase E RNA-binding domain AR2 drives sRNA decay in the absence of PNPase. *Proceedings of the National Academy of Sciences of the United States of America* **119,** e2208022119 (2022).
176. Ow, M. C. & Kushner, S. R. Initiation of tRNA maturation by RNase E is essential for cell viability *in E. coli*. *Genes & development* **16,** 1102–1115 (2002).
177. Mohanty, B. K., Petree, J. R. & Kushner, S. R. Endonucleolytic cleavages by RNase E generate the mature 3' termini of the three proline tRNAs in *Escherichia coli*. *Nucleic Acids Research* **44,** 6350–6362 (2016).
178. Li, Z. & Deutscher, M. P. RNase E plays an essential role in the maturation of *Escherichia coli* tRNA precursors. *RNA* **8,** 97–109 (2002).
179. Li, Z., Pandit, S. & Deutscher, M. P. RNase G (CafA protein) and RNase E are both required for the 5' maturation of 16S ribosomal RNA. *The EMBO journal* **18,** 2878–2885 (1999).
180. Klein, F. & Evguenieva-Hackenberg, E. RNase E is involved in 5'-end 23S rRNA processing in α-proteobacteria. *Biochemical and Biophysical Research Communications* **299,** 780–786 (2002).
181. Laalami, S., Cavaiuolo, M., Roque, S., Chagneau, C. & Putzer, H. *Escherichia coli* RNase E can efficiently replace RNase Y in *Bacillus subtilis*. *Nucleic Acids Research* **49,** 4643–4654 (2021).
182. Khemici, V., Poljak, L., Luisi, B. F. & Carpousis, A. J. The RNase E of *Escherichia coli* is a membrane-binding protein. *Molecular microbiology* **70,** 799–813 (2008).
183. Hadjeras, L. *et al.* Detachment of the RNA degradosome from the inner membrane of *Escherichia coli* results in a global slowdown of mRNA degradation, proteolysis of RNase E and increased turnover of ribosome-free transcripts. *Molecular microbiology* **111,** 1715–1731 (2019).
184. Carpousis, A. J., Campo, N., Hadjeras, L. & Hamouche, L. Compartmentalization of RNA degradosomes in bacteria controls accessibility to substrates and ensures concerted degradation of mRNA to nucleotides. *Annual review of microbiology* **76,** 533–552 (2022).
185. Aït-Bara, S. & Carpousis, A. J. RNA degradosomes in bacteria and chloroplasts: classification, distribution and evolution of RNase E homologs. *Molecular microbiology* **97,** 1021–1135 (2015).
186. Ortiz-Rodriguez, L. A., Azaldegui, C. A., Schrader, J. & Biteen, J. Dynamics of bacterial ribonucleoprotein bodies probed by single-molecule fluorescence imaging of RNase E. *Biophysical journal* **122,** 158a (2023).
187. Muthunayake, N. S., Tomares, D. T., Childers, W. S. & Schrader, J. M. Phase-separated bacterial ribonucleoprotein bodies organize mRNA decay. *Wiley Interdisciplinary Reviews: RNA* **11,** e1599 (2020).
188. Al-Husini, N. *et al.* BR-Bodies provide selectively permeable condensates that stimulate mRNA decay and prevent release of decay intermediates. *Molecular cell* **78,** 670-682 (2020).
189. Al-Husini, N., Tomares, D. T., Bitar, O., Childers, W. S. & Schrader, J. M. α-proteobacterial RNA degradosomes assemble liquid-liquid phase-separated RNP bodies. *Molecular cell* **71,** 1027-1039 (2018).
190. Collins, M. J., Tomares, D. T., Nandana, V., Schrader, J. M. & Childers, W. S. RNase E biomolecular condensates stimulate PNPase activity. *Scientific reports* **13,** 12937 (2023).
191. Bayas, C. A. *et al.* Spatial organization and dynamics of RNase E and ribosomes in *Caulobacter crescentus*. *Proceedings of the National Academy of Sciences of the United States of America* **115,** e3712-e3721(2018).
192. McDowall, K. J., Lin-Chao, S. & Cohen, S. N. A+U content rather than a particular nucleotide order determines the specificity of RNase E cleavage. *Journal of Biological Chemistry* **269,** 10790–10796 (1994).
193. Lin-Chao, S., Wong, T. T., McDowall, K. J. & Cohen, S. N. Effects of nucleotide sequence on the specificity of *rne*-dependent and RNase E-mediated cleavages of RNA I encoded by the pBR322 plasmid. *Journal of Biological Chemistry* **269,** 10797–10803 (1994).
194. Mackie, G. A. Ribonuclease E is a 5'-end-dependent endonuclease. *Nature* **395,** 720–723 (1998).
195. Lee, C.-R., Kim, M., Park, Y.-H., Kim, Y.-R. & Seok, Y.-J. RppH-dependent pyrophosphohydrolysis of mRNAs is regulated by direct interaction with DapF in *Escherichia coli*. *Nucleic Acids Research* **42,** 12746–12757 (2014).
196. Deana, A., Celesnik, H. & Belasco, J. G. The bacterial enzyme RppH triggers messenger RNA degradation by 5' pyrophosphate removal. *Nature* **451,** 355–358 (2008).
197. Bandyra, K. J., Wandzik, J. M. & Luisi, B. F. Substrate recognition and autoinhibition in the central ribonuclease RNase E. *Molecular cell* **72,** 275-285 (2018).
198. Islam, M. S., Bandyra, K. J., Chao, Y., Vogel, J. & Luisi, B. F. RNase E endonuclease activity and its

inhibition by pseudoridine. *bioRxiv* (Nov., 2023); preprint, not peer-reviewed, doi: 10.1101/2021.05.23.445298 (2021).
199. Callaghan, A. J. *et al.* Structure of *Escherichia coli* RNase E catalytic domain and implications for RNA turnover. *Nature* **437,** 1187–1191 (2005).
200. Garrey, S. M. *et al.* Substrate binding and active site residues in RNases E and G: role of the 5'-sensor. *Journal of Biological Chemistry* **284,** 31843–31850 (2009).
201. Wang, Z., Gerstein, M. & Snyder, M. RNA-Seq: a revolutionary tool for transcriptomics. *Nature reviews. Genetics* **10,** 57–63 (2009).
202. Conesa, A. *et al.* A survey of best practices for RNA-seq data analysis. *Genome biology* **17,** 13 (2016).
203. DeRisi, J. *et al.* Use of a cDNA microarray to analyse gene expression patterns in human cancer. *Nature Genetics* **14,** 457–460 (1996).
204. Chao, Y. *et al. In vivo* cleavage map illuminates the central role of RNase E in coding and non-coding RNA pathways. *Molecular cell* **65,** 39–51 (2017).
205. Clarke, J. E., Kime, L., Romero A, D. & McDowall, K. J. Direct entry by RNase E is a major pathway for the degradation and processing of RNA in *Escherichia coli*. *Nucleic Acids Research* **42,** 11733–11751 (2014).
206. Förstner, K. U., Reuscher, C. M., Haberzettl, K., Weber, L. & Klug, G. RNase E cleavage shapes the transcriptome of *Rhodobacter sphaeroides* and strongly impacts phototrophic growth. *Life science alliance* **1,** e201800080 (2018).
207. Hoyos, M., Huber, M., Förstner, K. U. & Papenfort, K. Gene autoregulation by 3' UTR-derived bacterial small RNAs. *eLife* **9,** e58836 (2020).
208. Hoffmann, U. A. *et al.* Transcriptome-wide *in vivo* mapping of cleavage sites for the compact cyanobacterial ribonuclease E reveals insights into its function and substrate recognition. *Nucleic Acids Research* **49,** 13075–13091 (2021).
209. Deutscher, M. P. & Li, Z. Exoribonucleases and their multiple roles in RNA metabolism. In *Progress in Nucleic Acid Research and Molecular Biology* (Academic Press), Vol. 66, pp. 67–105 (2000).
210. Deutscher, M. P. How bacterial cells keep ribonucleases under control. *FEMS Microbiology Reviews* **39,** 350–361 (2015).
211. Stickney, L. M., Hankins, J. S., Miao, X. & Mackie, G. A. Function of the conserved S1 and KH domains in polynucleotide phosphorylase. *Journal of bacteriology* **187,** 7214–7221 (2005).
212. Hardwick, S. W., Gubbey, T., Hug, I., Jenal, U. & Luisi, B. F. Crystal structure of *Caulobacter crescentus* polynucleotide phosphorylase reveals a mechanism of RNA substrate channelling and RNA degradosome assembly. *Open biology* **2,** 120028 (2012).
213. Lee, K. *et al.* RraA: A protein inhibitor of RNase E activity that globally modulates RNA abundance in *E. coli*. *Cell* **114,** 623–634 (2003).
214. Górna, M. W. *et al.* The regulatory protein RraA modulates RNA-binding and helicase activities of the *E. coli* RNA degradosome. *RNA* **16,** 553–562 (2010).
215. Gao, J. *et al.* Differential modulation of *E. coli* mRNA abundance by inhibitory proteins that alter the composition of the degradosome. *Molecular microbiology* **61,** 394–406 (2006).
216. Yeom, J.-H. *et al.* Inhibitory effects of RraA and RraB on RNAse E-related enzymes imply conserved functions in the regulated enzymatic cleavage of RNA. *FEMS Microbiology Letters* **285,** 10–15 (2008).
217. Göpel, Y., Papenfort, K., Reichenbach, B., Vogel, J. & Görke, B. Targeted decay of a regulatory small RNA by an adaptor protein for RNase E and counteraction by an anti-adaptor RNA. *Genes & development* **27,** 552–564 (2013).
218. Durica-Mitic, S., Göpel, Y., Amman, F. & Görke, B. Adaptor protein RapZ activates endoribonuclease RNase E by protein-protein interaction to cleave a small regulatory RNA. *RNA* **26,** 1198–1215 (2020).
219. Kalamorz, F., Reichenbach, B., März, W., Rak, B. & Görke, B. Feedback control of glucosamine-6-phosphate synthase GlmS expression depends on the small RNA GlmZ and involves the novel protein YhbJ in *Escherichia coli*. *Molecular microbiology* **65,** 1518–1533 (2007).
220. Göpel, Y., Khan, M. A. & Görke, B. Domain swapping between homologous bacterial small RNAs dissects processing and Hfq binding determinants and uncovers an aptamer for conditional RNase E cleavage. *Nucleic Acids Research* **44,** 824–837 (2016).
221. Robertson, H. D., Webster, R. E. & Zinder, N. D. A nuclease specific for double-stranded RNA. *Virology* **32,** 718–719 (1967).
222. Robertson, H. D., Webster, R. E. & Zinder, N. D. Purification and properties of ribonuclease III from *Escherichia coli*. *Journal of Biological Chemistry* **243,** 82–91 (1968).
223. Westphal, H. & Crouch, R. J. Cleavage of adenovirus messenger RNA and of 28S and 18S ribosomal RNA by RNase III. *Proceedings of the National Academy of Sciences of the United States of America* **72,** 3077–3081 (1975).
224. Nikolaev, N., Silengo, L. & Schlessinger, D. Synthesis of a large precursor to ribosomal RNA in a mutant of *Escherichia coli*. *Proceedings of the National Academy of Sciences of the United States of America* **70,** 3361–3365 (1973).
225. Dunn, J. J. & Studier, F. W. T7 early RNAs and *Escherichia coli* ribosomal RNAs are cut from large precursor RNAs *in vivo* by ribonuclease 3. *Proceedings of the National Academy of Sciences of the United States of America* **70,** 3296–3300 (1973).
226. King, T. C., Sirdeshmukh, R. & Schlessinger, D. RNase III cleavage is obligate for maturation but not for function of *Escherichia coli* pre-23S rRNA. *Proceedings of the National Academy of Sciences of the United States of America* **81,** 185–188 (1984).
227. Evguenieva-Hackenberg, E. & Klug, G. RNase III processing of intervening sequences found in helix 9 of 23S rRNA in the alpha subclass of *Proteobacteria*. *Journal of bacteriology* **182,** 4719–4729 (2000).
228. Kordes, E., Jock, S., Fritsch, J., Bosch, F. & Klug, G. Cloning of a gene involved in rRNA precursor processing and 23S rRNA cleavage in *Rhodobacter capsulatus*. *Journal of bacteriology* **176,** 1121–1127 (1994).

229. Blaszczyk, J. *et al.* Crystallographic and modeling studies of RNase III suggest a mechanism for double-stranded RNA cleavage. *Structure* **9,** 1225–1236 (2001).
230. Cerutti, H. & Casas-Mollano, J. A. On the origin and functions of RNA-mediated silencing: from protists to man. *Current genetics* **50,** 81–99 (2006).
231. Lejars, M., Kobayashi, A. & Hajnsdorf, E. RNase III, ribosome biogenesis and beyond. *Microorganisms* **9,** 2608 (2021).
232. Nicholson, A. W. Function, mechanism and regulation of bacterial ribonucleases. *FEMS Microbiology Reviews* **23,** 371–390 (1999).
233. Court, D. L. *et al.* RNase III: Genetics and function; structure and mechanism. *Annual review of genetics* **47,** 405–431 (2013).
234. Apirion, D. & Watson, N. Mapping and characterization of a mutation in *Escherichia coli* that reduces the level of ribonuclease III specific for double-stranded ribonucleic acid. *Journal of bacteriology* **124,** 317–324 (1975).
235. Dasgupta, S. *et al.* Genetic uncoupling of the dsRNA-binding and RNA cleavage activities of the *Escherichia coli* endoribonuclease RNase III—the effect of dsRNA binding on gene expression. *Molecular microbiology* **28,** 629–640 (1998).
236. Kindler, P., Keil, T. U. & Hofschneider, P. H. Isolation and characterization of a ribonuclease 3 deficient mutant of *Escherichia coli*. *Molecular & general genetics : MGG* **126,** 53–59 (1973).
237. Nashimoto, H. & Uchida, H. DNA sequencing of the *Escherichia coli* ribonuclease III gene and its mutations. *Molecular & general genetics : MGG* **201,** 25–29 (1985).
238. Weeks, R. & Ostermeier, M. Fitness and functional landscapes of the *E. coli* RNase III gene *rnc*. *Molecular biology and evolution* **40,** msad047 (2022).
239. MacRae, I. J. & Doudna, J. A. Ribonuclease revisited: structural insights into ribonuclease III family enzymes. *Current Opinion in Structural Biology* **17,** 138–145 (2007).
240. Maxwell, E. K., Ryan, J. F., Schnitzler, C. E., Browne, W. E. & Baxevanis, A. D. MicroRNAs and essential components of the microRNA processing machinery are not encoded in the genome of the ctenophore *Mnemiopsis leidyi*. *BMC Genomics* **13,** 714 (2012).
241. Stead, M. B. *et al.* Analysis of *Escherichia coli* RNase E and RNase III activity *in vivo* using tiling microarrays. *Nucleic Acids Research* **39,** 3188–3203 (2011).
242. Durand, S., Gilet, L., Bessières, P., Nicolas, P. & Condon, C. Three essential ribonucleases-RNase Y, J1, and III-control the abundance of a majority of *Bacillus subtilis* mRNAs. *PLoS genetics* **8,** e1002520 (2012).
243. Herskovitz, M. A. & Bechhofer, D. H. Endoribonuclease RNase III is essential in *Bacillus subtilis*. *Molecular microbiology* **38,** 1027–1033 (2000).
244. Durand, S., Gilet, L. & Condon, C. The essential function of *B. subtilis* RNase III is to silence foreign toxin genes. *PLoS genetics* **8,** e1003181 (2012).
245. Reif, C., Löser, C. & Brantl, S. *Bacillus subtilis* type I antitoxin SR6 promotes degradation of toxin *yonT* mRNA and is required to prevent toxic *yoyJ* overexpression. *Toxins* **10,** 74 (2018).
246. Vogel, J., Argaman, L., Wagner, E. G. H. & Altuvia, S. The small RNA IstR inhibits synthesis of an SOS-induced toxic peptide. *Current Biology* **14,** 2271–2276 (2004).
247. Gerdes, K., Nielsen, A., Thorsted, P. & Wagner, E. G. Mechanism of killer gene activation. Antisense RNA-dependent RNase III cleavage ensures rapid turnover of the stable *hok*, *srnB* and *pndA* effector messenger RNAs. *Journal of molecular biology* **226,** 637–649 (1992).
248. Mejía-Almonte, C. *et al.* Redefining fundamental concepts of transcription initiation in bacteria. *Nature reviews. Genetics* **21,** 699–714 (2020).
249. Wade, J. T. & Grainger, D. C. Pervasive transcription: illuminating the dark matter of bacterial transcriptomes. *Nature reviews. Microbiology* **12,** 647–653 (2014).
250. Toledo-Arana, A. & Lasa, I. Advances in bacterial transcriptome understanding: From overlapping transcription to the excludon concept. *Molecular microbiology* **113,** 593–602 (2020).
251. Lasa, I. *et al.* Genome-wide antisense transcription drives mRNA processing in bacteria. *Proceedings of the National Academy of Sciences of the United States of America* **108,** 20172–20177 (2011).
252. Lioliou, E. *et al.* Global regulatory functions of the *Staphylococcus aureus* endoribonuclease III in gene expression. *PLoS genetics* **8,** e1002782 (2012).
253. Geissmann, T. *et al.* A search for small noncoding RNAs in *Staphylococcus aureus* reveals a conserved sequence motif for regulation. *Nucleic Acids Research* **37,** 7239–7257 (2009).
254. Lioliou, E. *et al. In vivo* mapping of RNA-RNA interactions in *Staphylococcus aureus* using the endoribonuclease III. *Methods* **63,** 135–143 (2013).
255. Gatewood, M. L., Bralley, P., Weil, M. R. & Jones, G. H. RNA-Seq and RNA immunoprecipitation analyses of the transcriptome of *Streptomyces coelicolor* identify substrates for RNase III. *Journal of bacteriology* **194,** 2228–2237 (2012).
256. Helwak, A. & Tollervey, D. Mapping the miRNA interactome by cross-linking ligation and sequencing of hybrids (CLASH). *Nature protocols* **9,** 711–728 (2014).
257. McKellar, S. W. *et al.* RNase III CLASH in MRSA uncovers sRNA regulatory networks coupling metabolism to toxin expression. *Nature communications* **13,** 3560 (2022).
258. Mediati, D. G. *et al.* RNase III-CLASH of multi-drug resistant *Staphylococcus aureus* reveals a regulatory mRNA 3'UTR required for intermediate vancomycin resistance. *Nature communications* **13,** 3558 (2022).
259. Le Rhun, A. *et al.* Identification of endoribonuclease specific cleavage positions reveals novel targets of RNase III in *Streptococcus pyogenes*. *Nucleic Acids Research* **45,** 2329–2340 (2017).
260. Rath, E. C., Pitman, S., Cho, K. H. & Bai, Y. Identification of streptococcal small RNAs that are putative targets of RNase III through bioinformatics analysis of RNA sequencing data. *BMC Bioinformatics* **18,** 540 (2017).

261. Deltcheva, E. *et al.* CRISPR RNA maturation by trans-encoded small RNA and host factor RNase III. *Nature* **471,** 602–607 (2011).
262. Börner, J., Friedrich, T. & Klug, G. RNase III participates in control of quorum sensing, pigmentation and oxidative stress resistance in *Rhodobacter sphaeroides*. *Molecular microbiology* doi: 10.1111/mmi.15181 (2023).
263. Altuvia, Y. *et al. In vivo* cleavage rules and target repertoire of RNase III in *Escherichia coli*. *Nucleic Acids Research* **46,** 10380–10394 (2018).
264. Gordon, G. C., Cameron, J. C. & Pfleger, B. F. RNA sequencing identifies new RNase III cleavage sites in *Escherichia coli* and reveals increased regulation of mRNA. *mBio* **8,** e00128-17 (2017).
265. Miller, M. B. & Bassler, B. L. Quorum sensing in bacteria. *Annual review of microbiology* **55,** 165–199 (2001).
266. Ifill, G. *et al.* RNase III and RNase E influence post-transcriptional regulatory networks involved in virulence factor production, metabolism, and regulatory RNA processing in *Bordetella pertussis*. *mSphere* **6,** e0065021 (2021).
267. Hör, J., Matera, G., Vogel, J., Gottesman, S. & Storz, G. Trans-acting small RNAs and their effects on gene expression in *Escherichia coli* and *Salmonella enterica*. *EcoSal Plus* **9**. (2020).
268. Santiago-Frangos, A. & Woodson, S. A. Hfq chaperone brings speed dating to bacterial sRNA. *Wiley Interdisciplinary Reviews: RNA* **9,** e1475 (2018).
269. Melamed, S. *et al.* Global mapping of small RNA-target interactions in bacteria. *Molecular cell* **63,** 884–897 (2016).
270. Franze de Fernandez, M. T., Eoyang, L. & August, J. T. Factor fraction required for the synthesis of bacteriophage Qbeta-RNA. *Nature* **219,** 588–590 (1968).
271. Link, T. M., Valentin-Hansen, P. & Brennan, R. G. Structure of *Escherichia coli* Hfq bound to polyriboadenylate RNA. *Proceedings of the National Academy of Sciences of the United States of America* **106,** 19292–19297 (2009).
272. Schu, D. J., Zhang, A., Gottesman, S. & Storz, G. Alternative Hfq-sRNA interaction modes dictate alternative mRNA recognition. *The EMBO journal* **34,** 2557–2573 (2015).
273. Sauer, E., Schmidt, S. & Weichenrieder, O. Small RNA binding to the lateral surface of Hfq hexamers and structural rearrangements upon mRNA target recognition. *Proceedings of the National Academy of Sciences of the United States of America* **109,** 9396–9401 (2012).
274. Sauer, E. & Weichenrieder, O. Structural basis for RNA 3'-end recognition by Hfq. *Proceedings of the National Academy of Sciences of the United States of America* **108,** 13065–13070 (2011).
275. Wilusz, C. J. & Wilusz, J. Lsm proteins and Hfq: Life at the 3' end. *RNA biology* **10,** 592–601 (2013).
276. Updegrove, T. B., Zhang, A. & Storz, G. Hfq: the flexible RNA matchmaker. *Current Opinion in Microbiology* **30,** 133–138 (2016).
277. Andrade, J. M., dos Santos, R. F., Chelysheva, I., Ignatova, Z. & Arraiano, C. M. The RNA-binding protein Hfq is important for ribosome biogenesis and affects translation fidelity. *The EMBO journal* **37,** e97631 (2018).
278. Kufel, J., Allmang, C., Petfalski, E., Beggs, J. & Tollervey, D. Lsm Proteins are required for normal processing and stability of ribosomal RNAs. *Journal of Biological Chemistry* **278,** 2147–2156 (2003).
279. Kufel, J., Allmang, C., Verdone, L., Beggs, J. D. & Tollervey, D. Lsm proteins are required for normal processing of pre-tRNAs and their efficient association with La-homologous protein Lhp1p. *Molecular and cellular biology* **22,** 5248–5256 (2002).
280. Zhang, A. *et al.* Global analysis of small RNA and mRNA targets of Hfq. *Molecular microbiology* **50,** 1111–1124 (2003).
281. Lee, T. & Feig, A. L. The RNA binding protein Hfq interacts specifically with tRNAs. *RNA* **14,** 514–523 (2008).
282. Berghoff, B. A. *et al.* Contribution of Hfq to photooxidative stress resistance and global regulation in *Rhodobacter sphaeroides*. *Molecular microbiology* **80,** 1479–1495 (2011).
283. Sittka, A. *et al.* Deep sequencing analysis of small noncoding RNA and mRNA targets of the global post-transcriptional regulator, Hfq. *PLOS Genetics* **4,** e1000163 (2008).
284. Milner, J. L. & Wood, J. M. Insertion proQ220::Tn5 alters regulation of proline porter II, a transporter of proline and glycine betaine in *Escherichia coli*. *Journal of bacteriology* **171,** 947–951 (1989).
285. Smith, M. N., Crane, R. A., Keates, R. A. B. & Wood, J. M. Overexpression, purification, and characterization of ProQ, a posttranslational regulator for osmoregulatory transporter ProP of *Escherichia coli*. *Biochemistry* **43,** 12979–12989 (2004).
286. Chaulk, S. G. *et al.* ProQ is an RNA chaperone that controls ProP levels in *Escherichia coli*. *Biochemistry* **50,** 3095–3106 (2011).
287. Holmqvist, E., Li, L., Bischler, T., Barquist, L. & Vogel, J. Global maps of ProQ binding *in vivo* reveal target recognition via RNA structure and stability control at mRNA 3' ends. *Molecular cell* **70,** 971-982 (2018).
288. Smirnov, A. *et al.* Grad-seq guides the discovery of ProQ as a major small RNA-binding protein. *Proceedings of the National Academy of Sciences of the United States of America* **113,** 11591–11596 (2016).
289. Thomason, M. K. *et al.* Global transcriptional start site mapping using differential RNA sequencing reveals novel antisense RNAs in *Escherichia coli*. *Journal of bacteriology* **197,** 18–28 (2015).
290. Melamed, S., Adams, P. P., Zhang, A., Zhang, H. & Storz, G. RNA-RNA interactomes of ProQ and Hfq reveal overlapping and competing roles. *Molecular Cell* **77,** 411-425.e7 (2020).
291. Olejniczak, M. & Storz, G. ProQ/FinO-domain proteins: another ubiquitous family of RNA matchmakers? *Molecular microbiology* **104,** 905–915 (2017).
292. Gonzalez, G. M. *et al.* Structure of the *Escherichia coli* ProQ RNA-binding protein. *RNA* **23,** 696–711 (2017).
293. Quendera, A. P. *et al.* RNA-binding proteins driving the regulatory activity of small non-coding RNAs in bacteria. *Frontiers in Molecular Biosciences* **7,** 78 (2020).

294. Attaiech, L. *et al.* Silencing of natural transformation by an RNA chaperone and a multitarget small RNA. *Proceedings of the National Academy of Sciences of the United States of America* **113,** 8813–8818 (2016).
295. Chaulk, S. *et al. N. meningitidis* 1681 is a member of the FinO family of RNA chaperones. *RNA biology* **7,** 812–819 (2010).
296. Reinkensmeier, J. & Giegerich, R. Thermodynamic matchers for the construction of the cuckoo RNA family. *RNA biology* **12,** 197–207 (2015).
297. Grützner, J., Börner, J., Jäger, A. & Klug, G. The small RNA-binding protein CcaF1 promotes formation of photosynthetic complexes in *Rhodobacter sphaeroides*. *International journal of molecular sciences* **24,** 9515 (2023).
298. Paysan-Lafosse, T. *et al.* InterPro in 2022. *Nucleic Acids Research* **51,** D418-D427 (2023).
299. Kraus, A. *et al.* Arginine-rich small proteins with a domain of unknown function, DUF1127, play a role in phosphate and carbon metabolism of *Agrobacterium tumefaciens*. *Journal of bacteriology* **202,** e00309-20 (2020).
300. Budnick, J. A., Sheehan, L. M., Kang, L., Michalak, P. & Caswell, C. C. Characterization of three small proteins in *Brucella abortus* linked to fucose utilization. *Journal of bacteriology* **200,** e00127-18 (2018).
301. Robbe, C., Capon, C., Coddeville, B. & Michalski, J.-C. Structural diversity and specific distribution of O-glycans in normal human mucins along the intestinal tract. *The Biochemical journal* **384,** 307–316 (2004).
302. Hudson, A. W., Barnes, A. J., Bray, A. S., Ornelles, D. A. & Zafar, M. A. *Klebsiella pneumoniae* L-fucose metabolism promotes gastrointestinal colonization and modulates its virulence determinants. *Infection and Immunity* **90,** e0020622 (2022).
303. Stahl, M. *et al.* L-fucose utilization provides *Campylobacter jejuni* with a competitive advantage. *Proceedings of the National Academy of Sciences of the United States of America* **108,** 7194–7199 (2011).
304. Scott, K. P., Martin, J. C., Campbell, G., Mayer, C.-D. & Flint, H. J. Whole-genome transcription profiling reveals genes up-regulated by growth on fucose in the human gut bacterium "*Roseburia inulinivorans*". *Journal of bacteriology* **188,** 4340–4349 (2006).
305. Pacheco, A. R. *et al.* Fucose sensing regulates bacterial intestinal colonization. *Nature* **492,** 113–117 (2012).
306. Mistry, J. *et al.* Pfam: The protein families database in 2021. *Nucleic Acids Research* **49,** D412-D419 (2021).
307. Goodacre, N. F., Gerloff, D. L. & Uetz, P. Protein domains of unknown function are essential in bacteria. *mBio* **5,** e00744-13 (2013).
308. Hafner, M. *et al.* CLIP and complementary methods. *Nature Reviews Methods Primers* **1,** 20 (2021).

RNA BIOLOGY
2023, VOL. 20, NO. 1, 120–135
https://doi.org/10.1080/15476286.2023.2195733

Taylor & Francis
Taylor & Francis Group

RESEARCH PAPER

OPEN ACCESS Check for updates

Ribonuclease E strongly impacts bacterial adaptation to different growth conditions

Janek Börner [a*], Tobias Friedrich [b,c*], Marek Bartkuhn [b,d], and Gabriele Klug [a]

[a]Institute of Microbiology and Molecular Biology, Justus-Liebig-University Giessen, Giessen, Germany; [b]Biomedical Informatics and Systems Medicine, Justus-Liebig-University Giessen, Giessen, Germany; [c]Institute of Biochemistry, Justus-Liebig-University Giessen, Giessen, Germany; [d]Institute for Lung Health, Giessen, Germany

ABSTRACT

Adaptation of bacteria to changes in their environment is often accomplished by changes of the transcriptome. While we learned a lot on the impact of transcriptional regulation in bacterial adaptation over the last decades, much less is known on the role of ribonucleases. This study demonstrates an important function of the endoribonuclease RNase E in the adaptation to different growth conditions. It was shown previously that RNase E activity does not influence the doubling time of the facultative phototroph *Rhodobacter sphaeroides* during chemotrophic growth, however, it has a strong impact on phototrophic growth. To better understand the impact of RNase E on phototrophic growth, we now quantified gene expression by RNA-seq and mapped 5′ ends during chemotrophic growth under high oxygen or low oxygen levels and during phototrophic growth in the wild type and a mutant expressing a thermosensitive RNase E. Based on the RNase E-dependent expression pattern, the RNAs could be grouped into different classes. A strong effect of RNase E on levels of RNAs for photosynthesis genes was observed, in agreement with poor growth under photosynthetic conditions. RNase E cleavage sites and 5′ ends enriched in the *rne*^{ts} mutant were differently distributed among the gene classes. Furthermore, RNase E affects the level of RNAs for important transcription factors thus indirectly affecting the expression of their regulons. As a consequence, RNase E has an important role in the adaptation of *R. sphaeroides* to different growth conditions.

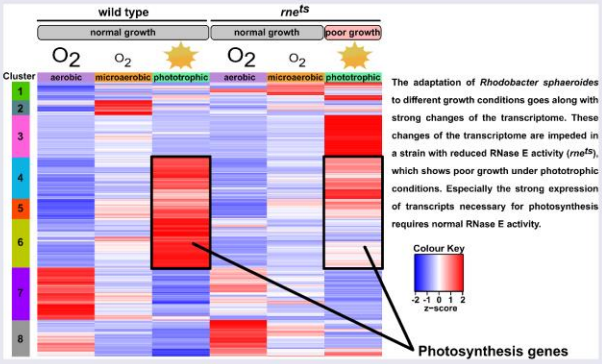

ARTICLE HISTORY
Revised 3 March 2023
Accepted 22 March 2023

KEYWORDS
Rhodobacter; RNase E; transcriptome; riboregulation; RNA processing; photosynthesis genes; bacterial adaptation

Introduction

Rhodobacter sphaeroides (recently renamed *Cereibacter sphaeroides*; [1]) is a facultative photosynthetic bacterium that adapts its metabolism to the oxygen and light conditions in the environment. At high oxygen tension no photosynthetic complexes are synthesized and ATP is generated by aerobic respiration. When oxygen tension drops, photosynthetic complexes are synthesized, but also at low oxygen levels (microaerobic conditions) aerobic respiration can generate ATP. When no oxygen is present and light is available, *R. sphaeroides* performs anoxygenic photosynthesis. In the absence of oxygen and light, fermentation or anaerobic respiration (in the presence of a suitable electron acceptor) can be performed. The photosynthetic complexes are assembled into an intracytoplasmic membrane system. At high or intermediate oxygen levels, formation of photosynthetic complexes is repressed by light [2,3]. This regulated formation of photosynthetic complexes by oxygen and light is important to avoid waste of energy for production of photosynthetic complexes when not required, but also to

CONTACT Gabriele Klug Gabriele.Klug@mikro.bio.uni-giessen.de Institute of Microbiology and Molecular Biology, Justus-Liebig-University Giessen, Heinrich-Buff-Ring 26-32, Giessen 35392, Germany
*These authors contributed equally to this work.

Supplemental data for this article can be accessed online at https://doi.org/10.1080/15476286.2023.2195733.

avoid photo-oxidative stress by the simultaneous presence of light, oxygen, and bacteriochlorophyll.

The regulatory mechanisms allowing the adaptation of *R. sphaeroides* to different growth conditions and to photo-oxidative stress have been intensely studied in the past. Not only regulation at the level of transcription, e.g. by alternative sigma factors, is important during adaptation (e.g. [4–7]), but also post-transcriptional regulation. Especially during adaptation to stationary phase, we observed pronounced changes of the proteome that were not reflected by corresponding changes of the transcriptome [8]. Our studies revealed also the importance of riboregulation during adaptation of *R. sphaeroides* (e.g. [9–15]). Riboregulation includes regulation through the action of ribonucleases (RNases) and regulation by small non-coding RNAs (sRNAs).

Riboregulation in *R. sphaeroides* was already demonstrated decades ago: the distribution of RNA-stabilizing elements (secondary structures) and destabilizing elements (RNase cleavage sites) leads to *puf* mRNA segments with different stabilities (Figure S1; [16,17]; reviewed in [18]). The polycistronic *pufQBALMX* mRNA encodes proteins of the reaction centre (*pufLM*), of the light-harvesting I complex (*pufB*A), a scaffolding protein (*pufX*), and a protein regulating porphyrin flux (*pufQ*, [19]). More recently, in *R. sphaeroides* the sRNA PcrX was identified that is processed from the 3' UTR (untranslated region) of the *puf* operon by RNase E cleavage [12]. PcrX targets the *pufX* mRNA region, promotes its degradation and thereby also influences the amounts of photosynthetic complexes. Furthermore, the antisense RNA asPcrL affects RNase III-dependent decay of the *pufL* mRNA segment [13]. Differences in the stability of the *puf* mRNA segments contribute to the stoichiometry of reaction centre and light-harvesting complexes, and influence growth of *Rhodobacter* when shifted to phototrophic conditions [9]. It was also demonstrated that the rate of initial endonucleolytic cleavage by RNase E within the *pufBALMX* mRNA segment is influenced by the oxygen concentration in the environment [20].

Considering the impact of mRNA degradation on regulation of *puf* gene expression, the influence of RNase E on the transcriptome of *R. sphaeroides* was analysed on a global level by RNA-seq from cultures grown at microaerobic conditions [21]. Since the *rne* gene cannot be deleted, the native *rne* gene was replaced by the *rne-3071* gene from *E. coli* that leads to production of a temperature-sensitive RNase E. A transcriptome analysis was performed by RNA-seq under microaerobic conditions. Despite the higher GC content of its genome, *R. sphaeroides* RNase E, like the *E. coli* enzyme, targets AU-rich sequences [21]. A strong effect of altered RNase E activity on the transcriptome was observed at 42°C, but many changes also occurred at 32°C, the optimal growth temperature for *R. sphaeroides*. *E. coli* RNase E can be part of a degradosome, a multienzyme complex composed of RNases, helicases and metabolic enzymes (reviewed in [22]). Degradosome complexes with varying composition were also found in several alphaproteobacteria, including *Rhodobacter capsulatus* [23], but also in cyanobacteria and Gram-positives [22]. The *E. coli* (gammaproteobacterium) degradosome localizes to the cytoplasmic membrane, the degradosome of the alphaproteobacterium *Caulobacter crescentus* localizes to BR-bodies, ribonucleoprotein condensates in the interior of the cell [22]. The localization of the degradosome of the alphaproteobacterium *R. sphaeroides* has not been analysed. Under microaerobic and phototrophic conditions, the cells are filled with intracytoplasmic membranes that accommodate the photosynthetic complexes [24]. In contrast to the *E. coli* RNase E, the RNase E enzymes of the alphaproteobacteria have an arginine-proline-rich region inserted into the S1 domain [25].

The $rne^{E.\ coli\ (ts)}$ mutant of *R. sphaeroides* showed a pronounced phenotype regarding the formation of photosynthetic complexes and phototrophic growth, whereas there was no effect on chemotrophic growth under microaerobic conditions [21].

To better understand the strong effect of RNase E on phototrophic growth of *R. sphaeroide*s, we compared RNA-seq data from the wild type and the rne^{ts} mutant not only during microaerobic (25–30 mM oxygen) growth at 32°C, but also under aerobic (160–180 mM oxygen), and phototrophic (no oxygen, 60 W/m^2 white light) growth conditions. We mapped 5' ends that are reduced in the mutant (log_2 fold change >1), indicating *bona fide* RNase E cleavage sites (scheme shown in Figure 1A). We also mapped 5' ends that are enriched in the rne^{ts} mutant. RNase E can bind to monophosphorylated 5' ends and will subsequently introduce cleavages in an overall 5'-3' direction (5' end-dependent degradation). Such monophosphorylated 5' ends can stem from previous endonucleolytic cleavage (by RNase E or RNase III) or by action of pyrophosphohydrolase on the 5' triphosphate of primary transcripts. Monophosphorylated 5' ends will be stabilized in the rne^{ts} mutant and are consequently enriched (Figure 1B).

Our data identified classes of genes with distinct RNase E-dependent expression patterns under different growth conditions. A strong impact of RNase E on expression of photosynthesis genes is in agreement with impeded growth under photosynthetic growth conditions. The effects of RNase E on mRNA classes (required for photosynthesis or motility) coincide with an effect of RNase E on the mRNAs for important transcriptional regulators for these classes.

Material and methods

Cultivation of bacterial strains

The *R. sphaeroides* 2.4.1 wild type ([26]; now renamed *Cereibacter sphaeroides*, [1]) and the *R. sphaeroides* rne^{ts} mutant [27] were cultivated in malate minimal medium [28] at 32°C. Both strains were either grown in the presence of high oxygen concentration of 180 µM dissolved oxygen (aerobic cultures), low oxygen concentration of 25 µM dissolved oxygen (microaerobic cultures) or in the absence of oxygen but illuminated with 60 W*m^{-2} white light (phototrophic cultures).

RNA isolation and RNA sequencing

20 ml of each culture were collected during exponential growth phase on ice at an OD_{660} of 0.4. Afterwards, cells were sedimented by centrifugation at 10,000 rpm for 10 min at 4°C (Sorvall RC 6 Plus centrifuge, Thermo Scientific). For

total RNA isolation the hot phenol method [29,30] was used. For removal of remaining DNA from RNA isolates the Turbo DNA-*free* kit (Invitrogen) was used following the manufacturer's protocol. To test for remaining DNA, PCR with specific primers against *rpoZ* was performed. DNA-free RNA was tested for RNA integrity by electrophoresis of 1.5 µg sample on denaturing 10% polyacrylamide TBE gels and subsequent staining with ethidium bromide, as well as on the Bioanalyzer (described in the data generation description of our deposited RNA-seq data in the GEO repository). The sequencing libraries were constructed as described earlier [31], using the NEBNext Multiplex Small RNA Library Prep Set for Illumina (NEB).

Spike-in quantitative reverse transcriptase PCR (qRT-PCR)

For quantification of RNA abundances by qRT-PCR a spike-in approach was used. For this, 1 ng of DNA-free spike-in *in vitro* transcribed *sinI* RNA from *Sinorhizobium meliloti* was added to the harvested cell pellet prior to RNA isolation [14]. The subsequent qRT-PCR of DNA-free RNA isolates was performed using the Brilliant III Ultra-Fast SYBR Green QRT-PCR Master Mix kit (Agilent Technologies) following the manufacturer's protocol. Relative RNA abundances were calculated from independent biological triplicates, each in technical replicates, using the Pfaffl quantification model (with efficiency correction) [32].

RNA half-life determination

To monitor RNA decay over time, 20 ml samples of biological triplicates of wild type and *rne*^{ts} mutant were sedimented as described above. One sample of each culture, referring as t0 (100%), was collected immediately before addition of 0.2 mg/ml rifampicin (SERVA electrophoresis GmbH), while the following samples were collected at the time points 3 min (t1), 6 min (t2), 9 min (t3), 15 min (t4) and 30 min (t5) after addition of rifampicin. RNA isolation by hot phenol extraction and quantification by qRT-PCR were performed as described above.

RNA-seq data processing

Alignment of the raw sequencing reads against the reference genome of *R. sphaeroides* (NC_007493.2, NC_007494.2, NC_009007.1, NC_007488.2, NC_007489.1, NC_007490.2, and NC_009008.1) was performed using the READemption pipeline [33] v.1.0.5. The aligned reads were stored as binary alignment maps (BAM) files in the 'output/align/alignments' folder created by READemption. Those BAM files were further processed within R v.4.1.2 [34] using a systemPipeR [35] v.1.26.3 with custom made parameter files for the different tools. For the analysis of gene expression, the read counts per gene were calculated using the summarizedOverlaps function with the corresponding gene transfer file (GTF) for each BAM file. DESeq2 [36] v.1.32 was used for the normalization of the reads and the identification of transcriptional changes. DESeq2's $\log_2$ fold change and adjusted p-value (Benjamini and Hochberg) were used for the identification of significantly differentially expressed genes (results of the DESeq2 analysis are listed in supplement table S3). The prediction of TSS and 5'/3' UTRs was performed earlier [37].

In order to define *bona fide* cleavage sites or 5' ends enriched in the mutant, the strand-specific coverage of each base of the genome based on the 5' counts of each read was generated using bedtools [38] genomecov function with '-d –5 -ibam -strand' parameters and the corresponding genome. To exclude bases with an insufficient coverage, a single base must have at least 10 counts in one of the replicates of the different conditions to be used for the identification of *bona fide* cleavage sites or 5' ends enriched in the mutant. The coverage of the remaining bases was normalized and the changes for

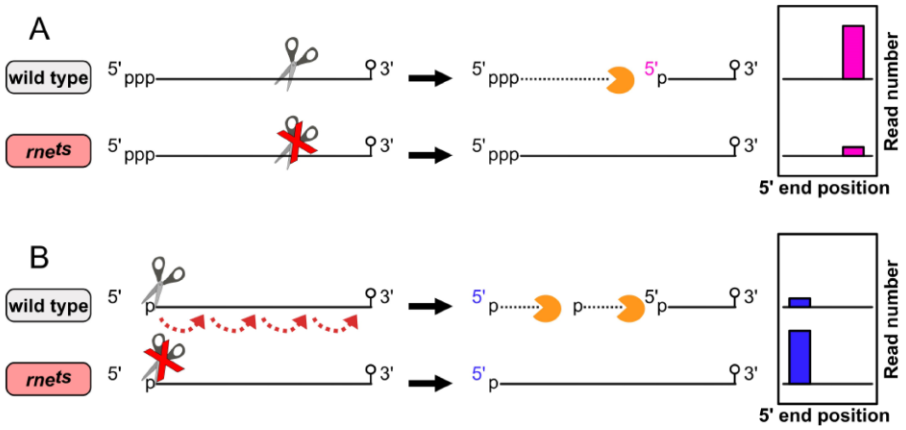

Figure 1. **Mapping of stable 5' ends from RNA-seq data**. Schematic overview for the identification rules used for mapping of *bona fide* cleavage sites, and 5' ends enriched in the *rne*^{ts} (modified from [21]). (A) Bacterial primary transcripts typically harbour triphosphorylated 5' ends, and 3' ends which are protected by RNA secondary structures like stem loops. Internal cleavage by RNase E generates monophosphorylated 5' ends and unprotected 3' ends. Subsequently, unprotected 3' ends are rapidly degraded by 3' to 5' exoribonucleases like PNPase or RNase R. Due to reduced RNase E activity in the *rne*^{ts} mutant, less internal cleavage by RNase E is catalysed, consequently leading to lower amounts of newly generated stable 5' ends in the *rne*^{ts} mutant (cleavage sites). (B) Since RNase E can be allosterically activated by monophosphorylated RNA substrates (5' end-dependent pathway), which are generated by endoribonuclease or pyrophosphohydrolase activity, these transcripts tend to accumulate in the mutant and can be identified by enriched 5' ends in the mutant.

each base between the *rne*^{ts} mutant and the wild type was calculated using DESeq2. Bases with a $\log_2$ fold change >1 and adjusted p-value <0.05 were defined as *bona fide* cleavage sites. 5' ends enriched in the mutant were defined using the same threshold for adjusted p-value but a $\log_2$ fold change < −1. Multiple adjacent cleavage sites or 5' ends enriched in the mutant within three bases to each other were reduced to one site using bedtools merge function with '-s -d 3 -o distinct' parameters.

The test for over representation of genes associated with GO terms (based on QuickGO taxon ID: 272943) for different groups of genes (e.g. significantly up-/downregulated) was performed using the fisher exact test for each GO term (pathway).

The GSEA was performed using the fGSEA R package [39] with gene sets based on all genes associated with a cleavage site or enriched 5' ends and the ranked list for all genes based on Wald statistic calculated by DESeq2.

p-values were normalized for multiple testing using the Benjamini and Hochberg strategy [40].

To compare the *rne* mRNA levels of the *E. coli* variant and the *R. sphaeroides* variant, the *E. coli* K12DH10B genome was downloaded from Illumina iGenomes. The sequence of the *E. coli* gene plus 500 bp upstream and downstream was extracted and added as a new chromosome to the FATSA file of *R. sphaeroides*. This combined FASTA file was used for alignment as described above. Counting of raw data for *E. coli* *rne*^{ts} mRNA reads and *R. sphaeroides rne* mRNA reads was performed using featureCounts from the Rsubread package [41]. These reads were size normalized and normalized for the longer length of the *E. coli* *rne*^{ts} gene.

RNase E activity reporter assay

For construction of the RNase E activity reporter, the mVenus open reading frame was cloned under transcriptional control of the strong constitutive 16S rRNA promoter (control plasmid). To monitor RNase E activity the well characterized RNase E cleavage site of the small RNA UpsM from *R. sphaeroides* [14] was introduced into the 5' UTR. All primers used for the cloning of the reporter plasmids are listed in supplement table S4. A scheme of the used constructs is depicted in Figure S2.

The sequence of the 16S rRNA promoter was amplified from the *R. sphaeroides* 2.4.1 genome by PCR using the oligonucleotides p16S_HindIII_for and p16S_ScaI_rev. The amplicon was inserted into pPHUmVenus [42] with *Hind*III and *Sca*I resulting in the plasmid pPHU231-p16S-mVenus (control plasmid). Subsequently, an 89 bp DNA fragment of the UpsM sequence was amplified using the primers UpsM90_ScaI_for and UpsM90_XbaI_rev, followed by insertion into pPHU-p16S-mVenus via *Sca*I and *Xba*I yielding the plasmid pPHU231-p16S-UpsM90-mVenus.

The plasmids pPHU231-p16S-mVenus and pPHU231-p16S-UpsM-90-mVenus were separately transferred into *R. sphaeroides* wild type and the *rne*^{ts} mutant by diparental conjugation using *E. coli* strain S17–1 [43]. Biological triplicates of the conjugants were cultivated under aerobic, microaerobic or phototrophic conditions. 100 µl of exponentially grown cultures were transferred into 96-well plates as technical duplicates, followed by measurements of OD_{660} and fluorescence of mVenus (extinction 515 nm, emission 548 nm) in a Tecan Infinity plate reader. The samples of phototrophic cultures were incubated at room temperature for 10 min after transfer into 96-well plates prior to the measurements, allowing maturation of mVenus fluorophore by oxygenation. As a control of background autofluorescence signals, empty vector controls of wild type and *rne*^{ts} mutant were cultivated and analysed according to the same described procedure.

Results and discussion

Effect of different growth conditions on the transcriptome of R. sphaeroides

We observed previously that reduced RNase E activity has a large impact on growth of *R. sphaeroides* under phototrophic, but not under chemotrophic growth at low oxygen tension (microaerobic conditions). In the previous study, the effect of RNase E on the transcriptome was only investigated under chemotrophic (microaerobic) conditions [21]. To better analyse the impact of RNase E on adaption of *R. sphaeroides* to different growth conditions, we now compared RNA-seq data of wild type and *rne*^{ts} mutant under phototrophic conditions and microaerobic conditions and also included chemotrophic growth under high oxygen tension (aerobic growth). Figure 2 demonstrates that growth behaviour under aerobic or microaerobic conditions is very similar in *R. sphaeroides* wild type, and growth of the *rne*^{ts} mutant is comparable. Under the chosen light condition, the wild type reaches a higher optical density when grown phototrophically. As already reported previously [21], the *rne*^{ts} mutant is strongly impeded in growth under these conditions.

To understand, why lower RNases E activity especially affects phototrophic growth, for each growth condition three RNA samples were analysed by RNA-seq, originating from three independent biological replicates. The PCA plot shown in Figure 3A demonstrates the good reproducibility of the sequencing triplicates. As expected, the highest variance between the different samples is based on the different growth conditions (aerobic, microaerobic, phototrophic) of *R. sphaeroides*. Of note, the microaerobic samples are in between the aerobic and phototrophic conditions, highlighting this intermediated growth condition. Interestingly, clear differences between *rne*^{ts} mutant and wild type samples are detectable for all conditions, suggesting that the enzyme mediates mild, albeit consistent effects under chemotrophic conditions, too. In line with the growth curve (Figure 2), the effects of the *rne*^{ts} mutant are by far the most visible under phototrophic growth conditions.

The influence of growth conditions on the transcriptome of *R. sphaeroides* wild type is also shown in Figure 3B. There is little change of the transcriptome when aerobic and microaerobic conditions are compared: about 90% of the genes show similar expression levels ($\log_2$ fold change >−1 and <1). 5% of the genes show significantly lower expression under aerobic conditions ($\log_2$ fold change <−1 and adjusted p-value <0.05), 4.6% of the genes show significantly higher

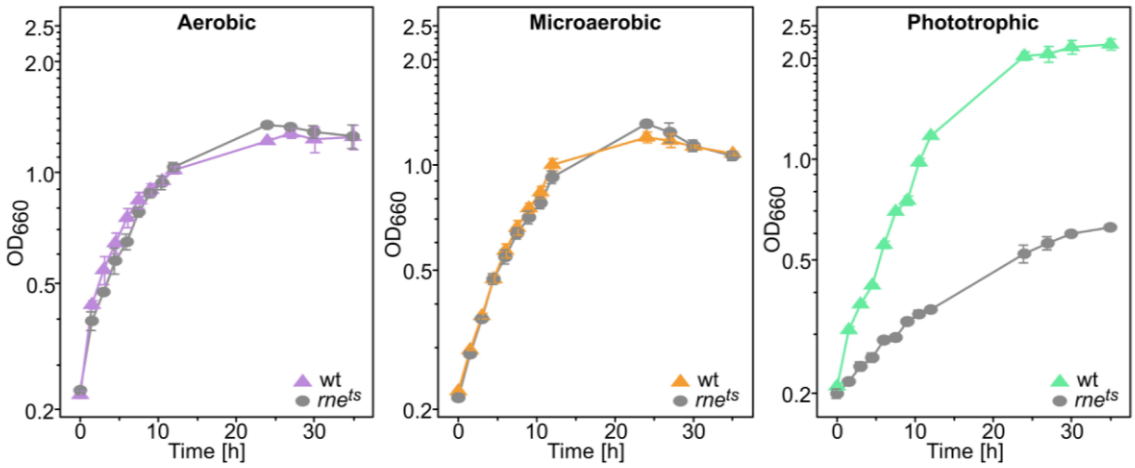

Figure 2. Growth behaviour of *R. sphaeroides* wild type and *rne*^{ts} mutant under aerobic, microaerobic, and phototrophic growth conditions. Exponentially grown pre-cultures were diluted to an OD_{660} of 0.2 and growth was followed by measuring the optical density (OD_{660}) of *R. sphaeroides* wild type and *rne*^{ts} mutant cultures for 35 hours. The mean and standard deviation of independent biological triplicates is shown.

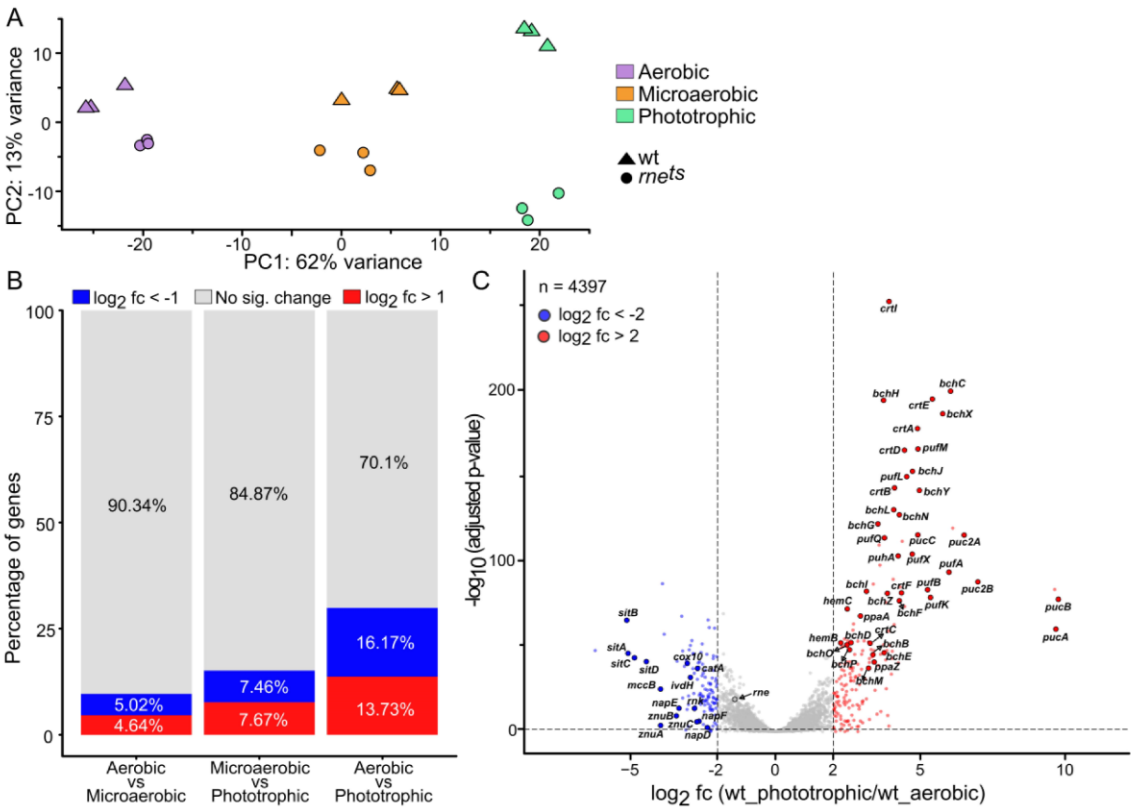

Figure 3. Significantly differentially expressed genes in *R. sphaeroides* among different environmental conditions. (A) Principle component analysis (PCA) showing the variation of the transcriptome of the two *R. sphaeroides* strains (wild type and *rne*^{ts} mutant) under aerobic, microaerobic, and phototrophic growth conditions. The transcriptome was analysed by RNA-seq. (B) Percentage of significantly differentially expressed genes in comparison between aerobic, microaerobic, and phototrophic growth conditions of *R. sphaeroides* wild type, including all genes with adjusted p-value <0.05 and $\log_2$ fold change >1 (upregulated) or <−1 (downregulated). (C) Volcano plot highlighting significantly differentially expressed genes between phototrophic and aerobic growth conditions.

expression ($\log_2$ fold change >1 and adjusted p-value <0.05). When microaerobic and phototrophic growth conditions are compared, differences in the transcriptome are slightly larger. About 7.5% of all genes show significantly lower expression under microaerobic conditions and about 7.7% of the genes show significantly higher expression. Expression levels show much stronger differences between aerobic and phototrophic conditions: 16.2% of the genes show significantly lower

expression levels under aerobic conditions, 13.7% show significantly higher expression levels.

This result reflects, that the change of parameters concerning oxygen concentration and light between aerobic and phototrophic growth is the biggest. In previous work, *R. sphaeroides* transcriptomes under different growth conditions were analysed using microarrays. Pappas et al. (2004) reported decreased expression of about 10% of the transcripts in aerobic cultures versus phototrophic cultures, and increased expression levels for about 12% of the transcripts. These changes are in the same range as observed in our data set.

The different expression pattern between phototrophic and aerobic conditions is further visualized in a volcano plot (Figure 3C). Among the genes with significantly higher expression ($\log_2$ fold change >2 and adjusted p-value <0.05) under phototrophic conditions are many photosynthesis genes (45 genes of a total of 180): *puf* and *puc* genes encoding pigment-binding proteins, *bch* genes for bacteriochlorophyll synthesis, *hem* genes for the synthesis of protoporphyrin IX, *crt* genes for carotenoid synthesis, *ppaA* for a transcriptional regulator of photosynthesis genes. The products of those genes are required for phototrophic growth but not or to a lesser extent under aerobic conditions, when the presence of photosynthetic complexes may cause photo-oxidative stress. Similar expression patterns were also observed in a previous microarray study [44]. Strongly reduced expression levels under phototrophic growth are observed e.g. for a number of genes for ribosomal proteins or genes involved in metal transport (*sit, zur, exbD*). Interestingly the *rne* transcript shows higher abundance (2.7-fold) under aerobic conditions than under phototrophic conditions.

Figure S3 shows the result of a gene ontology term enrichment analysis including all significantly upregulated genes as shown in the volcano plot (Figure 3C). This analysis also confirms a significant role of those RNAs in photosynthesis and closely associated functions.

Effect of RNase E on global changes of the transcriptome under different growth conditions

As a next step we compared the changes of the transcriptome under different growth conditions in the wild type and the *rne*^{ts} mutant strain (Figure 4A). Only transcripts with a strong and statistically significant differential expression ($\log_2$ fold change >2 or <−2 and adjusted p-value <0.05) between growth conditions or strains are included (446 transcripts in total). The left part of the figure shows the expression profiles in the wild type. Individual expression levels are compared to the average (colour coded). Based on their expression pattern under different growth conditions and in different strains the transcripts are grouped into eight different clusters by unsupervised agglomerative hierarchical clustering. When microaerobic and aerobic conditions are compared in the wild type, major changes occur in cluster 2, which shows much stronger expression under microaerobic conditions, and in cluster 7, which shows much stronger expression under aerobic conditions. When microaerobic and phototrophic conditions are compared, the change in expression pattern is more drastic: clusters 4, 5, and 6 show strongly increased expression under phototrophic conditions, transcript levels of clusters 7 and 8 are rather decreased.

Our previous study focused exclusively on the identification of differential 5' ends, which are affected by RNase E in

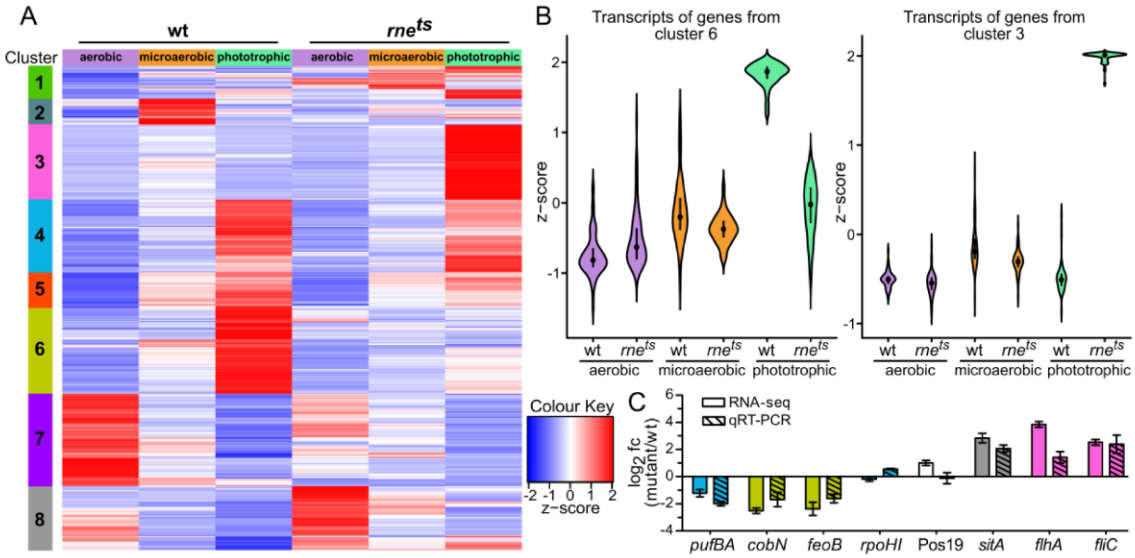

Figure 4. The *rne*^{ts} mutant has a highly altered transcriptome, especially under phototrophic conditions. (A) Heatmap illustrating the z-standardized transcriptomic changes of transcripts of the top deregulated genes (adjusted p-value <0.05 and $\log_2$ fold change >2 or <−2; $n = 446$) based on all growth conditions, highlighting transcriptomic changes among aerobic, microaerobic, and phototrophic growth conditions of *R. sphaeroides* wild type and the *rne*^{ts} mutant. The clustering was performed according to the Euclidean distance. (B) Quantification of the z-standardized gene expression of RNAs from cluster 6 and cluster 3 (as shown in panel A). (C) Spike-in quantitative reverse transcriptase PCR with total RNA obtained from phototrophically grown wild type and *rne*^{ts} mutant. The relative abundance of selected RNAs (bars are coloured according to the clusters of the heatmap) in the *rne*^{ts} mutant, is shown.

R. sphaeroides under microaerobic conditions [21]. In this study, we were also interested in differential 5' ends under aerobic and phototrophic conditions, and especially in RNA expression levels in the mutant under the different growth conditions. The right part of Figure 4A shows the expression levels under the three growth conditions for the *rne*^{ts} mutant. The expression profiles shown in Figure 4A clearly demonstrate a particularly strong impact of RNase E under phototrophic conditions. In microaerobic conditions, the expression profiles are quite similar between the two strains. Major differences occur in cluster 2 which shows clearly lower expression when RNase E activity is reduced and in cluster 1 with higher expression in the mutant. Cluster 2 comprises 24 genes, of which 12 encode hypothetical proteins (Table S1). Two genes encode Fru-1,6-bisphospatase, two encode uncharacterized transcriptional regulators, two encode subunits of ABC transporters, one encodes a protein for conjugational transfer. Further annotations are: putative chemoreceptor protein, metalloprotease, NADH-ubiquinone oxidoreductase subunit, fosmidomycin resistance protein, D-malate dehydrogenase.

Cluster 1 comprises 29 genes, four of them for tRNAs (Table S1). 14 genes encode hypothetical proteins, two genes flagellar proteins and nine genes proteins of various predicted functions. RSs_1624 is a UTR-derived sRNA. Due to the lacking characterization of most proteins, the biological consequences of changed transcript levels of cluster 1 and 2 remain elusive.

Under aerobic conditions cluster 7 shows very strong expression in the wild type, which is much weaker in the *rne*^{ts} mutant. 85 genes belong to this cluster, among them the *rne* gene for RNase E, the *rnpA* gene for the RNase P protein component, RSP_0624 coding for RNase G, nine genes for ribosomal proteins, two for sRNAs, and 29 genes encoding hypothetical proteins. Considering the *rne* gene, the RNA-seq results cannot be compared between wild type and mutant, since the *rne*^{ts} transcript of the mutant only partly maps to the *R. sphaeroides* genome. Other genes in cluster 7 encode proteins with unknown or diverse metabolic or regulatory functions (Table S1). Cluster 8 comprises 59 genes and shows clearly stronger expression under aerobic conditions than in other growth conditions in the mutant, but only slightly increased expression in the wild type. Like in cluster 7, many mRNAs of cluster 8 encode proteins with unknown (23 hypothetical proteins) or diverse metabolic or regulatory functions (Table S1). Furthermore, cluster 8 includes genes encoding catalase (*catA*), nitrate reductase (*napBDEF*), pyrroloquinoline quinone biosynthesis proteins (*pqqACD*), several proteins involved in metal transport (*sitACD, znuABC, zur*), sugar transport (RSP_2367, 2368), subunits of a TRAP-T transporter (RSP_1418–1420), and two predicted transcriptional regulators (RSP_2950 and RSP_3448).

Under phototrophic conditions cluster 4, 5, and 6 are strongly induced in the wild type. There is weaker induction of cluster 4 and 5 genes in the mutant, but no or only very weak induction of cluster 6 under phototrophic conditions. Cluster 6 comprises 81 genes, about 20 encode proteins with known functions in photosynthesis. They are required for syntheses of bacteriochlorophyll, carotenoids, protoporphyrin and cobalamin (which is required for bacteriochlorophyll synthesis, reviewed in [45]), or the synthesis of pigment-binding proteins. 17 genes with a role in photosynthesis are also found in cluster 4, which comprises 67 genes including six genes for sRNAs of unknown function. Cluster 4 includes most *puf* and *puc* transcripts that encode pigment binding proteins, *bchD* and *bchI* for bacteriochlorophyll synthesis, *hemC* encoding porphobilinogen deaminase, and *cycA* and *cycC* encoding cytochrome c_2 that is required for photosynthetic electron transport. Interestingly, the transcript encoding the alternative sigma factor RpoHI is also part of cluster 6. RpoHI has an important function in many stress responses, including photooxidative stress and stationary phase [6,31,37,46,47]. The association of cluster 6 and cluster 3 genes with different GO terms is shown in Figure S4.

Expression of cluster 6 and cluster 3 genes is also visualized in the violin plot in Figure 4B. It underlines the similar expression of the clusters in mutant and wild type in aerobic and microaerobic conditions but very different expression patterns during phototrophic growth.

Cluster 5 comprises only 31 genes, half of them with a role in pigment synthesis, three genes for proteins required for formation of photosynthetic complexes (*pucC*, *pufQ*, RSP_0276).

Considering the high number of genes required for photosynthesis in clusters 4–6, the poor growth of the *rne*^{ts} mutant under phototrophic conditions is not surprising.

Very pronounced differences in expression between mutant and wild type under phototrophic conditions are also seen for cluster 3, which consists of 69 genes and shows much stronger expression in the mutant. 12 genes encode hypothetical proteins, 48 genes encode proteins for flagellar synthesis or chemotaxis. Expression of cluster 3 genes is rather similar in the wild type under all three conditions and also between wild type and mutant during chemotrophic growth. This is also visualized by the violin plot in Figure 4B.

For some selected genes we confirmed the expression changes between mutant and wild type for phototrophic growth by real-time RT-PCR (Figure 4C). The DESeq2 analysis quantifies all reads obtained for a gene, while in the real-time RT-PCR expression of only a small part of an RNA (about 200 nt) is monitored. This may account for slight differences in the observed expression changes between the two methods.

Cleavage by RNase E is strongly influenced by growth conditions

As a next step, *bona fide* RNase E cleavage sites (5' ends significantly reduced in *rne*^{ts} mutant: $\log_2$ fold change <-1 and adjusted p-value <0.05) were identified for the different data sets, as well as the 5' ends that are significantly enriched in the mutant ($\log_2$ fold change >1 and adjusted p-value <0.05) (Figure 5). By far the most cleavage sites were detected under aerobic conditions (4206 total), followed by phototrophic conditions (2765 total) and microaerobic conditions (2007 total) (Figure 5A). For an important and validated cleavage site of RNase E within *pufL* in *R. capsulatus* an influence of oxygen tension during growth on cleavage was already noted decades ago [20]. This study demonstrates for

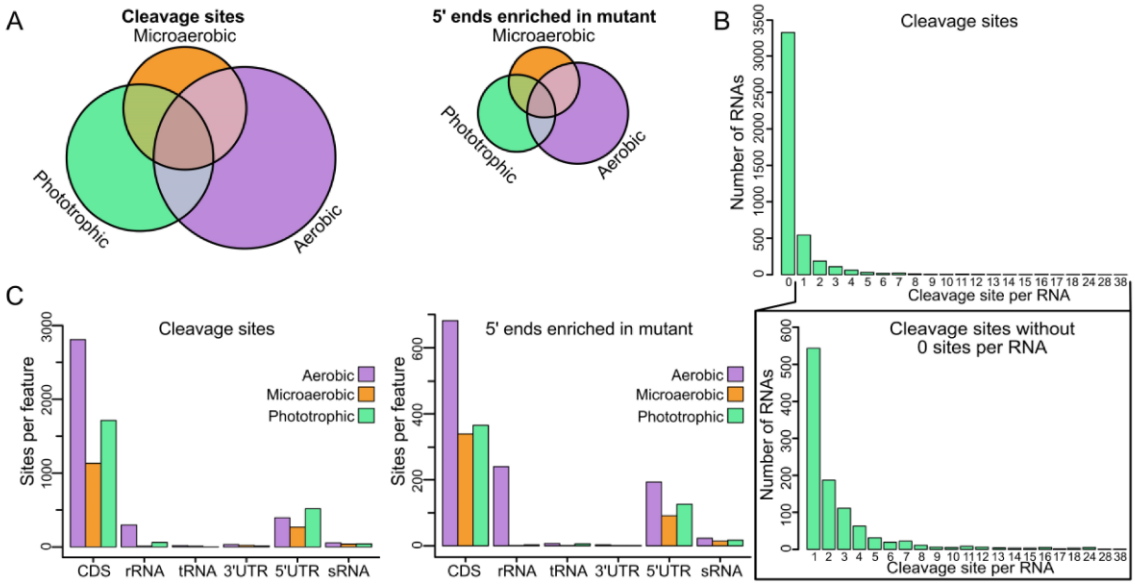

Figure 5. RNA-seq based identification of *bona fide* RNase E cleavage sites and enriched 5′ ends in the mutant. (A) Number of mapped RNase E cleavage sites and enriched 5′ ends in the mutant under aerobic, microaerobic, and phototrophic growth conditions. The circles and their overlaps are proportional according to the amount of identified sites. (B) Number of RNAs with mapped cleavage sites under phototrophic conditions. A magnified version is depicted in the lower panel, missing RNAs without cleavage sites. (C) Distribution of cleavage sites and enriched 5′ ends in the mutant among annotated genomic features.

the first time a major influence of growth conditions on RNase-mediated processing and maturation.

With 1108 mapped cleavage sites, the overlap between aerobic/microaerobic conditions was the biggest, whereas for microaerobic/phototrophic conditions an overlap of 905 cleavage sites, and for aerobic/phototrophic conditions an overlap of 569 cleavage sites was identified. In total, less 5' ends enriched in the mutant were detected than cleavage sites, while the distribution among the different growth conditions was similar.

No RNase E cleavage sites were mapped for a high percentage of transcripts (about 2700 under all conditions; about 3300 under phototrophic conditions). This implies that many changes in the transcriptome are rather due to altered production of the transcripts or to turn-over by other RNases than to altered turn-over by RNase E. However, not all existing cleavage sites will meet our criteria ($\log_2$ fold changes and p-values). Nevertheless, they may contribute to turn-over of transcripts. Unexpectedly, the overlap of cleavage sites in different growth conditions was also rather small: 2830 cleavage sites were detected only in aerobic conditions, 1535 cleavage sites only in phototrophic conditions, which could be due to generally differential RNA abundances between the three conditions, a fact that may influence the likelihood to map *bona fide* cleavage sites. Since the mutant showed a strongly impaired growth phenotype under phototrophic conditions, we were especially interested in the distribution of cleavage sites per RNA during phototrophic growth (Figure 5B). While most RNAs (about 3300) were found to harbour no *bona fide* cleavage site (by our definition), we observed a wide spread distribution of cleavage sites per RNA for those RNAs with cleavage site(s). For a majority of RNAs 1–7 cleavage sites were mapped, while we also found RNAs with over 20 *bona fide* cleavage sites per RNA.

In addition to the number of cleavage sites per RNA under phototrophic conditions, we investigated the distribution of all cleavage sites and 5' ends significantly enriched in the mutant under aerobic, microaerobic and phototrophic conditions among annotated genomic features (Figure 5C). For all three conditions, most cleavage sites were mapped within coding sequences (CDS), followed by 5' UTRs and rRNAs, except for aerobic conditions where we mapped an unexpected high number of enriched 5' ends in the mutant within rRNAs. In comparison with our previously published data [21], the distribution of sites among genomic features is generally similar. rRNAs are part of large transcripts that undergo several maturation steps including the action of RNase E, RNase III, RNase P and RNase J [48–51]. These processes generate many intermediate and mature monophosphorylated 5' ends, which are likely to accumulate in the *rne*^{ts} mutant. Although previous microarray data indicated that rRNA/total RNA ratios did not change drastically between different growth conditions [52], the enrichment of these rRNA 5' ends under aerobic conditions in the mutant remains to be elucidated. Nevertheless, a biological effect on the growth behaviour caused by the higher amounts of rRNA 5' ends mapped under aerobic conditions in the mutant was not visible (Figure 2).

We also analysed the correlation of cleavage site distribution and differences in gene expression between the *rne*^{ts} mutant and the wild type under phototrophic growth conditions. Most RNAs with mapped RNase E cleavage sites do not show significantly increased or decreased expression levels in the mutant under phototrophic

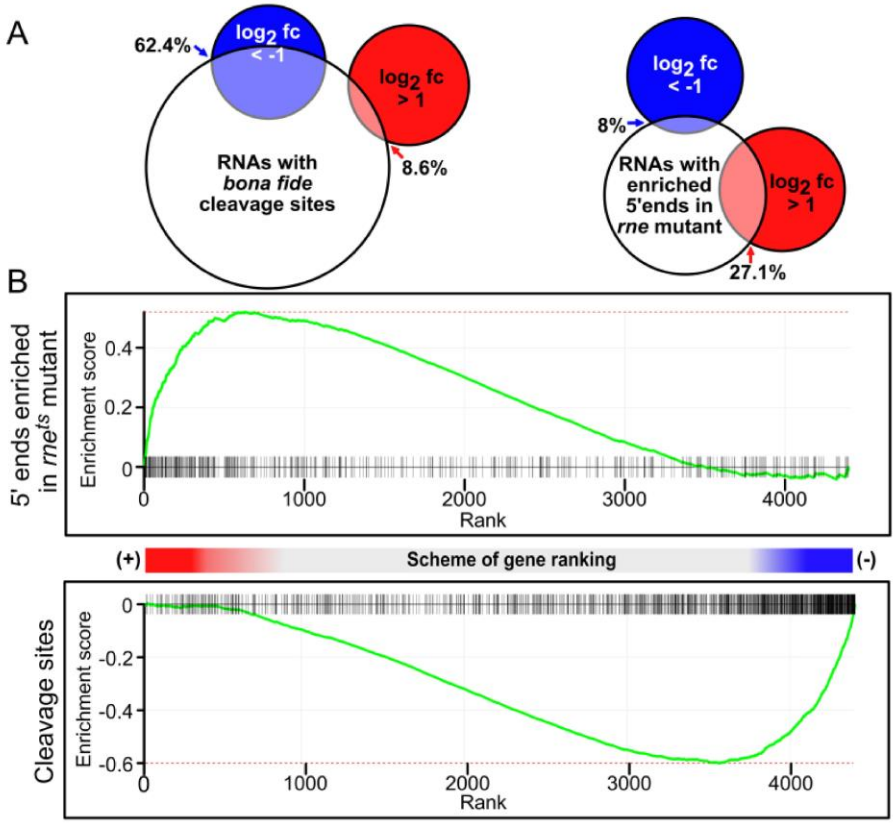

Figure 6. RNAs with cleavage sites significantly correlate with weakly expressed genes in the mutant under phototrophic conditions. (A) Overlap of significantly differentially expressed genes (mutant/wild type) with RNAs harbouring cleavage sites or enriched 5′ ends in the mutant under phototrophic conditions, including all RNAs with adjusted p-value <0.05 and $\log_2$ fold change >1 or <−1. (B) Gene set enrichment analysis (GSEA) including all genes of *R. sphaeroides*. The distribution of cleavage sites (bottom panel) or 5′ ends enriched in the mutant (top panel) within the DESeq2 ranked gene list was analysed. The RNAs were ranked based on their expression changes according to the Wald statistics calculated by DESeq2 between both strains under phototrophic conditions. Each black line represents an RNA. RNAs with highest expression (rne^{ts}_phototrophic/wt_phototrophic) are localized at the red end of the gene ranking scheme, whereas RNAs with lowest expression are localized at the blue end. The enrichment score is a running sum, which increases if an RNA possesses a cleavage site or mutant enriched 5′ end.

conditions. Interestingly, 62.4% of all RNAs with decreased levels in the mutant (adjusted p-value <0.05 and $\log_2$ fold change <−1) under phototrophic conditions contain RNase E cleavage sites (Figure 6A), while only 8.6% of the RNAs with increased expression in the mutant (adjusted p-value <0.05 and $\log_2$ fold change >1) under phototrophic conditions contain RNase E cleavage sites. A different result is seen for 5' ends that are enriched in the mutant: Only 8% of the RNAs with decreased levels in the mutant under phototrophic conditions contain enriched 5' ends in the mutant, while 27.1% of the RNAs with increased level contain enriched 5' ends. In addition, the median $\log_2$ fold change of all genes with mapped cleavage sites is about −0.4 (rne^{ts}_phototrophic/wt_phototrophic), while genes with enriched 5' ends in the mutant show a slight increase with a median $\log_2$ fold change of about 0.2 (Figure S5). Considering that we identified 1040 RNAs with cleavage sites and 436 RNAs with enriched 5' ends in the mutant under phototrophic conditions, these median $\log_2$ fold changes of such a number of RNAs are remarkable.

In order to further analyse the distribution of cleavage sites and enriched 5' ends in the mutant on a global scale, we performed a gene set enrichment analysis (GSEA) (Figure 6B). Here, we ranked all RNAs based on their expression change between rne^{ts} mutant and wild type under phototrophic conditions from maximal increased ratio (red) to maximal decreased ratio (blue) (Scheme of gene ranking), according to the DESeq2 analysis (Wald statistic). Next, we defined sets of RNAs based on association with cleavage sites or enriched 5' ends in the mutant, respectively. The enrichment score is a running sum, which increases if an RNA possesses an enriched 5' end in the mutant (top panel) or cleavage site (bottom panel), and decreases if an RNA does not possess any of both sites. Transcripts with and without cleavage sites are equally distributed among RNAs with highly increased expression in the mutant under phototrophic conditions (rank 0 to ~600) reflected by the straight line. Among the RNAs with ranks in between rank ~600 to ~3500 transcripts without cleavage sites dominate, leading to a decrease of the enrichment score. Among the RNAs with highest rank (rank

~3500 to ~4300; strongest decreased expression mutant versus wild type) many transcripts have cleavage sites, leading to a strong increase of the enrichment score. In conclusion, we compared both sets of RNAs with the ranked list and found both sets globally associated, with induced expression for enriched 5' ends in the mutant (p-value $<10^{-10}$) or reduced expression for cleavage sites (p-value $<10^{-10}$). These results show, that RNAs with diminished abundances in the mutant possess a particularly high amount of cleavage sites, which was also indicated as highly significant by hypergeometric test (enrichment over background distribution of cleavage sites: 6.23-fold; p-value $<2.2^{-16}$). *Vice versa*, RNAs with elevated abundances in the mutant were found to have a high number of 5' ends enriched in the mutant.

We also compared the number of cleavage sites and enriched 5' ends in each cluster of the heatmap to the mean distribution for each growth condition (Figure S6; Table S2). About 50% of the cleavage sites (cluster mean) of the mean background distribution were detected for cluster 6 transcripts under aerobic conditions but 2.7-fold (266%) more cleavage sites under microaerobic conditions, and even 7-fold (708%) more cleavage sites under phototrophic conditions (Figure S6; Table S2). Compared to the background mean over all transcripts, less enriched 5' ends were detected in cluster 3 (cluster mean) under aerobic and microaerobic conditions but almost twice as much 5' ends were enriched in phototrophic conditions (Figure S6; Table S2).

One concern in our analysis was that in general more RNase E cleavage sites and more enriched 5' ends in the mutant may be detected when the RNA levels between mutant and wild type show stronger variation. Cleavage sites may be mapped when transcript levels are much higher in the wild type than in the mutant and *vice versa* for enriched 5' ends in the mutant. This is already partially excluded by the GSEA shown in Figure 6, as also many cleavage sites are found in transcripts with increased levels in the mutant. Additionally, Figure S6 shows that such a correlation between expression change and number of cleavage sites is visible in some but not all cases. E. g. quite often both, cleavage sites and enriched 5' ends are increased under the same condition. Cluster 1 shows higher expression under phototrophic conditions in the mutant, but no cleavage sites are detected under phototrophic conditions. Cluster 8 shows similar expression in both strains under microaerobic conditions, but the number of enriched 5' ends in the mutant is 5-fold above background level.

To further exclude that the change of read number between wild type and mutant leads to changed levels in the detected 5' ends, we plotted the number of cleavage sites per RNA against the $\log_2$ fold change of the RNA between wild type and *rne*^{ts} mutant under phototrophic conditions. As seen in Figure S7 no correlation between the fold change of an RNA and the number of detected cleavage sites is visible. Taken these results together, we conclude that the accumulation or reduction of cleavage sites and enriched 5' ends in the mutant observed in the clusters is not an artefact of the analysis. Note that in contrast to the GSEA (Figure 6B), the analysis shown in Figure S7 does not include RNAs without cleavage sites.

Levels of mRNAs for regulators of photosynthesis and motility gene expression are affected by RNase E

The effect of RNase E on the level of a certain mRNA may be direct by the processing of this particular mRNA. Our results support some correlation between the presence of RNase E cleavage sites or enriched 5' ends and expression change between microaerobic and phototrophic growth conditions (Figure S5; Figure 6B). Another possibility is an indirect effect through RNase E-mediated cleavage of an mRNA for e.g. a transcriptional regulator of this RNA. The fact that some of the clusters defined in Figure 4A contain many mRNAs with similar function and/or transcribed from the same chromosomal locus, supports the presence of such indirect effects in addition to the direct effects. Therefore, we gave special attention to the effect of RNase E on mRNAs for known regulators of photosynthesis gene expression.

PrrB/PrrA (sensor kinase and response regulator of a two-component system), PpsR/AppA, and FnrL (transcriptional activator) are important protein regulators that affect expression of many photosynthesis genes (overview shown in Figure 7). Real-time RT-PCR quantification confirmed a reduction in the levels of *prrB* and *appA* mRNAs between *rne*^{ts} mutant versus wild type under phototrophic conditions (Figure 8). While the RNA-seq read coverage (Figure S9) showed similar abundances for the *appA* transcript in wild type under microaerobic and phototrophic conditions, *appA* mRNA was clearly less abundant in the *rne*^{ts} mutant under phototrophic conditions. The *prrB* transcript showed higher abundance under phototrophic conditions in the wild type but not or to a lesser extent in the mutant (Figure S8). Since PrrB as well as AppA are important regulators of photosynthesis gene expression, the effect of RNase E on their transcript levels will indirectly affect expression of many photosynthesis genes (Figure 7). As a result of PrrB/PrrA being activators and AppA an anti-repressor, higher levels of these proteins in the wild type will lead to stronger activation of photosynthesis genes in comparison to the mutant.

Although our study focused on the impact of RNase E on phototrophic growth, our data also revealed a strong influence of RNase E on genes of cluster 3, which was opposite to the effect seen on photosynthesis genes (Figure 4A,B) and includes many motility genes. Figs. 8 and S10 show that *rpoN2* mRNA is much more abundant in the mutant than in the wild type under phototrophic conditions. The alternative sigma factor RpoN2 is the master regulator of flagellar and motility genes [53–55], which are part of cluster 3 and show much stronger expression in the mutant under phototrophic conditions (Figure 4A).

How does RNase E affect mRNA levels of regulators of photosynthesis or motility genes?

Transcriptional start sites have been previously mapped for the *R. sphaeroides* transcriptome [37]. For the *appA* mRNA RNase E cleavage sites were mostly detected in the 5' UTR, which is transcribed from a promoter with the −35 region located around position 156.784. The screen shot in Figure S9

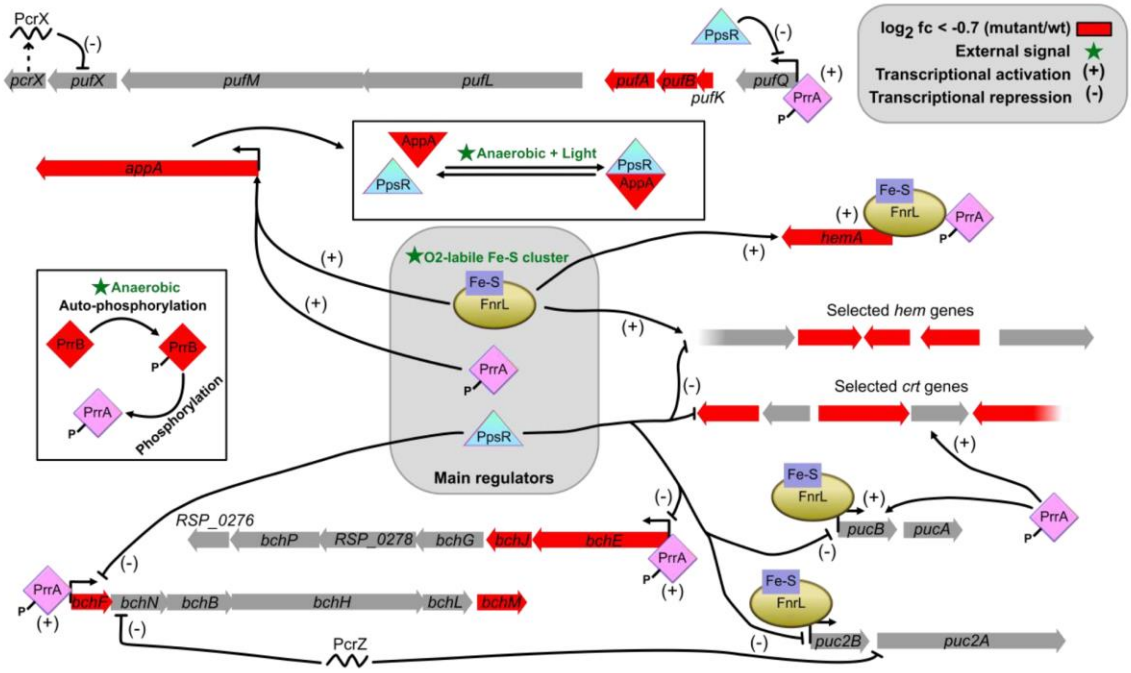

Figure 7. Schematic representation of the photosynthesis gene transcription regulation model in *R. sphaeroides*. The transcription of photosynthesis genes is controlled by multiple different activators and repressors to ensure a tight regulation upon changing environmental conditions. The regulation network consists of three main regulatory systems which are able to sense and signal changes in oxygen and light availability: (1) the activating PrrA/PrrB two component system senses oxygen availability, (2) the activator FnrL, which senses oxygen availability by an oxygen labile iron sulphur cluster, (3) the PpsR/AppA repressor/anti-repressor system which senses light and oxygen availability by a BLUF- and a SCHIC-domain, respectively, within the anti-repressor AppA. On post-transcriptional layer small regulatory RNAs (like PcrZ and PcrX) where found to fine-tune photosynthesis gene expression. RNAs with $\log_2$ fold change <−0.7 (*rne*^{ts}_phototrophic/wt_phototrophic) are marked in red colour.

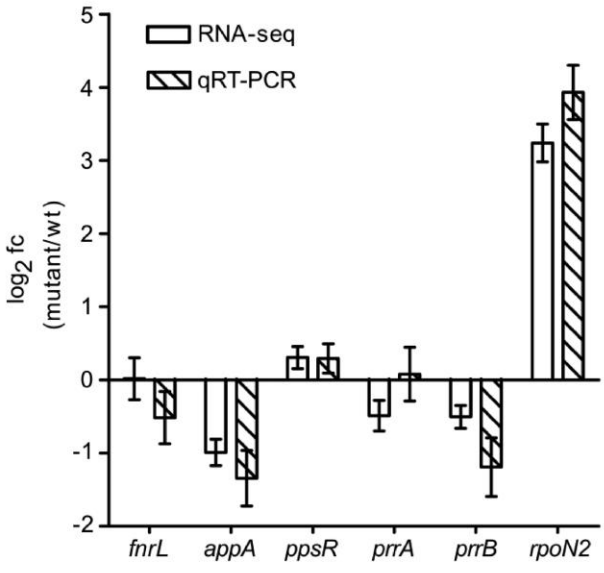

Figure 8. qRT-PCR for quantification ofmRNAs encoding transcriptional main regulators. Spike-in quantitative reverse transcriptase PCR with total RNA obtained from phototrophically grown wild type and *rne*^{ts} mutant. The relative abundances (mutant/wt) were calculated from independent biological triplicates.

shows that the distribution of RNase E cleavage sites differs between microaerobic and phototrophic conditions. Cleavage sites at positions 156.448, 156.587 and 156.478 were only mapped under phototrophic conditions. However, we cannot directly link cleavage site distribution to mRNA levels. Other cleavage sites were only mapped under microaerobic conditions. *prrB* is also transcribed from an own promoter with the −35 region around position 105.845 (Figure S8). The first two nucleotides of the *prrB* mRNA were mapped as RNase E cleavage sites, although the first nucleotide (transcription start site: TSS) is rather expected to be enriched in the *rne*^{ts} mutant, due to the impeded 5' end-dependent decay. In addition, RNase E cleavage sites are mapped to two further positions within the 5' UTR. Another RNase E cleavage site occurs only under phototrophic conditions at position 106.116 (Figure S8).

An influence of RNase E on the level of gene expression is likely to be due to an effect on transcript stability. To test this, we determined the half-lives of *appA* and *prrB*, in wild type and mutant under microaerobic and phototrophic growth (Figure 9). The half-life of *appA* under phototrophic conditions in the wild type was longer (about 4 min) than that in the *rne*^{ts} mutant (about 2 min 15 sec). The half-life of *prrB* was also clearly shorter under phototrophic conditions in the *rne*^{ts} mutant (1 min 35 sec) than in the wild type (about 3 min). Thus, both transcripts showed faster turn-over in the mutant under phototrophic conditions.

In agreement with the different expression patterns of cluster 6 and cluster 3 RNAs, the expression pattern of *rpoN2* mRNA is different from that of *appA* and *ppsR*: under phototrophic conditions *rpoN2* levels are much higher

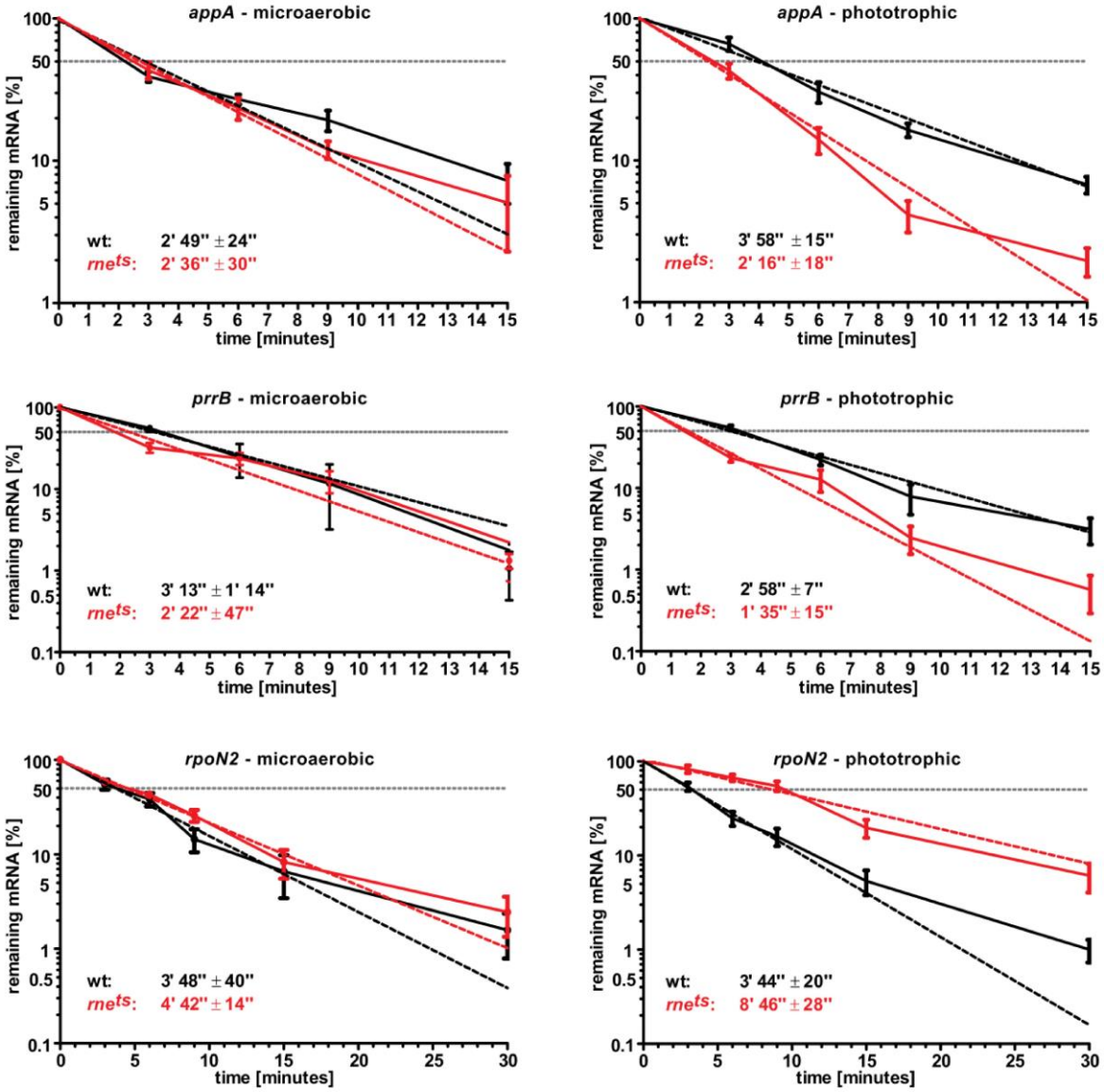

Figure 9. mRNA half-lives of *appA*, *prrB* and *rpoN2* under microaerobic and phototrophic growth conditions. The half-lives of mRNAs encoding important regulatory proteins for photosynthesis and motility were investigated under microaerobic and phototrophic conditions. Cultures were treated with 0.2 mg/ml rifampicin and samples were collected at the time points $t = 0$, 3, 6, 9, 15 and 30 minutes after addition of rifampicin. Total RNA was isolated using the hot phenol method, traces of DNA removed by DNase treatment and mRNA abundances relative to a spike-in RNA control of known sequence and quantity were determined by qRT-PCR using specific primers against *appA*, *prrB* or *rpoN2*. The decay of mRNA within biological triplicates of wild type (black) and *rne*^{ts} mutant (red) was fitted to semi-logarithmic trend lines (dashed lines). The standard deviation of the biological triplicates is shown as error bars. The calculated mRNA half-lives and their standard deviations are given in the bottom of each panel.

in the mutant. Our analysis revealed a strong enrichment of the TSS in the mutant exclusively under phototrophic conditions (Figure S10). In accordance with this observation the half-life of *rpoN2* is strongly increased in the mutant under phototrophic conditions (about 4 min 42 sec under microaerobic conditions, 8 min 46 sec in phototrophic conditions), while the half-life is the same under both growth conditions in the wild type (about 3 min 48 sec and 3 min 44 sec) (Figure 9). Higher RNA stability in the mutant can e.g. result from impeded 5' end-dependent degradation pathway. The opposite effects of RNase E (destabilizing versus stabilizing) during phototrophic growth on *appA*, *prrB* versus *rpoN2* expression correlates well with the different expression patterns of cluster 3 and cluster 6 mRNAs. Despite the distinct expression pattern of cluster 3 RNAs, we did not observe a clear effect of RNase E on the swimming motility of *R. sphaeroides* under phototrophic conditions (data not shown).

Concluding remarks and outlook

Although an impact of ribonucleases on the bacterial transcriptome is described in several studies (e.g. [15,56–61]), such strong effects of an RNase on certain growth conditions as observed for *R. sphaeroides* ([21]; Figure 2 this study) are rare. In *E. coli* inactivation of the *rne* gene results in loss of colony forming ability on solid media [62] and in filamentous growth in liquid culture [63]. The filamentous phenotype was attributed to an effect of RNase E on the FtsZ/FtsA ratio [64]. Furthermore, a role of RNases in stress response is well established [15,65–69].

The present study links expression patterns of mRNAs under different growth conditions to the action of RNase E. A certain distribution of cleavage sites and enriched 5' ends in the mutant in defined mRNA clusters contributes to the observed expression pattern of those mRNA clusters. Furthermore, the action of RNase E on mRNAs for regulatory proteins indirectly affects their regulons. Indeed, the effect of RNase E on expression of photosynthesis genes and their regulators fits to the observed growth phenotype. An open question remains, why RNase E cleavages and enriched 5' ends in the mutant show such variation under the different growth conditions?

Our differential expression analysis hints to higher *rne* mRNA levels under aerobic conditions compared to phototrophic conditions in the wild type (Figure 3C) and in the mutant strain (data not shown). However, the quantification of mRNA levels gives no information on the RNase E activities under different conditions and if RNase E level/activity would vary between aerobic and phototrophic growth conditions, we should see a similar effect on all mRNAs that are recognized by RNase E, which is not the case. Nevertheless, we established a reporter assay to test for RNase E activity under different growth conditions. A short 89 nt sequence containing a well-defined RNase E recognition site was cloned in front of the mVenus reporter gene (Figure S2). This construct was transferred to the wild type and the *rne*^{ts} cells by diparental conjugation and the resulting fluorescence was determined under the different growth conditions. The fluorescence caused by this construct was compared to the reporter construct without the newly incorporated RNase E cleavage site to include all putative effects of RNase E on other parts of the resulting mRNA. In the wild type strain the reporter with cleavage site showed much less activity than the control under all conditions (Figure 10). This difference was much smaller in the *rne*^{ts} mutant. Figure 10 demonstrates that the biggest influence of RNase E on the activity of the reporter is seen under phototrophic conditions (about 6.8-fold difference between wild type and mutant; aerobic and microaerobic growth: about 3-fold difference). We cannot make confident conclusions about the total RNase activities under the different conditions, since the growth conditions also influence the activity of the reporter protein, but it is clear that phototrophic conditions differ from chemotrophic conditions in the ratio of RNase E activity in wild type and *rne*^{ts} mutant. These strong differences in activity may well account for the strong effect of reduced RNase E activity especially during phototrophic growth but does not explain that not all RNAs with RNase E cleavage sites are affected.

It is also conceivable that the growth conditions affect RNA structure and subsequently substrate recognition by RNase E. Such changes may be influenced by the sequence and may thus be very different for individual RNAs. We also have to consider that not only ribonuclease and substrate are involved in the cleavage process. It was reported that the composition and activity of the degradosome complex in *R. capsulatus* vary under different oxygen concentrations [23]. Since the degradosome complexes in *E. coli* and *R. sphaeroides* vary, the oxygen condition may have different influence on the composition and activity of the degradosome in the *rne*^{ts} mutant. Due to the binding of the *E. coli* enzyme to the cytoplasmic membrane, intracellular membranes may also have different effects on the activity of the degradosomes in the wild type and the *rne*^{ts} strain. However, as not only phototrophic cells but also microaerobic cells are full of

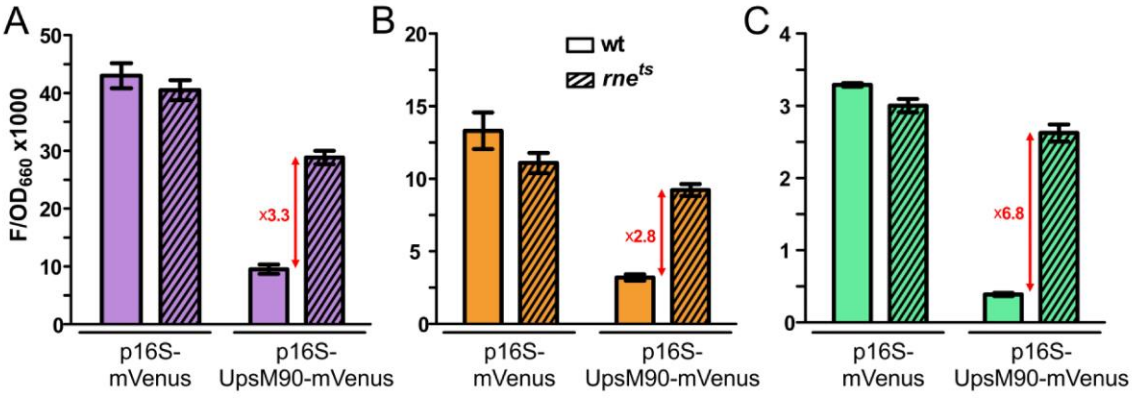

Figure 10. RNase E activity reporter measurements under aerobic, microaerobic and phototrophic growth conditions. The fluorescence intensity of mVenus was measured in biological triplicates *in vivo* under aerobic (A), microaerobic (B) and phototrophic (C) conditions, normalized by subtraction of the background fluorescence from an empty vector control and divided to the optical density OD_{660}. The standard deviations are given as error bars. Cells carrying the plasmid pPHU-p16s-mVenus represent a control, where the mVenus open reading frame is under transcriptional control of the constitutive 16S rRNA promoter from *R. sphaeroides*. pPHU-p16S-Upsm90-mVenus was used to assess RNase E activity by introduction of an 89 nt 5′ UTR directly upstream of the mVenus open reading frame, harbouring a well characterized RNase E cleavage site originating from the small RNA UpsM of *R. sphaeroides*.

intracytoplasmic membrane vesicles, this is unlikely to account for the higher number of RNase E cleavage sites under phototrophic conditions.

It is also conceivable that the substitution of the native *R. sphaeroides rne* gene by a variant of the gammaproteobacterium *E. coli* contributes to the disruption of posttranscriptional gene expression regulation. As mentioned above, this could be due to the different architectures of the two enzymes (presence of the membrane targeting sequence and variances in protein interaction sites on the scaffold domain), but also to different activities of the catalytic RNase domains. Differentially specialized substrate recognition may be a possible factor that can lead to defective RNA processing. However, our analyses revealed that the vast majority of 5' end positions are identical in both strains. As the bacterial RNA degradosome is a very complex machinery, it is hard to distinguish between distinct effects of the single components (RNase E interaction partners or catalysis by RNase E itself) in our analysis.

Additionally, RNA chaperones like Hfq [70–72] or CsrA [73] play an important role in RNase E-mediated cleavage as well as adapter proteins like RapZ [74] or RNase E inhibitors like RraA in *E. coli* [75]. An *R. sphaeroides* strain lacking the Hfq protein has a pleiotropic phenotype including altered pigmentation and photooxidative stress resistance [76]. Recently, the DUF1127 protein CcaF1 was identified as a new type of RNA binding protein in *R. sphaeroides* and shown to assist in RNase E-dependent RNA processing [31]. CcaF1 has an important function in stress defence. *hfq* and *ccaF1* mRNA levels were similar under microaerobic and phototrophic conditions. We conclude that an effect of these RNA-binding proteins on RNase E mediated cleavage is unlikely to account for the observed growth-dependent effects of RNase E on the transcriptome, but cannot exclude post-transcriptional regulation of *hfq* or *ccaF1* expression. A second DUF1127 protein of *R. sphaeroides*, RSP_0557, was also shown to bind to many RNAs and to affect their levels [31]. Under phototrophic conditions RSP_0557 mRNA levels are much higher than under microaerobic and aerobic growth in the wild type. In the mutant, similar low RSP_0557 mRNA levels are observed under both conditions. Therefore, RSP_0557 may be a candidate for a mediator of growth-dependent RNA cleavage for a specific set of transcripts. Interestingly, the RSP_0557 mRNA (about 340 nt) possesses one of the highest *bona fide* RNase E cleavage site densities under phototrophic growth conditions (12 cleavage sites), and contains considerably less cleavage sites under microaerobic conditions (two cleavage sites) (Figure S11). An influence of RSP_0557 abundance on RNase E-dependent cleavage and of RNase E on RSP_0557 abundance would constitute a feed-back mechanism. Such regulatory loops put considerable constrains to the analysis of the role of individual components in a network. It is known, that RSP_0557 expression is controlled by the RpoHI/HII alternative sigma factors [77]. As a consequence, RSP_0557 mRNA increases during transition to stationary phase [42], in response to high oxygen levels, and under heat stress [78]. Thus, growth conditions influence RSP_0557 levels also independently of RNase E. The role of RSP_0557 as RNA chaperone requires, however, further analyses.

It is unlikely that the exact mechanisms behind the influence of growth conditions on RNase E-mediated cleavage can be identified by global studies. It will be necessary to select some RNase E substrates and to include different mutants for ribonucleases, transcriptional regulators and RNA-binding proteins. Unfortunately, it will not be possible to use defined *in vitro* systems for such studies. While the *in vitro* systems can limit the number of involved RNAs and proteins, they do not allow to look at the effect of environmental factors and growth conditions.

In summary, our data set provides insights into direct (RNase E-mediated RNA processing) and indirect (RNase E-dependent abundance of transcriptional regulators) effects that contribute to the strong impact of RNase E on growth under different environmental conditions. Especially the effect of RNase E on the stability of RNAs for important regulators of photosynthesis genes indirectly affects the expression of many photosynthesis genes and consequently the formation of photosynthetic complexes and phototrophic growth. The study underlines the importance of RNases in the adaptation of bacteria to changing growth conditions.

Acknowledgments

We thank Daniel-Timon Spanka for initial read mapping and DESeq2 analysis, Andreas Jäger for technical support, Konrad Förstner and Muhammad Elhossary for advice and discussion, and Tilman Borggrefe for financial support. We thank the Core Unit Systems Medicine at the University of Würzburg, particularly Panagiota Arampatzi and Elena Katzowitsch, for support with the cDNA library preparation and RNA-seq.

Data availability statement

The FASTQ files of all replicates from RNA sequencing are available in the NCBI Gene Expression Omnibus (GEO) repository [79] with the accession number GSE200990. https://ncbi.nlm.nih.gov/geo/query/acc.cgi?acc=GSE200990

Disclosure statement

No potential conflict of interest was reported by the authors.

Funding

Deutsche Forschungsgemeinschaft [Kl 561/41-1, RTG 2355]; IZKF at the University Würzburg [project Z-6]. Funding for open access charge: Deutsche Forschungsgemein-schaft/University of Giessen

ORCID

Janek Börner http://orcid.org/0000-0003-4824-9393
Tobias Friedrich http://orcid.org/0000-0003-4014-8678
Marek Bartkuhn http://orcid.org/0000-0001-6872-9082
Gabriele Klug http://orcid.org/0000-0002-3527-5093

References

[1] Hördt A, López MG, Meier-Kolthoff JP, et al. Analysis of 1,000+ type-strain genomes substantially improves taxonomic classification of alphaproteobacteria. Front Microbiol. 2020;11:468.

[2] Shimada H, Iba K, Takamiya K. Blue-light irradiation reduces the expression of *puf* and *puc* Operons of *Rhodobacter sphaeroides* under semi-aerobic conditions. Plant Cell Physiol. 1992;33:471–475.

[3] Braatsch S, Gomelsky M, Kuphal S, et al. A single flavoprotein, AppA, integrates both redox and light signals in *Rhodobacter sphaeroides*. Mol Microbiol. 2002;45:827–836.

[4] Anthony JR, Newman JD, Donohue TJ. Interactions between the *Rhodobacter sphaeroides* ECF sigma factor, sigma(e), and its anti-sigma factor, ChrR. J Mol Biol. 2004;341:345–360.

[5] Nuss AM, Glaeser J, Klug G. RpoH(II) activates oxidative-stress defense systems and is controlled by RpoE in the singlet oxygen-dependent response in *Rhodobacter sphaeroides*. J Bacteriol. 2009;191:220–230.

[6] Nuss AM, Glaeser J, Berghoff BA, et al. Overlapping alternative sigma factor regulons in the response to singlet oxygen in *Rhodobacter sphaeroides*. J Bacteriol. 2010;192:2613–2623.

[7] Dufour YS, Imam S, Koo BM, et al. Convergence of the transcriptional responses to heat shock and singlet oxygen stresses. PLoS Genet. 2012;8:e1002929.

[8] Bathke J, Konzer A, Remes B, et al. Comparative analyses of the variation of the transcriptome and proteome of *Rhodobacter sphaeroides* throughout growth. BMC Genomics. 2019;20:358.

[9] Klug G, Adams CW, Belasco J, et al. Biological consequences of segmental alterations in mRNA stability: effects of deletion of the intercistronic hairpin loop region of the *Rhodobacter capsulatus puf* operon. Embo J. 1987;6:3515–3520.

[10] Mank NN, Berghoff BA, Hermanns YN, et al. Regulation of bacterial photosynthesis genes by the small noncoding RNA PcrZ. Proc Natl Acad Sci U S A. 2012;109:16306–16311.

[11] Billenkamp F, Peng T, Berghoff BA, et al. A cluster of four homologous small RNAs modulates C1 metabolism and the pyruvate dehydrogenase complex in *Rhodobacter sphaeroides* under various stress conditions. J Bacteriol. 2015;197:1839–1852.

[12] Eisenhardt KMH, Reuscher CM, Klug G. PcrX, an sRNA derived from the 3'- UTR of the *Rhodobacter sphaeroides puf* operon modulates expression of *puf* genes encoding proteins of the bacterial photosynthetic apparatus. Mol Microbiol. 2018;110:325–334.

[13] Reuscher CM, Klug G. Antisense RNA asPcrL regulates expression of photosynthesis genes in *Rhodobacter sphaeroides* by promoting RNase III-dependent turn-over of *puf* mRNA. RNA Biol. 2021;18:1445–1457.

[14] Grützner J, Remes B, Eisenhardt KMH, et al. sRNA-mediated RNA processing regulates bacterial cell division. Nucleic Acids Res. 2021;49:7035–7052.

[15] Spanka DT, Reuscher CM, Klug G. Impact of PNPase on the transcriptome of *Rhodobacter sphaeroides* and its cooperation with RNase III and RNase E. BMC Genomics. 2021;22:106.

[16] Chen CYA, Beatty TJ, Cohen SN, et al. An intercistronic stem-loop structure functions as an mRNA decay terminator necessary but insufficient for *puf* mRNA stability. Cell. 1988;52:609–619.

[17] Klug G, Cohen SN. Combined actions of multiple hairpin loop structures and sites of rate-limiting endonucleolytic cleavage determine differential degradation rates of individual segments within polycistronic *puf* operon mRNA. J Bacteriol. 1990;172:5140–5146.

[18] Evguenieva-Hackenberg E, Klug G. Chapter 7 RNA degradation in archaea and gram-negative bacteria different from *Escherichia coli*. In: Condon C, editor. Progress in molecular biology and translational science. Amsterdam, Boston: Elsevier Academic Press; 2009. pp. 275–317.

[19] Chidgey JW, Jackson PJ, Dickman MJ, et al. PufQ regulates porphyrin flux at the haem/bacteriochlorophyll branchpoint of tetrapyrrole biosynthesis via interactions with ferrochelatase. Mol Microbiol. 2017;106:961–975.

[20] Klug G. A DNA sequence upstream of the *puf* operon of *Rhodobacter capsulatus* is involved in its oxygen-dependent regulation and functions as a protein binding site. Mol Gen Genet. 1991;226:167–176.

[21] Förstner KU, Reuscher CM, Haberzettl K, et al. RNase E cleavage shapes the transcriptome of *Rhodobacter sphaeroides* and strongly impacts phototrophic growth. Life Sci Alliance. 2018;1: e201800080.

[22] Carpousis AJ, Campo N, Hadjeras L, et al. Compartmentalization of RNA degradosomes in bacteria controls accessibility to substrates and ensures concerted degradation of mRNA to nucleotides. Annu Rev Microbiol. 2022;76:533–552.

[23] Jäger S, Hebermehl M, Schiltz E, et al. Composition and activity of the *Rhodobacter capsulatus* degradosome vary under different oxygen concentrations. J Mol Microbiol Biotechnol. 2004;7:148–154.

[24] Golecki JR, Oelze J. Differences in the architecture of cytoplasmic and intracytoplasmic membranes of three chemotrophically and phototrophically grown species of the Rhodospirillaceae. J Bacteriol. 1980;144:781–788.

[25] Aït-Bara S, Carpousis AJ. RNA degradosomes in bacteria and chloroplasts: classification, distribution and evolution of RNase E homologs. Mol Microbiol. 2015;97:1021–1135.

[26] van Niel CB. The culture, general physiology, morphology, and classification of the non-sulfur purple and brown bacteria. Bacteriol Rev. 1944;8:1–118.

[27] Weber L, Thoelken C, Volk M, et al. The conserved Dcw gene cluster of *R. sphaeroides* is preceded by an uncommonly extended 5' leader featuring the sRNA UpsM. PLoS ONE. 2016;11: e0165694.

[28] Remes B, Berghoff BA, Förstner KU, et al. Role of oxygen and the OxyR protein in the response to iron limitation in *Rhodobacter sphaeroides*. BMC Genomics. 2014;15:794.

[29] Janzon L, Löfdahl S, Arvidson S. Evidence for a coordinate transcriptional control of alpha-toxin and protein a synthesis in *Staphylococcus aureus*. FEMS Microbiol Lett. 1986;33:193–198.

[30] Damm K, Bach S, Müller KMH, et al. Impact of RNA isolation protocols on RNA detection by Northern blotting. Methods Mol Biol. 2015;1296:29–38.

[31] Grützner J, Billenkamp F, Spanka D-T, et al. The small DUF1127 protein CcaF1 from *Rhodobacter sphaeroides* is an RNA-binding protein involved in sRNA maturation and RNA turnover. Nucleic Acids Res. 2021;49:3003–3019.

[32] Pfaffl MW. A new mathematical model for relative quantification in real-time RT-PCR. Nucleic Acids Res. 2001;29:e45.

[33] Förstner KU, Vogel J, Sharma CM. Reademption - a tool for the computational analysis of deep-sequencing-based transcriptome data. Bioinformatics. 2014;30:3421–3423.

[34] R Core Team. A language and environment for statistical computing. Vienna, Austria: R foundation of statistical computing; 2021.

[35] Backman TWH, Girke T. systemPipeR: NGS workflow and report generation environment. BMC Bioinf. 2016;17:388.

[36] Love MI, Huber W, Anders S. Moderated estimation of fold change and dispersion for RNA-seq data with DESeq2. Genome Biol. 2014;15:550.

[37] Remes B, Rische-Grahl T, Müller KMH, et al. An RpoHI-dependent response promotes outgrowth after extended stationary phase in the Alphaproteobacterium *Rhodobacter sphaeroides*. J Bacteriol. 2017;199.

[38] Quinlan AR, Hall IM. Bedtools: a flexible suite of utilities for comparing genomic features. Bioinformatics. 2010;26:841–842.

[39] Korotkevich G, Sukhov V, Budin N, et al. Fast gene set enrichment analysis. bioRxiv. 2016 [2021 Feb 1]. pre-print: not peer-reviewed. DOI:10.1101/060012

[40] Benjamini Y, Hochberg Y. Controlling the false discovery rate: a practical and powerful approach to multiple testing. J R Stat Soc Ser B Methodol. 1995;57:289–300.

[41] Liao Y, Smyth GK, Shi W. The R package Rsubread is easier, faster, cheaper and better for alignment and quantification of RNA sequencing reads. Nucleic Acids Res. 2019;47:e47.

[42] McIntosh M, Eisenhardt K, Remes B, et al. Adaptation of the Alphaproteobacterium *Rhodobacter sphaeroides* to stationary phase. Environ Microbiol. 2019;21:4425–4445.

[43] Simon R, Priefer U, Pühler A. A broad host range mobilization system for *in vivo* genetic engineering: transposon mutagenesis in gram negative bacteria. Biotechnology. 1983;1:784–791.
[44] Pappas CT, Sram J, Moskvin OV, et al. Construction and validation of the *Rhodobacter sphaeroides* 2.4.1 DNA microarray: transcriptome flexibility at diverse growth modes. J Bacteriol. 2004;186:4748–4758.
[45] Klug G. Beyond catalysis: vitamin B12 as a cofactor in gene regulation. Mol Microbiol. 2014;91:635–640.
[46] Karls RK, Brooks J, Rossmeissl P, et al. Metabolic roles of a *Rhodobacter sphaeroides* member of the sigma32 family. J Bacteriol. 1998;180:10–19.
[47] Peng T, Berghoff BA, Oh JI, et al. Regulation of a polyamine transporter by the conserved 3' UTR-derived sRNA SorX confers resistance to singlet oxygen and organic hydroperoxides in *Rhodobacter sphaeroides*. RNA Biol. 2016;13:988–999.
[48] Srivastava AK, Schlessinger D. Mechanism and regulation of bacterial ribosomal RNA processing. Annu Rev Microbiol. 1990;44:105–129.
[49] Evguenieva-Hackenberg E. Bacterial ribosomal RNA in pieces. Mol Microbiol. 2005;57:318–325.
[50] Deutscher MP. Chapter 9 Maturation and degradation of ribosomal RNA in bacteria. In: Condon C, editor. Progress in molecular biology and translational science. Amsterdam, Boston: Elsevier Academic Press; 2009. pp. 369–391.
[51] Rische T, Klug G. The ordered processing of intervening sequences in 23S rRNA of *Rhodobacter sphaeroides* requires RNase J. RNA Biol. 2012;9:343–350.
[52] Roh JH, Smith WE, Kaplan S. Effects of oxygen and light intensity on transcriptome expression in *Rhodobacter sphaeroides* 2.4.1. Redox active gene expression profile. J Biol Chem. 2004;279:9146–9155.
[53] Poggio S, Osorio A, Dreyfus G, et al. The four different sigma(54) factors of *Rhodobacter sphaeroides* are not functionally interchangeable. Mol Microbiol. 2002;46:75–85.
[54] Poggio S, Osorio A, Dreyfus G, et al. Transcriptional specificity of RpoN1 and RpoN2 involves differential recognition of the promoter sequences and specific interaction with the cognate activator proteins. J Biol Chem. 2006;281:27205–27215.
[55] Vega-Baray B, Domenzain C, Rivera A, et al. The flagellar set Fla2 in *Rhodobacter sphaeroides* is controlled by the CckA pathway and is repressed by organic acids and the expression of Fla1. J Bacteriol. 2015;197:833–847.
[56] Le Rhun A, Lécrivain AL, Reimegård J, et al. Identification of endoribonuclease specific cleavage positions reveals novel targets of RNase III in *Streptococcus pyogenes*. Nucleic Acids Res. 2017;45:2329–2340.
[57] Altuvia Y, Bar A, Reiss N, et al. *In vivo* cleavage rules and target repertoire of RNase III in *Escherichia coli*. Nucleic Acids Res. 2018;46:10380–10394.
[58] Broglia L, Lécrivain A-L, Renault TT, et al. An RNA-seq based comparative approach reveals the transcriptome-wide interplay between 3'-to-5' exoRnases and RNase Y. Nat Commun. 2020;11:1587.
[59] Duggal Y, Fontaine BM, Dailey DM, et al. RNase I modulates *Escherichia coli* motility, metabolism, and resistance. ACS Chem Biol. 2020;15:1996–2004.
[60] Hoffmann UA, Heyl F, Rogh SN, et al. Transcriptome-wide *in vivo* mapping of cleavage sites for the compact cyanobacterial ribonuclease E reveals insights into its function and substrate recognition. Nucleic Acids Res. 2021;49:13075–13091.
[61] Ifill G, Blimkie T, Lee AHY, et al. RNase III and RNase E influence posttranscriptional regulatory networks involved in virulence factor production, metabolism, and regulatory RNA processing in *Bordetella pertussis*. mSphere. 2021;6:e0065021.
[62] Deana A, Belasco JG. The function of RNase G in *Escherichia coli* is constrained by its amino and carboxyl termini. Mol Microbiol. 2004;51:1205–1217.
[63] Goldblum K, Apririon D. Inactivation of the ribonucleic acid-processing enzyme ribonuclease E blocks cell division. J Bacteriol. 1981;146:128–132.
[64] Tamura M, Lee K, Miller CA, et al. RNase E maintenance of proper FtsZ/FtsA ratio required for nonfilamentous growth of *Escherichia coli* cells but not for colony-forming ability. J Bacteriol. 2006;188:5145–5152.
[65] Goverde RL, Huis In't Veld JH, Kusters JG, et al. The psychrotrophic bacterium *Yersinia enterocolitica* requires expression of *pnp*, the gene for polynucleotide phosphorylase, for growth at low temperature (5 degrees C). Mol Microbiol. 1998;28:555–569.
[66] Apura P, Lorenzo VD, Arraiano CM, et al. Ribonucleases control distinct traits of *Pseudomonas putida* lifestyle. Environ Microbiol. 2021;23:174–189.
[67] Manasherob R, Miller C, Kim K, et al. Ribonuclease E modulation of the bacterial SOS response. PLoS ONE. 2012;7:e38426.
[68] Rosenzweig JA, Chopra AK. The exoribonuclease Polynucleotide Phosphorylase influences the virulence and stress responses of yersiniae and many other pathogens. Front Cell Infect Microbiol. 2013;3:81.
[69] Lejars M, Hajnsdorf E. RNase III participates in the adaptation to temperature shock and oxidative stress in *Escherichia coli*. Microorganisms. 2022;10:699.
[70] Vogel J, Luisi BF. Hfq and its constellation of RNA. Nat Rev Microbiol. 2011;9:578–589.
[71] Sauer E. Structure and RNA-binding properties of the bacterial LSm protein Hfq. RNA Biol. 2013;10:610–618.
[72] Wagner EGH. Cycling of RNAs on Hfq. RNA Biol. 2013;10:619–626.
[73] Stenum TS, Holmqvist E. CsrA enters Hfq's territory: regulation of a base-pairing small RNA. Mol Microbiol. 2022;117:4–9.
[74] Göpel Y, Papenfort K, Reichenbach B, et al. Targeted decay of a regulatory small RNA by an adaptor protein for RNase E and counteraction by an anti-adaptor RNA. Genes Dev. 2013;27:552–564.
[75] Lee K, Zhan X, Gao J, et al. RraA: a protein inhibitor of RNase E activity that globally modulates RNA abundance in *E. coli*. Cell. 2003;114:623–634.
[76] Berghoff BA, Glaeser J, Sharma CM, et al. Contribution of Hfq to photooxidative stress resistance and global regulation in *Rhodobacter sphaeroides*. Mol Microbiol. 2011;80:1479–1495.
[77] Müller KMH, Berghoff BA, Eisenhardt BD, et al. Characteristics of Pos19 - a small coding RNA in the oxidative stress response of *Rhodobacter sphaeroides*. PLoS ONE. 2016;11:e0163425.
[78] McIntosh M, Köchling T, Latz A, et al. A major checkpoint for protein expression in *Rhodobacter sphaeroides* during heat stress response occurs at the level of translation. Environ Microbiol. 2021;23:6483–6502.
[79] Edgar R, Domrachev M, Lash AE. Gene Expression Omnibus: NCBI gene expression and hybridization array data repository. Nucleic Acids Res. 2002;30:207–210.

Received: 21 July 2023 | Revised: 21 September 2023 | Accepted: 26 September 2023

DOI: 10.1111/mmi.15181

RESEARCH ARTICLE

WILEY

RNase III participates in control of quorum sensing, pigmentation and oxidative stress resistance in *Rhodobacter sphaeroides*

Janek Börner [1] | Tobias Friedrich [2,3] | Gabriele Klug [1]

[1]Institute of Microbiology and Molecular Biology, Justus-Liebig-University Giessen, Giessen, Germany

[2]Biomedical Informatics and Systems Medicine, Justus-Liebig-University Giessen, Giessen, Germany

[3]Institute of Biochemistry, Justus-Liebig-University Giessen, Giessen, Germany

Correspondence
Gabriele Klug, Institute of Microbiology and Molecular Biology, Justus-Liebig-University Giessen, Heinrich-Buff-Ring 26-32, Giessen 35392, Germany.
Email: gabriele.klug@mikro.bio.uni-giessen.de

Funding information
Deutsche Forschungsgemeinschaft, Grant/Award Number: KI563/41-1

Abstract

RNase III is a dsRNA-specific endoribonuclease, highly conserved in bacteria and eukarya. In this study, we analysed the effects of inactivation of RNase III on the transcriptome and the phenotype of the facultative phototrophic α-proteobacterium *Rhodobacter sphaeroides*. RNA-seq revealed an unexpectedly high amount of genes with increased expression located directly downstream to the rRNA operons. Chromosomal insertion of additional transcription terminators restored wild type-like expression of the downstream genes, indicating that RNase III may modulate the rRNA transcription termination in *R. sphaeroides*. Furthermore, we identified RNase III as a major regulator of quorum-sensing autoinducer synthesis in *R. sphaeroides*. It negatively controls the expression of the autoinducer synthase CerI by reducing *cerI* mRNA stability. In addition, RNase III inactivation caused altered resistance against oxidative stress and impaired formation of photosynthetically active pigment-protein complexes. We also observed an increase in the CcsR small RNAs that were previously shown to promote resistance to oxidative stress. Taken together, our data present interesting insights into RNase III-mediated regulation and expand the knowledge on the function of this important enzyme in bacteria.

KEYWORDS
bacterial photosynthesis, quorum sensing, *Rhodobacter*, riboregulation, RNase III, stress response

1 | INTRODUCTION

For many years, it was assumed that in bacteria regulation of gene expression occurs nearly exclusively on the levels of transcription and translation, however, the last decades have unveiled the crucial role of riboregulation. Riboregulation describes the action of ribonucleases, noncoding regulatory RNAs and RNA-binding proteins that often influence gene expression by stabilisation or destabilisation of messenger RNAs, which consequently affects the translatome and thereby the proteome. Bacteria use riboregulation to quickly and cost-efficiently adapt gene expression to changing environmental conditions, which is reflected by generally much shorter RNA half-lives (often in a range of minutes) in bacteria, compared to eukaryotes (often in a range of hours) (Belasco & Brawerman, 1993).

While being first discovered in *Escherichia coli* in 1967 (Robertson et al., 1967, 1968), RNase III was intensely studied in

the following years for its ability to specifically cleave double-stranded RNA (dsRNA) substrates. The physiological functions of RNase III were described mainly in the maturation of the ribosomal RNA (Dunn & Studier, 1973; Nikolaev et al., 1973) and processing of viral RNA (Westphal & Crouch, 1975). In many α-proteobacteria, RNase III is also responsible for the fragmentation of the 23S rRNA (Evguenieva-Hackenberg & Klug, 2000). Genome-sequencing approaches revealed that the enzyme is highly conserved not only in bacteria, but homologues are present in nearly every living organism, except of many archaeal species (Nicholson, 2014). Prokaryotic members of the RNase III family have a simple architecture, often only consisting of a catalytically active C-terminal RNase III Domain (RIIID) and an N-terminal dsRNA binding domain. Eukaryotic members of the RNase III family can possess two RIIID (Drosha and Dicer) and additionally, a helicase and a PAZ (Piwi Argonaute Zwille) domain (Dicer), which are used to establish RNA–RNA interactions for gene silencing via RNA interference (Carmell & Hannon, 2004; Court et al., 2013; Kang & Hata, 2012).

A well-studied example of the direct action of RNase III on mRNAs is the processing of the *pnp* transcript in many bacteria (Carzaniga et al., 2009; Gatewood et al., 2011; Portier et al., 1987; Régnier & Grunberg-Manago, 1990; Snow et al., 2020). The *pnp* mRNA encodes the polynucleotide phosphorylase (PNPase), an important exoribonuclease with 3′ to 5′ phosphorolytic activity. As a primary transcript *pnp* harbours a stabilising 5′ RNA structure and is highly stable resulting in frequent translation. However, degradation of the *pnp* transcript is initiated through recognition of the 5′ RNA structure by RNase III and followed by dsRNA cleavage. Subsequently, one strand of the opened 5′ double-strand structure is removed by PNPase, resulting in a single-stranded 5′ end region of *pnp* accessible for RNase E-mediated degradation.

In particular, the development of low-cost high throughput RNA sequencing (RNA-seq) methods in the beginning of the early 2000s and its applications revealed new functions of RNase III. RNase III was previously known to primarily affect maturation of ribosomal and transfer RNAs, but the spectrum of other RNAs recognised by RNase III has been largely expanded in the last decades (Altuvia et al., 2018; Gatewood et al., 2012; Ifill et al., 2021; Rath et al., 2017).

Moreover, the discovery of a variety of novel regulatory non-coding RNAs through RNA-seq has rekindled interest in RNase III. Non-coding regulatory RNAs are part of the riboregulation network and were not only described in bacteria (in bacteria called sRNAs) but also in numerous other organisms (reviewed in Jørgensen et al., 2020; Mahendran et al., 2022; Papenfort & Melamed, 2023; Storz et al., 2011). sRNAs can exert their regulatory effects on gene expression by specific base pairing with their target mRNAs, and thereby form RNA–RNA duplexes, which are often recognised by RNase III as a substrate (Lioliou et al., 2012; McKellar et al., 2022; Mediati et al., 2022). While a direct action of RNase III in sRNA-mediated regulation of plasmid copy numbers was already described quite early (Blomberg et al., 1990; Conrad & Campbell, 1979), other established functions of RNase III acting on sRNA-mediated regulation were found in regulation of type I toxin-antitoxin systems (Gerdes et al., 1992; Vogel et al., 2004), stress responses (Afonyushkin et al., 2005; Lalaouna et al., 2019; Opdyke et al., 2011) or virulence of pathogenic bacteria (Boisset et al., 2007; Huntzinger et al., 2005; Romby et al., 2006).

We discovered several small regulatory RNAs (sRNAs) (Berghoff et al., 2009), which affect important physiological processes like, for example, growth and cell division (Grützner, Remes, et al., 2021), stress resistance (Adnan et al., 2015; Billenkamp et al., 2015; Müller et al., 2016; Peng et al., 2016) and formation of photosynthesis complexes (Eisenhardt et al., 2018; Mank et al., 2012; Reuscher & Klug, 2021) in the model organism *Rhodobacter sphaeroides* (recently renamed to *Cereibacter sphaeroides*, Hördt et al., 2020). *R. sphaeroides* is a gram-negative purple non-sulphur bacterium with versatile metabolism, able to live under a variety of different environmental conditions, which makes it a well-suited model to study adjustment of gene expression to changing environmental conditions.

To investigate the functional role of RNase III in *R. sphaeroides*, especially its impact on regulation of gene expression, we inactivated the catalytic activity of RNase III by exchanging two highly conserved amino acids (G48S, D49R) within the active centre of the native enzyme. An obvious effect of the RNase III deficiency was pronounced in a drastically reduced photopigment production. Moreover, we could observe increased cell survival rates of the mutant upon oxidative stress exposure, which are accompanied by elevated expression of CcsR sRNAs, which counteract oxidative stress through negative regulation of a glutathione-dependent metabolic pathway, leading to accumulation of antioxidative glutathione. Strikingly, we found a novel regulatory function of RNase III in the quorum-sensing system of *R. sphaeroides*, where RNase III negatively controls the expression of the quorum-sensing autoinducer synthase (*cerI*) by mRNA destabilisation, consequently resulting in reduced autoinducer production. Interestingly, lack of RNase III activity does not only affect 23S rRNA fragmentation but also transcript levels of genes located downstream of the three rRNA operons.

2 | RESULTS

2.1 | Inactivation of the *R. sphaeroides* RNase III leads to strong decrease in pigmentation

Like in the well-studied γ-proteobacterium *E. coli*, the RNase III encoding gene (*rnc*) in *R. sphaeroides* is chromosomally organised in an operon consisting of three genes, giving rise to a polycistronic mRNA. While in *E. coli*, the *rnc* gene is the first gene of the operon, followed by the *era* gene (encoding a GTPase important for cell cycle control) and the *recO* gene (encoding a DNA repair protein), in *Rhodobacter* the first gene is *lep* for leader peptidase, followed by the *rnc* gene and the *era* gene on last position (Rauhut et al., 1996).

In the first approach, we constructed an *R. sphaeroides rnc* deletion mutant (Δ*rnc*), by substitution of the native *R. sphaeroides* gene with a kanamycin resistance cassette, leading to loss of RNase III activity but also showing polar effects of the mutation. A strong phenotype was visible in a drastic filamentation morphology of the Δ*rnc*-mutant stain, which we could attribute to a reduced *era* mRNA

level in the mutant. To exclude polar effects, we next inactivated RNase III catalytic activity through the exchange of two highly conserved amino acids (G48S, D49R) within the RIIID signature motif (Figure S1). This approach relies on mutations described in previous studies (Apirion & Watson, 1975; Dasgupta et al., 1998; Kindler et al., 1973; Nashimoto & Uchida, 1985) and was adapted in our study to the *R. sphaeroides* RNase III enzyme.

To test for loss of RNase III activity, we checked the ability of the *R. sphaeroides* enzyme to fragment ribosomal RNAs. Like several other α-proteobacteria, *R. sphaeroides* fragments the large 23S rRNA into smaller pieces, thereby generating a 14S, 5.8S-like and an additional 16S rRNA molecule (Evguenieva-Hackenberg, 2005; Evguenieva-Hackenberg & Klug, 2000; Zahn et al., 2000). This process is strictly RNase III-dependent in *R. sphaeroides*. To analyse the rRNA expression pattern of the mutated cells, generated by the exchange of the two mentioned amino acids (Figure S1), we isolated and visualised total RNA by gel electrophoresis and ethidium bromide staining (Figure S2). The presence of intact 23S rRNA and the absence of 14S and 5.8S-like rRNA fragments in total RNA of the mutated cells (*rnc*_GD48,49SR; from now referred to as *rnc*$^-$ strain) confirmed the inactivity of RNase III. As a control, we constructed a plasmid (pRK-*rnc*) harbouring a copy of the native *rnc* gene under transcriptional control of the native promoter and transferred it to the *rnc*$^-$ cells by diparental conjugation (complementation strain). Analysis of the rRNAs from total RNA samples of the complementation strain revealed the restoration of a wild type-like cleavage pattern, indicating that the loss of RNase III can be complemented by ectopic expression of the native *rnc* gene (Figure S2). Band intensities showed some variation between the complemented strain and the wild type and an additional band occurred in the complemented strain. This may be due to different RNase levels in the two strains caused by expression from the pRK vector. Only the wild type and *rnc* mutant were used in our further analyses.

To analyse the growth behaviour of the *rnc*$^-$ strain in comparison to the wild type, we cultivated both strains under aerobic (high oxygen tension), microaerobic (low oxygen tension) or phototrophic conditions (anaerobic, illuminated with white light) in malate minimal medium and followed the OD_{660} over a time of 35 h (Figure 1). While in the presence of oxygen *R. sphaeroides* performs chemotrophic growth through aerobic respiration, photosynthesis is used for energy conservation in the absence of oxygen and the presence of light (phototrophic conditions). As a result, only a minor growth deficiency of the mutant was visible under aerobic and phototrophic conditions, while under microaerobic conditions, the growth of mutant and wild type was similar.

During the growth analyses, we observed a paler colour of the mutant cultures as an obvious phenotype. Since the colour of *R. sphaeroides* cultures is defined by their type and degree of pigmentation, we analysed the production of photopigments. For this, we first performed a spectral analysis of both strains grown in a minimal medium under microaerobic or phototrophic growth conditions (Figure 2a). The spectra of the mutant showed a strongly decreased absorbance at wavelengths, where carotenoids and bacteriochlorophyll possess specific absorbance maxima. The photosynthetic apparatus of *R. sphaeroides* comprises the reaction centre (RC) and two light-harvesting complexes (LHI and LHII). The reduced absorbance at these specific wavelengths was more pronounced under microaerobic growth conditions.

Next, we extracted the photopigments of both strains via acetone/methanol extraction (Figure 2b). The measured amounts of extracted pigments confirmed our expectations, indicating that the *rnc*$^-$ strain in general produces much less pigments than the wild type, in particular under microaerobic conditions. Since the pigments are required to build the photosynthetic complexes, lower pigment production will result in decreased amounts of pigment–protein complexes.

2.2 | RNA-seq analysis reveals global effects of RNase III on gene expression in *R. sphaeroides*

We previously showed that RNase E has a remarkably strong effect on the growth of *R. sphaeroides* under phototrophic conditions

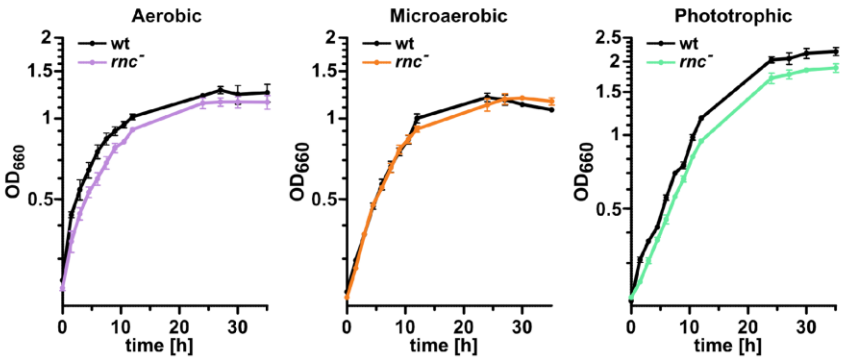

FIGURE 1 Growth behaviour of the *rnc*$^-$-mutant strain under various growth conditions. The growth behaviour of the *R. sphaeroides* wild type and *rnc*$^-$ strain was analysed by monitoring the optical density (OD_{660}) over 35 h. Cells were either cultivated under aerobic, microaerobic or phototrophic conditions in a malate minimal medium. The mean value of biological triplicates is shown. The standard deviation is given as error bars.

that correlate with strong changes of the transcriptome (Börner et al., 2023; Förstner et al., 2018). We were also interested in investigating the global effects of RNase III on the transcriptome especially in regards to growth under different environmental conditions. We cultivated the *rnc*⁻ mutant and wild type under aerobic, microaerobic or phototrophic conditions to mid-exponential growth phase and collected samples for RNA-seq analysis. To compare the RNA expression profiles, we performed unsupervised agglomerative hierarchical clustering, grouping all transcripts according to their expression level between two growth conditions, in either wild type or mutant (Figure 3).

To first investigate the growth condition-dependent effect on RNA abundance changes, all transcripts with $\log_2$ fold change >1 or <−1, adjusted *p*-value <0.05 (between two growth conditions) and a minimum of at least 10 reads in one library were counted as significantly differentially regulated between two growth conditions. For further analysis of the RNase III-dependent influence on the transcriptome, the RNA expression profiles of all significantly differentially regulated genes (from the comparison of the two growth conditions) within wild type or mutant were plotted side by side in the form of three independent heat maps (Figure 3). While the majority of the transcriptome showed very similar expression changes between mutant and wild type (visible in a similar blue/red tone between wild type and mutant column), some RNAs showed different expression changes between the two strains (selected regions of interest are marked as 1–9 in Figure 3). The number of RNAs contained per each region and their annotated features are shown in Table 1. A list of all RNAs per region is shown in Supplementary Table S1.

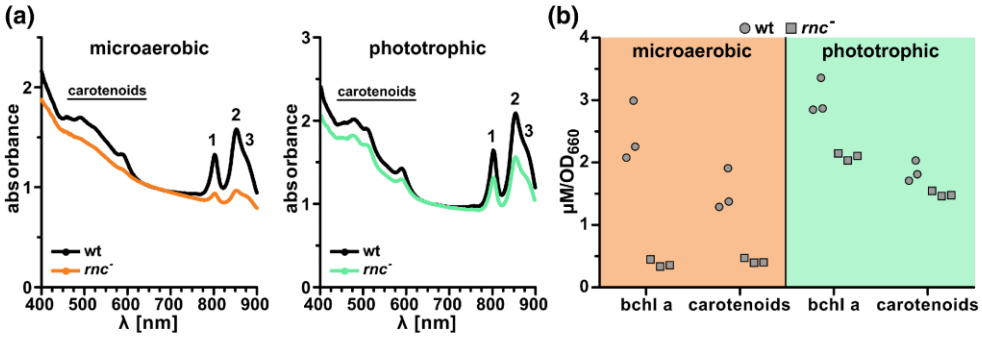

FIGURE 2 Loss of RNase III activity leads to impaired production of photosynthetic complexes. (a) Whole-cell absorbance spectra of microaerobically or phototrophically grown wild type and mutant cells. The specific absorbance maxima for photosynthetic complexes are marked as 1–3 (1: RC and LH II; 2: LH II; 3: RC and LH I). The mean values of biological triplicates are shown. (b) Photometrically determined amounts of bacteriochlorophyll a (bchl a) and carotenoids from acetone/methanol extracts of wild type and mutant cells. The strains were grown under phototrophic or microaerobic conditions as biological triplicates.

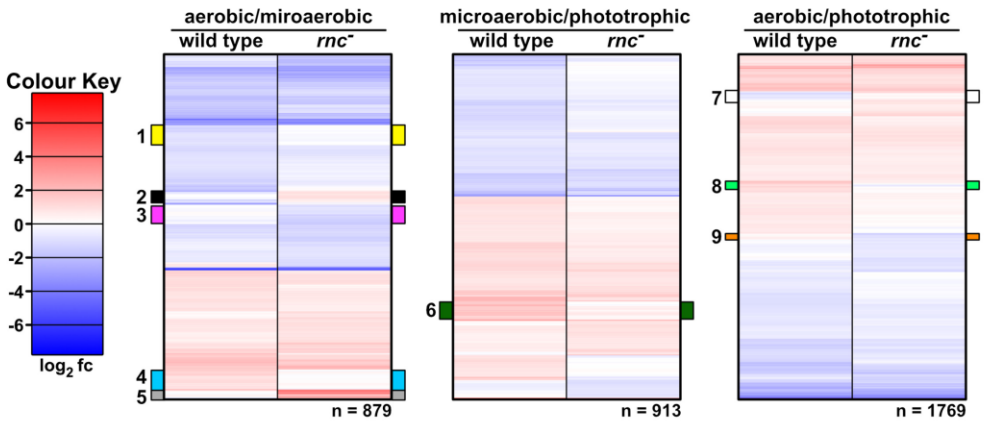

FIGURE 3 RNA-seq-based global RNA expression patterns. Heat maps illustrate global changes in RNA expression between the different growth conditions, within wild type or mutant. Ratios ($\log_2$ fold changes) were calculated from RNA-seq data obtained from aerobically, microaerobically or phototrophically grown biological triplicates of wild type (left panel) or *rnc*⁻ (right panel) strain. All RNAs with significantly differential abundances ($\log_2$ fold change >1 or <−1, p-adjusted value <0.05, with a mean read count of at least 10 between all samples) were plotted per heat map. RNAs within one heat map were grouped into clusters according to their expression pattern between the two indicated growth conditions within a strain by unsupervised agglomerative hierarchical clustering. The total number of displayed RNAs is indicated at the bottom right of each heat map. A positive expression change is highlighted in red and a negative expression change in blue colour (colour key).

TABLE 1 Distribution of functional RNA types among regions of the heat maps.

Region	RNAs in total	rRNA	tRNA	sRNA	mRNAs with predicted function	mRNAs for hypothetical proteins
1	47	2	–	–	20	15
2	27	–	1	3	12 (5)	11 (3)
3	40	–	–	–	13	27
4	47	–	6	–	22	19
5	23	–	–	2	7	14
6	46	–	–	–	29	17
7	44	3	5	1	13 (7)	21 (5)
8	13	–	–	–	8	5
9	11	–	–	–	5	6

Note: The table shows the total content of RNAs per region of the heat maps from Figure 3. The number of contained RNAs was further divided according to their annotated RNA type (rRNA, tRNA, sRNA and mRNA). The numbers per annotated type are given in the following rows. mRNAs with predicted function and mRNAs for hypothetical proteins are separately listed. Numbers in parentheses indicate the amount of RNAs located in close proximity downstream to one of the rRNA operons.

For most of the defined regions, no functional groups among the genes are obvious. Region 1 contains the *traB*, *F*, *G*, *N* and *W* genes for proteins related to plasmid conjugation and *groEL* and *groES* for heat shock chaperonins. As well, *tra* genes as *gro* genes are co-transcribed. While *groEL* and *groES* are localised on chromosome I, *tra* genes are localised on mega plasmid D. Region 6 contains several genes involved in metal transport (*znuAB*, *zur* and *sitD*).

Interestingly, when looking at the read coverage files using the Integrated Genome Browser (Freese et al., 2016), we noticed that a large proportion of enriched RNAs in the mutant are located directly downstream of rRNA operons (one rRNA operon is located on the large first chromosome, and two more rRNA operons on the second chromosome) (Figure 4). A screenshot visualising the total RNA-seq read coverage at the genomic locus of the first rRNA operon, taken from the Integrated Genome Browser, is shown in Figure S3. A list of all genes located directly downstream to rRNA operons (as seen in Figure 4), including the DESeq2 results (mutant/wt under microaerobic conditions) of those genes, is given in Supplementary Table S2. To validate the enrichment of RNAs located directly downstream of the rRNA operons, as seen in the RNA-seq read coverage (Figure 4), qRT-PCR was performed for four different loci, located downstream of the rRNA operons (locus A and locus B: downstream to rRNA operon 1; locus C: downstream to rRNA operon 2; locus D: downstream to rRNA operon 3). qRT-PCR for all four tested loci confirmed high enrichment of the tested RNA segments in the *rnc*$^-$-mutant strain compared to the wild type under microaerobic conditions (Figure 4c), as also seen in the read coverage plots in Figure 4a,b as well as the DESeq2 results shown in Supplementary Table S2. To test, if the enrichment of these loci is due to increased transcription, possibly by partially unterminated transcription read-through of the rRNA genes, we chromosomally integrated additional transcription terminators directly downstream, adjacent to the rRNA operons in the *rnc*$^-$-mutant strain by homologues recombination (insertion regions are marked as green arrows in Figure 4a,b), and repeated qRT-PCR for the four different loci A-D with samples of the modified *rnc*$^-$ mutants, harbouring additional transcription terminators. Strikingly, we observed a strong reduction of RNA abundances, compared to the quantification of the previous *rnc*$^-$ samples with native transcription terminators. While still being slightly enriched, the RNA abundances at all four loci nearly reached wild type level.

To further characterise the effects of RNase III on the *R. sphaeroides* transcriptome, we used an RNA-seq-based prediction protocol to globally map bona-fide RNase III cleavage sites, comparable to approaches recently published by our group for RNase E (Börner et al., 2023; Förstner et al., 2018). For this, we analysed the 5′ end positions of each RNA-seq read obtained from wild type and *rnc*$^-$ strain under aerobic, microaerobic or phototrophic growth conditions. As an endoribonuclease, RNase III can cleave RNA substrates internally and as a result may generate new stable RNA 5′ ends. If stable, these new 5′ ends will consequently produce higher 5′ end read counts at positions, where RNase III catalysed RNA hydrolysis (RNase III-dependent 5′ ends). As a consequence, these RNase III-dependent 5′ end read counts can be enriched in the wild type, in comparison to the mutant (where RNase III is unable to hydrolyse RNAs), and were further defined by us as significantly enriched in the wild type with setting cut-off parameters as $\log_2$ fold change >1 (wt/mutant) and adjusted *p*-value <0.05, with a minimum read count of at least 10 in one of the libraries (from now on referred to as RNase III cleavage sites).

Through our prediction approach, we were able to identify RNase III cleavage sites under all three tested growth conditions, where most sites were detected under aerobic conditions ($n = 2220$), less under phototrophic conditions ($n = 1093$) and least under microaerobic conditions ($n = 565$) (Figure 5a). The biggest overlap of cleavage sites was found between microaerobic/phototrophic and microaerobic/aerobic conditions, which reflects that microaerobic conditions represent an intermediate state between growth at high oxygen conditions (aerobic) and complete absence of oxygen (phototrophic).

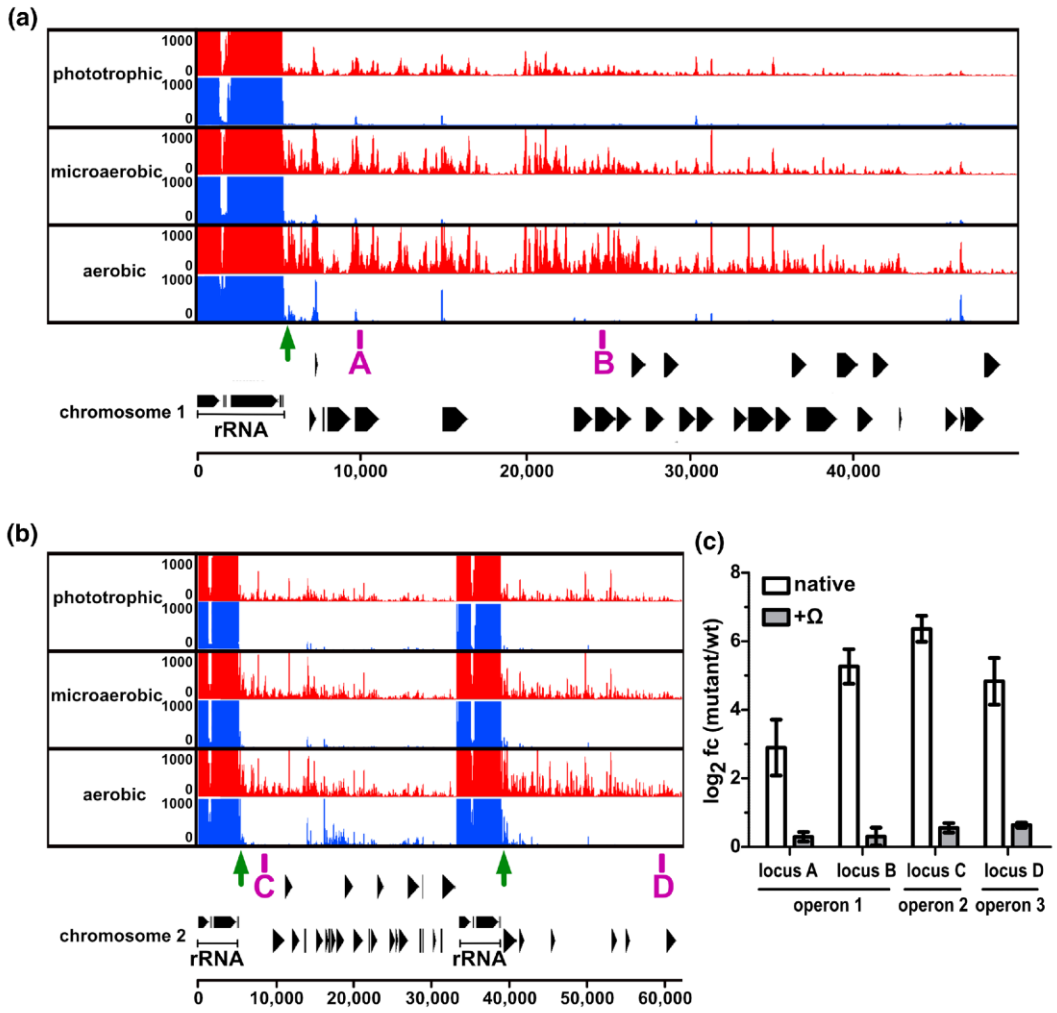

FIGURE 4 RNA-seq read coverage of the genomic regions located downstream to rRNA operons. (a,b) The total read coverage of cDNA libraries from exponentially grown wild type (blue) and *rnc*⁻ (red) strain samples is shown. Samples were collected during growth under either aerobic, microaerobic or phototrophic conditions. The read coverage was plotted from wiggle files of merged independent biological triplicates with the integrated genome browser. The scale bar of the read coverage has an identical height for all tracks. Annotated genes are shown in black. Green arrows indicate the locations, where transcriptional terminators have been chromosomally integrated. Validation by qRT-PCR was performed for four different loci (A–D; magenta boxes). (c) Spike-in qRT-PCR for quantification of RNA loci located downstream of the three rRNA operons. 20 ng DNA-free total RNA of microaerobically grown biological triplicates of *R. sphaeroides* wild type and *rnc*⁻ strain were analysed (white bars). Additionally, wild type samples were compared to modified *rnc*⁻ strains, harbouring inserted transcriptional terminators directly downstream of the rRNA operons (see panels a and b of this figure). The relative abundance (mutant/wt) is shown. The standard deviation of the mean is indicated as an error bar.

To characterise the cleavage sites on a global scale, we grouped the RNAs harbouring cleavage sites among annotated genomic features (Figure 5b). Our analysis revealed a predominant quantity of cleavage sites within coding sequences (CDS), where most cleavage sites were found under aerobic conditions, followed by phototrophic conditions, and least under microaerobic conditions. The second biggest group to contain RNase III cleavage sites were ribosomal RNAs, followed by 5′ UTRs and sRNAs.

Additionally, we quantified the cleavage site per RNA ratios under each of the three growth conditions and found an enormous variation of cleavage sites per RNA (Figure 5c). The vast majority of RNAs lacked any RNase III cleavage site (≈85% under aerobic conditions; ≈95% under microaerobic conditions; ≈89% under phototrophic conditions), while second most RNAs contained a single RNase III cleavage site. Interestingly, we could identify several RNAs with more than 50 cleavage sites per transcript, nearly exclusively under phototrophic conditions. The highest number of sites per RNA was found within all three copies of 23S rRNA under phototrophic conditions (each with 75 sites per RNA), followed by 16S rRNA (66, 51 and 47 sites RNA). Under aerobic conditions, the *fusA1* transcript, encoding translation elongation factor G, was detected as the RNA with the most cleavage sites (57 sites).

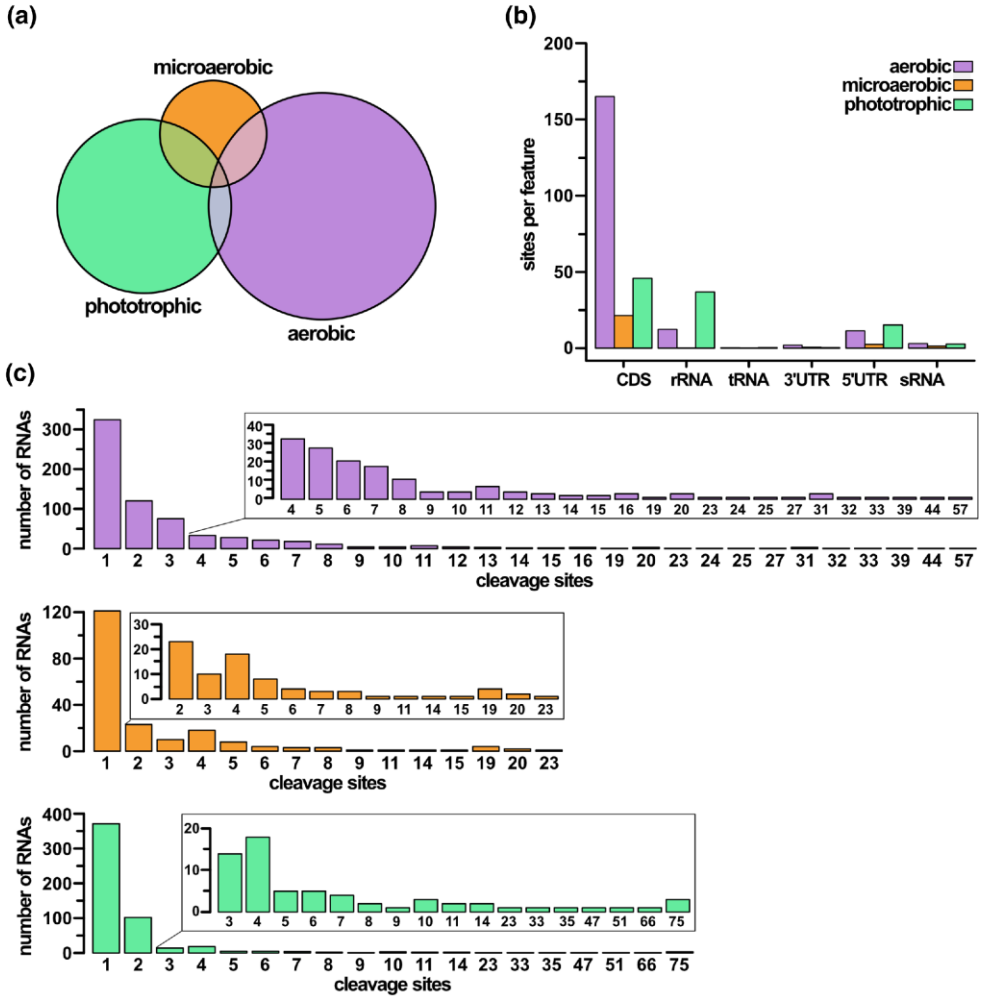

FIGURE 5 Distribution of mapped RNase III cleavage sites. (a) Amount of mapped RNase III cleavage sites per growth condition. The circle and overlaps illustrate the proportional quantity of identified RNase III cleavage sites. (b) Distribution of cleavage sites per annotated genomic feature. (c) Number of RNAs and their respective amount of identified cleavage sites.

Since our analysis pointed towards high amounts of RNase III cleavage sites especially under aerobic conditions, we constructed an in vivo RNase III activity reporter (equivalent to our recently published ribonuclease E activity reporter, Börner et al., 2023) to study the growth condition-dependent effects of RNase III. We fused the well-characterised RNase III cleavage site of the native pre-16S rRNA to the mVenus encoding gene (indicator construct: pPHU231-5′UTR-mV), allowing RNase III to introduce cleavage within the 5′ UTR of the reporter mRNA generating a monophosphorylated 5′ end, which can subsequently activate 5′ end-dependent RNA decay by RNase E. As a background control for RNase III activity on mVenus expression, we used an almost identical plasmid, with the sole exception, that it did not contain the introduced cleavage site but only the ribosome binding site within the 5′ UTR of mVenus (control construct: pPHU231-p16S-mV). The scheme of both reporter constructs is depicted in Figure 6a.

After conjugation of the reporter plasmids to either wild type or *rnc*⁻ cells, we cultivated the resulting conjugants under aerobic, microaerobic or phototrophic conditions and determined the normalised fluorescence units (F/OD_{660}) of the mid-exponential cultures in a Tecan plate reader. A strong effect of the growth conditions on the measured fluorescence was visible, which is partly due to the influence of oxygen on mVenus fluorescence. Only a minor difference in normalised fluorescence units was observed between wild type and *rnc*⁻ cells for the control construct, as the wild type produced only slightly higher fluorescence values (Figure 6b). On the other hand, a strong effect of the RNase III deficiency in the form of highly elevated fluorescence units generated by the indicator construct was visible (Figure 6c), which served as a proof of function of our construct. Interestingly, we did not observe an equal ratio in fluorescence of wild type to mutant throughout the three growth conditions: the fluorescence units under microaerobic and phototrophic conditions differed by factors of 1.9 and 2.6, respectively,

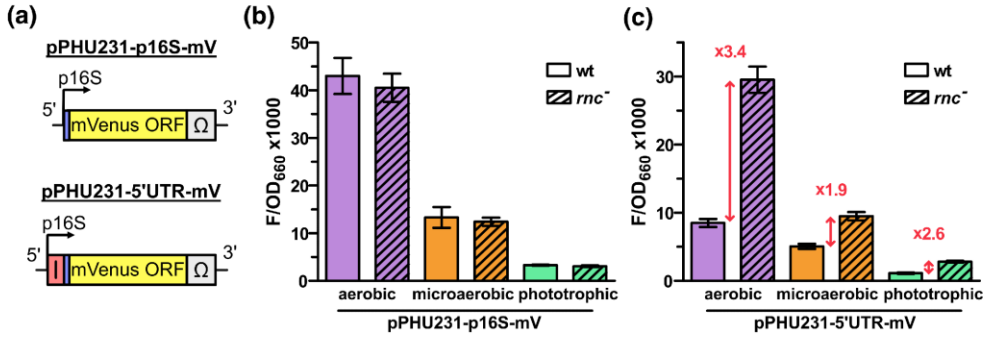

FIGURE 6 Reporter system-based evaluation of the in vivo RNase III cleavage activity. (a) Schematic overview of the reporter constructs. The mVenus gene (yellow) is under transcriptional control of the strong constitutive 16S rRNA promoter of *R. sphaeroides*, preceded by an optimised artificial ribosome binding site (blue), and followed by a transcriptional terminator (grey) (control construct: pPHU231-p16S-mV) as described in Börner et al. (2023). To investigate RNase III cleavage activity, the well-characterised RNase III cleavage site of the native 5′ pre-16S rRNA (red) was introduced in the 5′ UTR directly upstream of the ribosome binding site (indicator construct: pPHU231-5′UTR-mV). Biological triplicates of wild type and *rnc*⁻ mutant, carrying the reporter plasmids pPHU231-p16S-mVenus (b) and pPHU231-5′UTR-mVenus (c) were cultivated under aerobic, microaerobic or phototrophic conditions until exponential growth phase. The mean values of normalised fluorescence intensities (F/OD_{660}) and their standard deviations are shown. The ratio between wild type and mutant mean values is indicated in red colour above the two corresponding bars.

while under aerobic conditions, a stronger increment (factor 3.4) was measured. This supports variations of the impact of RNase III under different growth conditions.

2.3 | Elevated CcsR expression is accompanied by increased resistance towards oxidative stress upon loss of RNase III activity

Recent studies of our group identified a novel small RNA-binding protein, CcaF1, which is co-expressed with four homologous CcsR sRNAs (CcsR1-4) from a single promoter (Billenkamp et al., 2015; Grützner, Billenkamp, et al., 2021). While CcaF1 binds to various RNA targets (Grützner, et al., 2023; Grützner, Billenkamp, et al., 2021), affecting their stability and regulating gene expression, the CcsR sRNAs inhibit a glutathione-dependent C1 metabolic pathway, leading to increased levels of antioxidative glutathione, which provides protection against reactive oxygen species and enhancing cell viability. Previous work documented a direct correlation between CcsR levels and stress resistance (Billenkamp et al., 2015; Grützner, Billenkamp, et al., 2021).

As our RNA-seq data indicated a strong enrichment of CcsR sRNAs in the *rnc*⁻ mutant compared to the wild type in the presence of oxygen (read coverage shown in Figure S4a,b), we were interested in further validating these results. To investigate the expression of CcsR, especially in regard to its function during stress conditions, we induced the stress response of *R. sphaeroides* through incubation at an elevated temperature (42°C) or treatment with paraquat (superoxide radical-inducing agent), $CdCl_2$, H_2O_2 or tBOOH (tertiary butyl alcohol, organic hydroperoxide), followed by isolation of total RNA. Northern blot analysis confirmed the RNA-seq result of an enriched CcsR1 steady-state level in the mutant during standard microaerobic growth conditions at 32°C (Figure 7a). The sequence of the four CcsR sRNAs is almost identical, but the chosen oligonucleotide probe allows specific detection of CcsR1, which is representative of CcsR1-4 levels (Billenkamp et al., 2015). For all tested stress conditions, both strains showed an increase in CcsR1 expression, which confirms the induction of stress condition, as CcsR is transcribed from an RpoHI/RpoHII-dependent promoter. RpoHI and RpoHII are alternative sigma factors, actively replacing the house-keeping sigma factor during heat and oxidative stress in *R. sphaeroides* (Nuss et al., 2010). Interestingly, the mutant showed much higher CcsR1 levels than the wild type under all tested stress conditions, except for heat stress, where CcsR1 expression was slightly reduced in the mutant compared to the wild type. Furthermore, we analysed CcsR1 expression by northern blot analysis of total RNA samples from the *rnc* complementation strain (*rnc*⁻::pRK-*rnc*). Restoration of the wild type-like CcsR1 abundance within the complementation strain proved the influence of RNase III on CcsR1 expression (Figure 7b).

As the RNA steady-state level is defined by the individual transcription rate, as well as the RNA stability, we constructed a reporter plasmid harbouring a transcriptional fusion of the CcsR expression controlling pCcaF1 promoter and the gene of the yellow fluorescent protein mVenus (pPHU-pCcaF1-mV). The reporter plasmid and the related empty control vector were transferred to *R. sphaeroides* wild type and *rnc*⁻ cells by diparental conjugation. Fluorescence measurements of the microaerobically grown conjugants revealed a stronger reporter signal within the *rnc*⁻ background (fluorescence units around 35% increased), pointing towards higher promoter activity and more frequent transcription of CcsR from pCcaF1 upon loss of RNase III activity (Figure 7c).

As the CcsR sRNAs are transcribed from an RpoHI/RpoHII-dependent promoter, we also quantified mRNA level for the alternative sigma factors RpoE, RpoHI and RpoHII by qRT-PCR (Figure S5). The results show that *rpoE* and *rpoHII* mRNA levels were increased in the *rnc*⁻ mutant compared to the wild type. As a master regulator,

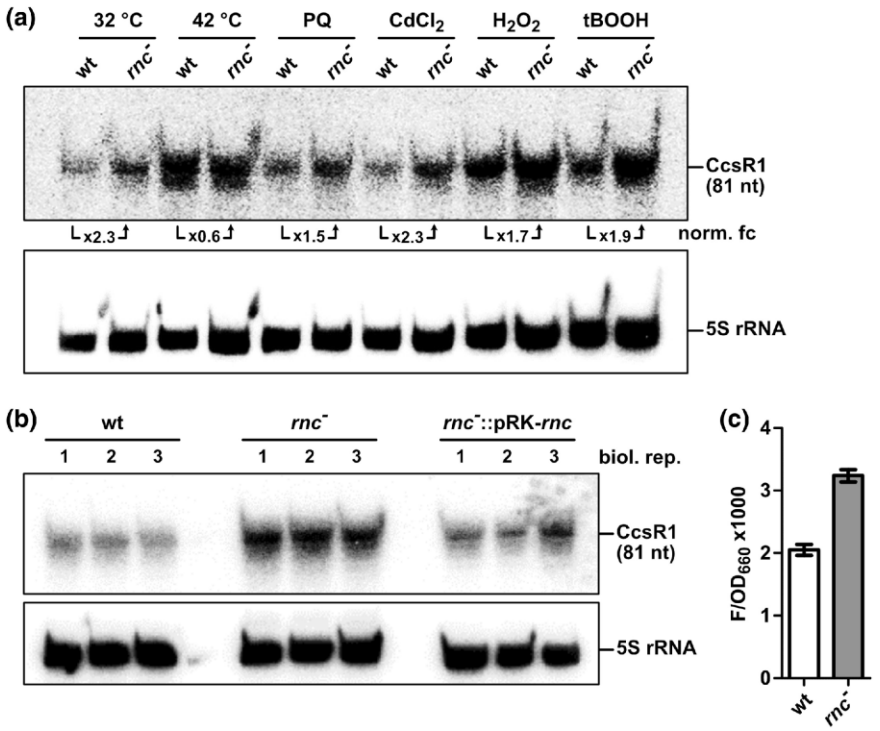

FIGURE 7 RNase III affects stress-dependent expression of CcsR. Northern blot analysis for evaluation of the CcsR1 sRNA steady-state level. 7 µg total RNA from microaerobic cells were analysed. RNAs were detected by hybridisation with a radiolabelled antisense DNA probe specific for CcsR1. Visualisation of the 5S rRNA served as a loading control. (a) To induce the stress response, wild type and *rnc*⁻ cultures were either grown for 1 h at 42°C or treated with 0.3 mM paraquat (PQ), 0.1 mM $CdCl_2$, 0.5 mM H_2O_2 or 0.3 mM tBOOH prior to sample collection and RNA isolation. The fold change (mutant/wt) after normalisation to the loading control is indicated below the corresponding bands. (b) RNA originating from biological triplicates of wild type, *rnc*⁻ mutant, and the RNase complementation strain (*rnc*⁻::pRK-*rnc*) was analysed by northern blot. (c) In vivo promoter activity reporter assay. Microaerobically grown biological triplicates of wild type and mutant cells, carrying the transcriptional fusion of pCcaF1 and mVenus on plasmid pPHU-pCcaF1-mV, were used for measurements of mVenus fluorescence intensity. Mean values of the normalised fluorescence units (F/OD_{660}) and their standard deviations are shown.

RpoE activates the expression of RpoHII in *R. sphaeroides*, specifically during oxidative and heat stress conditions (Dufour et al., 2012; Nuss et al., 2009). Interestingly, with our RNA-seq-based prediction approach, no bona fide RNase III cleavage sites were mapped to either of the mRNAs.

To investigate the transcript stability of CcsR in vivo, we cultivated the wild type and *rnc*⁻ strain under microaerobic conditions to mid-exponential growth phase (≈OD_{660} 0.5) and added rifampicin to inactivate the DNA-dependent RNA polymerase. Samples collected either prior to the addition of rifampicin (referred to as 100% RNA content), or after rifampicin addition were used for northern blot analyses. The half-life experiments confirmed our previously obtained data of a generally enriched CcsR1 steady level in the *rnc*⁻ strain. Interestingly, we did not observe a major difference in transcript stabilities, between mutant and wild type strain, as the northern blot signal for the mutant samples only decreased slightly faster than the signals from the wild type samples (Figure 8a). To calculate the half-lives of CcsR1 in the different strains, we quantified the CcsR1 signals and normalised them to the signal intensities of the 5S rRNA loading control, followed by fitting the normalised data points to semi-logarithmic trend lines. The calculation revealed only a minor difference in CcsR1 stability, with a calculated half-life of around 7.1 min for the wild type and around 6.4 min for the mutant (Figure 8b).

Since the mutant strain accumulates CcsR through increased transcription rate, and one function of CcsR is to downregulate glutathione-dependent metabolism in *R. sphaeroides* helping to counteract oxidative stress, we next tested the survival of the mutant strain under certain stress conditions. For this, we selected several stress agents causing oxidative cell damage, and treated exponentially grown wild type and mutant cells. To assess stress resistance and subsequent cell survival rate, we plated a dilution of the treated cultures on agar plates and counted resulting colonies from the differentially treated approaches after 2 days of growth at 32°C in the dark. An untreated approach, where no stress-inducing agents were added, served as a reference (100% cell survival rate) (Figure 9a). Our data show comparable survival rates of mutant and wild type strains after exposure to elevated temperatures at 42°C (heat shock, causing protein denaturation) or treatment with cadmium chloride. As a heavy metal, cadmium acts toxic on cells, causing protein denaturation through disruption of protein disulphide bridges, and release of protein-bound Fe^{2+} through binding

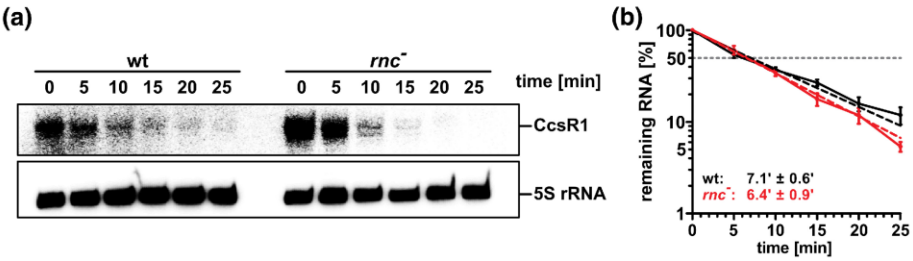

FIGURE 8 The stability of CcsR is unaffected by a loss of RNase III activity. (a) Northern blot analysis for evaluation of the CcsR1 half-lives. Microaerobic wild type and *rnc*⁻-mutant cultures were treated with 0.2 mg/mL rifampicin. Samples were collected prior ($t = 0$ min) and 5, 10, 15, 20 and 25 min after the rifampicin treatment. 10 µg total RNA were electrophoretically separated on a denaturing 10% polyacrylamide gel and subsequently immobilised on a nylon membrane by blotting and UV crosslinking. RNAs were detected by hybridisation of the membrane with a radiolabelled antisense DNA probe specific for CcsR1. Visualisation of the 5S rRNA served as a loading control. (b) Decrease of CcsR1 sRNA levels after rifampicin treatment. Transcript stabilities were calculated by quantification of the northern blot signal intensities of wild type (black) and mutant (red) samples, normalisation to the loading control and fitting of the data points to semi-logarithmic trend lines (dashed lines). Northern blots with samples from independent biological triplicates of wild type and mutant were used for calculation.

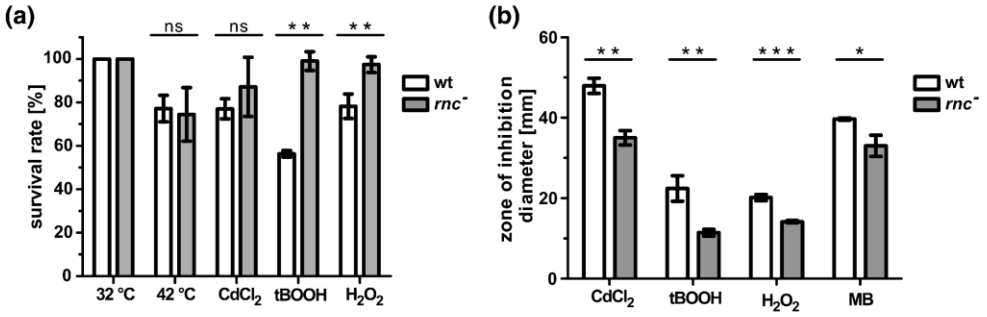

FIGURE 9 RNase III affects the stress resistance of *R. sphaeroides*. (a) Normalised survival rates (cfu/mL) of wild type and mutant under several stress conditions. The mean values and their standard deviation of normalised biological triplicates are shown as white (wild type) and grey (mutant) bars. Cells grown at 32°C served as a reference. For assessing survival, the cultures were shifted to 42°C for 1 h (heat shock) or incubated with either 0.01 mM $CdCl_2$, 0.3 mM tBOOH or 0.5 mM H_2O_2 for 20 min before plating on solid malate minimal medium. Student's two-sided t-test was used to assess the statistical significance of the difference in mean values (ns: not significant; **p-value <0.01). (b) Zone of inhibition assay showing the stress resistance of wild type (white) and mutant (grey) cells on a solid medium. 0.1 M $CdCl_2$, 0.5 M tBOOH, 1 M H_2O_2 or 0.01 M methylene blue (MB) were spotted on sterilised filter discs in the centre of *Rhodobacter*-containing soft agar plates. The mean zone of inhibition diameter of biological triplicates is depicted. Standard deviations are given as error bars. Student's two-sided *t*-test was used to assess the statistical significance of the difference in mean values (*p-value <0.05, **p-value <0.01, ***p-value <0.001).

competition with divalent cation co-factors leading to the generation of hydroxyl radicals by the Fenton reaction and other reactive oxygen species by downstream processes. For cultures treated with tBOOH (organic peroxide) or H_2O_2, we observed a higher rate of colony-forming units from the mutant compared to the wild type, comparable to the colony-forming units of the untreated approach, indicating an increased stress resistance under these conditions.

In addition to our stress experiments with liquid cultures, we performed zone of inhibition assays to evaluate the stress resistance of both strains grown on a solid medium (Figure 9b). Notable, a more pronounced zone of inhibition in this assay indicates a decreased stress resistance. Interestingly, the mutant strain showed significantly smaller zones of inhibition than the wild type after treatment with cadmium chloride, which suggests an elevated stress resistance of the mutant against cadmium toxicity on a solid medium, and is more pronounced than the respective stress resistance in liquid medium (Figure 9a). For tBOOH and H_2O_2 stress, the zone of inhibition data showed similar results as previously obtained from the survival assay (indicating a higher stress resistance of the mutant). Additionally, we tested the photooxidative stress resistance of the mutant by applying methylene blue onto the culture containing soft agar plates, followed by incubation under white light. In this approach, methylene blue acts as a photosensitiser by energy transfer to molecular triplet oxygen and subsequent electron spin-flip leading to the generation of singlet oxygen, in the presence of light (DeRosa & Crutchley, 2002). As already observed for cultures treated with $CdCl_2$ or peroxide, the mutant strain showed a higher survival rate than the wild type.

In addition to small regulatory RNAs, ROS-detoxifying enzymes like superoxide dismutases and catalases play a well-studied and crucial role in counteracting oxidative stress. While the model organism *E. coli* possesses three superoxide dismutase enzymes (*sodA*, *sodB* and *sodC*), only a single superoxide dismutase has been found in *Rhodobacter capsulatus* (Cortez et al., 1998) and a single superoxide dismutase (*sodC*) is annotated in *R. sphaeroides*. Nevertheless, our RNA-seq approach did not reveal any effect of RNase III on the abundance of *sodC* in *R. sphaeroides*. Interestingly, the catalase encoding mRNA, *catA*, showed an increased steady-state level in the *rnc*⁻ mutant in our RNA-seq data, which also was validated by qRT-PCR with a $\log_2$ fold change ≈ 1.8 (mutant/wt) under microaerobic growth conditions. *catC*, which encodes another catalase in *R. sphaeroides* showed no expression changes between wild type and RNase III mutant in our RNA-seq analysis under all three growth conditions (data not shown).

Taken together, our data indicate a higher stress resistance of the mutant against all tested ROS-causing agents, except for $CdCl_2$ on solid media (while here also a higher mean cfu/mL was calculated, the standard deviation between the independent biological replicates was too large to be considered as significant). A higher stress resistance upon heat shock could not be seen in our data.

2.4 | RNase III controls quorum sensing in *R. sphaeroides*

Since its first discovery in *Aliivibrio fischeri* (Nealson et al., 1970), quorum sensing (QS) has been intensely investigated in many bacterial species and has been described as the ability to sense and respond to cell density in a bacterial population. The well-studied LuxI/LuxR QS system of *A. fischeri* comprises besides five other proteins a signal receptor (LuxR) sensing the presence of autoinducer molecules and controlling the transcription of QS-regulated genes, and an autoinducer synthase (LuxI), whose expression is induced upon perceived QS signals (Engebrecht & Silverman, 1984). The existence of Lux-type systems has later been reported for many bacterial species (Fuqua et al., 1994; Greenberg et al., 1979; Salmond et al., 1995), underlining its biological relevance. While the LuxI/LuxR-type system is one of the most simply built, a variety of more complex QS systems has been described in last decades, where a surprisingly high amount of physiological functions have been found to show QS-dependent regulation (e.g. antibiotic production/resistance, virulence, biofilm formation, sporulation or morphology) (reviewed in Miller & Bassler, 2001; Whitehead et al., 2001).

In *R. sphaeroides*, the LuxR-type signal receptor is encoded by the *cerR* gene, whereas *cerI* codes for the LuxI-type acyl-homoserine lactone (AHL, autoinducer) synthase. RNA-seq data of the *rnc*⁻-mutant strain revealed an elevated *cerI* mRNA level under microaerobic and phototrophic conditions, where the enrichment over the wild type was highest under microaerobic conditions (Figure S6). To test whether the accumulation of *cerI* mRNA in *R. sphaeroides* has any physiological effect on AHL production, we used an *S. meliloti* reporter strain (McIntosh et al., 2019). This strain is characterised by a disrupted QS system unable to synthesise AHLs. Additionally, the strain carries a low copy reporter plasmid, introducing a transcriptional fusion of promoter pSMb20911 with the mVenus gene. In this in vivo system, pSMb20911 is repressed by rising AHL concentrations and thereby the expression of mVenus is negatively regulated. This coupling between rising AHL concentration and decreasing fluorescence signal enables to quantify unknown AHL concentrations.

To assess the correlation between fluorescence signal and AHL concentration, we collected cell-free supernatant from mid-exponential *R. sphaeroides* wild type cultures and incubated separate reporter strain cultures with increasing ratios of supernatant per blank medium (growth in 0%–100% supernatant). The resulting fluorescence units were plotted and used as reference correlation (Figure 10a, grey box). To quantify the AHL amounts produced by the *rnc*⁻ strain, we next compared fluorescence units of the in vivo system, generated through incubation with 25% cell-free supernatant from mutant or wild type. Remarkably, a strongly diminished signal (≈1500 F/OD_{600}) was obtained from reporter cultures grown with supernatant of the *rnc*⁻ strain, which was even lower than the signal generated by growth in 100% wild type supernatant (≈2200 F/OD_{600}), indicating immense repression of mVenus caused by hyperproduction of AHLs in the *rnc*⁻ mutant (factor: >4). As a control, we tested the effect of 400 nM commercially obtained AHL on our reporter system, which resulted in just slightly fewer fluorescence units (≈1000 F/OD_{600}) than measured while evaluating the *rnc*⁻ strain supernatant (Figure 10a).

To validate the effects on the *cerI*/*cerR* system observed in our RNA-seq data (Figure S6), we analysed the total RNA of independent biological triplicates from wild type and *rnc*⁻ strain by qRT-PCR (Figure 10b). As expected, the mutant showed a strong enrichment of *cerI* transcript compared to the wild type ($\log_2$ fold change mutant/wt ≈ 2.5), while for *cerR* only a mild effect was visible. Since the LuxI/LuxR-type system represents a positive feed-forward loop, the accumulation of autoinducer leads to an increment of the *cerI* mRNA level, through decreased repression of *cerI* transcription by *cerR*. Nevertheless, we were interested to further investigate the impact of RNase III on this system by analysis of the in vivo *cerI* mRNA stabilities in the wild type and *rnc*⁻ background. For this, we added rifampicin to exponentially grown wild type and mutant cultures, collected samples at distinct time points after addition of rifampicin and analysed the total RNA of these samples by qRT-PCR. As a result, we plotted the decreasing *cerI* mRNA level per time and fitted the data points to semi-logarithmic trend lines. While the wild type showed a specific *cerI* half-life of around 4 min, our analysis revealed an increased stability in the mutant with a half-life of around seven to 9 min, indicating a relevant destabilising effect on RNase III on the *cerI* transcript.

3 | DISCUSSION

Our comparative RNA-seq analysis revealed a considerable impact of RNase III on the transcriptome of *R. sphaeroides* that was,

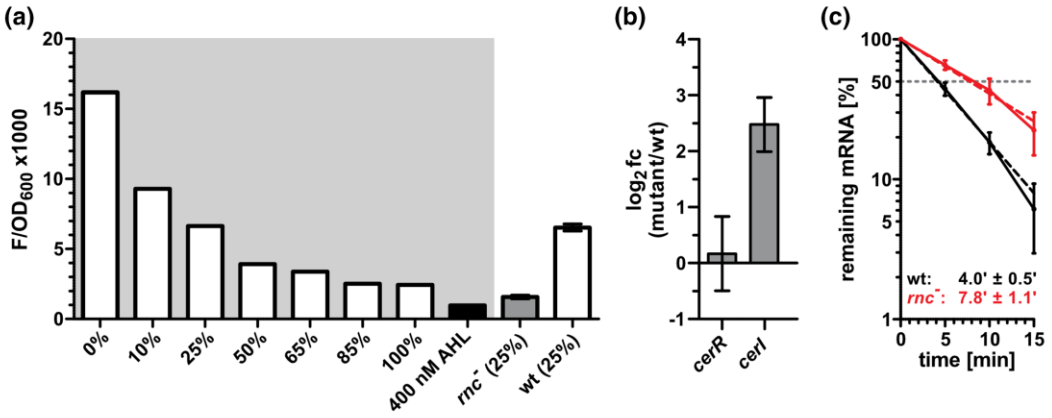

FIGURE 10 The production of quorum-sensing autoinducer molecules is negatively affected by RNase III. (a) In vivo reporter system for detection of quorum-sensing autoinducer levels. An *S. meliloti* reporter strain (McIntosh et al., 2019) was used to evaluate concentrations of secreted autoinducer molecules from cell-free supernatants of wild type (white) and *rnc*⁻ (grey) cultures. The *S. meliloti* reporter strain was grown in increasing amounts (0%–100%) of supernatant from microaerobically grown *R. sphaeroides* wild type cultures (assessment of repression, grey box) or in 25% supernatant from the microaerobically grown *R. sphaeroides rnc*⁻ strain. A reporter culture grown with 400 nM oxo-C16:1-HL served as a reference (black bar). The resulting mVenus expression is shown as normalised fluorescence (F/OD_{600}). (b) Spike-in quantitative reverse transcriptase PCR for quantification of *cerR* and *cerI* from *R. sphaeroides* wild type and *rnc*⁻ strain. 20 ng DNA-free total RNA of microaerobically grown biological triplicates was analysed. The relative abundance (mutant/wt) is shown. The standard deviation of the mean is indicated as an error bar. (c) Determination of *cerI* transcript stabilities in wild type and mutant strain. 20 ng DNA-free total RNA, isolated from cell samples collected either prior ($t = 0$ min) or 5 min, 10 min, 15 min after the addition of 0.2 mg/mL rifampicin, were analysed by spike-in quantitative reverse transcriptase PCR. Mean values of biological triplicates were fitted to semi-logarithmic trend lines (dashed lines).

however, less pronounced than the impact of RNase E (Börner et al., 2023). An unexpectedly high amount of enriched RNAs in the mutant originated from loci directly downstream of rRNA operons (Figure 4), resulting in a strongly increased read coverage obtained by RNA-seq that was confirmed for selected genes by qRT-PCR. We hypothesised that these increased transcript levels are due to partially unterminated transcription of the rRNA genes leading to read-through into the downstream located genes, or due to increased DNA accessibility, for example, by a higher degree of DNA structure relaxation in the mutant strain. The chromosomal insertion of additional transcription terminators directly downstream to rRNA operons resulted in a drastic decrease of the tested transcript levels (Figure 4c), nearly restoring wild type-like RNA abundances, suggesting that transcription termination of rRNA is affected in the *rnc*⁻ strain. In a recently published RNA-seq study with an *E. coli* RNase III mutant (Maes et al., 2017), such an enrichment of transcripts located downstream to rRNA was not visible. As for our own data set, no rRNA depletion was applied to the chosen *E. coli* data set. This implies an effect of RNase III that is not general but maybe specific to bacteria with RNase III-dependent 23S rRNA fragmentation. Presently, this possibility cannot be validated due to the lack of suitable data sets.

The biosynthesis of rRNA, including transcription elongation and rRNA processing, is a highly complex but crucial growth-rate limiting step, which is only poorly understood in many bacterial species. The elongation of rRNA transcription has been reported to include several factors, importantly, the Nus proteins involved in anti-termination at several rho-dependent termination sites. To achieve anti-termination and to promote read-through, NusA and NusB can assemble with RNA sequences of the nascent rRNA transcript, known as *boxA* sites, and form RNA loops to interact with the DNA-dependent RNA polymerase (Cagliero et al., 2014; Das, 1993). Our RNA-seq analysis did not point towards the altered expression of *nusA* and *nusB* in the RNase III mutant, making it unlikely that a transcription read-through caused by the *nus* system *in trans* is responsible for the measured enrichment of RNA directly downstream of the rRNA operons.

The proper processing of rRNA ensures maturation of the precursors to functional end products (some tRNA genes are co-transcribed with the 16S, 23S and 5S rRNA genes), involves several ribonucleases like RNase E, RNase J, YbeY, and RNase III (reviewed in Deutscher, 2009; Srivastava & Schlessinger, 1990) and occurs simultaneously during transcription (French & Miller, 1989). The important role of RNase III in the processing the rRNA transcript to 23S, 16S and 5S rRNAs is well established as well and its role in further rRNA fragmentation α-proteobacteria is well recognised (Apirion et al., 1976; Evguenieva-Hackenberg, 2005; King et al., 1984). As seen in Figure S2 of our study, this process is strictly RNase III-dependent in *R. sphaeroides*. Therefore, it is conceivable that the lack of 23S rRNA fragmentation is affecting rRNA transcription termination via a yet unknown mechanism *in cis*, for example, by altering the RNA secondary structure and transcription rate. YbeY is another endoribonuclease conserved in many bacteria and reported to participate in rRNA processing. In *E. coli*, a deletion of *ybeY* led to the generation of immature 16S rRNA, aberrant ribosome biogenesis, and impaired rRNA transcription anti-termination (Davies

et al., 2010; Grinwald & Ron, 2013; Jacob et al., 2013). However, we did not see an effect of YbeY on the transcript levels downstream of the rRNA operons when testing total RNA samples from an *R. sphaeroides* Δ*ybeY* mutant (Spanka & Klug, 2021) by qRT-PCR (data not shown).

The transcriptome-wide mapping of RNase III cleavage sites revealed a lower number of identified sites compared to our previous mapping of RNase E cleavage sites (between 565 and 2220 cleavage sites found for RNase III, compared to 2007–4206 cleavage sites found for RNase E), which suggests a weaker global regulatory role of RNase III in comparison to RNase E in *R. sphaeroides*. This is in agreement with the number of mRNAs with changed levels in the two strains and with the drastic effect of the *rne* mutation during phototrophic growth (Börner et al., 2023; Förstner et al., 2018).

Loss of RNase III activity caused some clear phenotypic effects in *R. sphaeroides*: reduced pigmentation, alteration of stress resistance and of the quorum-sensing regulatory circuit. Strongly reduced pigmentation occurred especially under microaerobic conditions (Figure 2), when photopigments and photosynthesis complexes are already produced but not necessary for ATP generation (Gregor & Klug, 1999). Under phototrophic conditions, this effect was less pronounced, although photosynthesis complexes are necessary for ATP production (Figure 1).

Our global gene expression analysis of the RNase III mutant did not point towards generally reduced mRNA levels of photosynthesis-related genes (e.g. *crt* and *bch* genes for carotenoid and bacteriochlorophyll synthesis, and *puf* or *puc* genes encoding pigment-binding proteins), as it was recently reported for the *R. sphaeroides* rne^{ts} mutant with reduced RNase E activity (Börner et al., 2023). While we observed decreased mRNA abundances of some known regulators of photosynthesis gene expression in our recent study of the rne^{ts} mutant, our data for the RNase III mutant revealed increased mRNAs levels for the photosynthesis regulators AppA, PpsR and FnrL in the *rnc* mutant under microaerobic and phototrophic conditions (Figures S7a,b and S8). The PpsR/AppA repressor/antirepressor system regulates many photosynthesis genes in response to light and oxygen (Braatsch et al., 2002; Gomelsky & Kaplan, 1997; Han et al., 2007; Masuda & Bauer, 2002), among them also *bch* and *crt* genes. The redox-responsive FnrL also affects the expression of many photosynthesis genes (Imam et al., 2014).

We recently showed that the small RNA-binding DUF1127-domain protein CcaF1 promotes the formation of photosynthesis complexes in *R. sphaeroides* (Grützner et al., 2023). *ccaF1* is co-transcribed with the CcsR sRNAs and also shows higher levels in the rnc^- mutant. This excludes the possibility that diminished pigmentation in the mutant strain is due to reduced *ccaF1* transcript levels. Taken together, our RNA-seq data cannot unequivocally explain the effect of RNase III on pigmentation. However, the formation of photosynthetic complexes includes many regulatory circuits (Eisenhardt et al., 2018, 2021; Mank et al., 2012; Reuscher & Klug, 2021) and its regulation is very complex and may also involve yet unknown factors.

A functional role of RNases in the stress response of numerous microorganisms has been reported already in the past. Often a reduction or lack of the native RNase activity leads to enhanced susceptibility towards various cellular stresses, like oxidative, osmotic or temperature stress (Duggal et al., 2020; Förstner et al., 2018; Lejars & Hajnsdorf, 2022; Möller et al., 2019; Spanka et al., 2021). In contrast, our data (Figure 9) document a higher resistance of *R. sphaeroides* against oxidative stress when RNase III activity is lacking. Interestingly, we observed that the higher resistance of the mutant against oxidative stress is accompanied by elevated CcsR levels. The northern blot data (Figure 8) show that the rnc^- mutant accumulates CcsR1, compared to the wild type, under non-stress conditions and all tested oxidative stress conditions, but not during heat shock, where expression of CcsR1 was lower than in the wild type. As reported in our previous studies (Billenkamp et al., 2015; Grützner, Billenkamp, et al., 2021), CcsR has an important function in the oxidative stress response of *R. sphaeroides* by affecting glutathione levels through direct binding to *flhR* mRNA encoding a transcriptional activator. Additionally, enrichment of CcsR indirectly decreases the levels of mRNAs encoding subunits of the pyruvate dehydrogenase complex, which is a primary target of reactive oxygen species (ROS) (Billenkamp et al., 2015). It is likely that the enhanced stress resistance against the tested ROS-inducing agents is caused by an accumulation of CcsR. This is supported by the observation that the cell survival rate and CcsR abundance are not affected by RNase III upon heat stress. Furthermore, our results show that the higher levels of CcsR in the mutant are rather due to an increased transcription rate (Figure 7c) than to increased sRNA stability (Figure 8), suggesting an indirect regulatory effect of RNase III on CcsR expression. Presumably, the elevated *rpoE* and *rpoHII* mRNA levels (Figure S5) in the mutant contribute to the higher CcsR abundance.

In a previous study, we could show that RSP_0557, another small protein with DUF1127 domain expressed from a different locus than *ccaF1-ccsR*, has RNA-binding activity and interacts with CcsR transcripts and other RNAs in *R. sphaeroides* (Grützner, Billenkamp, et al., 2021). Our RNA-seq data showed increased mRNA abundances of *RSP_0557* in the RNase III mutant compared to the wild type, under all three growth conditions (Figure S9). The enrichment was further validated by qRT-PCR under microaerobic conditions ($\log_2$ fold change mutant/wt ≈ 1.6). Therefore, it is conceivable that also an increased level of RSP_0557 influences CcsR expression, e.g. by altering the maturation efficiency of *ccaF1-ccsR* precursor transcript to mature CcsR sRNAs.

Since catalases are known to degrade hydrogen peroxide to water and molecular oxygen, and the mutant strain did show increased resistance against hydrogen peroxide, it can be assumed that the enrichment of *catA* mRNA in the mutant positively contributes to the increased survival rate under this specific stress conditions. However, catalases have been reported to be highly specific to hydrogen peroxide and are not expected to accept organic peroxides as a substrate. In a conclusion, the increased survival rate of the rnc^- mutant under tBOOH stress can probably not be explained solely by an elevated catalase level. Like the formation of photosynthesis complexes, the oxidative stress response of

R. sphaeroides includes a complex network of different regulators (Eisenhardt et al., 2021).

Strikingly, we found a novel physiological function of RNase III in the regulation of quorum sensing, by controlling the expression of the autoinducer synthase (*cerI*). For RNase E, another important endoribonuclease which is essential in many gram-negative bacteria, an impact on the expression of the autoinducer synthase is already well described (e.g. in the closely related α-proteobacterium *S. meliloti* (Baumgardt et al., 2014)). In our study on *R. sphaeroides*, qRT-PCR (Figure 10) and RNA-seq (read coverage shown in Figure S6) independently confirmed the enrichment of *cerI* mRNA in the *rnc*⁻ mutant strain, indicating an action of RNase III on the Lux-type QS system. Analysis of the *cerI* mRNA half-life (Figure 10c) revealed increased stability in the mutant strain. Interestingly, we were able to show that RNase III deficiency leads to hyperproduction of AHLs in *R. sphaeroides* (Figure 10a), probably through the enrichment of *cerI* mRNA thus accumulating CerI enzyme in the mutant. For the second component of the *R. sphaeroides* Lux-type system, the signal receptor *cerR*, we did not observe an mRNA enrichment (Figure 10b). As the Lux-type QS system represents a positive feed-forward loop, where AHLs bind to *cerR* and as a complex activate transcription of *cerI*, it is conceivable that also *cerR* is differentially expressed at high AHL concentrations. However, as *cerR* is preceded by its own promoter and we did not find any relevant increase or decrease in *cerR* abundance, we conclude that the transcription of *cerR* is regulated independently of the transcription of *cerI*. Interestingly, we were able to map several bona fide RNase III cleavage sites inside the open reading frame of the *cerI* mRNA as seen in Figure S6 (three under aerobic conditions, one under aerobic conditions), which could account for the measured stabilisation and accumulation of *cerI* mRNA in the *rnc*⁻ mutant (Figure 10b,c).

Not all *rnc*-dependent effects observed in our transcriptome analysis may be a direct consequence of RNase III cleavage. This can also be seen in a correlation analysis (Figure S10), where we plotted all annotated RNAs from the RNA-seq analysis according to their expression change against the amount of mapped bona fide RNase III cleavage sites. As we observed a widespread expression change of RNAs without mapped cleavage sites, only a slight tendency towards reduced abundance in the mutant was visible for RNAs harbouring mapped cleavage sites. In addition, RNAs with increased amount of mapped cleavage sites showed an unaffected (log_2 fold change mutant/wt of nearly 0) or even increased abundance in the mutant.

On one hand, RNase III directly affects, for example, mRNAs for transcriptional regulators or regulatory small RNAs that in turn will regulate the expression of other genes. Furthermore, as described in the introduction, RNase III is known to regulate the expression of *pnp* for PNPase, which acts as a 3′ to 5′ exoribonuclease. Lack of RNase III activity leads to changed *pnp* levels in *R. sphaeroides* and also to changed *rne* levels (as seen per DESeq2 analysis in Supplementary Tables S3 and S4). We have previously shown that also PNPase and RNase E have strong effects on the *R. sphaeroides* transcriptome and influence stress resistance (Förstner et al., 2018; Spanka et al., 2021). As previous publications, this study emphasises the important role of RNases in bacterial gene regulation.

4 | EXPERIMENTAL PROCEDURES

4.1 | Cultivation of bacterial strains

R. sphaeroides and *Sinorhizobium meliloti* were cultivated in malate minimal medium (Remes et al., 2014) at 32°C. Cultivation of *Escherichia coli* S17-1 (Simon et al., 1983) for cloning procedures and diparental conjugation (Klug & Drews, 1984) was performed in standard I medium (Roth) at 37°C and 180 rpm. *R. sphaeroides* strains were grown either at a high oxygen concentration of 160–180 μM dissolved oxygen (aerobic cultures), low oxygen concentration of 25–30 μM dissolved oxygen (microaerobic cultures) or anaerobically with 60 $W * m^{-2}$ white light (phototrophic cultures).

For determination of RNA half-lives, 0.2 mg/mL rifampicin (Serva Electrophoresis) was added to exponentially grown biological triplicates of *R. sphaeroides* wild type and *rnc*_GD48,49SR-mutant strain (*rnc*⁻). Cell samples were collected prior to the addition ($t = 0$ min) and 5, 10, 15, 20 and 25 min afterwards.

For induction of the bacterial stress response, biological triplicates of wild type and mutant strain were grown microaerobically to mid-exponential growth phase followed by incubation in the presence of 0.25 mM paraquat (Sigma-Aldrich), 0.3 mM tBOOH (Sigma-Aldrich), 0.01 mM $CdCl_2$ (Sigma-Aldrich) or 0.5 mM H_2O_2 (Roth) for 20 min prior to sample collection. For heat stress, the exponential cultures were shifted to 42°C for 60 min.

4.2 | Construction of the *R. sphaeroides* RNase III mutant

All oligonucleotides used in this study are listed in Supplementary Table S5. To inactivate the catalytic function of RNase III in *R. sphaeroides*, two relevant amino acids in the active centre of the native enzyme were substituted (G48S, D49R). For this, the whole 690 bp open reading frame of the native RNase III encoding gene (*rnc*) of *R. sphaeroides* 2.4.1 was amplified by PCR using the oligonucleotides rnc_frag_for_BamHI and rnc_frag_rev_KpnI. The resulting amplicon was ligated into the pJet1.2/blunt vector (Thermo Scientific) following the manufacturer's protocol, yielding plasmid pJet-rnc. To mutate the nucleotides of interest within the *rnc* gene by side-directed mutagenesis, plasmid pJet-rnc was amplified by PCR using the oligonucleotides rnc_rolling_for and rnc_rolling_rev, yielding plasmid pJet-rnc-mut. Subsequently, pJet-rnc-mut was restricted using restriction enzymes *Bam*HI and *Xba*I. The resulting 705 bp fragment was electrophoretically separated on a 1% (w/v) agarose TAE gel, extracted using the innuPREP DOUBLEpure kit (Analytik Jena) according to the manufacturer's protocol, and inserted into the suicide vector pK18mobII-*sacB* (Schäfer et al., 1994) by *Bam*HI and

*Xba*I, yielding plasmid pK18-rnc-mut. Subsequently, pK18-rnc-mut was transferred in *R. sphaeroides* 2.4.1 wild type by diparental conjugation with *E. coli* S17-1 and used for chromosomal integration via homologous recombination (double cross-over).

For complementation of the RNase III deficiency, the native *rnc* gene was cloned under transcriptional control of the native *lep-rnc-era* promoter on the expression vector pRK4352 (Mank et al., 2012). The 400 bp promoter region directly upstream of the *lep* gene was amplified by PCR using the oligonucleotides Prnc_for_HindIII and Prnc_rev_BamHI. The resulting amplicon was inserted to pRK4352 via *Hin*dIII and *Bam*HI, followed by insertion of the previously generated *rnc* containing 690 bp fragment via *Bam*HI and *Kpn*I, yielding plasmid pRK-*rnc*. pRK-*rnc* was transferred to the *R. sphaeroides* RNase III mutant by diparental conjugation using *E. coli* S17-1.

To insert additional transcription terminators directly downstream to the rRNA operons within the *rnc*$^-$ mutant, we cloned three DNA fragments for homologues recombination into modified pK18 plasmids, pK1.2 (Kretz et al., 2023), harbouring an array of four *rrnB* T1 transcription terminators (Ham et al., 2006). The three fragments for homologues recombination were amplified from genomic DNA of *R. sphaeroides* 2.4.1 by PCR using oligonucleotide pairs Term1_for_HindIII and Term1_rev_XbaI, Term2_for_HindIII and Term2_rev_XbaI and Term3_for_HindIII and Term3_rev_XbaI. Subsequently, the amplicons were inserted into pK1.2 with *Hin*dIII and *Xba*I. The resulting plasmids were transferred to the *R. sphaeroides rnc*$^-$ strain by diparental conjugation using *E. coli* S17-1 followed by chromosomal integration via homologues recombination (single cross-over), introducing the *rrnB* T1 transcription terminator array at the targeted sequences downstream of the *R. sphaeroides* rRNA operons.

4.3 | Analysis of photopigments

Biological triplicates of wild type and *rnc*$^-$ mutant were grown under microaerobic or phototrophic conditions to mid-exponential growth phase. Cells from 1 mL of culture were sedimented by centrifugation for 10 min at 8000 rpm and cell pellets were resuspended in 50 µL ddH_2O. 500 µL acetone/methanol (7:2, v/v) were added to extract the photopigments. Cell debris was removed by centrifugation for 5 min at 13,000 rpm, and the supernatant was used for absorbance measurements at $\lambda = 770$ nm (bacteriochlorophyll a) and $\lambda = 585$ nm (carotenoids). Concentrations were calculated using the extinction coefficient 76 $mM^{-1}cm^{-1}$ (bacteriochlorophyll a) or 128 $mM^{-1}cm^{-1}$ (carotenoids).

For analysis of whole-cell spectra, 800 µL cell culture samples were collected, and the absorbance values between $\lambda = 400$ nm and $\lambda = 900$ nm were measured on a spectrophotometer (Specord 50, Analytik Jena) and subsequently normalised to OD_{660}.

4.4 | Assessment of bacterial stress resistance

For survival assays, biological triplicates of wild type and *rnc*$^-$ mutant were grown microaerobically to mid-exponential growth phase. The bacterial stress response was induced as described above. 10^{-5} dilutions of the cultures were plated on malate minimal agar plates and incubated for 48 h at 32°C. Colony-forming units per mL were calculated, and the survival rate at 32°C without stress agents was used as a reference.

The zone of inhibition assay was performed as described previously (Grützner, Billenkamp, et al., 2021). 5 µL of 0.1 M $CdCl_2$, 0.5 M tBOOH, 1 M H_2O_2 and 0.01 M methylene blue were spotted on the filter discs. The agar plates were either incubated in the dark or illuminated with 85 µmol $m^{-2}s^{-1}$ white light (only for plates treated with methylene blue).

4.5 | AHL measurements

To assess concentrations of secreted AHLs from *R. sphaeroides* wild type and *rnc*$^-$ mutant, a previously established *S. meliloti* reporter strain (McIntosh et al., 2019) was used, that carries a transcriptional fusion of the SMb20911 promoter (promoter controlling the transcription of an uncharacterised small open reading frame in *S. meliloti* 1021) and the mVenus gene on a low copy plasmid. Since the SMb20911 promoter is fully active in the absence of AHLs and becomes repressed by rising AHL concentration, the resulting mVenus fluorescence (extinction: 515 nm; emission: 548 nm) is negatively correlated to the applied AHL concentration.

The *S. meliloti* reporter strain was grown in malate minimal medium and increasing amounts (0%–100%) of cell-free supernatant from microaerobically grown *R. sphaeroides* wild type cultures, to assess the correlation between autoinducer concentration and reduction of mVenus signal. To quantify the secreted AHL amounts of the *R. sphaeroides rnc*$^-$ strain, biological triplicates of the *S. meliloti* reporter strain were cultivated in 25% cell-free supernatant from the microaerobically grown *R. sphaeroides rnc*$^-$ strain and malate minimal medium. A reporter culture grown in malate minimal medium with 400 nM commercially obtained oxo-C16:1-HL (N-3-oxo-hexadec-11(Z)-enoyl-L-homoserine lactone; Cayman Chemical) served as reference.

4.6 | Quantification of RNA abundances

RNA isolation was performed as described previously (Börner et al., 2023), using the hot phenol technique (Damm et al., 2015; Janzon et al., 1986).

For northern blot analysis, either 7 µg or 10 µg total RNA was electrophoretically separated on denaturing 10% polyacrylamide gels, transferred to 0.45 µM nylon membranes by semidry electroblotting and subsequently immobilised by UV crosslinking. For specific detection, immobilised RNAs were hybridised with radiolabelled antisense DNA oligonucleotides (listed in Supplementary Table S5) in Church buffer with low stringency (Church & Gilbert, 1984). After hybridisation, membranes were washed with 5× SSC buffer containing 0.01% SDS twice under rotation

at 42°C, dried and exposed to a phosphor imaging screen (Bio-Rad). Phosphor imaging signals were evaluated using the Quantity One® 1-D analysis software (Bio-Rad). For removal of the hybridised DNA oligonucleotides, membranes were incubated in 5× SSC buffer containing 0.1% SDS for 20 min at 95°C and 80 rpm. 3′ end labelling of DNA oligonucleotides was performed using [γ-^{32}P] ATP (Hartmann Analytic) and T4 polynucleotide kinase (NEB) following the manufacturer's protocol.

Quantitative-reverse transcriptase PCR (qRT-PCR) and RNA sequencing of DNA-free total RNA were performed as described in Börner et al., 2023. The oligonucleotides used for qRT-PCR are listed in Supplementary Table S5.

4.7 | Bioinformatics analysis

Samples from biological triplicates of wild type and *rnc*$^-$-mutant strains, grown under aerobic, microaerobic or phototrophic growth conditions, were analysed by RNA sequencing. Raw sequencing data were aligned to the reference genome of *R. sphaeroides* (NC_007493.2, NC_007494.2, NC_009007.1, NC_007488.2, NC_007489.1, NC_007490.2 and NC_009008.1), saved as binary alignment maps (BAM) files and converted to coverage tracks (wiggle) using the READemption pipeline (Förstner et al., 2014) v.1.0.5. Wiggle files for the individual samples that belong to the same condition were merged within R v.4.1.2 using rtracklayer v.1.56.1 (Lawrence et al., 2009). Read counts per gene were identified using the summarize Overlaps function (Lawrence et al., 2013) based on the BAM files and the gene transfer file (GTF) file of *R. sphaeroides*. Transcriptome changes between the growth conditions (aerobic, microaerobic or phototrophic) were individually calculated for the wild type and *rnc*$^-$ mutant using DESeq2 v. 1.32 (Love et al., 2014). In order to identify differentially expressed genes between wild type and mutant, the individual significantly differentially regulated genes ($\log_2$ fold change >1 or <−1, adjusted *p*-value <0.05, mean of read counts >10) of both wild type and mutant between different growth conditions were plotted as heat maps. These heat maps were unsupervised agglomerative hierarchical clustered to reveal different expression patterns between wild type and mutant.

Identification and annotation of bona fide cleavage sites were previously described in detail (Börner et al., 2023). In short, strand-specific 5′ counts were compared between wild type and mutant using DESeq2 v.1.32 and subsequently filtered for minimal counts of >10, $\log_2$ fold change >1 and adjusted *p*-value <0.05. Multiple 5′ ends that fulfil all criteria and were localised within three base positions adjacent to each other were merged. Annotation of the features associated with cleavage sites was performed based on the *R. sphaeroides* GTF file using the GenomicRanges (Lawrence et al., 2013) package.

In order to compare the transcriptomic effects of RNase III between *R. sphaeroides* and *E. coli*, raw RNA-seq reads from *E. coli* wild type and RNase III mutant were downloaded from the ArrayExpress repository (accession number: E-MTAB-9507). These raw reads were aligned against the K12 DH10B *E. coli* reference genome and coverage tracks (wiggle) were generated using READemption v.1.0.5.

4.8 | RNase III activity reporter assay

To investigate the RNase III activity in vivo, a new reporter plasmid similar to our previously described construct for assaying RNase E activity (Börner et al., 2023) was generated. For this, we introduced the well-known RNase III cleavage site of the native pre-16S rRNA into the previously constructed pPHU231-p16S-mVenus plasmid (Börner et al., 2023).

The 82 bp genomic sequence of the pre-16S rRNA cleavage site was amplified by PCR using oligonucleotides 5′_16S_for_ScaI and 5′_16S_rev_XbaI, followed by insertion into pPHU231-p16S-mVenus via *Sca*I and *Xba*I yielding plasmid pPHU231-5′UTR-mVenus (indicator plasmid). Subsequently, the plasmid was transferred to *rnc*$^-$ and wild type cells by diparental conjugation using the *E. coli* S17-1 strain.

Cultivation of the conjugants and measurements of the resulting mVenus fluorescence were performed as described previously (Börner et al., 2023). As a reference, the mVenus fluorescence generated by the wild type and *rnc*$^-$ strain carrying the control plasmid (pPHU231-p16S-mVenus) was analysed.

AUTHOR CONTRIBUTIONS

Gabriele Klug: Methodology; conceptualization; funding acquisition; writing – original draft; writing – review and editing; data curation; supervision; formal analysis; project administration; resources. **Janek Börner:** Conceptualization; methodology; investigation; writing – original draft; writing – review and editing; validation; data curation; visualization; project administration; formal analysis. **Tobias Friedrich:** Investigation; writing – review and editing; visualization; data curation; formal analysis; software.

ACKNOWLEDGEMENTS

We thank Kerstin Haberzettl and Andrea Weisert for excellent technical assistance with DNA cloning procedures, Florian Gerken and Fabian Droß for experimental support, Florian Leinberger for assistance with RNA-seq cross-sample normalisation and Matthew McIntosh for help and fruitful discussions concerning the quorum-sensing system investigations. This work was funded by Deutsche Forschungsgemeinschaft (DFG KI563/41-1). Open Access funding enabled and organized by Projekt DEAL.

CONFLICT OF INTEREST STATEMENT

None declared.

DATA AVAILABILITY STATEMENT

The RNA-seq data analysed in this study are publicly available in the NCBI Gene Expression Omnibus (GEO, https://www.ncbi.nlm.nih.gov/geo/) repository with the accession numbers GSE200990 (wild type samples) and GSE236804 (RNase III mutant samples).

ETHICS STATEMENT

The authors declare that no human or animal subjects were used in this study.

ORCID

Janek Börner https://orcid.org/0000-0003-4824-9393
Tobias Friedrich https://orcid.org/0000-0003-4014-8678
Gabriele Klug https://orcid.org/0000-0002-3527-5093

REFERENCES

Adnan, F., Weber, L. & Klug, G. (2015) The sRNA SorY confers resistance during photooxidative stress by affecting a metabolite transporter in *Rhodobacter sphaeroides*. *RNA Biology*, 12, 569–577.

Afonyushkin, T., Vecerek, B., Moll, I., Bläsi, U. & Kaberdin, V.R. (2005) Both RNase E and RNase III control the stability of *sodB* mRNA upon translational inhibition by the small regulatory RNA RyhB. *Nucleic Acids Research*, 33, 1678–1689.

Altuvia, Y., Bar, A., Reiss, N., Karavani, E., Argaman, L. & Margalit, H. (2018) In vivo cleavage rules and target repertoire of RNase III in *Escherichia coli*. *Nucleic Acids Research*, 46, 10380–10394.

Apirion, D., Neil, J. & Watson, N. (1976) Revertants from RNase III negative strains of *Escherichia coli*. *Molecular & General Genetics*, 149, 201–210.

Apirion, D. & Watson, N. (1975) Mapping and characteryation of a mutation in *Escherichia coli* that reduces the level of ribonuclease III specific for double-stranded ribonucleic acid. *Journal of Bacteriology*, 124, 317–324.

Baumgardt, K., Charoenpanich, P., McIntosh, M., Schikora, A., Stein, E., Thalmann, S. et al. (2014) RNase E affects the expression of the acyl-homoserine lactone synthase gene *sinI* in *Sinorhizobium meliloti*. *Journal of Bacteriology*, 196, 1435–1447.

Belasco, J.G. & Brawerman, G. (Eds.). (1993) *Control of messenger RNA stability*. New York, NY: Academic Press.

Berghoff, B.A., Glaeser, J., Sharma, C.M., Vogel, J. & Klug, G. (2009) Photooxidative stress-induced and abundant small RNAs in *Rhodobacter sphaeroides*. *Molecular Microbiology*, 74, 1497–1512.

Billenkamp, F., Peng, T., Berghoff, B.A. & Klug, G. (2015) A cluster of four homologous small RNAs modulates C1 metabolism and the pyruvate dehydrogenase complex in *Rhodobacter sphaeroides* under various stress conditions. *Journal of Bacteriology*, 197, 1839–1852.

Blomberg, P., Wagner, E.G. & Nordström, K. (1990) Control of replication of plasmid R1: the duplex between the antisense RNA, CopA, and its target, CopT, is processed specifically in vivo and in vitro by RNase III. *The EMBO Journal*, 9, 2331–2340.

Boisset, S., Geissmann, T., Huntzinger, E., Fechter, P., Bendridi, N., Possedko, M. et al. (2007) *Staphylococcus aureus* RNAIII coordinately represses the synthesis of virulence factors and the transcription regulator Rot by an antisense mechanism. *Genes & Development*, 21, 1353–1366.

Börner, J., Friedrich, T., Bartkuhn, M. & Klug, G. (2023) Ribonuclease E strongly impacts bacterial adaptation to different growth conditions. *RNA Biology*, 20, 120–135.

Braatsch, S., Gomelsky, M., Kuphal, S. & Klug, G. (2002) A single flavoprotein, AppA, integrates both redox and light signals in *Rhodobacter sphaeroides*. *Molecular Microbiology*, 45, 827–836.

Cagliero, C., Zhou, Y.N. & Jin, D.J. (2014) Spatial organization of transcription machinery and its segregation from the replisome in fast-growing bacterial cells. *Nucleic Acids Research*, 42, 13696–13705.

Carmell, M.A. & Hannon, G.J. (2004) RNase III enzymes and the initiation of gene silencing. *Nature Structural & Molecular Biology*, 11, 214–218.

Carzaniga, T., Briani, F., Zangrossi, S., Merlino, G., Marchi, P. & Dehò, G. (2009) Autogenous regulation of *Escherichia coli* polynucleotide phosphorylase expression revisited. *Journal of Bacteriology*, 191, 1738–1748.

Church, G.M. & Gilbert, W. (1984) Genomic sequencing. *Proceedings of the National Academy of Sciences of the United States of America*, 81, 1991–1995.

Conrad, S.E. & Campbell, J.L. (1979) Role of plasmid-coded RNA and ribonuclease III in plasmid DNA replication. *Cell*, 18, 61–71.

Cortez, N., Carrillo, N., Pasternak, C., Balzer, A. & Klug, G. (1998) Molecular cloning and expression analysis of the *Rhodobacter capsulatus sodB* gene, encoding an iron superoxide dismutase. *Journal of Bacteriology*, 180, 5413–5420.

Court, D.L., Gan, J., Liang, Y.-H., Shaw, G.X., Tropea, J.E., Costantino, N. et al. (2013) RNase III: genetics and function; structure and mechanism. *Annual Review of Genetics*, 47, 405–431.

Damm, K., Bach, S., Müller, K.M.H., Klug, G., Burenina, O.Y., Kubareva, E.A. et al. (2015) Impact of RNA isolation protocols on RNA detection by Northern blotting. *Methods in Molecular Biology (Clifton, N.J.)*, 1296, 29–38.

Das, A. (1993) Control of transcription termination by RNA-binding proteins. *Annual Review of Biochemistry*, 62, 893–930.

Dasgupta, S., Fernandez, L., Kameyama, L., Inada, T., Nakamura, Y., Pappas, A. et al. (1998) Genetic uncoupling of the dsRNA-binding and RNA cleavage activities of the *Escherichia coli* endoribonuclease RNase III—the effect of dsRNA binding on gene expression. *Molecular Microbiology*, 28, 629–640.

Davies, B.W., Köhrer, C., Jacob, A.I., Simmons, L.A., Zhu, J., Aleman, L.M. et al. (2010) Role of *Escherichia coli* YbeY, a highly conserved protein, in rRNA processing. *Molecular Microbiology*, 78, 506–518.

DeRosa, M.C. & Crutchley, R.J. (2002) Photosensitized singlet oxygen and its applications. *Coordination Chemistry Reviews*, 233, 351–371.

Deutscher, M.P. (2009) Maturation and degradation of ribosomal RNA in bacteria. *Progress in Molecular Biology and Translational Science*, 85, 369–391.

Dufour, Y.S., Imam, S., Koo, B.-M., Green, H.A. & Donohue, T.J. (2012) Convergence of the transcriptional responses to heat shock and singlet oxygen stresses. *PLoS Genetics*, 8, e1002929.

Duggal, Y., Fontaine, B.M., Dailey, D.M., Ning, G. & Weinert, E.E. (2020) RNase I modulates *Escherichia coli* motility, metabolism, and resistance. *ACS Chemical Biology*, 15, 1996–2004.

Dunn, J.J. & Studier, F.W. (1973) T7 early RNAs and *Escherichia coli* ribosomal RNAs are cut from large precursor RNAs in vivo by ribonuclease 3. *Proceedings of the National Academy of Sciences of the United States of America*, 70, 3296–3300.

Eisenhardt, K.M.H., Remes, B., Grützner, J., Spanka, D.-T., Jäger, A. & Klug, G. (2021) A complex network of sigma factors and sRNA StsR regulates stress responses in *R. sphaeroides*. *International Journal of Molecular Sciences*, 22, 7557.

Eisenhardt, K.M.H., Reuscher, C.M. & Klug, G. (2018) PcrX, an sRNA derived from the 3′- UTR of the *Rhodobacter sphaeroides puf* operon modulates expression of *puf* genes encoding proteins of the bacterial photosynthetic apparatus. *Molecular Microbiology*, 110, 325–334.

Engebrecht, J. & Silverman, M. (1984) Identification of genes and gene products necessary for bacterial bioluminescence. *Proceedings of the National Academy of Sciences of the United States of America*, 81, 4154–4158.

Evguenieva-Hackenberg, E. (2005) Bacterial ribosomal RNA in pieces. *Molecular Microbiology*, 57, 318–325.

Evguenieva-Hackenberg, E. & Klug, G. (2000) RNase III processing of intervening sequences found in helix 9 of 23S rRNA in the alpha subclass of *Proteobacteria*. *Journal of Bacteriology*, 182, 4719–4729.

Förstner, K.U., Reuscher, C.M., Haberzettl, K., Weber, L. & Klug, G. (2018) RNase E cleavage shapes the transcriptome of *Rhodobacter*

sphaeroides and strongly impacts phototrophic growth. *Life Science Alliance*, 1, e201800080.

Förstner, K.U., Vogel, J. & Sharma, C.M. (2014) READemption-a tool for the computational analysis of deep-sequencing-based transcriptome data. *Bioinformatics*, 30, 3421–3423.

Freese, N.H., Norris, D.C. & Loraine, A.E. (2016) Integrated genome browser: visual analytics platform for genomics. *Bioinformatics*, 32, 2089–2095.

French, S.L. & Miller, O.L. (1989) Transcription mapping of the *Escherichia coli* chromosome by electron microscopy. *Journal of Bacteriology*, 171, 4207–4216.

Fuqua, W.C., Winans, S.C. & Greenberg, E.P. (1994) Quorum sensing in bacteria: the LuxR-LuxI family of cell density-responsive transcriptional regulators. *Journal of Bacteriology*, 176, 269–275.

Gatewood, M.L., Bralley, P. & Jones, G.H. (2011) RNase III-dependent expression of the *rpsO-pnp* operon of *Streptomyces coelicolor*. *Journal of Bacteriology*, 193, 4371–4379.

Gatewood, M.L., Bralley, P., Weil, M.R. & Jones, G.H. (2012) RNA-Seq and RNA immunoprecipitation analyses of the transcriptome of *Streptomyces coelicolor* identify substrates for RNase III. *Journal of Bacteriology*, 194, 2228–2237.

Gerdes, K., Nielsen, A., Thorsted, P. & Wagner, E.G. (1992) Mechanism of killer gene activation. Antisense RNA-dependent RNase III cleavage ensures rapid turn-over of the stable *hok*, *srnB* and *pndA* effector messenger RNAs. *Journal of Molecular Biology*, 226, 637–649.

Gomelsky, M. & Kaplan, S. (1997) Molecular genetic analysis suggesting interactions between AppA and PpsR in regulation of photosynthesis gene expression in *Rhodobacter sphaeroides* 2.4. 1. *Journal of Bacteriology*, 179, 128–134.

Greenberg, E.P., Hastings, J.W. & Ulitzur, S. (1979) Induction of luciferase synthesis in *Beneckea harveyi* by other marine bacteria. *Archives of Microbiology*, 120, 87–91.

Gregor, J. & Klug, G. (1999) Regulation of bacterial photosynthesis genes by oxygen and light. *FEMS Microbiology Letters*, 179, 1–9.

Grinwald, M. & Ron, E.Z. (2013) The *Escherichia coli* translation-associated heat shock protein YbeY is involved in rRNA transcription antitermination. *PLoS ONE*, 8, e62297.

Grützner, J., Billenkamp, F., Spanka, D.-T., Rick, T., Monzon, V., Förstner, K.U. et al. (2021) The small DUF1127 protein CcaF1 from *Rhodobacter sphaeroides* is an RNA-binding protein involved in sRNA maturation and RNA turnover. *Nucleic Acids Research*, 49, 3003–3019.

Grützner, J., Börner, J., Jäger, A. & Klug, G. (2023) The small RNA-binding protein CcaF1 promotes formation of photosynthetic complexes in *Rhodobacter sphaeroides*. *International Journal of Molecular Sciences*, 24, 9515.

Grützner, J., Remes, B., Eisenhardt, K.M.H., Scheller, D., Kretz, J., Madhugiri, R. et al. (2021) sRNA-mediated RNA processing regulates bacterial cell division. *Nucleic Acids Research*, 49, 7035–7052.

Ham, T.S., Lee, S.K., Keasling, J.D. & Arkin, A.P. (2006) A tightly regulated inducible expression system utilizing the *fim* inversion recombination switch. *Biotechnology and Bioengineering*, 94, 1–4.

Han, Y., Meyer, M.H., Keusgen, M. & Klug, G. (2007) A haem cofactor is required for redox and light signalling by the AppA protein of *Rhodobacter sphaeroides*. *Molecular Microbiology*, 64, 1090–1104.

Hördt, A., López, M.G., Meier-Kolthoff, J.P., Schleuning, M., Weinhold, L.-M., Tindall, B.J. et al. (2020) Analysis of 1,000+ type-strain genomes substantially improves taxonomic classification of *alphaproteobacteria*. *Frontiers in Microbiology*, 11, 468.

Huntzinger, E., Boisset, S., Saveanu, C., Benito, Y., Geissmann, T., Namane, A. et al. (2005) *Staphylococcus aureus* RNAIII and the endoribonuclease III coordinately regulate *spa* gene expression. *The EMBO Journal*, 24, 824–835.

Ifill, G., Blimkie, T., Lee, A.H.Y., Mackie, G.A., Chen, Q., Stibitz, S. et al. (2021) RNase III and RNase E influence posttranscriptional regulatory networks involved in virulence factor production, metabolism, and regulatory RNA processing in *Bordetella pertussis*. *mSphere*, 6, 10–1128.

Imam, S., Noguera, D.R. & Donohue, T.J. (2014) Global analysis of photosynthesis transcriptional regulatory networks. *PLoS Genetics*, 10, e1004837.

Jacob, A.I., Köhrer, C., Davies, B.W., RajBhandary, U.L. & Walker, G.C. (2013) Conserved bacterial RNase YbeY plays key roles in 70S ribosome quality control and 16S rRNA maturation. *Molecular Cell*, 49, 427–438.

Janzon, L., Löfdahl, S. & Arvidson, S. (1986) Evidence for a coordinate transcriptional control of alpha-toxin and protein a synthesis in *Staphylococcus aureus*. *FEMS Microbiology Letters*, 33(2–3), 193–198.

Jørgensen, M.G., Pettersen, J.S. & Kallipolitis, B.H. (2020) sRNA-mediated control in bacteria: an increasing diversity of regulatory mechanisms. *Biochimica et Biophysica Acta (BBA) - Gene Regulatory Mechanisms*, 1863, 194504.

Kang, H. & Hata, A. (2012) Control of Drosha-mediated microRNA maturation by smad proteins. In: *Eukaryotic RNases and their partners in RNA degradation and biogenesis, part B*. New York, NY: Elsevier, pp. 123–136.

Kindler, P., Keil, T.U. & Hofschneider, P.H. (1973) Isolation and characterization of a ribonuclease 3 deficient mutant of *Escherichia coli*. *Molecular & General Genetics*, 126, 53–59.

King, T.C., Sirdeshmukh, R. & Schlessinger, D. (1984) RNase III cleavage is obligate for maturation but not for function of *Escherichia coli* pre-23S rRNA. *Proceedings of the National Academy of Sciences of the United States of America*, 81, 185–188.

Klug, G. & Drews, G. (1984) Construction of a gene bank of *Rhodopseudomonas capsulata* using a broad host range DNA cloning system. *Archives of Microbiology*, 139, 319–325.

Kretz, J., Israel, V. & McIntosh, M. (2023) Design–build–test of synthetic promoters for inducible gene regulation in alphaproteobacteria. *ACS Synthetic Biology.*, 12, 2663–2675.

Lalaouna, D., Baude, J., Wu, Z., Tomasini, A., Chicher, J., Marzi, S. et al. (2019) RsaC sRNA modulates the oxidative stress response of *Staphylococcus aureus* during manganese starvation. *Nucleic Acids Research*, 47, 9871–9887.

Lawrence, M., Gentleman, R. & Carey, V. (2009) rtracklayer: an R package for interfacing with genome browsers. *Bioinformatics*, 25, 1841–1842.

Lawrence, M., Huber, W., Pagès, H., Aboyoun, P., Carlson, M., Gentleman, R. et al. (2013) Software for computing and annotating genomic ranges. *PLoS Computational Biology*, 9, e1003118.

Lejars, M. & Hajnsdorf, E. (2022) RNase III participates in the adaptation to temperature shock and oxidative stress in *Escherichia coli*. *Microorganisms*, 10, 699.

Lioliou, E., Sharma, C.M., Caldelari, I., Helfer, A.-C., Fechter, P., Vandenesch, F. et al. (2012) Global regulatory functions of the *Staphylococcus aureus* endoribonuclease III in gene expression. *PLoS Genetics*, 8, e1002782.

Love, M.I., Huber, W. & Anders, S. (2014) Moderated estimation of fold change and dispersion for RNA-seq data with DESeq2. *Genome Biology*, 15, 550.

Maes, A., Gracia, C., Innocenti, N., Zhang, K., Aurell, E. & Hajnsdorf, E. (2017) Landscape of RNA polyadenylation in *E. coli*. *Nucleic Acids Research*, 45, 2746–2756.

Mahendran, G., Jayasinghe, O.T., Thavakumaran, D., Arachchilage, G.M. & Silva, G.N. (2022) Key players in regulatory RNA realm of bacteria. *Biochemistry and Biophysics Reports*, 30, 101276.

Mank, N.N., Berghoff, B.A., Hermanns, Y.N. & Klug, G. (2012) Regulation of bacterial photosynthesis genes by the small noncoding RNA PcrZ. *Proceedings of the National Academy of Sciences of the United States of America*, 109, 16306–16311.

Masuda, S. & Bauer, C.E. (2002) AppA is a blue light photoreceptor that antirepresses photosynthesis gene expression in *Rhodobacter sphaeroides*. *Cell*, 110, 613–623.

McIntosh, M., Serrania, J. & Lacanna, E. (2019) A novel LuxR-type solo of *Sinorhizobium meliloti*, NurR, is regulated by the chromosome replication coordinator, DnaA and activates quorum sensing. *Molecular Microbiology*, 112, 678–698.

McKellar, S.W., Ivanova, I., Arede, P., Zapf, R.L., Mercier, N., Chu, L.-C. et al. (2022) RNase III CLASH in MRSA uncovers sRNA regulatory networks coupling metabolism to toxin expression. *Nature Communications*, 13, 3560.

Mediati, D.G., Wong, J.L., Gao, W., McKellar, S., Pang, C.N.I., Wu, S. et al. (2022) RNase III-CLASH of multi-drug resistant *Staphylococcus aureus* reveals a regulatory mRNA 3′ UTR required for intermediate vancomycin resistance. *Nature Communications*, 13, 3558.

Miller, M.B. & Bassler, B.L. (2001) Quorum sensing in bacteria. *Annual Review of Microbiology*, 55, 165–199.

Möller, P., Busch, P., Sauerbrei, B., Kraus, A., Förstner, K.U., Wen, T.-N. et al. (2019) The RNase YbeY is vital for ribosome maturation, stress resistance, and virulence of the natural genetic engineer *Agrobacterium tumefaciens*. *Journal of Bacteriology*, 201, e00730-18.

Müller, K.M.H., Berghoff, B.A., Eisenhardt, B.D., Remes, B. & Klug, G. (2016) Characteristics of Pos19—a small coding RNA in the oxidative stress response of *Rhodobacter sphaeroides*. *PLoS ONE*, 11, e0163425.

Nashimoto, H. & Uchida, H. (1985) DNA sequencing of the *Escherichia coli* ribonuclease III gene and its mutations. *Molecular & General Genetics*, 201, 25–29.

Nealson, K.H., Platt, T. & Hastings, J.W. (1970) Cellular control of the synthesis and activity of the bacterial luminescent system. *Journal of Bacteriology*, 104, 313–322.

Nicholson, A.W. (2014) Ribonuclease III mechanisms of double-stranded RNA cleavage. *Wiley Interdisciplinary Reviews. RNA*, 5, 31–48.

Nikolaev, N., Silengo, L. & Schlessinger, D. (1973) Synthesis of a large precursor to ribosomal RNA in a mutant of *Escherichia coli*. *Proceedings of the National Academy of Sciences of the United States of America*, 70, 3361–3365.

Nuss, A.M., Glaeser, J., Berghoff, B.A. & Klug, G. (2010) Overlapping alternative sigma factor regulons in the response to singlet oxygen in *Rhodobacter sphaeroides*. *Journal of Bacteriology*, 192, 2613–2623.

Nuss, A.M., Glaeser, J. & Klug, G. (2009) RpoH(II) activates oxidative-stress defense systems and is controlled by RpoE in the singlet oxygen-dependent response in *Rhodobacter sphaeroides*. *Journal of Bacteriology*, 191, 220–230.

Opdyke, J.A., Fozo, E.M., Hemm, M.R. & Storz, G. (2011) RNase III participates in GadY-dependent cleavage of the *gadX-gadW* mRNA. *Journal of Molecular Biology*, 406, 29–43.

Papenfort, K. & Melamed, S. (2023) Small RNAs, large networks: post-transcriptional regulons in gram-negative bacteria. *Annual Review of Microbiology*, 77, 23–43.

Peng, T., Berghoff, B.A., Oh, J.-I., Weber, L., Schirmer, J., Schwarz, J. et al. (2016) Regulation of a polyamine transporter by the conserved 3′ UTR-derived sRNA SorX confers resistance to singlet oxygen and organic hydroperoxides in *Rhodobacter sphaeroides*. *RNA Biology*, 13, 988–999.

Portier, C., Dondon, L., Grunberg-Manago, M. & Régnier, P. (1987) The first step in the functional inactivation of the *Escherichia coli* polynucleotide phosphorylase messenger is a ribonuclease III processing at the 5′ end. *The EMBO Journal*, 6, 2165–2170.

Rath, E.C., Pitman, S., Cho, K.H. & Bai, Y. (2017) Identification of streptococcal small RNAs that are putative targets of RNase III through bioinformatics analysis of RNA sequencing data. *BMC Bioinformatics*, 18, 111–120.

Rauhut, R., Jäger, A., Conrad, C. & Klug, G. (1996) Identification and analysis of the *rnc* gene for RNase III in *Rhodobacter capsulatus*. *Nucleic Acids Research*, 24, 1246–1251.

Régnier, P. & Grunberg-Manago, M. (1990) RNase III cleavages in non-coding leaders of *Escherichia coli* transcripts control mRNA stability and genetic expression. *Biochimie*, 72, 825–834.

Remes, B., Berghoff, B.A., Förstner, K.U. & Klug, G. (2014) Role of oxygen and the OxyR protein in the response to iron limitation in *Rhodobacter sphaeroides*. *BMC Genomics*, 15, 794.

Reuscher, C.M. & Klug, G. (2021) Antisense RNA asPcrL regulates expression of photosynthesis genes in *Rhodobacter sphaeroides* by promoting RNase III-dependent turn-over of *puf* mRNA. *RNA Biology*, 18, 1445–1457.

Robertson, H.D., Webster, R.E. & Zinder, N.D. (1967) A nuclease specific for double-stranded RNA. *Virology*, 32, 718–719.

Robertson, H.D., Webster, R.E. & Zinder, N.D. (1968) Purification and properties of ribonuclease III from *Escherichia coli*. *The Journal of Biological Chemistry*, 243, 82–91.

Romby, P., Vandenesch, F. & Wagner, E.G.H. (2006) The role of RNAs in the regulation of virulence-gene expression. *Current Opinion in Microbiology*, 9, 229–236.

Salmond, G.P., Bycroft, B.W., Stewart, G.S. & Williams, P. (1995) The bacterial 'enigma': cracking the code of cell-cell communication. *Molecular Microbiology*, 16, 615–624.

Schäfer, A., Tauch, A., Jäger, W., Kalinowski, J., Thierbach, G. & Pühler, A. (1994) Small mobilizable multi-purpose cloning vectors derived from the *Escherichia coli* plasmids pK18 and pK19: selection of defined deletions in the chromosome of *Corynebacterium glutamicum*. *Gene*, 145, 69–73.

Simon, R., Priefer, U. & Pühler, A. (1983) A broad host range mobilization system for in vivo genetic engineering: transposon mutagenesis in gram negative bacteria. *Bio/Technology*, 1, 784–791.

Snow, S., Bacon, E., Bergeron, J., Katzman, D., Wilhelm, A., Lewis, O. et al. (2020) Transcript decay mediated by RNase III in *Borrelia burgdorferi*. *Biochemical and Biophysical Research Communications*, 529, 386–391.

Spanka, D.-T. & Klug, G. (2021) Maturation of UTR-derived sRNAs is modulated during adaptation to different growth conditions. *International Journal of Molecular Sciences*, 22, 12260.

Spanka, D.-T., Reuscher, C.M. & Klug, G. (2021) Impact of PNPase on the transcriptome of *Rhodobacter sphaeroides* and its cooperation with RNase III and RNase E. *BMC Genomics*, 22, 106.

Srivastava, A.K. & Schlessinger, D. (1990) Mechanism and regulation of bacterial ribosomal RNA processing. *Annual Review of Microbiology*, 44, 105–129.

Storz, G., Vogel, J. & Wassarman, K.M. (2011) Regulation by small RNAs in bacteria: expanding frontiers. *Molecular Cell*, 43, 880–891.

Vogel, J., Argaman, L., Wagner, E.G.H. & Altuvia, S. (2004) The small RNA IstR inhibits synthesis of an SOS-induced toxic peptide. *Current Biology*, 14, 2271–2276.

Westphal, H. & Crouch, R.J. (1975) Cleavage of adenovirus messenger RNA and of 28S and 18S ribosomal RNA by RNase III. *Proceedings of the National Academy of Sciences of the United States of America*, 72, 3077–3081.

Whitehead, N.A., Barnard, A.M., Slater, H., Simpson, N.J. & Salmond, G.P. (2001) Quorum-sensing in gram-negative bacteria. *FEMS Microbiology Reviews*, 25, 365–404.

Zahn, K., Inui, M. & Yukawa, H. (2000) Divergent mechanisms of 5′ 23S rRNA IVS processing in the alpha-proteobacteria. *Nucleic Acids Research*, 28, 4623–4633.

SUPPORTING INFORMATION

Additional supporting information can be found online in the Supporting Information section at the end of this article.

How to cite this article: Börner, J., Friedrich, T. & Klug, G. (2023) RNase III participates in control of quorum sensing, pigmentation and oxidative stress resistance in *Rhodobacter sphaeroides*. *Molecular Microbiology*, 00, 1–19. Available from: https://doi.org/10.1111/mmi.15181

International Journal of *Molecular Sciences*

MDPI

Article

The Small RNA-Binding Protein CcaF1 Promotes Formation of Photosynthetic Complexes in *Rhodobacter sphaeroides*

Julian Grützner †, Janek Börner †, Andreas Jäger and Gabriele Klug *

Institute of Microbiology and Molecular Biology, Justus Liebig University Giessen, Heinrich-Buff-Ring 26-32, 35392 Giessen, Germany; janek.boerner@mikro.bio.uni-giessen.de (J.B.); andreas.jaeger@mikro.bio.uni-giessen.de (A.J.)
* Correspondence: gabriele.klug@mikro.bio.uni-giessen.de
† These authors contributed equally to this work.

Abstract: In natural habitats, bacteria frequently need to adapt to changing environmental conditions. Regulation of transcription plays an important role in this process. However, riboregulation also contributes substantially to adaptation. Riboregulation often acts at the level of mRNA stability, which is determined by sRNAs, RNases, and RNA-binding proteins. We previously identified the small RNA-binding protein CcaF1, which is involved in sRNA maturation and RNA turnover in *Rhodobacter sphaeroides*. *Rhodobacter* is a facultative phototroph that can perform aerobic and anaerobic respiration, fermentation, and anoxygenic photosynthesis. Oxygen concentration and light conditions decide the pathway for ATP production. Here, we show that CcaF1 promotes the formation of photosynthetic complexes by increasing levels of mRNAs for pigment synthesis and for some pigment-binding proteins. Levels of mRNAs for transcriptional regulators of photosynthesis genes are not affected by CcaF1. RIP-Seq analysis compares the binding of CcaF1 to RNAs during microaerobic and photosynthetic growth. The stability of the *pufBA* mRNA for proteins of the light-harvesting I complex is increased by CcaF1 during phototrophic growth but decreased during microaerobic growth. This research underlines the importance of RNA-binding proteins in adaptation to different environments and demonstrates that an RNA-binding protein can differentially affect its binding partners in dependence upon growth conditions.

Keywords: RNA-binding proteins; riboregulation; *Rhodobacter*; RNA stability; phototrophic growth; RIPseq

Citation: Grützner, J.; Börner, J.; Jäger, A.; Klug, G. The Small RNA-Binding Protein CcaF1 Promotes Formation of Photosynthetic Complexes in *Rhodobacter sphaeroides*. *Int. J. Mol. Sci.* **2023**, *24*, 9515. https://doi.org/10.3390/ijms24119515

Academic Editor: Andreas Burkovski

Received: 12 May 2023
Revised: 24 May 2023
Accepted: 25 May 2023
Published: 30 May 2023

1. Introduction

Members of the genus *Rhodobacter* are characterized by high metabolic versatility, which allows them to adapt to changing environmental conditions. While aerobic respiration takes place in the presence of oxygen, anoxygenic photosynthesis (in the presence of light), anaerobic respiration, or fermentation (both in the absence of light) can generate ATP under anoxic conditions. Many studies have addressed the adaptation of *Rhodobacter capsulatus* and *Rhodobacter sphaeroides* (now renamed *Cereibacter* [1]) to changing oxygen and light conditions in the past (reviewed in [2–4]). Several proteins directly or indirectly affecting the rates of transcription of photosynthesis genes in response to oxygen levels were identified (the names of the *R. capsulatus* proteins given in parentheses): the two-component system PrrA/PrrB (RegA/RegB) [5,6], the repressor–anti-repressor systems PpsR (CrtJ)/AppA and PpaA (AerR) [7–9], and FnrL [10,11]. AppA and PpaA (AerR) do not only function as oxygen-sensors but also as photoreceptors that sense light via a heme or cobalamin cofactor [8,12–15].

Besides this protein-based regulation, riboregulation has an important role in the control of photosynthesis gene expression in *Rhodobacter*. More than two decades ago, the differential stabilities of segments of the polycistronic *puf* operon (encoding components

of the photosynthetic complexes) of *R. capsulatus* were reported to affect the ratios of the reaction center (RC) and light-harvesting (LH) I complexes [16]. Later on, the important roles of the *R. sphaeroides* sRNAs PcrZ, PcrX, and asPcrL in regulated photosynthesis gene expression were demonstrated [17–19]. Hfq, an RNA chaperone interacting with many sRNAs, contributes to the photo-oxidative stress resistance of *R. sphaeroides* and also affects its levels of photosynthetic complexes [20,21]. In addition, a remarkable strong effect of the endoribonuclease RNase E on phototrophic but not on chemotrophic growth was observed [22]. RNase E was shown to differentially affect the stability of mRNAs for the important regulators AppA and PrrB under microaerobic and phototrophic growth conditions [23].

Recently, we identified a new type of small RNA-binding protein in *R. sphaeroides*: CcaF1 (conserved CcsR associated factor 1) [24]. The *ccaF1* gene is co-transcribed with four CcsR RNAs that modulate the C1 metabolism and have an important role in stress defense [25] (Figure 1A). *ccaF1* encodes a small protein of 71 amino acids that comprises a DUF1127 domain. An association of short DUF1127 proteins with CcsR-like sRNAs is often found in alphaproteobacteria and was labeled CIN1 locus [26]. The CcaF1 protein of *R. sphaeroides* affects CcsR levels in trans and alters stress resistance. Together with RNase E, CcaF1 is involved in the processing of the *ccaF1*–CcsR transcript and in the maturation of the CcsR RNAs. But CcaF1 also affects levels of many other RNAs in *R. sphaeroides*, including RNAs for photosynthesis genes, and it affects the stability of the *pufBA* mRNA. Overexpression of *ccaF1* strongly impedes growth under microaerobic conditions [24].

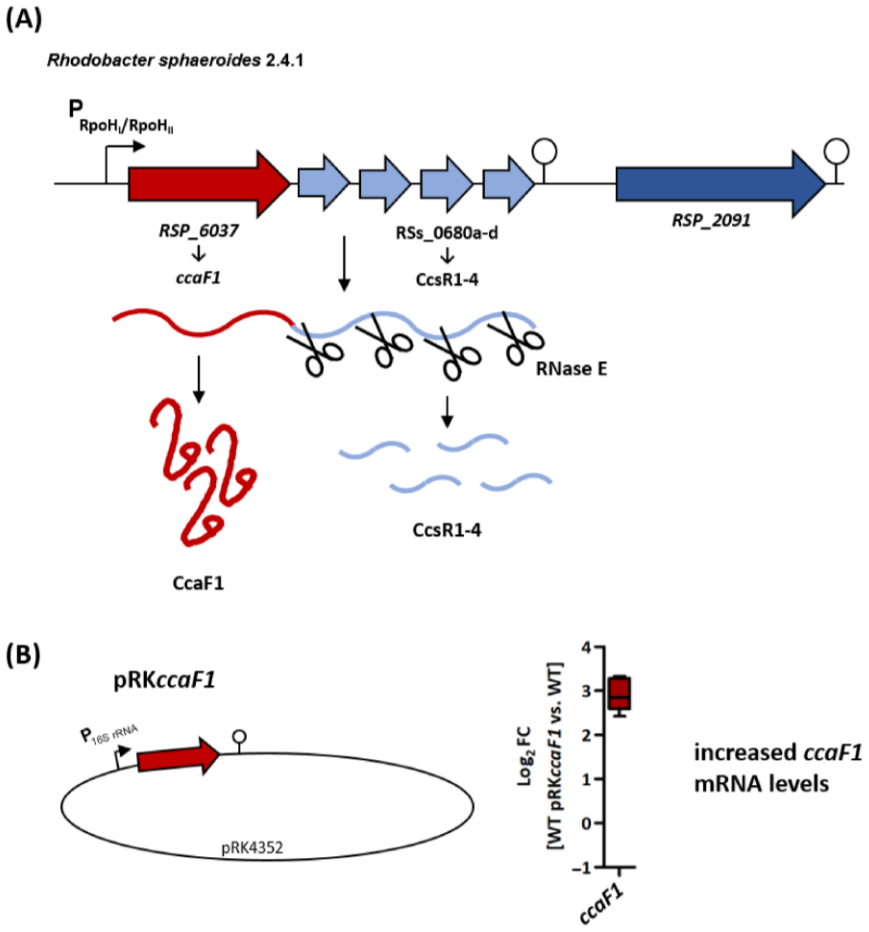

Figure 1. (**A**) Genomic context of the DUF1127 protein CcaF1 (dark red) and the CcsR1-4 sRNAs (light blue) from *R. sphaeroides* 2.4.1. The protein–sRNA operon is preceded by an RpoH$_I$/RpoH$_{II}$

promoter (black arrow), and a Rho-independent terminator structure is located at the 3′ end (modified from [25]). The transcribed RNA precursor is processed by the endoribonuclease RNase E into the *ccaF1* mRNA and the CcsR1-4 sRNAs [24]. (**B**) Schematic overview of the plasmids introduced in the *R. sphaeroides* wild type. In strain WT pRK*ccaF1*, the *ccaF1* gene is transcribed from a strong 16S rRNA promoter, leading to a strongly increased *ccaF1* mRNA level. This finding was confirmed by a quantitative real-time RT-PCR with total RNA samples from biological triplicates of the *ccaF1* overexpression strain (WT pRK*ccaF1*) and the empty vector control, as shown in the right panel.

Based on these findings, we were interested in the role of CcaF1 in phototrophic growth. Our data demonstrate that CcaF1 has a mild promoting effect on doubling time during phototrophic growth and influences the transition of *R. sphaeroides* from chemotrophic to phototrophic growth. Co-immunoprecipitation demonstrates that CcaF1 directly binds to several mRNAs for proteins with a direct function in photosynthesis.

2. Results

2.1. CcaF1 Affects Phototrophic Growth and Pigmentation of R. sphaeroides

It was not possible to generate a viable strain lacking *ccaF1* [25]. Therefore, we compared strain WT pRK*ccaF1* (wild type carrying the *ccaF1* overexpression plasmid) to strain WT pRK4352 (empty vector control) [24]. Plasmid pRK4352 carries a strong rRNA promoter from *R. sphaeroides;* in plasmid pRK*ccaF1*, the *ccaF1* gene is transcribed from this promoter, leading to strongly increased *ccaF1* mRNA levels (Figure 1B). Strain WT pRK*ccaF1* was strongly impeded in growth compared to the wild type or control strain WT pRK4352 when incubated under microaerobic conditions [24].

When the strains were cultivated microaerobically and then shifted to phototrophic growth, doubling of WT pRK*ccaF1* was slightly faster in the exponential phase than the control (Figure 2A). Both strains reached a similar optical density in the stationary phase.

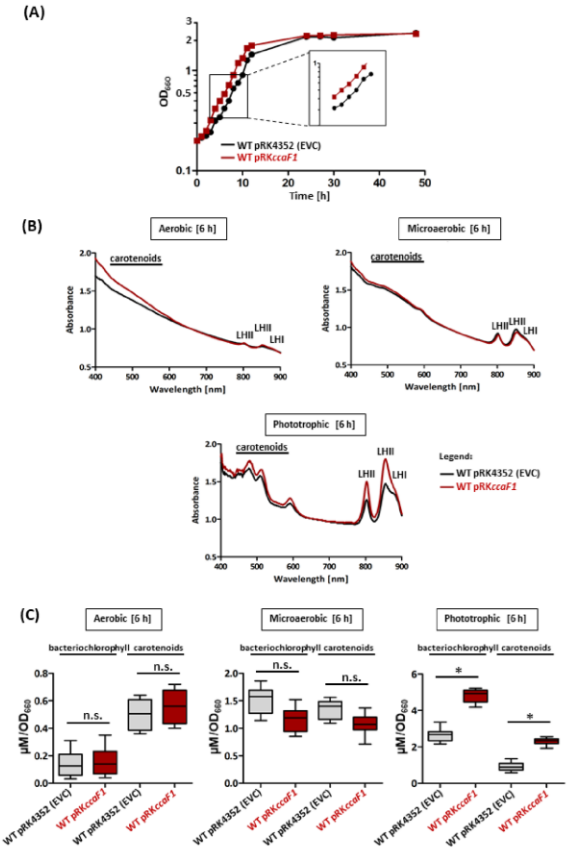

Figure 2. (**A**) Growth behavior of *R. sphaeroides* WT pRK4352 (EVC; black) or *R. sphaeroides* with the *ccaF1* overexpression plasmid (pRK*ccaF1*; red) was monitored over 48 h. The plotted optical densities

at 660 nm (OD_{660}) represent the mean of at least three independent experiments. The standard deviation of the mean was calculated (error bars are not visible due to a high reproducibility). (**B**) Whole-cell spectra were analyzed for the empty vector control and the *ccaF1* overexpression strain (pRK*ccaF1*; red). Microaerobic overnight cultures were diluted on the next day to an OD_{660} 0.2 and incubated further under aerobic, microaerobic, or phototrophic growth conditions for 8 h (See bacterial strains and growth conditions). After 8 h under aerobic, microaerobic, or phototrophic growth conditions, the absorbance was measured from 400 nm to 900 nm. The peaks at 800 and 850 nm represent specific absorbance maxima of the light-harvesting complex II (LHII), and the peak at 870 nm stems from absorbance of the light-harvesting complex I (LHI). The absorbance of the reaction center at 800 and 870 nm is covered by the absorbances of the more abundant LH complexes. Shown are results of three independent experiments, each performed in technical duplicates. (**C**) The bacteriochlorophyll and carotenoid contents in the *R. sphaeroides* WT *ccaF1* overexpression strain (pRK*ccaF1*; red) or the empty vector control (pRK4352; gray) were analyzed. To calculate the bacteriochlorophyll content (µM), the absorbance was normalized to the OD_{660}, and the extinction coefficient of 76 mM^{-1} cm^{-1} was applied. The carotenoid-specific absorbance was measured at 484 nm. To calculate the carotenoid content (µM), the absorbance was normalized to the OD_{660}, and the extinction coefficient of 128 mM^{-1} cm^{-1} was applied. Shown are results of nine independent experiments, each performed in technical duplicates (mean values and their standard deviation are shown). Student's two-sided t-test was applied to assess the statistical significance of differences in pigment amount mean values between EVC and *R. sphaeroides* pRK*ccaF1* (*: $p < 0.05$; n.s.: not significant).

Figure 2B shows that after 6 h under phototrophic growth, the strain overexpressing *ccaF1* accumulated higher amounts of photosynthetic complexes than the EVC. After 6 h under microaerobic conditions, in which the formation of photosynthetic complexes in *Rhodobacter* is already induced, the absorption spectra were almost identical between the overexpressing strain and the control (Figure 2B).

A quantitative analysis of the bacteriochlorophyll and carotenoid levels in both strains under the different growth conditions is shown in Figure 2C. While the differences in bacteriochlorophyll and carotenoid content between the two strains were not significantly different under aerobic and microaerobic conditions, significantly higher pigment levels were observed under phototrophic conditions in the pRK*ccaF1*-carrying strain (bacteriochlorophyll levels increased by a factor of 2.1, carotenoid levels by a factor of 2.8) compared to the EVC.

2.2. Levels of Some mRNAs for Pigment Synthesis and for Pigment-Binding Proteins Are Affected by CcaF1

To form photosynthetic complexes, the pigment-binding PufBALM and PucBA proteins and the assembly factor PufX, as well as photopigments, are required. Previous analyses under microaerobic conditions demonstrated an effect of CcaF1 on the level and stability of the *pufBA* mRNA [24]. Figure 3A shows northern blots for total RNA from cells isolated after 6 h of phototrophic growth and hybridized either against a *pufBA* or *pucBA* DNA probe. In strain WT pRK*ccaF1,* the levels of the *pufBA* mRNA-encoding pigment-binding proteins of the LHI complex were clearly increased in comparison to the control strain. Such an increase was not observed for the *pucBA* mRNA, encoding proteins of the LHII complex. We also analyzed the effect of CcaF1 on the abundance of sRNAs with a known function in the regulation of photosynthesis gene expression. Northern blots revealed a minor change in PcrZ levels, which is processed to a stable smaller 3′ fragment [17]; in PcrX that is processed from the 3′ UTR of the *pufBALMX* mRNA [18]; and in asPufL, which is antisense to a part of *pufL* [19]. These observations were also confirmed by real time RT-PCR (Figure 3B), which revealed increased levels of mRNAs for bacteriochlorophyll synthesis: *bchE* (encoding magnesium-protoporphyrin IX monomethyl ester oxidative cyclase), *bchL* (light-independent protochlorophyllide reductase), and *bchM* (Mg-protoporphyrin IX methyl transferase), which belongs to two different operons. Likewise, increased mRNA levels upon overexpression of *CcaF1* were shown for two genes for

carotenoid synthesis: *crtE* (geranylgeranyl pyrophosphate synthetase) and *crtI* (phytoene dehydrogenase), belonging to different operons. The *pufLM* mRNA encoding the L and M proteins of the photosynthetic reaction center showed a slight increase in the overexpression strain, as well as the sRNA PcrX that is co-transcribed with the *pufBALM* genes. Real-time RT-PCR also revealed slightly increased levels of PcrZ and asPufL upon overexpression of *ccaF1*; slightly decreased levels of *ppaA* and *ppsR*; and no effect on levels of *appA* and *fnrL* (Figure 3B). This finding suggests that the increased amounts of photosynthetic complexes in the overexpression strain is rather due to increased mRNA levels for Puf proteins and for pigment synthesis than to altered mRNA levels for transcription regulators of photosynthesis genes.

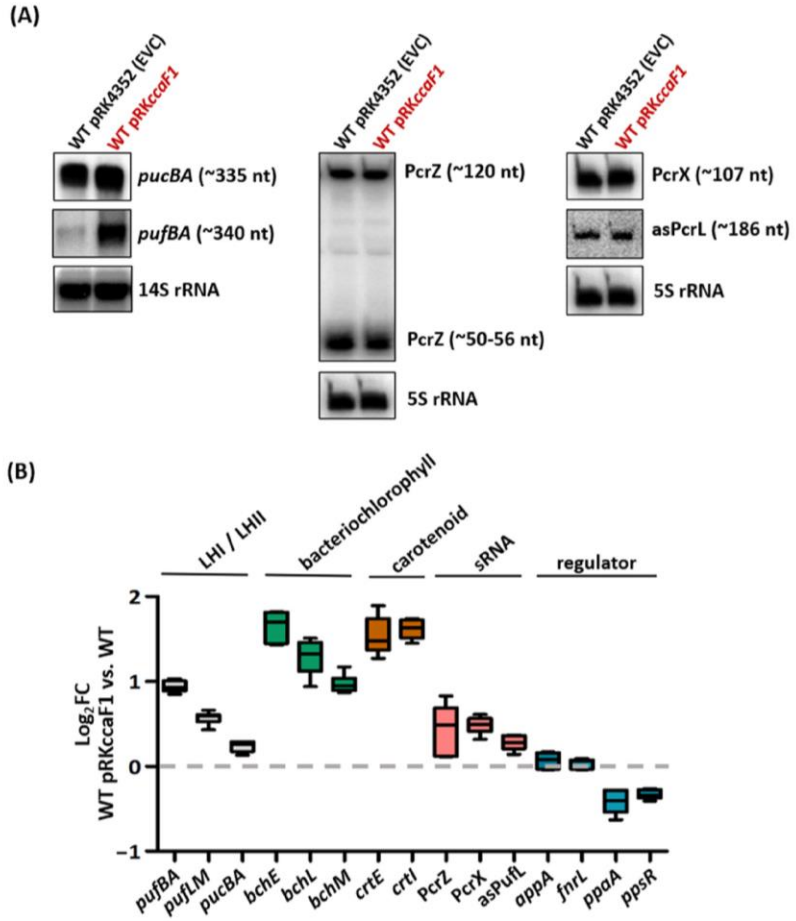

Figure 3. (**A**) Northern blot analysis of *R. sphaeroides* WT pRK4352 (EVC) and *ccaF1* overexpression (pRK*ccaF1*). Samples were taken after 8 h under phototrophic growth conditions, and total RNA was isolated. For detection of mRNA transcripts (*pufBA* and *pucBA*), 10 µg total RNA were separated on a 1% agarose (*w/v*) formaldehyde gel. The 14S rRNA served as a loading control. *R. sphaeroides* cleaves the 23S RNA into fragments of 16S and 14S. For the detection of small RNAs (PcrZ, PcrX, asPufL), 8 µg total RNA were separated on a 10% polyacrylamide gel containing 7 M urea. The 5S rRNA served as a loading control. (**B**) The abundance changes of mRNAs encoding pigment-binding proteins of the LHI/II complex (*pufBA*, *pucBA*), bacteriochlorophyll synthesis (*bchE*, *bchL*, *bchM*), carotenoid synthesis (*crtE*, *crtI*) and photosynthesis regulators (*appA*, *fnrL*, *ppaA*, *ppsR*), and the sRNA PcrZ were analyzed by quantitative real-time RT-PCR. In addition, 20 ng DNA-free total RNA were used for real-time RT-PCR. Changes in abundance were normalized to *rpoZ* (housekeeping gene). Shown are results of three independent experiments, each performed in technical duplicates.

2.3. CcaF1 Increases the Half-Life of pufBA under Phototrophic Growth

Our previous study revealed that overexpression of *ccaF1* under microaerobic conditions decreased the *pufBA* mRNA half-life from about 22 min to only 12 min, while there was no significant effect on the *pucBA* mRNA (18–20 min half-life) [24]. Figure 4A shows northern blots for phototrophic cultures. While the half-life of *pucBA* was about 26 min for both strains, the half-life of the *pufBA* mRNA was almost doubled in WT pRK*ccaF1* (about 39 min versus about 20 min in the control) (Figure 4A). Under microaerobic conditions, overexpression of *ccaF1* resulted in decreased *pufBA* mRNA half-life [24].

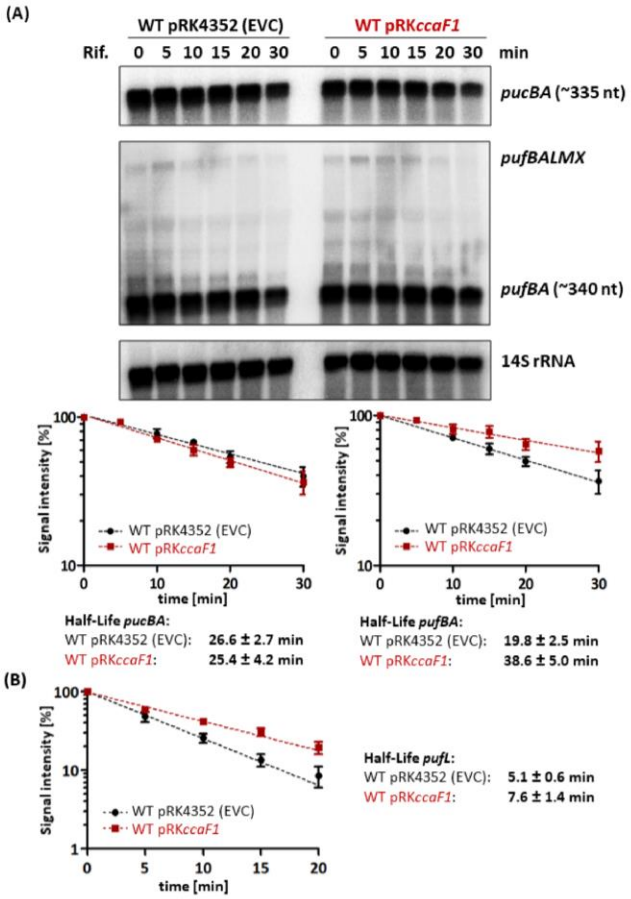

Figure 4. Determination of *pucBA*, *pufBA*, and *pufL* mRNA half-lives in the empty vector control (pRK4352) and upon *ccaF1* overexpression (pRK*ccaF1*). Samples were taken at different time points after adding rifampicin (Rif.). The average half-life was calculated from three independent experiments, and the standard deviation is indicated. (**A**) Total RNA was isolated and separated on a 1% agarose formaldehyde gel. After blotting, the mRNAs of *pucBA*, *pufBALMX*, and *pufBA* were hybridized to specific radio-labelled PCR-products. For quantification, RNA signal intensities were normalized to signals of the 14S rRNA loading control. (**B**) To quantify *pufL*-specific mRNA levels, 20 ng DNA-free total RNA and *pufL*-specific primers were used for real-time RT-PCR. Changes in abundance were normalized to *rpoZ* (housekeeping gene).

As seen in Figure 4A, the *pufBALMX* mRNA is hardly detectable by northern blot. Therefore, we monitored the decay of the *pufL* segment by using real-time RT-PCR (Figure 4B). While the half-life of the shorter *pufBA* fragment was strongly stabilized upon overexpression of *ccaF1*, only a moderate stabilizing effect was observed for the *pufL* segment (8 min versus 5 min in the control).

2.4. CcaF1 Interacts with Some Photosynthesis mRNAs, but Not with mRNAs for Transcriptional Regulators

We applied co-immunoprecipitation (CoIP) to test for a direct interaction of CcaF1 and mRNAs for pigment-binding proteins, enzymes of pigment synthesis, or regulatory proteins and sRNAs under phototrophic conditions. After sequencing of samples obtained from CoIP (RIP-Seq), the data were processed into wiggle files and visualized in the Integrated Genome Browser (screenshots displayed in Figure 5). We compared this data set to the RIP-Seq results under microaerobic conditions and to a CoIP with non-tagged CcaF1 (negative control). At the bottom, RNA-seq data from total RNA, both under microaerobic and phototrophic conditions is shown.

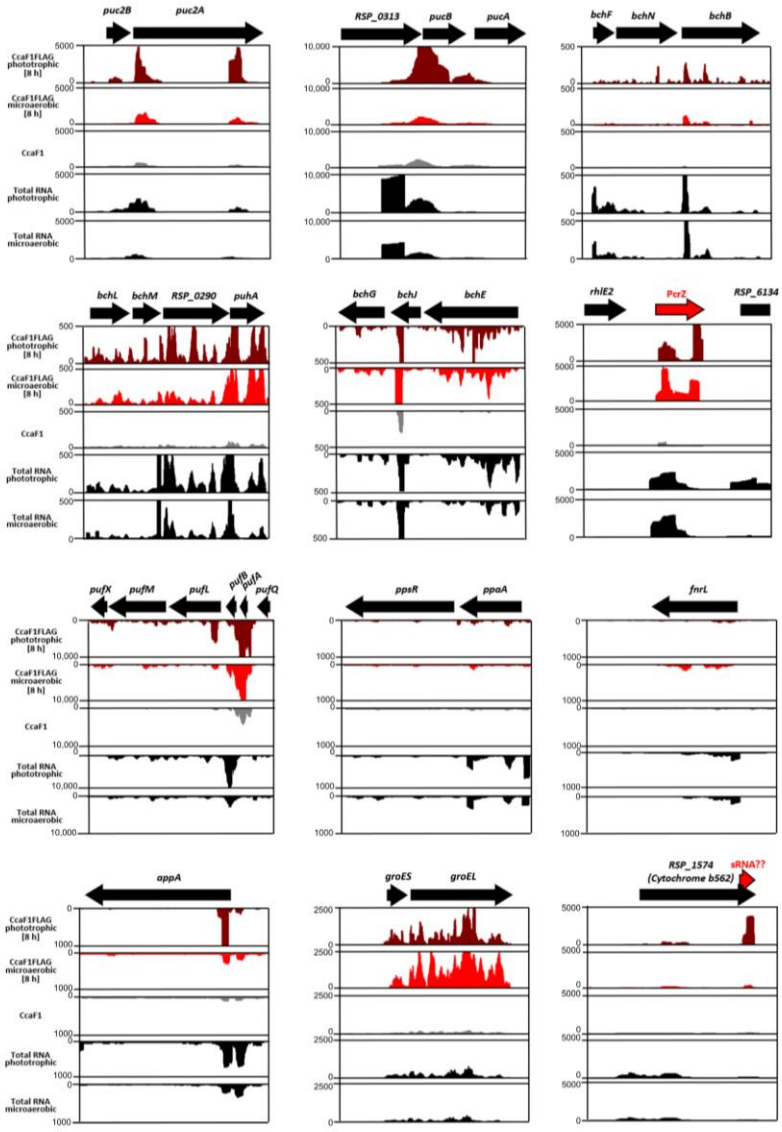

Figure 5. Analysis of co-immunoprecipitated RNA using CcaF1 with 3xFLAG-tag (CcaF1FLAG) or without 3xFLAG-tag (CcaF1, untagged control) on the plasmid pRK4352 by RNA-Seq (RIP-Seq). The CoIP was performed as described in [24]. Read coverage plots from the Integrated Genome Browser display the sequencing reads for selected RNAs. The read coverage plots of CcaF1FLAG under phototrophic growth conditions are shown in dark red, under microaerobic growth conditions in red, CcaF1 without FLAG-tag (control) in grey, and total RNA under microaerobic and phototrophic growth conditions in black.

Six hours after transition to phototrophic growth, we observed higher levels of *pucBA*, *puc2BA*, *bchN*, *bchB*, *bchL*, *bchM* mRNAs (from the same operon), *bchE*, *bchJ*, and *bchG* mRNAs (from the same operon) in CoIP RNA, compared to RIP-Seq from microaerobic cultures. *R. sphaeroides* harbours two *pucBA* operons [27]. The Puc2A protein is much longer than PucA and is not assembled into LHII complexes like PucA, PucB, and Puc2B [28]. Moreover, *pufBA* showed similar enrichment in phototrophic and microaerobic conditions, but the read coverage pattern was somewhat different.

The 3′ segment of sRNA PcrZ was more enriched in the RIP-Seq under phototrophic than under microaerobic conditions. A remarkable strong enrichment under phototrophic conditions was observed for the 3′ part of *RSP_1574* (mRNA for cytochrome b562 from the cytochrome bc1 complex that is involved in respiratory and cyclic photosynthetic electron transport). The *groEL* mRNA is shown as an example for an mRNA that is more enriched under microaerobic conditions. The *ccaF1* mRNA level was increased in total RNA from phototrophic cultures compared to chemotrophic cultures (Figure S1).

Figure S2 shows gels of the CoIP RNAs and confirms the interaction of CcaF1 to *pufBA*, *pucBA*, *bchB*, *bchE*, *bchN*, *bchM*, and PcrZ. The mRNAs for the regulators of photosynthesis genes FnrL, PpaA, and PpsR showed no interaction with CcaF1. There was a strong enrichment for the 3′ end of the *appA*-coding mRNA but not for the downstream region.

We quantified the enrichment of RNAs in the CoIP samples with real-time RT-PCR (Figure 6). This approach confirmed high enrichment factors (14–43 fold) for *pufBA*, *pucBA*, *bch* mRNAs, and the sRNA PcrZ in the CoIP. While mRNAs for the regulators FnrL, PpaA, and PpsR were not enriched, the 5′ part of *appA* showed a 1.8-fold enrichment.

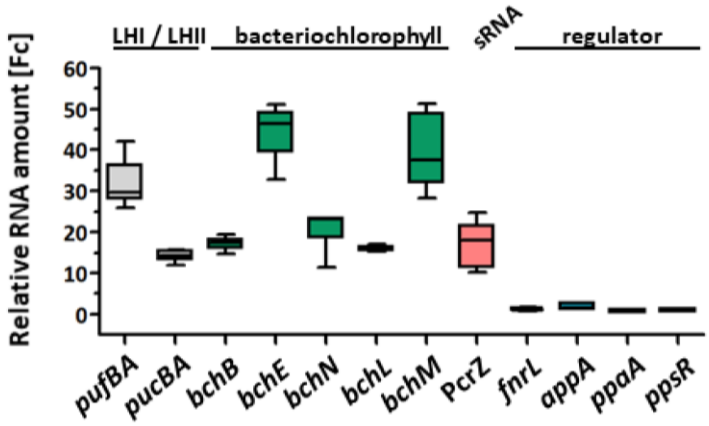

Figure 6. Validation of co-immunoprecipitated RNA by real-time RT-PCR using CcaF1 with 3xFLAG-tag (CcaF1FLAG) or without 3xFLAG-tag (CcaF1, untagged control) on the plasmid pRK4352. 20 ng DNA-free total microaerobic overnight cultures were diluted on the next day to an OD_{660} 0.2 and incubated under phototrophic growth conditions for 8 h (see bacterial strains and growth conditions). The RNA from independent biological triplicates was analyzed. The fold change between flag-tagged CcaF1 versus the non-flag-tagged CcaF1 (control) samples is plotted.

3. Discussion

Bacteria have a remarkable ability to cope with different environmental conditions by adjusting their metabolism and by mounting stress responses. This requires regulation of gene expression and involves a multitude of different mechanisms to adjust the transcriptome and the proteome. These mechanisms of regulation also include RNA-binding proteins that often work together with sRNAs (e.g., [29]). The role of some bacterial RNA-binding proteins has been intensely studied in the past. The small Hfq protein (77 amino acids, as in *R. sphaeroides*) is a global regulator of sRNA-based networks in many bacterial species, and deletion mutants of Hfq have often pleiotropic phenotypes [30]. Such pleiotropic effects are also described for *Rhodobacter*, including an influence on the formation of pigment-protein complexes [20]. The FinO domain protein ProQ was later identified as

another global RNA-binding protein that interacts with many sRNAs and mRNAs [31]. So far, no ProQ homolog was identified in *R. sphaeroides*. Recently, KH-domain proteins were also shown to be important for sRNA function [32]. Small proteins with DUF 1127 domains have been found in many bacterial species, but their interaction with RNAs was so far only reported for *R. sphaeroides* [24].

This study demonstrates a differential impact of CcaF1 on gene expression and growth during chemotrophic or phototrophic cultivation. While overexpression of *ccaF1* strongly impedes chemotrophic growth under microaerobic conditions [24], it has a small growth-promoting effect on phototrophic cultures. Thus, CcaF1 contributes to the transition of *R. sphaeroides* between different growth conditions.

The slight growth-promoting effect of CcaF1 under phototrophic conditions is linked with increased amounts of photosynthetic complexes and increased levels of mRNAs that are required for pigment synthesis or synthesis of the *puf* mRNA for the reaction center and LHI proteins. Surprisingly, an increase of the *pucBA* mRNAs for LHII proteins was not observed. LHII is the most abundant complex under photosynthetic conditions [33]. The ratio of RC and LHI complexes is relatively constant (about 1:14). Interestingly, this ratio is a consequence of the differential stabilities of segments of the polycistronic *pufBALMX* mRNA. Deletion of a hairpin loop that stabilizes the 3′ end of the *pufBA* mRNA results in altered ratios of RC to LHI [16]. The ratio of LHII to the RC–LHI core complexes is flexible and also influenced by growth conditions [34]. After a shift from chemotrophic to phototrophic growth, *puf* and *puc* mRNAs are induced; RC–LHI complexes occur first, and then LHII associates to the RC–LHI core complexes [35]. For the increased formation of LHII complexes upon overexpression of *ccaF1*, as seen in the spectra in Figure 2B, obviously no overproduction of the *pucBA* mRNA is required. It is conceivable that the *pucBA* levels produced without *ccaF1* overexpression are sufficient for this overall increase, which is controlled by RC–LHI complexes into the membrane.

The increased levels of *pufBA* mRNA in the presence of higher amounts of CcaF1 are linked with an increased half-life under phototrophic conditions. CcaF1 was shown to promote RNase E-mediated maturation of the CcsR1 RNAs but also to decrease the half-life of several tested RNAs (including that of *pufBA*) under microaerobic conditions. The half-lives of other RNAs that were shown to bind to CcaF1 by CoIP were not affected [24], as also shown in Figure 4 for *pucBA* mRNA under phototrophic conditions. This implies that CcaF1 can promote degradation of bound RNA but can also stabilize RNA or not affect the half-life. This effect depends most likely on the features of the RNA targets, like the presence and localization of RNase E cleavage sites. It is surprising that the effect of CcaF1 on *pufBA* stability is the opposite in microaerobic and phototrophic conditions. It is unlikely that the target RNAs adopt significantly different structures under the different growth conditions. It is known that binding to the membrane has a strong influence on RNase E activity in the gammaproteobacterium *E. coli*, while in the alphaproteobacterium *Caulobacter crescentus* RNase E localizes to BR bodies [36]. Data on the localization of RNase E in the alphaproteobacterium *Rhodobacter* are not available, as the *Rhodobacter* enzyme possesses no membrane-targeting sequence. Under microaerobic as well as under phototrophic conditions, photosynthetic complexes are formed and inserted into intracytoplasmic membrane vesicles that are absent in aerobic cultures. As seen in Figure 2B, the amounts of photosynthetic complexes that correlate to the amounts of intracytoplasmic membranes are higher under phototrophic growth. It is, however, unlikely that this difference would cause opposite effects of CcaF1 on the stability of certain targets. It is likely that further yet unknown factors are involved in the CcaF1–target RNA–RNase E interplay that still need identification.

Remarkably, the amounts of mRNAs for known regulators of the formation of components of the photosynthetic apparatus (AppA, FnrL, PpaA, PpsR) and for PcrX were not or were only slightly affected by CcaF1. This underlines that CcaF1 directly affects the amounts of some of its binding partners by affecting stability and that the changes in the amounts of *pufBA*, *bch*, and *crt* mRNAs are not the consequence of an indirect effect by

these regulators. This finding emphasizes the important role of RNA-binding proteins in the regulation of bacterial gene expression and in bacterial adaptation.

4. Materials and Methods

4.1. Bacterial Strains and Growth Conditions

All *R. sphaeroides* strains are listed in Table S1 and were cultivated in malate minimal-salt medium or on solid medium containing 1.6% (*w*/*v*) agar at 32 °C in the dark [37]. For strain construction see Grützner et al. [24]. When necessary, tetracycline (2 µg mL^{-1}) was added to liquid and solid growth media.

For all experiments (growth behavior, pigment analysis, and determination of RNA half-life) Erlenmeyer flasks were filled up to 80% with malate minimal-salt medium, inoculated 1% with the corresponding *R. sphaeroides* strain (see Table S1), and incubated overnight under microaerobic growth conditions (140 rpm, 32 °C). The microaerobic preculture with an OD_{660} around 0.6 was diluted on the next day to an OD_{660} 0.2 and shifted to aerobic (baffled Erlenmeyer flasks were filled up to 25% and shaken at 180 rpm, 32 °C), microaerobic (Erlenmeyer flasks were filled up to 80% and shaken at 180 rpm, 32 °C), or phototrophic (sealed Meplat bottles were filled up to 100% and illuminated with 60 W/m^2 white light at 32 °C) growth conditions.

To monitor the growth behavior, the optical density (OD) was measured every 1.5 h at 660 nm (Specord 50, Analytic Jena AG, Jena, Germany).

4.2. Pigment Analysis

For pigment analysis, *R. sphaeroides* strains were cultivated overnight under microaerobic growth conditions, diluted to an OD_{660} 0.2, and incubated for 8 h under aerobic, microaerobic, or phototrophic growth conditions (see bacterial strains and growth conditions). For whole-cell absorbance spectra, 1 mL of the culture was transferred into a cuvette, and the absorbance was measured in a spectral photometer at wavelengths of 400–900 nm. The amounts of bacteriochlorophyll and carotenoids were measured as previously described [38].

4.3. Determination of RNA Half-Life

To analyze the half-life of specific RNA transcripts, microaerobic precultures of *R. sphaeroides* were diluted to an OD_{660} 0.2 and incubated under phototrophic growth conditions for 8 h (see bacterial strains and growth conditions). After taking sample t_0 (10–15 mL), rifampicin was added to a final concentration of 0.2 mg mL^{-1}. The 10–15 mL samples were taken at indicated time points after addition of rifampicin and harvested by centrifugation (10,000 rpm, 10 min, 4 °C). Afterwards the total RNA was isolated and used for northern blot analysis or real-time RT-PCR.

4.4. RNA Isolation

To analyze specific RNA transcripts, microaerobic precultures of *R. sphaeroides* were diluted to an OD_{660} 0.2 and incubated under phototrophic growth conditions for 8 h (see bacterial strains and growth conditions). The cells were harvested by centrifugation at 10,000 rpm for 10 min at 4 °C. For northern blot analysis, quantitative real-time RT-PCR and RNA sequencing of total RNA by the hot-phenol method [39], were used. The RNA was precipitated with 1/10x vol. 3 M sodium acetate pH 4.5 and 2.5x vol. 96% ethanol overnight at −20 °C. For quantitative real-time RT-PCR, the remaining DNA was removed by TURBO DNase treatment (Invitrogen/Thermo Fischer Scientific, Rockford, IL, USA). The absence of DNA contamination was tested by PCR using oligonucleotides targeting *gloB* (RSP_0799) [40]. RNA integrity was tested on a 10% polyacrylamide gel containing 7 M urea and subsequent staining with ethidium bromide, as well as on the Bioanalyzer (described in the data generation description of our deposited RNA-Seq data in the GEO repository). The sequencing libraries were constructed as described earlier [24], using

the NEBNext Multiplex Small RNA Library Prep Set for Illumina (NEB, Frankfurt am Main, Germany).

4.5. Northern Blot Analysis

For the detection of small RNAs, 8 µg total RNA were separated on a 10% polyacrylamide gel containing 7 M urea and transferred to a nylon membrane (Roth, Karlsruhe, Germany) by semi-dry electroblotting [41]. For detection of the sRNAs, specific oligodeoxynucleotides (listed in Table S2) were labeled with [γ-^{32}P]-ATP (Hartmann Analytic, Braunschweig, Germany) by a T4 polynucleotide kinase end-labeling reaction (Fermentas/Thermo Fisher Scientific, Rockford, IL, USA).

For the detection of mRNA transcripts, 10 µg total RNA were separated on a 1% agarose (*w/v*) formaldehyde gel and transferred to a nylon membrane (Roth, Karlsruhe, Germany) by vacuum blotting [12]. For detection of mRNA transcripts, specific PCR products (primer listed in Table S2) were labelled with [α-^{32}P]-CTP (Hartmann Analytics, Braunschweig, Germany) by using the Prime-a-Gene Labeling System (Promega, Mannheim, Germany).

The membranes were hybridized overnight using the Church and Gilbert buffer system [42], washed with 0.01% SDS and 5x SSC in ddH_2O and exposed on phosphorimaging screens (Bio-Rad, Feldkirchen, Germany). To analyze the intensities of the phosphorimaging signals the 1D-Quantity One software version 4.6.8 Basic (Bio-Rad, Feldkirchen, Germany) was used.

4.6. Co-Immunoprecipitation

For CoIP, microaerobic precultures of *R. sphaeroides* WT pRK*ccaF1*FLAG_NT and *R. sphaeroides* pRK*ccaF1* as an untagged control [24] were diluted to an OD_{660} 0.2 and incubated under phototrophic growth conditions for 8 h (see bacterial strains and growth conditions). The cells (from 100 mL culture) were harvested by centrifugation at 10,000 rpm at 4 °C. The CoIP was performed as described in Grützner et al. and Pfeiffer et al. [24,43]. The precipitated CoIP RNA was treated by TURBO DNase (Invitrogen/Thermo Fischer Scientific, Rockford, IL, USA) to remove any DNA contamination. The isolated RNA was analyzed by RNA sequencing and quantitative real-time RT-PCR.

4.7. Quantitative Real-Time RT-PCR

For quantitative real-time RT-PCR, the Brilliant III Ultra-Fast SYBR® Green qPCR Master Mix Kit (Agilent, Santa Clara, CA, USA) was used as described in the manufacturer's manual. The 10 µL reaction mixtures contained 5 µL Master Mix (supplied), 0.1 µL DTT (100 mM, supplied), 0.5 µL RiboBlock solution (supplied), 0.4 µL water, 1 µL of each primer (10 pmol/L), and 2 µL DNA-free RNA (20 ng/µL). The reactions were performed in a spectrofluorometric thermal cycler (Bio-Rad, Feldkirchen, Germany), and the resulting data were visualized using the Bio-Rad CFX Manager 3.0 software. All real-time RT-PCR experiments were performed in technical duplicates with samples originating from biological triplicates. For all primers, a no-template control was included, to confirm the absence of DNA contamination. RNA abundances were normalized to *rpoZ*. Fold changes were calculated according to Pfaffl [44].

4.8. RNA-Seq Data Processing

The RNA-Seq data processing was performed as described in Börner et al. [23]. The alignment of the raw sequencing reads against the reference genome of *R. sphaeroides* (NC_007493.2, NC_007494.2, NC_009007.1, NC_007488.2, NC_007489.1, NC_007490.2, and NC_009008.1) was performed using the READemption pipeline v.1.0.5 [45]. Processed wiggle files were visualized using the Integrated Genome Browser software version 9.1.10 [46].

Supplementary Materials: The supporting information can be downloaded at: https://www.mdpi.com/article/10.3390/ijms24119515/s1. References [12,17,23–25,41,47–49] are cited in the supplementary materials Tables S1 and S2.

Author Contributions: Conceptualization, J.G. and G.K.; methodology, J.G., J.B. and A.J.; validation, J.G., J.B., A.J. and G.K.; investigation, J.G., J.B. and A.J.; resources, G.K.; data curation, J.G. and J.B.; writing—original draft preparation, J.G., J.B. and G.K.; writing, review, and editing, G.K., J.G. and J.B.; visualization, J.G.; supervision, G.K.; project administration, G.K.; funding acquisition, J.G. and G.K. All authors have read and agreed to the published version of the manuscript.

Funding: This work was funded by Deutsche Forschungsgemeinschaft (DFG 563/41-1 and GRK 2355).

Institutional Review Board Statement: Not applicable.

Informed Consent Statement: Not applicable.

Data Availability Statement: The RNA-Seq data are available in the NCBI gene expression omnibus (GEO) repository. The RIP-Seq analysis (CoIP) data are listed in GSE145045 [24] and in GSE230031. The RNA sequencing of the total RNA is listed in GSE200990 [23].

Acknowledgments: We thank Andrea Weisert and Florian Gerken for excellent technical assistance. We further thank Tara Procida, Jochen Wilhelm, and Marek Bartkuhn (Institute for Lung Health, Giessen, Germany) for fruitful discussions regarding the design of the RNA-Seq approach, support with the cDNA library preparation, and RNA-Seq data generation, along with Tobias Friedrich for RNA-Seq data processing.

Conflicts of Interest: The authors declare no conflict of interest.

References

1. Hördt, A.; López, M.G.; Meier-Kolthoff, J.P.; Schleuning, M.; Weinhold, L.-M.; Tindall, B.J.; Gronow, S.; Kyrpides, N.C.; Woyke, T.; Göker, M. Analysis of 1,000+ type-strain genomes substantially improves taxonomic classification of *Alphaproteobacteria*. *Front. Microbiol.* **2020**, *11*, 468. [CrossRef] [PubMed]
2. Pemberton, J.M.; Horne, I.M.; McEwan, A.G. Regulation of photosynthetic gene expression in purple bacteria. *Microbiology (Reading)* **1998**, *144 Pt 2*, 267–278. [CrossRef] [PubMed]
3. Gregor, J.; Klug, G. Regulation of bacterial photosynthesis genes by oxygen and light. *FEMS Microbiol. Lett.* **1999**, *179*, 1–9. [CrossRef] [PubMed]
4. Mackenzie, C.; Eraso, J.M.; Choudhary, M.; Roh, J.H.; Zeng, X.; Bruscella, P.; Puskás, A.; Kaplan, S. Postgenomic adventures with *Rhodobacter sphaeroides*. *Annu. Rev. Microbiol.* **2007**, *61*, 283–307. [CrossRef]
5. Oh, J.I.; Kaplan, S. Generalized approach to the regulation and integration of gene expression. *Mol. Microbiol.* **2001**, *39*, 1116–1123. [CrossRef]
6. Elsen, S.; Swem, L.R.; Swem, D.L.; Bauer, C.E. RegB/RegA, a highly conserved redox-responding global two-component regulatory system. *Microbiol. Mol. Biol. Rev.* **2004**, *68*, 263–279. [CrossRef]
7. Gomelsky, M.; Kaplan, S. Molecular genetic analysis suggesting interactions between AppA and PpsR in regulation of photosynthesis gene expression in *Rhodobacter sphaeroides* 2.4.1. *J. Bacteriol.* **1997**, *179*, 128–134. [CrossRef]
8. Gomelsky, M.; Klug, G. BLUF: A novel FAD-binding domain involved in sensory transduction in microorganisms. *Trends Biochem. Sci.* **2002**, *27*, 497–500. [CrossRef]
9. Gomelsky, L.; Sram, J.; Moskvin, O.V.; Horne, I.M.; Dodd, H.N.; Pemberton, J.M.; McEwan, A.G.; Kaplan, S.; Gomelsky, M. Identification and *in vivo* characterization of PpaA, a regulator of photosystem formation in *Rhodobacter sphaeroides*. *Microbiology (Reading)* **2003**, *149*, 377–388. [CrossRef]
10. Zeilstra-Ryalls, J.H.; Kaplan, S. Aerobic and anaerobic regulation in *Rhodobacter sphaeroides* 2.4.1: The role of the *fnrL* gene. *J. Bacteriol.* **1995**, *177*, 6422–6431. [CrossRef]
11. Zeilstra-Ryalls, J.H.; Kaplan, S. Role of the *fnrL* gene in photosystem gene expression and photosynthetic growth of *Rhodobacter sphaeroides* 2.4.1. *J. Bacteriol.* **1998**, *180*, 1496–1503. [CrossRef]
12. Braatsch, S.; Gomelsky, M.; Kuphal, S.; Klug, G. A single flavoprotein, AppA, integrates both redox and light signals in *Rhodobacter sphaeroides*. *Mol. Microbiol.* **2002**, *45*, 827–836. [CrossRef] [PubMed]
13. Masuda, S.; Bauer, C.E. AppA is a blue light photoreceptor that antirepresses photosynthesis gene expression in *Rhodobacter sphaeroides*. *Cell* **2002**, *110*, 613–623. [CrossRef] [PubMed]
14. Klug, G. Beyond catalysis: Vitamin B12 as a cofactor in gene regulation. *Mol. Microbiol.* **2014**, *91*, 635–640. [CrossRef] [PubMed]
15. Fang, M.; Bauer, C.E. The Vitamin B12-dependent photoreceptor AerR relieves photosystem gene repression by extending the interaction of CrtJ with photosystem promoters. *mBio* **2017**, *8*, e00261-17. [CrossRef] [PubMed]

16. Klug, G.; Adams, C.W.; Belasco, J.; Doerge, B.; Cohen, S.N. Biological consequences of segmental alterations in mRNA stability: Effects of deletion of the intercistronic hairpin loop region of the *Rhodobacter capsulatus puf* operon. *EMBO J.* **1987**, *6*, 3515–3520. [CrossRef]
17. Mank, N.N.; Berghoff, B.A.; Hermanns, Y.N.; Klug, G. Regulation of bacterial photosynthesis genes by the small noncoding RNA PcrZ. *Proc. Natl. Acad. Sci. USA* **2012**, *109*, 16306–16311. [CrossRef]
18. Eisenhardt, K.M.H.; Reuscher, C.M.; Klug, G. PcrX, an sRNA derived from the 3'- UTR of the *Rhodobacter sphaeroides puf* operon modulates expression of *puf* genes encoding proteins of the bacterial photosynthetic apparatus. *Mol. Microbiol.* **2018**, *110*, 325–334. [CrossRef]
19. Reuscher, C.M.; Klug, G. Antisense RNA asPcrL regulates expression of photosynthesis genes in *Rhodobacter sphaeroides* by promoting RNase III-dependent turn-over of *puf* mRNA. *RNA Biol.* **2021**, *18*, 1445–1457. [CrossRef]
20. Berghoff, B.A.; Glaeser, J.; Sharma, C.M.; Zobawa, M.; Lottspeich, F.; Vogel, J.; Klug, G. Contribution of Hfq to photooxidative stress resistance and global regulation in *Rhodobacter sphaeroides*. *Mol. Microbiol.* **2011**, *80*, 1479–1495. [CrossRef]
21. Hess, W.R.; Berghoff, B.A.; Wilde, A.; Steglich, C.; Klug, G. Riboregulators and the role of Hfq in photosynthetic bacteria. *RNA Biol.* **2014**, *11*, 413–426. [CrossRef] [PubMed]
22. Förstner, K.U.; Reuscher, C.M.; Haberzettl, K.; Weber, L.; Klug, G. RNase E cleavage shapes the transcriptome of *Rhodobacter sphaeroides* and strongly impacts phototrophic growth. *Life Sci. Alliance* **2018**, *1*, e201800080. [CrossRef] [PubMed]
23. Börner, J.; Friedrich, T.; Bartkuhn, M.; Klug, G. Ribonuclease E strongly impacts bacterial adaptation to different growth conditions. *RNA Biol.* **2023**, *20*, 120–135. [CrossRef] [PubMed]
24. Grützner, J.; Billenkamp, F.; Spanka, D.T.; Rick, T.; Monzon, V.; Förstner, K.U.; Klug, G. The small DUF1127 protein CcaF1 from *Rhodobacter sphaeroides* is an RNA-binding protein involved in sRNA maturation and RNA turnover. *Nucleic Acids Res.* **2021**, *49*, 3003–3019. [CrossRef]
25. Billenkamp, F.; Peng, T.; Berghoff, B.A.; Klug, G. A cluster of four homologous small RNAs modulates C1 metabolism and the pyruvate dehydrogenase complex in *Rhodobacter sphaeroides* under various stress conditions. *J. Bacteriol.* **2015**, *197*, 1839–1852. [CrossRef]
26. Reinkensmeier, J.; Giegerich, R. Thermodynamic matchers for the construction of the cuckoo RNA family. *RNA Biol.* **2015**, *12*, 197–207. [CrossRef]
27. Zeng, X.; Choudhary, M.; Kaplan, S. A second and unusual *pucBA* operon of *Rhodobacter sphaeroides* 2.4.1: Genetics and function of the encoded polypeptides. *J. Bacteriol.* **2003**, *185*, 6171–6184. [CrossRef]
28. Lu, Y.; Zhang, H.; Cui, W.; Saer, R.; Liu, H.; Gross, M.L.; Blankenship, R.E. Top-Down mass spectrometry analysis of membrane-bound light-harvesting complex 2 from *Rhodobacter sphaeroides*. *Biochemistry* **2015**, *54*, 7261–7271. [CrossRef]
29. Quendera, A.P.; Seixas, A.F.; Dos Santos, R.F.; Santos, I.; Silva, J.P.N.; Arraiano, C.M.; Andrade, J.M. RNA-binding proteins driving the regulatory activity of small non-coding RNAs in bacteria. *Front. Mol. Biosci.* **2020**, *7*, 78. [CrossRef]
30. Holmqvist, E.; Vogel, J. RNA-binding proteins in bacteria. *Nat. Rev. Microbiol.* **2018**, *16*, 601–615. [CrossRef]
31. Holmqvist, E.; Berggren, S.; Rizvanovic, A. RNA-binding activity and regulatory functions of the emerging sRNA-binding protein ProQ. *Biochim. Biophys. Acta Gene Regul. Mech.* **2020**, *1863*, 194596. [CrossRef] [PubMed]
32. Olejniczak, M.; Jiang, X.; Basczok, M.M.; Storz, G. KH domain proteins: Another family of bacterial RNA matchmakers? *Mol. Microbiol.* **2022**, *117*, 10–19. [CrossRef]
33. Hu, X.; Ritz, T.; Damjanović, A.; Autenrieth, F.; Schulten, K. Photosynthetic apparatus of purple bacteria. *Q. Rev. Biophys.* **2002**, *35*, 1–62. [CrossRef] [PubMed]
34. Schumacher, A.; Drews, G. The formation of bacteriochlorophyll protein complexes of the photosynthetic apparatus of *Rhodopseudomonas capsulata* during early stages of development. *Biochim. Biophys. Acta* **1978**, *501*, 183–194. [CrossRef] [PubMed]
35. Klug, G.; Kaufmann, N.; Drews, G. Gene expression of pigment-binding proteins of the bacterial photosynthetic apparatus: Transcription and assembly in the membrane of *Rhodopseudomonas capsulata*. *Proc. Natl. Acad. Sci. USA* **1985**, *82*, 6485–6489. [CrossRef] [PubMed]
36. Carpousis, A.J.; Campo, N.; Hadjeras, L.; Hamouche, L. Compartmentalization of RNA degradosomes in bacteria controls accessibility to substrates and ensures concerted degradation of mRNA to nucleotides. *Annu. Rev. Microbiol.* **2022**, *76*, 533–552. [CrossRef]
37. Remes, B.; Berghoff, B.A.; Förstner, K.U.; Klug, G. Role of oxygen and the OxyR protein in the response to iron limitation in *Rhodobacter sphaeroides*. *BMC Genom.* **2014**, *15*, 794. [CrossRef]
38. Han, Y.; Meyer, M.H.F.; Keusgen, M.; Klug, G. A haem cofactor is required for redox and light signalling by the AppA protein of *Rhodobacter sphaeroides*. *Mol. Microbiol.* **2007**, *64*, 1090–1104. [CrossRef]
39. Janzon, L.; Löfdahl, S.; Arvidson, S. Evidence for a coordinate transcriptional control of alpha-toxin and protein a synthesis in *Staphylococcus aureus*. *FEMS Microbiol. Lett.* **1986**, *33*, 193–198. [CrossRef]
40. Glaeser, J.; Klug, G. Photo-oxidative stress in *Rhodobacter sphaeroides*: Protective role of carotenoids and expression of selected genes. *Microbiology (Reading)* **2005**, *151*, 1927–1938. [CrossRef]
41. Berghoff, B.A.; Glaeser, J.; Sharma, C.M.; Vogel, J.; Klug, G. Photooxidative stress-induced and abundant small RNAs in *Rhodobacter sphaeroides*. *Mol. Microbiol.* **2009**, *74*, 1497–1512. [CrossRef] [PubMed]
42. Church, G.M.; Gilbert, W. Genomic sequencing. *Proc. Natl. Acad. Sci. USA* **1984**, *81*, 1991–1995. [CrossRef] [PubMed]

43. Pfeiffer, V.; Sittka, A.; Tomer, R.; Tedin, K.; Brinkmann, V.; Vogel, J. A small non-coding RNA of the invasion gene island (SPI-1) represses outer membrane protein synthesis from the *Salmonella* core genome. *Mol. Microbiol.* **2007**, *66*, 1174–1191. [CrossRef]
44. Pfaffl, M.W. A new mathematical model for relative quantification in real-time RT-PCR. *Nucleic Acids Res.* **2001**, *29*, e45. [CrossRef]
45. Förstner, K.U.; Vogel, J.; Sharma, C.M. READemption-a tool for the computational analysis of deep-sequencing-based transcriptome data. *Bioinformatics* **2014**, *30*, 3421–3423. [CrossRef] [PubMed]
46. Freese, N.H.; Norris, D.C.; Loraine, A.E. Integrated genome browser: Visual analytics platform for genomics. *Bioinformatics* **2016**, *32*, 2089–2095. [CrossRef]
47. Simon, R.; O'Connell, M.; Labes, M.; Puhler, A. Plasmid vectors for the genetic analysis and manipulation of rhizobia and other gram-negative bacteria. *Meth. Enzymol.* **1986**, *118*, 640–659. [CrossRef]
48. Van Niel, C.B. The culture, general physiology, morphology, and classification of the non-sulfur purple and brown bacteria. *Bacteriol. Rev.* **1944**, *8*, 1–118. [CrossRef]
49. Jäger, A.; Braatsch, S.; Haberzettl, K.; Metz, S.; Osterloh, L.; Han, Y.; Klug, G. The AppA and PpsR proteins from Rhodobacter sphaeroides can establish a redox-dependent signal chain but fail to transmit blue-light signals in other bacteria. *J. Bacteriol.* **2007**, *189*, 2274–2282. [CrossRef]

Selbstständigkeitserklärung

Hiermit versichere ich, die vorgelegte Thesis selbstständig und ohne unerlaubte fremde Hilfe und nur mit den Hilfen angefertigt zu haben, die ich in der Thesis angegeben habe. AlleTextstellen, die wörtlich oder sinngemäß aus veröffentlichten Schriften entnommen sind, und alle Angaben die auf mündlichen Auskünften beruhen, sind als solche kenntlichgemacht. Bei den von mir durchgeführten und in der Thesis erwähnten Untersuchungen habe ich die Grundsätze guter wissenschaftlicher Praxis, wie sie in der ‚Satzung der Justus-Liebig-Universität zur Sicherung guter wissenschaftlicher Praxis' niedergelegt sind, eingehalten. Entsprechend § 22 Abs. 2 der Allgemeinen Bestimmungen für modularisierte Studiengänge dulde ich eine Überprüfung der Thesis mittels Anti-Plagiatssoftware.

Datum	Unterschrift